THE PHOTOCHEMICAL AND THERMAL DECOMPOSITION OF FERRIC OXALATE

A Thesis for the Degree of Doctor of Philosophy

presented by

Gordon James McLennan, B.Sc.

University of Edinburgh

January, 1962

CONTENTS

CONTENTS (Contd.)

INTRODUCTION

In the last forty years very considerable progress has been made in the chemistry of the solid state. It has frequently been of advantage to have a systematic study of solid state decompositions which can be brought about both thermally and photochemically; the azide salts have for example received particular attention. Ferric oxalate comes into this class of compounds and has the advantage that its overall decomposition can be represented by the simple equation (1)

$$Fe_2(C_2O_4)_3 \longrightarrow 2FeC_2O_4 + 2CO_2$$

The general Schroedinger equation as applied to an ionic solid shows that the permitted energy levels lie in a series of bands which are separated from each other by several electron volts. The first "full" band is normally filled with electrons and the second, - next defined in energy terms - the conductance band, is normally empty; the substance is then an insulator. On absorption of sufficient energy supplied by radiation, an electron is elevated from the full band into the conductance band where there is an abundance of empty states. Under the influence of an applied electric field the electron, thus elevated, therefore can move freely through the crystal. The corresponding gap in the full band is called a positive hole and, by virtue of exchange with an electron from a neighbouring ion, is mobile. Thus both the electron and the positive hole may contribute to the conductivity.

While photoconductivity has been observed with many ionic solids, in the general case the first absorption maximum in the long wavelength end of the absorption spectrum does not correspond to the energy required to elevate an electron into the conductance band, but rather to a lower energy which is associated with the formation as an excited species called an exciton (2). This is regarded as an electron associated with its positive hole and is thus a neutral species: so despite the fact that it is mobile it does not contribute to the electronic conductivity of the solid. It has been found to be a kinetically significant factor in many photochemical reactions.

The excited species normally returns to the ground state by a radiationless transition, i.e. by dissipating its energy thermally to the lattice. However, if the potential energy curves of the ground and excited states do not overlap then reversion to the ground state can only take place by re-emission of radiation, i.e. luminescence. Another form of fluorescence, phosphorescence, takes place if the excited species is trapped in a metastable state at an impurity centre (copper, silver or gold, in zinc sulphide) and re-emission of radiation takes place after a certain time interval, dependent on the stability of the metastable state.

These phenomena represent effects of radiation which are reversible since the crystal can be restored to its ground state. In certain salts, the silver halides, metallic azides and oxalates, the effect of radiation may be permanent and result in a definite chemical change.

Three classes of photochemical decomposition can be distinguished with the metallic azides. They are shown below.

Mercury azide[3]	Alkali and Alkali earth azides e.g. Barium azide[4]	Thallous azide[5]
No photoconductivity	No photoconductivity	Photoconductivity
Rate of reaction proportional to light intensity (I)	Rate $\propto I^2$	Rate $\propto I$
$3Hg_2(N_3)_2 \rightarrow 2Hg_3N_2 + 7N_2$	$Ba(N_3)_2 \rightarrow Ba + 3N_2$	$2TlN_3 \rightarrow 3N_2 + 2Tl$
Activation energy = 8 K. cals./mole.	5 K. cals./mole.	8 K. cals./mole.
No exciton peaks in the u.v. spectra (at -180°C)	Exciton peaks in u.v. spectra	Exciton peaks in u.v. spectra

Deb and Yoffe (3) concluded that mercury azide is a covalent compound and that decomposition proceeds by a molecular rather than an electronic mechanism. On absorption of light an excited azide molecule is formed, this decomposes unimolecularly to give the primary product of the reaction and nitrogen. Depicting the reaction as $A \rightarrow B + N_2$, the detailed mechanism is:

$$A + h\nu \underset{k_2}{\overset{k_1}{\rightleftharpoons}} A^{*} \text{ (excited state)}$$

$$A^{*} \xrightarrow[k_3]{} B + N_2$$

On the assumption that the concentration of A^{*} remains effectively constant then by applying a steady state equation, where k is the rate constant for the appropriate process, it

follows that:

$$\frac{d(N_2)}{dt} = k_3 A^* = \frac{k_1 k_3 A}{k_2 + k_3}$$

Now, since the quantum efficiency is low, $k_2 \gg k_3$, and since

$$k_1 = \left(\frac{\alpha}{h\nu}\right) I \quad \text{where } I = \text{intensity of illumination}$$

and α is the absorption coefficient

$$\text{then } \frac{d(N_2)}{dt} = \frac{k_3}{k_2} A\left(\frac{\alpha}{h\nu}\right) I$$

and E, the activation energy for the whole reaction = $E_3 - E_2 \approx E_3$ (since E_2 will be small).

Therefore the rate of the reaction is proportional to the light intensity, the concentration, i.e. the surface area of A, and the absorption coefficient, and the activation energy of the reaction is approximately equal to that of the dissociation of the complex A^*.

Since in the decomposition of thallous azide photoconductivity was observed, the production of electrons and/or positive holes is indicated. Also the activation energies of the photodecomposition and photoconductivity were the same; if the primary act of absorption causes the formation of electrons and positive holes the activation energy of photoconductivity should be approximately zero. This was observed with light of wavelength less than 3,800 Å, and the reaction is regarded as taking place between the positive holes to produce nitrogen, the electron neutralising the thallium ion to give the metal.

However, at the longer wavelengths Deb and Yoffe considered that the electrons were produced by thermal dissociation of optically formed excitons. The energy required for this is approximately 2 K. cals/mole (6) and so the mechanism is quite feasible at room temperature.

The mechanism for the reaction is thus considered to be the optical formation of an exciton which dissociates to give an electron and a positive hole. Two positive holes react to form three molecules of nitrogen, and the thallium ion diffuses to metal specks, where the electron is trapped, to form the metal atom.

The scheme is thus:

$$N_3' + h\nu \underset{2}{\overset{1}{\rightleftharpoons}} N_3'^{*} \quad \text{(exciton)}$$

$$N_3'^{*} \underset{4}{\overset{3}{\rightleftharpoons}} N_3 + \epsilon$$

$$2N_3 \xrightarrow{5} 3N_2$$

$$Tl^{+} + Tl_n + \epsilon \longrightarrow Tl_{n+1}$$

On application of the steady state equation with reference to the number of positive holes, electrons and excitons then:

$$\frac{d(N_2)}{dt} = k_5(N_3)^2$$

$$\frac{d(N_3'^{*})}{dt} = k_1(N_3')\, I - k_2(N_3'^{*}) - k_3(N_3'^{*})$$

Now k_1 and $k_2 \gg k_3$

$$\therefore (N_3'^{*}) = \frac{k_1}{k_2}(N_3')\, I$$

Once metal specks are formed step 4 becomes unimportant since electrons will be trapped by them rather than recombine with the positive holes.

$$\therefore \quad \frac{d(N_3)}{dt} = k_3(N_3'^{*}) - k_5(N_3)^2 = 0$$

$$\therefore \quad \frac{d(N_2)}{dt} = k_3(N_3'^{*}) = \frac{k_1 k_3}{k_2}(N_3') I$$

$$\text{and } E = E_1 + E_3 - E_2 \approx E_3$$

As before the rate is first order and proportional to the light intensity and the activation energy is approximately equal to that of the dissociation of the exciton.

Finally in the case of barium azide the rate of reaction is proportional to the square of the light intensity, and therefore the ultimate decomposition involves two azide radicals.

Now Thomas and Tompkins (4) using the steady state treatment with reference to the number of traps present in the crystal showed that if the reacting species were azide radicals then theoretical reasoning could not account for the experimental results. If, however, the decomposition proceeds through the reaction of two neutral excitons, then the steady state treatment yields the experimentally determined dependence on the rate of intensity and temperature.

Thus the mechanism is considered to be the excitation of azide ions to give excitons. These migrate through the crystal, until trapped at certain points in the lattice. The exact nature of these traps is unimportant since the exciton is neutral.

Those excitons which are not trapped before all their kinetic energy is dissipated revert to the ground state. Those excitons which are trapped are stable for a certain time and then again revert to the ground state; if before this happens a second exciton is trapped there is the possibility that they will react. Since the azide ion is excited only a small amount of energy may need to be acquired thermally to ensure reaction. On decomposition three molecules of nitrogen are formed, two vacant anion sites and two electrons are produced. The latter associate to form F centres and the trap is regenerated.

The difference in the mechanism of decomposition between thallous and barium azides can be related to the stability of their respective excitons. In the case of barium azide the dissociation energy is approximately 14 K. cals./mole (6), so that the exciton is stable at room temperatures. Whereas, as mentioned previously, the dissociation of an azide exciton is quite probable at room temperature.

The experimental results for the photochemical decomposition of silver oxalate (7) are very similar to those of barium azide and a similar mechanism was proposed for the reaction. Absorption of light creates an exciton which may be trapped at a lattice imperfection. There it may absorb a second quantum of light to become a double exciton, which can either revert to the single exciton or decompose to give carbon dioxide, two F centres, and regenerate the trap.

$$C_2O_4'' + h\nu \rightleftharpoons (C_2O_4')' \quad \text{(single exciton)}$$

$$(C_2O_4')' + h\nu \rightleftharpoons (C_2O_4)'' \quad \text{(double exciton)}$$

$$(C_2O_4)'' \longrightarrow 2CO_2 + 2F + \square \quad \text{(trap)}$$

It is of interest at this stage to examine the results of experiments conducted on the photolysis of ferric oxalate in aqueous solutions. The first significant results were obtained by Allmand and Webb (8), Allmand and Young (9) and Livingston (10). Livingston showed that the rate of reaction was proportional to the light intensity, the reaction continued to completion and the quantum efficiency, 0.5, was doubled in the presence of oxygen. He considered that the light was absorbed by the ferritrioxalate ion, the predominating complex in the conditions he used, to form an excited ion. This could decompose in one of two ways: in the absence of oxygen, a bimolecular reaction with a normal ferrotrioxalate ion as shown:

$$\left[Fe(C_2O_4)_3\right]^{III*} + \left[Fe(C_2O_4)_3\right]^{III*} \longrightarrow 2\left[Fe(C_2O_4)_2\right]'' + C_2O_4'' + 2CO_2$$

or in the presence of oxygen:

$$\left[Fe(C_2O_4)_3\right]^{III*} + O_2 + H_2O \longrightarrow \left[Fe(C_2O_4)_2\right]' + HO_2' + OH' + 2CO_2$$

$$\left[Fe(C_2O_4)_2\right]' + C_2O_4'' \longrightarrow \left[Fe(C_2O_4)_3\right]'''$$

This explains the doubled quantum efficiency in the presence of oxygen.

However, more recently Parker (11) has extended the conditions under which the reaction was previously studied and in conjunction with Hatchard (12) using flash photolysis techniques obtained

results from which they postulated the following scheme:

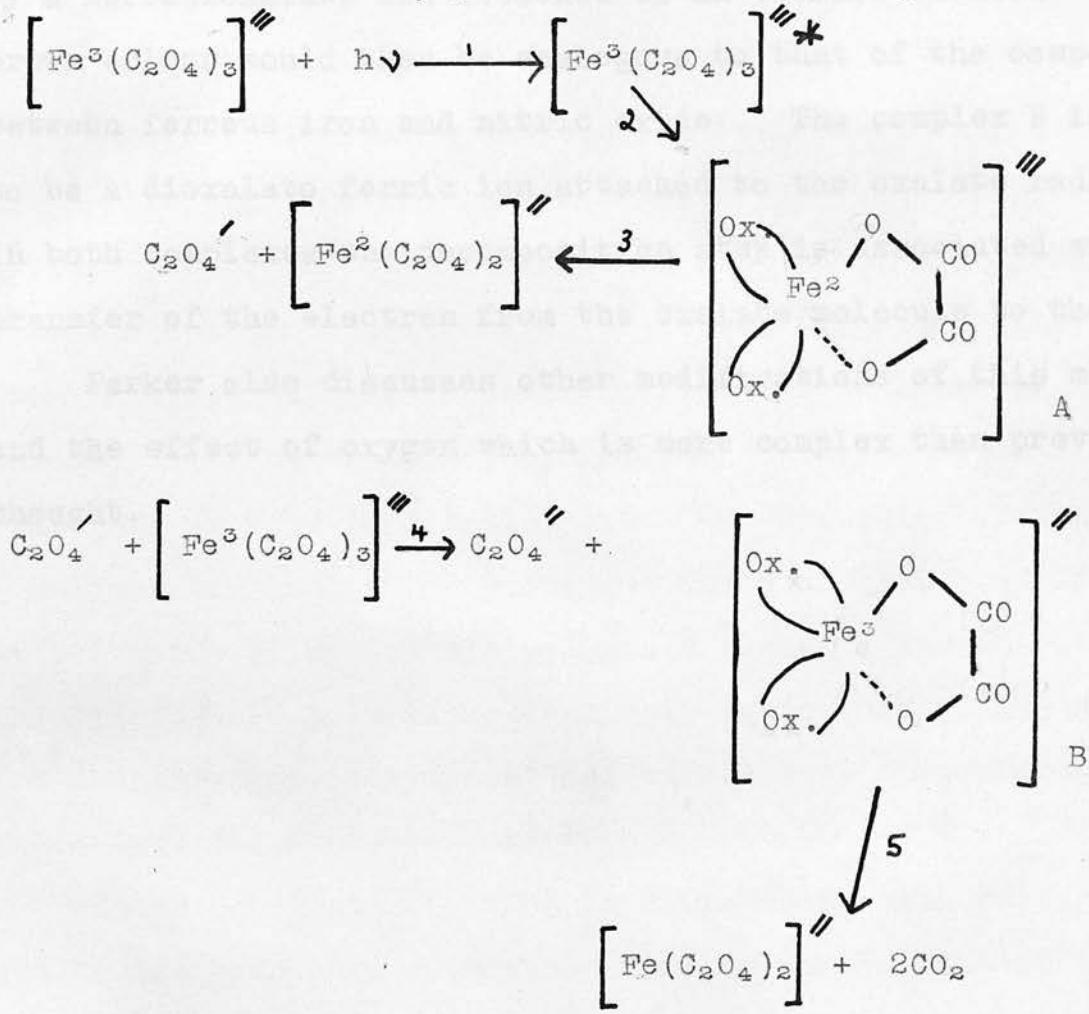

Analogous schemes can be written for the mono and dioxalato complexes which have been shown by spectro-photometric methods to exist in acid solutions. The rate controlling step is considered to be either 3 or 5, from the flash photolysis experiments more probably step 5.

On radiation of a frozen solution of the ferrioxalate ion, a brown substance was obtained which on examination by paramagnetic resonance showed the presence of free radicals. It is possible that this could be the metastable state A and could be represented

by a ferrodioxalate ion attached to an oxalate radical. The brown colour would then be analogous to that of the compound between ferrous iron and nitric oxide. The complex B is thought to be a dioxalato ferric ion attached to the oxalate radical. In both complexes the decomposition step is associated with the transfer of the electron from the oxalate molecule to the iron.

Parker also discusses other modifications of this mechanism and the effect of oxygen which is more complex than previously thought.

THERMAL DECOMPOSITIONS

Inorganic thermal decompositions can be readily divided into exothermic and endothermic reactions. In the latter, as represented by the decomposition of some salts and hydrates, dissociation and recombination processes may occur simultaneously causing complications in both experimental techniques and in the theoretical interpretation of results. Nevertheless, these reactions provide information about the mechanism of interface reactions and nucleation processes which are not readily obtainable by the study of exothermic processes alone. Investigations in this field have been almost entirely restricted to the study of the dissociation of hydrates and carbonates. ~~Ferric oxalate falls into the former category~~.

Water of crystallisation in hydrates is held partly in co-ordination complexes round the metallic ions of the lattice and partly as structural water. The former in the case of simple hydrates appears to be more loosely held within the lattice than the structural water. Thus for copper sulphate penta-hydrate four molecules of water are easily removed at room temperature in vacuo, but the last can only be removed at high temperatures, the process being accompanied by hydrolysis of the sulphate.

The rate of dehydration is normally studied by weight loss methods utilising either a micro balance or suspension from a calibrated spring. One of two factors controls this rate. Firstly the rate of loss of water from the transition layer

existing between hydrated and dehydrated material. If this is the rate controlling factor then, on the assumption that the nature of the transition layer does not change, the dehydration will proceed at a constant rate. The second factor is the rate of diffusion through the dehydrated layer. If the impedance offered by the dehydrated layer to the water molecules is significant, then the overall rate of dehydration will fall off as this layer increases in thickness. The rate of evaporation of water molecules from the external surface of the crystal is probably not significant as dehydrations proceed at a rate very much slower than that of evaporation from a surface into a vacuum.

As such dehydrations involve the removal of molecules from a solid surface, the semi-empirical Polanyi-Wigner equation (13) was applied. This equation states that the rate of reaction (r) at a solid surface is:

$$r = N \gamma e^{-E/RT}$$

which is essentially the simple Arrhenius equation with the pre-exponential constant comprised of two factors: N the number of molecules/cm.^{2} of interface and γ the lattice vibration frequency calculated to be about 10^{13}.

In the case of copper sulphate pentahydrate both Garner and Tanner (14) and Smith and Topley (15) found that the rate of dehydration to the monohydrate fell off to some extent with time, indicating an impedance by the dehydration layer to the water molecules. The effect, although significant, was not large:

the monohydrate was produced as a pseudomorph of the pentahydrate and thus large intergranular spaces were present and offered only a partial barrier to the diffusing water molecules. The activation energy was calculated to be between 16 and 18 K. cals./mole which is comparable to the heat of dissociation, indicating that this was a controlling factor in the rate of dehydration. Substitution of the results in the Polanyi-Wigner equation gave a normal value of γ. Garner (16) thus concluded that, in the dehydration of copper sulphate pentahydrate to the monohydrate the mechanism of formation of the new phase was closely connected with the mechanism of destruction of the old phase and little or no energy in excess of the heat of dissociation was required.

Chrome alum (17) on the other hand gave a constant rate of dehydration which indicated that the loss of water from the transition layer was the rate determining factor. The energy of activation was calculated to be 31 K. cals./mole which was considerably greater than the heat of dissociation (10 K. cals./mole). Determination of the lattice vibration frequency from the Polanyi-Wigner equation gave a high value: 10^{25}. Similarly in the case of calcium carbonate hexahydrate (18), a value of γ was obtained which was significantly larger than 10^{13}. Several theories have been put forward to account for these differences, which Garner discusses fully in his "Chemistry of the Solid State," chapter 8.

Exothermic decompositions of the type:

$$A_{solid} \longrightarrow B_{solid} + C_{gas}$$

have been widely studied since the course of the reaction is readily followed by measuring the pressure of the product gas. The pressure time curves so obtained are usually sigmoid in shape and from them in the majority of cases three stages of the reaction can be detected; an initial reaction occurring on the surface of the crystals, followed by the formation of minute fragments of the new phase B in the old phase A, called nucleation, and finally a reaction occurring at the interface between the phase A and the phase B.

The first stage is not clearly understood but is thought, in some cases at least, to consist of surface decomposition with the formation of anion vacancies. The characteristic mobility possessed by these vacancies determines to some extent the subsequent formation of nuclei. Since the new phase B will generally possess a different molar volume and crystal structure from the phase A, its formation will cause local deformation of the parent lattice. Most crystals are imperfect and contain many crystal defects. It has been shown that these consist of dislocations (19), cation, anion vacancies, Smekal cracks, etc. At these points the lattice strength will have a minimum value and thus nucleation processes will be preferred in their vicinity, as shown by the work of Hedges and Mitchell on silver bromide (20).

Nuclei larger than a certain size, growth nuclei, are stable, those smaller, germ nuclei, are not and tend to disappear unless local energy conditions allow them to grow to a stable size. The ensuing kinetics of decomposition are now governed by the

relative values of the activation free energy of growth of the existing nuclei (ΔG_1) and that of the formation of further nuclei (ΔG_2). If $\Delta G_1 < \Delta G_2$ then growth of the existing nuclei will be preferred to the formation of more nuclei. Thus compact individual nuclei of phase B will be formed in the matrix of A. This has been observed with barium azide (21) and copper sulphate pentahydrate (22). If on the other hand the two free energies are approximately equal then a large number of small nuclei will be formed and as a result the acceleration period of the decomposition is considerably reduced as was observed with mercuric oxalate (23). In the case of silver and lead azide (24) nucleation is very rapid and there is almost instantaneous coverage of the surface with a film of the solid product. Thus the most rapid rate of reaction is at the beginning and the subsequent rate is controlled by the movement of the interface towards the centre of the crystal.

The "normal" growth of nuclei takes place according to a power law relationship corresponding to the equation $p \propto t^n$ where p is the pressure of the product gas, t is the time of the reaction and n usually an integer. Where the decomposition is concerned with growth from a fixed number of nuclei, n has the value 2 or 3, corresponding to two or three dimensional growth. This is demonstrated by calcium azide (25), aged mercury fulminate (26) (n = 3), small crystals of barium styphnate monohydrate (27) and dehydrated lead styphnate (28) (n = 2). Where the number of nuclei also increase with time values for

n of 4, for silver oxalate (29), and 6 for barium azide (30) have been recorded.

Although the power law has proved satisfactory in explaining many reactions, Garner and Hailes (31) found that it was inadequate in explaining the decomposition of fresh mercury fulminate. They introduced the concept of the growth of nuclei propagated by a branching chain mechanism which leads to an exponential law: $p = Ce^{kt}$, where C and k are constants. Although this equation has been experimentally verified, the exact nature of the chains is somewhat obscure.

Prout and Tompkins (32) found that for the decomposition of potassium permanganate neither of the above laws fitted the experimental results. They modified the exponential equation by allowing for the interference between the branching nuclei, this leading to the formulation of the well known equation:

$$\ln. \frac{\alpha}{1 - \alpha} = kt + c ,$$

where α is the fraction decomposed, k is the branching coefficient and c a constant. They considered that the strain set up by the formation of the new phase created cracks in the crystal and the branching nucleation was connected with these cracks.

These mechanisms hold up to the maximum rate of the reaction. However, after this, overlap between the nuclei causes a fall off in the rate and the remainder of the decomposition is called the decay stage. This is governed usually by one of two equations.

Where the complex interface resulting from the overlap of large nuclei breaks down, blocks of undecomposed material are isolated and the rate of reaction is proportional to the amount of substance undecomposed, leading to the unimolecular decay law:

$$\ln.(1 - \alpha) = kt$$

Secondly where the surface of the crystal is covered by a film of product, the movement of the resultant interface towards the centre of the crystal is found to be expressed by the equation:

$$1 - (1 - \alpha)^{\frac{1}{3}} = kt$$

called the "contracting sphere" equation. Both these equations have been experimentally verified in many cases. Many other theoretical equations governing the rate of formation and growth of nuclei have been developed and a full review of these is given in Garner's "Chemistry of the Solid State," chapters 7 and 9.

While a considerable quantity of information can be deduced from the pressure time curves, evidence from other physical measurements, e.g. infra red and ultra violet spectroscopy and conductivity, is of great value.

Oxalate Salts

Although only the decomposition kinetics of the heavy metal oxalates have been studied in detail, qualitative decomposition results have been recorded on many others and they are readily classified into three groups by their primary decomposition products.

Firstly the divalent metal oxalates (33) which decompose to

give the metal oxide, carbon monoxide and carbon dioxide. Secondary reactions can take place by the reduction of the metal oxide by carbon monoxide. The proportions of the various products depend on the rate of decomposition of the oxalate and the ease of reduction of the metal oxide. In the case of nickel oxalate (34) only the metal and carbon dioxide are obtained.

The second group are those which decompose to give the carbonate and carbon monoxide, these consist of the rare earth (35), alkali (36) and alkaline earth (37) metal oxalates. In the study of these considerable use has been made of differential thermal analysis. This technique is of great value in examining the decomposition of the oxalate salt hydrates qualitatively as well as giving results leading to the easy calculation of activation energies.

The third group are the heavy metal oxalates, which decompose to give varying quantities of the metal, metal oxide, carbon monoxide and carbon dioxide.

The kinetics of the decomposition of silver oxalate have been extensively studied, (it decomposes to give silver and carbon dioxide) and two sets of results can be distinguished. For the acceleratory period both a power law $\alpha = ct^n$ (38,39) and an exponential law $\alpha = Ce^{kt}$ (40) relationship have been reported. In the former case n was approximately 4 and on pre-irradiation with ultra violet light fell towards the value 3. This was ascribed to the first order ~~of~~ formation of certain sites of

compact nuclei which grow three-dimensionally, the number of unfertilised sites being reduced as the period of ultra violet light exposure is increased. Where the exponential law fitted it was found that k but not C was sensitive to the method of preparation, whereas C but not k was increased by exposure to ultra violet light. Recent results (41) show that annealing silver oxalate at 80°C prior to decomposition gives more reproduceable results and it is then found that the acceleratory period of the decomposition is best fitted by the Prout Tompkins equation and the decay by the "contracting sphere" equation. The effect of ultra violet light is thought to be the conversion of branching points from germ nuclei to growth nuclei and thus the reaction will then be fitted by a cubic power law. This is a considerably simplified picture, particularly with respect to the effect of ultra violet light irradiation. Nucleation by a mechanism similar to that for silver bromide is discounted since ionic conductivity measurements show that there is no increase in conductivity either with photolysis or during thermal decomposition.

The decomposition of lead oxalate (42) appears to be quite satisfactorily explained by the Prout Tompkins equation, the energy of activation being the same for the acceleration and decay processes. Grinding of the crystals reduces the induction period but does not substantially alter the rate constants of the reaction. The effect is thus to increase the initial number of nuclei and so cause earlier interference

between the branching chains leading to a shorter acceleration period.

Prout and Tompkins (43) in their examination of the decomposition of mercuric oxalate found that there was a short acceleration period described by the equation:

$$\frac{dp}{dt} = kt + C$$

where k and C are constants. Now, since it is a precipitated solid, mercuric oxalate is probably highly nucleated and thus the short period of acceleration is the spreading of the reaction, from a large number of initial centres, over the surface of the crystal. After the maximum rate, the rate of reaction will be governed by the rate of the movement of the resultant interface towards the centre of the crystal. Thus the kinetics should be described by the equation:

$$kt = 1 - (1 - \alpha)^{\frac{1}{3}}$$

which is equivalent to $(\frac{dp}{dt})^{\frac{1}{2}} \propto t$

and this was found to fit the experimental results. The presence of water vapour was found to retard the reaction; this is a further indication that the reaction takes place on the surface, since the water will be adsorbed by the reactive centres and the induction period will be due to the desorption of this vapour.

On irradiation with ultra violet light the salt was found to darken, without evolution of gas. This was thought to

consist of the production of mercury and mercurous oxalate. On decomposition of the irradiated salt a rapid increase in pressure was observed; however, the subsequent kinetics were unchanged. This rapid increase of pressure was associated with the unimolecular decay of the mercurous oxalate. The primary act of irradiation was envisaged as the freeing of an electron from a surface oxalate group, which is subsequently trapped by a mercury atom in the second layer. If the mercury collects two electrons, the metal is formed and accounts for the darkening. The process thus corresponds to an electron transference which when followed by intra-molecular change results in the production of the mercurous oxalate.

Finally, with nickel oxalate Scaife and Allen (34) found that the reaction was comprised of two parts, an initial reaction described by the equation:

$$p = k(t - t_o)^{\frac{1}{2}}$$

where t_o is the time correction for the period of heating, for about the first 6% of decomposition, followed by an initially constant rate of reaction which falls off with time.

The mechanism for the first process is based on the hypothesis that oxalate ions can diffuse in the surface layers. At the end of this process, the lattice on the surface breaks down and a fresh surface of oxalate ions is exposed which decomposes, initially at a constant rate with the formation of metallic nickel. No nickel appears to be formed in the first process.

It has been assumed in all these reactions that the diffusion of the product gas from the solid has not been a kinetically significant factor. However, it has been reported that in the thermal decomposition of potassium manganese trioxalate and potassium cobalt trioxalate (44) diffusion does play an important role in the kinetics of the reaction. This possibility of diffusion must be kept in mind in all investigations based on gas pressure measurements.

The following pages contain a report on the investigation of the decomposition, both photochemical and thermal, of ferric oxalate crystals. Preliminary trials showed that reasonable rates of decomposition might be followed by gas pressure measurements for reasonable light intensities at room temperature and also for thermal decompositions in the neighbourhood of 100°C. Such crystals contain water and the complications of water liberation must be kept in mind.

It was hoped that such studies in conjunction with electrical conductivity measurements with and without illumination, would provide additional evidence and confirmation of existing theories of oxalate decomposition.

EXPERIMENTAL METHODS

SECTION 1: PREPARATION AND PURIFICATION OF CHEMICALS

Ferric oxalate was prepared by the method described by Weinland and Rein (45). 4 gms. of ferric nitrate nonahydrate ($Fe(NO_3)_3\ 9H_2O$) and 2.4 gms. of oxalic acid dihydrate were thoroughly crushed and dissolved in 30 gms. of 70% nitric acid. The solution was filtered through a sintered glass filter to remove the small amount of undissolved material and allowed to stand in a desiccator containing concentrated sulphuric acid. After twenty four hours a yellow solid had precipitated; this was filtered as before, washed with ice cold water and dried over concentrated sulphuric acid. The product was lightly ground in a hand mortar ('crushed powder').

The entire operation was carried out in dim light to avoid decomposition.

The oxalate was analysed in the following manner. A solution of approximately 0.3 gms. of the oxalate in dilute sulphuric acid was made up, from which the iron was precipitated, by ammonia, as the hydroxide. The remaining oxalate solution was then titrated with standard permanganate in the usual way. The ferric iron solution obtained by dissolving the hydroxide precipitate was reduced with zinc and sulphuric acid to give the corresponding ferrous solution. This was again titrated with standard permanganate solution. Typical results are shown below as are the theoretical percentages for iron and oxalate in $Fe_2(C_2O_4)_3\ n\ H_2O$ for values of n = 4, 5, 6.

Weight of Oxalate (gm.)	Vol. of $KMnO_4$ 1972 N mls.	% oxalate	Vol. of $KMnO_4$ mls.	% iron
0.3015	19.62	56.5	6.46	23.9
0.3976	25.98	56.7	8.63	23.9
n				
4		58.9		25.0
5		56.7		24.0
6		54.6		23.1

The experimental results of 56.6% and 23.9% are therefore consistent with the formula $Fe_2(C_2O_4)_3 \cdot 5\ H_2O$.

Gases

Cylinder oxygen was passed slowly over phosphoric oxide, through a trap surrounded by liquid oxygen into an evacuated gas storage bulb attached to the apparatus. The bulb was rinsed twice with 50 mm. of oxygen and evacuated to 10^{-3} mm. before 760 mm. oxygen was finally admitted.

Cylinder carbon dioxide was also passed over phosphoric oxide into an evacuated storage bulb. From this it was condensed into a trap, surrounded by liquid oxygen, pumped free of permanent gas impurities and expanded back into the bulb. This was repeated twice.

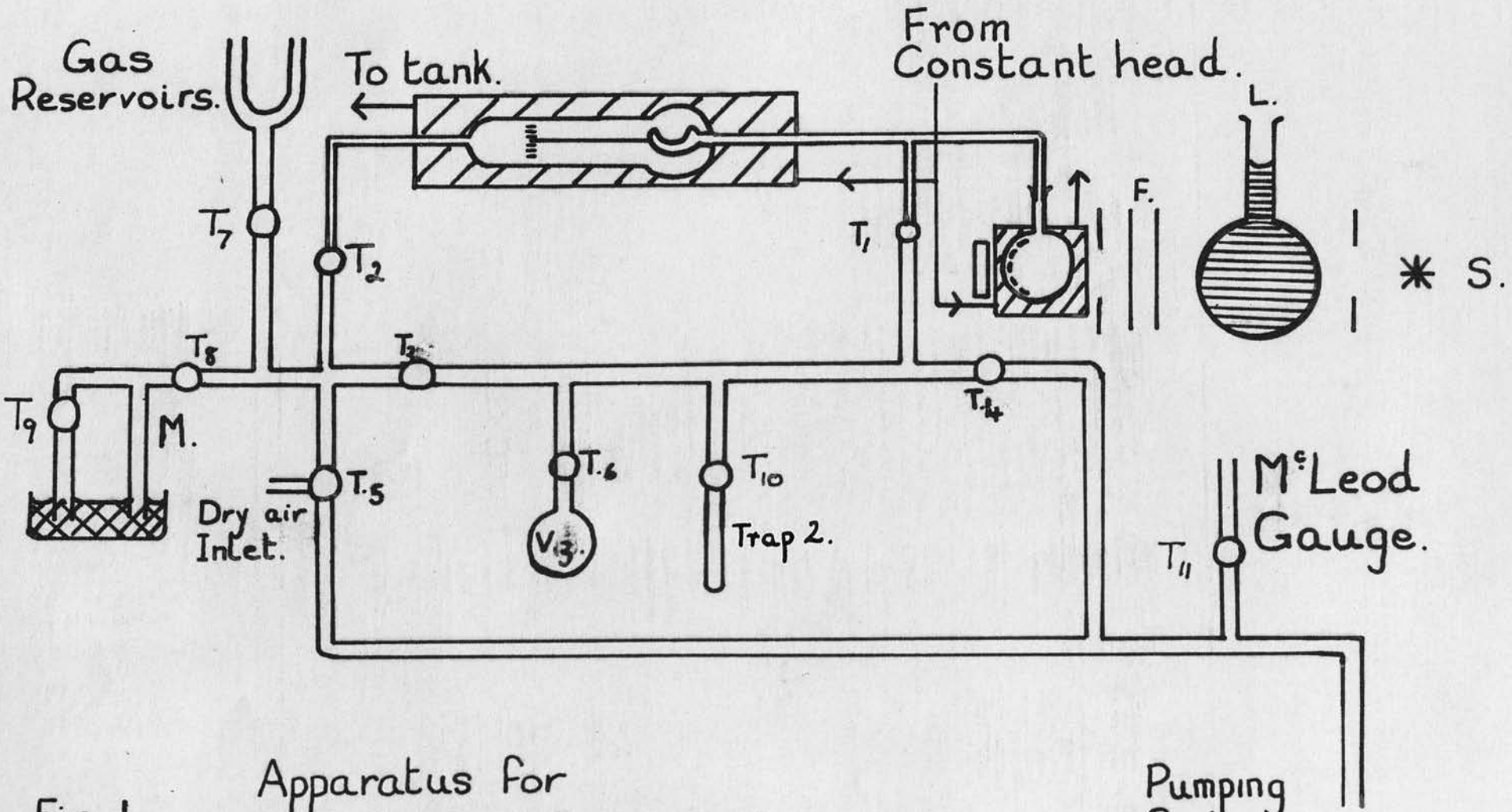

Fig. 1. Apparatus for Photochemical Decomposition.

SECTION 2: APPARATUS FOR PHOTOCHEMICAL DECOMPOSITION MEASUREMENTS

The apparatus shown in diagrammatic form opposite was used to measure small pressure changes in gases at pressures from 0 - 50 mm. occurring during the illumination of ferric oxalate films. It was constructed almost entirely of soda glass. All "Quickfit" joints and high vacuum taps were lubricated with Apieson grease L for normal low temperatures; at higher temperatures silicone high vacuum grease was employed.

A silica mercury diffusion pump, backed by a Speedivac oil pump, was used to evacuate the system. Three pressure measuring instruments were used: (1) mercury manometer (M) for pressure differences from 2 mm. upwards, (2) Bourdon gauge for changes of 0.01 mm. upwards, (3) McLeod gauge for pressures of 10^{-1} mm. to 10^{-6} mm.

Because of the sensitivity of the Bourdon gauge the volume in which it was used had to be kept at a steady temperature. This was achieved with a water circling divided flow arrangement. Water from a large reservoir was pumped up to a constant head device from which it flowed down in two streams, one round the gauge jacket and the other round the reaction vessel.

The temperature of the thermostat bath was maintained by means of an electric heater in conjunction with a chloroform mercury regulator and a sunvic relay. This water was constantly stirred. The rates of flow of water through the well lagged lines to the

gauge could be controlled by a screw clip at the constant head outlet. Under these conditions the temperature was controlled to within 0.01°C.

Calibration of the Bourdon gauge

A telescope with a vertical scale in the eyepiece was focussed on the illuminated platinum tip of the gauge pointer and adjusted till the pointer fell in the centre of the scale. The gauge was calibrated in mm. of mercury per telescope scale division. This was effected by repeatedly reducing the pressure in the gauge, compensating the gauge jacket, noting the total number of scale divisions traversed by the gauge pointer and measuring the total pressure change by the mercury manometer.

The apparatus was filled with dry air through the air leak at T_5 to a known pressure as recorded by the manometer (M). The tap T_3 was then closed. The reaction vessel was then evacuated through T_4 and the compensating evacuation through T_5. The evacuation was continued until the pressure of the entire system had been lowered by about 30 mm. The sensitivity of the gauge was then found by dividing this pressure by the total number of scale divisions traversed. With one gauge the following results were obtained.

Total pressure change = 26.5 mm.

Number of scale divisions travelled = 870

870 divs. = 26.5 mm.

1 div. = 0.0304 mm.

on repetition

1 div. = 0.0304 mm.

and 1 div. = 0.0301 mm.

Sensitivity of gauge = 0.0303 mm. Hg./div.

Determination of reaction space volume

In order to calculate the molar quantities of gases reacting in the system it is necessary that the total volume of the reaction vessel gas space be known. In this determination the required volume was found by expanding a known pressure of gas in the unknown volume into a known volume and measuring the resultant pressure.

Referring to fig. 1 - the volume of V_3 was determined by weighing the bulb empty and full of water up to the tap T_6. With the reaction volume and jacket connected about 10 cm. of dry air was admitted to them and measured on the manometer. The taps T_3 and T_1 were then closed and the volumes V_2 (where V_2 is given by the volume enclosed by taps T_1, T_3, T_6, T_{10} and T_4) and V_3 evacuated. The air in V_1 was then expanded into V_2, the gauge pointer being kept in the central position by simultaneous removal of air from the jacket. When equilibrium was attained the pressure was recorded, the air then expanded into V_3 and the final manometer

reading taken. Knowing P_1, P_2, P_3 and V_3 the volume V_1 can be calculated:

$$P_1 V_1 = P_2(V_2 + V_1) = P_3(V_1 + V_2 + V_3)$$

$$= P_3\left(\frac{P_1 V_1}{P_2} + V_3\right)$$

$$\therefore P_1 V_1 P_2 = P_3 P_1 V_1 + P_3 V_3 P_2$$

$$\therefore V_1 = \frac{P_2 P_3 V_3}{P_1(P_2 - P_3)}$$

A typical result is shown below:

P_1 = 102.7 mm.

P_2 = 71.2 mm.

P_3 = 38.0 mm.

V_3 = 54.7 mls.

$\therefore V_1$ = 43.0 mls.

on repetition V_1 = 43.2 mls.

Volume of reaction space = 43.1 mls.

Optical System

The radiation source (S) was an Osira mercury vapour lamp, the beam of which was passed through a two litre spherical glass flask (L) containing a solution of copper sulphate (≡ 1 cm. of a solution containing 100 gm. of $CuSO_4.5H_2O$/l.). This served both as a filter for infra red and ultra violet rays and as a lens. Various filter combinations were used to pass whatever lines of the mercury spectrum were required. The following table gives the combinations used.

Wavelength in Å of light transmitted	Filter combination used
3650	Wood's glass plate 2 mm. thick
4050	1 cm. saturated aqueous copper nitrate solution and 1 cm. iodine in carbon tetrachloride 7.5 gm./litre
4360	1 cm. cuprammonium sulphate solution; 50 gm. $CuSO_4.5H_2O$, 600 mls. 0.88 ammonia in 1 litre aqueous solution, and 1 cm. saturated aqueous sodium nitrite solution
5460	Chance glass OY 3
5790	1 cm. potassium dichromate solution 150 gm./litre

Solutions were contained in 1 cm. glass filter cells. In all experiments the light beam was transmitted through at least 6 mm. of soda glass and about 20 cm. of water. Under these conditions very little light of wave-length less than 3650 Å was expected to reach the sample under irradiation. The input to the 230 volt - 125 watt lamp was stabilised by a voltage stabiliser and the lamp protected by a choke and condenser arrangement.

SECTION 3: TYPICAL REACTION PROCEDURE

Preparation of Films

The films of ferric oxalate were of two types and were prepared in the following way.

Firstly up to 300 mgm. as required were weighed into a spherical reaction vessel. A few drops of water were added and the contents of the flask swirled to form an even film about 2 cms. in diameter on one side of the reaction flask. The flask was then attached to the apparatus in a horizontal position and the water pumped off.

Secondly 10 mgm. of the ferric oxalate were weighed into a flat sided reaction vessel, to which approximately 1 ml. of distilled water was added. When the oxalate had dissolved the flask was attached horizontally to the apparatus and carefully evacuated. This gave a yellow glassy almost transparent film as compared to the thick powdery film obtained by the other method. These operations were carried out in dim light, the films being protected from stray light as completely as possible. When the films were dry the reaction vessel was attached to the apparatus and was evacuated at 10^{-3} mm. for 16 hours.

Reaction Pressure Measurements

Pressure changes arising from photochemical reactions investigated were measured on the Bourdon gauge. Before readings were started the thermostatted water was circulated for ½ hour to

give steady temperatures. Taps T_1 and T_2 were then closed and if after a further ½ hour no leak was apparent, the illumination was started. The light was switched on ¼ hour before it was required to ensure that there would be a steady light intensity for the reaction.

The position of the gauge pointer was read every five minutes, or at longer intervals when the reaction was slower, during a typical decomposition. When the pointer reached about 30 scale divisions from the centre zero, the pressure in the gauge jacket was rapidly raised or lowered to bring the pointer 30 divisions on the other side of the zero. This was repeated as often as was necessary throughout a run.

Examination of the gaseous products

On suitable illumination photodecomposition of ferric oxalate films was accompanied by increases in gas pressure and as will be described later a further residual pressure increase took place after the illumination was discontinued. To include the gas, evolved in the latter process, in the measurements the film was normally left for seventeen hours after the illumination was stopped. The product gases were then condensed into the trap (2) fig. 1 by surrounding it with liquid nitrogen, and then separately re-expanded into the reaction space by surrounding (2) with the appropriate temperature baths. The pressures of the gases were then recorded.

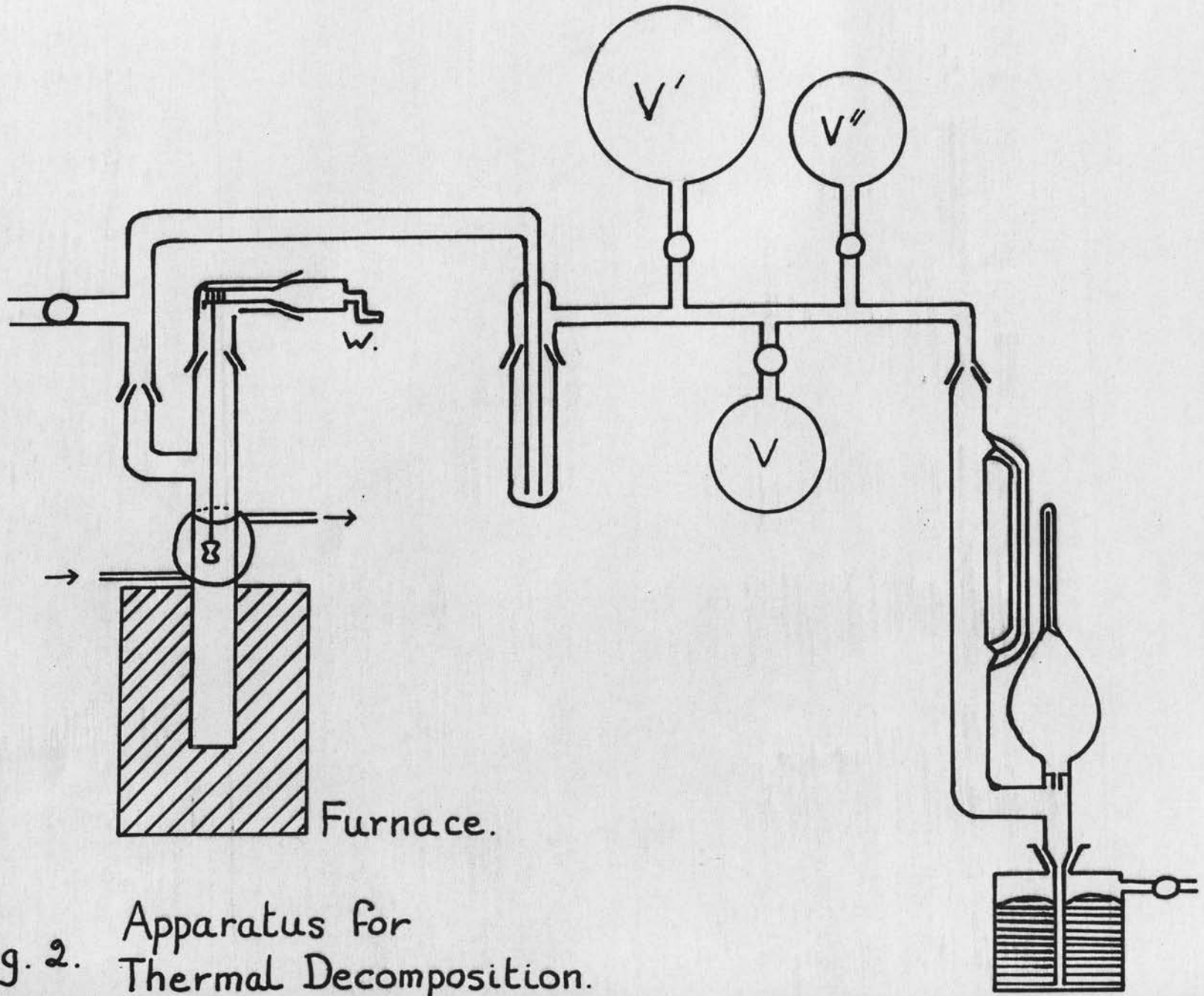

Fig. 2. Apparatus for Thermal Decomposition.

SECTION 4; APPARATUS FOR THERMAL DECOMPOSITION MEASUREMENTS

It was intended for the study of the thermal decomposition of the oxalate to replace the water jacket round the reaction vessel with an electric furnace. This, cylindrical in shape, consisted of two halves which fitted round the reaction vessel. This system would facilitate investigations of the decompositions under the simultaneous effects of light and heat as well as enabling direct comparisons between the two types of decomposition to be made. Unfortunately, however, this system was found to be unsuitable because of temperature variation. Nevertheless it was used for qualitative experiments.

The apparatus finally used is shown in diagrammatic form opposite (fig. 2). It was a simple static system where the pressure of the gas evolved into a known volume was measured on the McLeod gauge. The reaction vessel was centrally situated in the furnace, the input to which was kept constant by means of a simmerstat in conjunction with a voltage stabiliser. It was found that if the room temperature was kept reasonably constant that the temperature of the furnace could be maintained within $0.5^{\circ}C$. This temperature could be adjusted by altering the input voltage with a variac and was measured with a thermometer. The trap filled with a cardice/acetone mixture removed the water vapour produced during the reaction and minimised the diffusion of mercury from the McLeod gauge to the reaction vessel.

The sample to be decomposed was contained in a small bucket

which was constructed from 2 cm.^{2} of 0.025 mm. thick platinum foil. This could be lowered into or raised from the furnace at any given time by means of the winch (W) to which the bucket was attached by a length of fine platinum wire.

The volumes V' and V" consisted of two bulbs which could be connected to the reaction line to maintain the pressures in the desired range. The volume of each section of the system was measured by expanding a known pressure of dry air from the known volume (V) into each section and measuring the resultant pressure on the manometer. The volumes given are a mean of three values and were found with the reaction vessel and trap at room temperature.

Volume of reaction space = 542 ml.

V" = 1,080 ml.

V' = 3,000 ml.

Calibration of McLeod gauge

To calibrate the McLeod gauge two factors are required, the volume/mm. of the capillary and the volume of the bulb. These were obtained as follows: the length of a thread of mercury, introduced into the capillary, was measured using a travelling microscope. On weighing the quantity of mercury used, the volume of the mercury and thus the volume/mm. of the capillary could be obtained. A mean value of three determinations was obtained. The volume of the bulb was found by weighing it empty and filled with water, and again the final value taken was the mean of three determinations.

Experimental Procedure

With the weighed sample (approximately 10 mgm.) in the platinum bucket, held in the cooled part of the reaction vessel, the total volume was pumped out at 10^{-5} mm. for 16 hours. The system was then isolated from the pumps and if after 1 hour no leak had developed, the sample was lowered into the furnace so that it made good contact with the bottom of the reaction vessel. By preliminary experiments it was estimated that the bucket took less than 2 minutes to reach the temperature of the reaction vessel. With the trap held at $-80^{\circ}C$. the McLeod gauge measured the pressure of carbon dioxide evolved. Pressure readings were taken at suitable intervals.

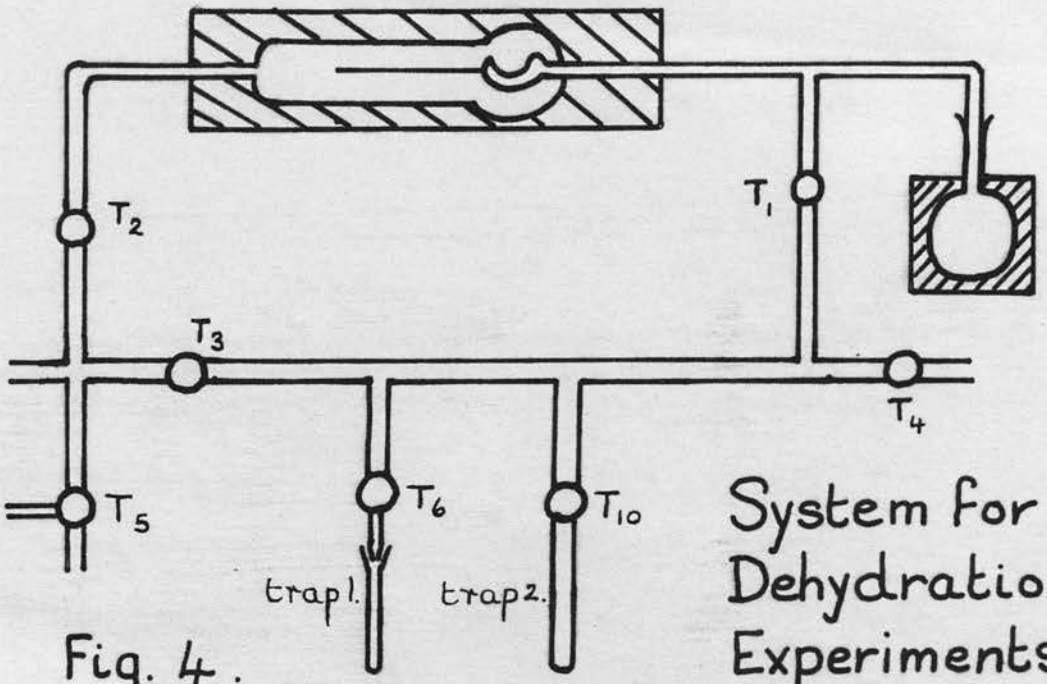

System for Dehydration Experiments.

Fig. 4.

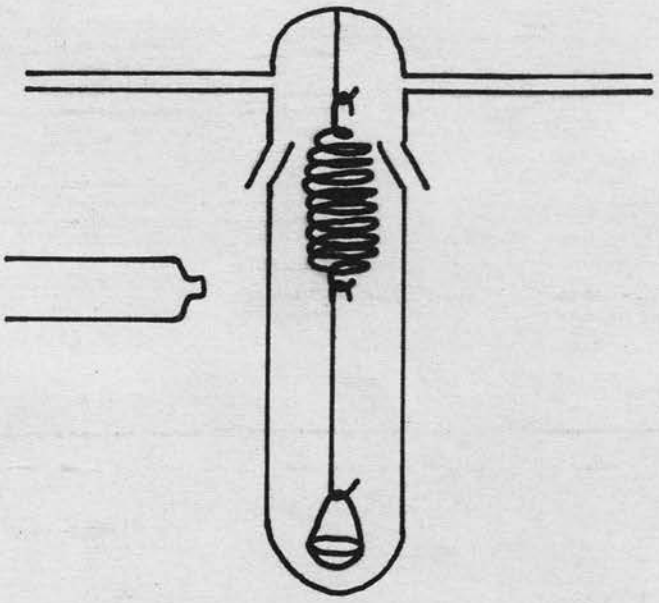

Calibrated Spring System.

Fig. 3.

SECTION 5: DEHYDRATION EXPERIMENTS

The dehydrations were studied either by weight loss methods with a calibrated spring arrangement or by measuring the pressure of water vapour evolved, on the bourdon gauge. Three sets of dehydration experiments were performed.

(1) Measurement of the extent of dehydration.

(2) Measurement of dissociation pressures.

(3) Measurement of the rates of dehydration.

The weight loss method was used for (1), however, it was found to be unsatisfactory for (2) and (3), and thus the vapour pressure method was used for these experiments and to confirm the results obtained for (1).

Weight loss method

The system used was a simplified version of the McBain-Baker sorption balance (fig. 3). The spring, constructed from copper-beryllium wire, was suspended from the apparatus by a glass hook. The sample was contained in a glass bucket which was attached to the spring by a length of fine glass rod, so that the sample was near the bottom of the containing vessel and could be shielded from stray light. The telescope was focussed on the lower end of the spring, the calibration results of which are shown below and in the graph (fig. 5).

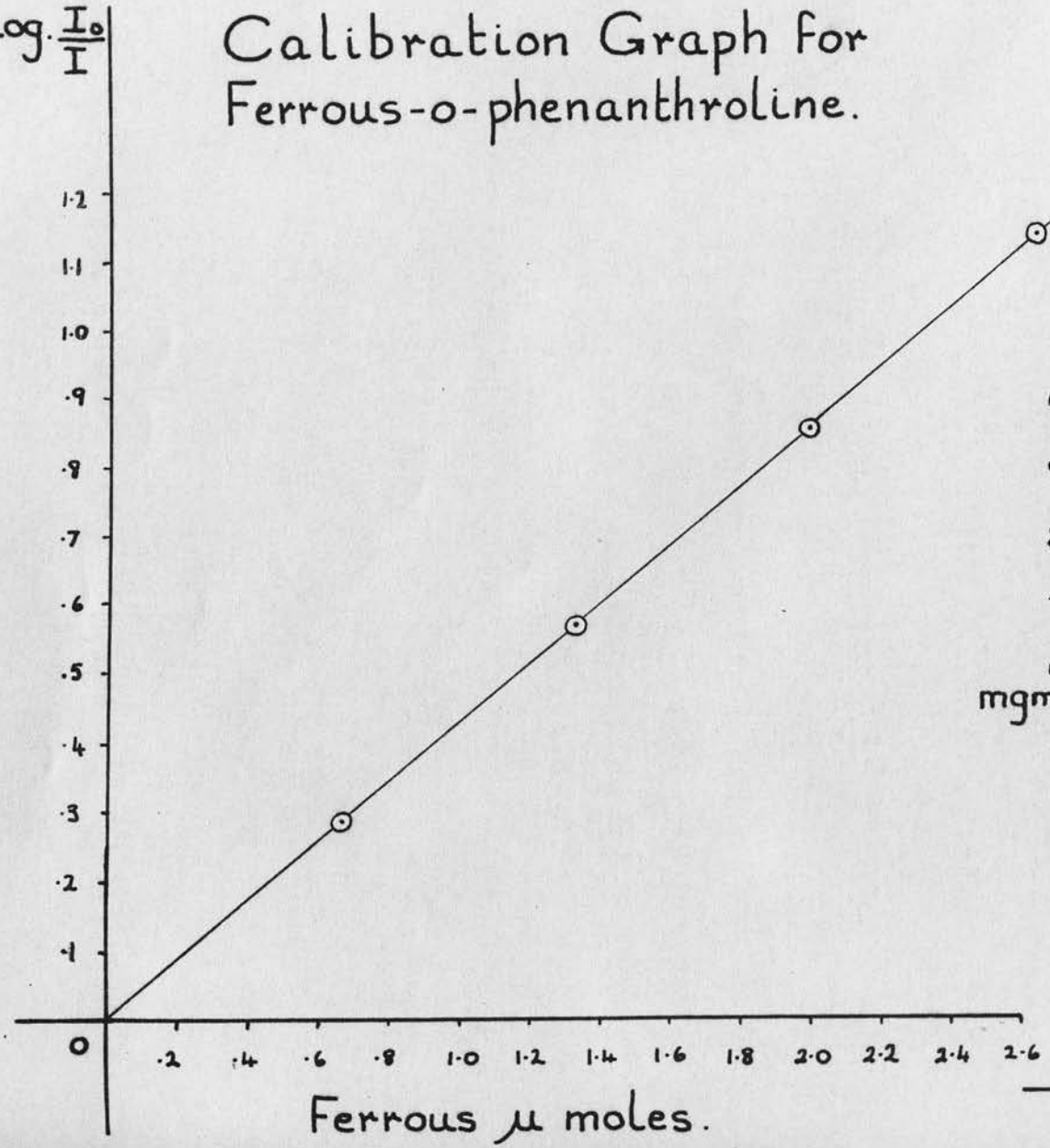
Log. $\frac{I_0}{I}$
Calibration Graph for
Ferrous-o-phenanthroline.
1·2
1·1
1·0
·9
·8
·7
·6
·5
·4
·3
·2
·1
0
·2
·4
·6
·8
1·0
1·2
1·4
1·6
1·8
2·0
2·2
2·4
2·6
Ferrous μ moles.

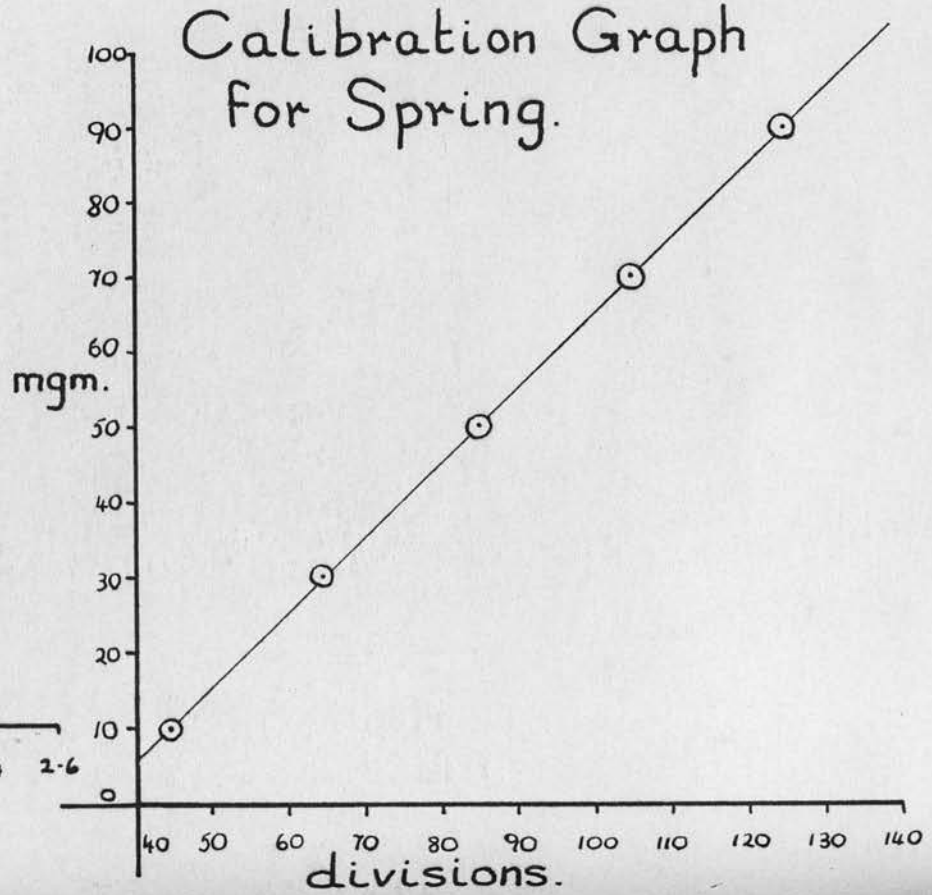
Calibration Graph
for Spring.
mgm.
100
90
80
70
60
50
40
30
20
10
0
40
50
60
70
80
90
100
110
120
130
140
divisions.

Weight mgm.	Telescope Reading divs.
10	44.5
30	64.5
50	85.0
70	105.0
90	125.0

From the graph the sensitivity of the spring = 1.00 mgm./div.

For measurements with the spring, 100 mgm. samples were used. The initial reading was taken under normal conditions, the apparatus was then evacuated and readings taken until a constant weight loss was recorded.

Vapour Pressure Methods

The system used is shown in fig. 4, being similar to the apparatus used for the photochemical decomposition except that trap (1) replaced the volume V_3. For the measurement of the extent of dehydration the following procedure was adopted. Samples of the hydrates, from 10-30 mgm., were placed in the detachable trap (1), which was then attached to the apparatus with T_6 closed. After the rest of the apparatus was fully evacuated T_6 was opened and the trap evacuated; at the same time it was surrounded by a cardice/acetone mixture to prevent dehydration at that stage. After evacuation T_4 was closed and the freezing mixture removed from (1) and placed round (2) (where

carbon dioxide was also evolved liquid nitrogen was used to surround (2)), trap (1) was then surrounded by a water bath or furnace at the temperature at which the dehydration was to be investigated.

After a suitable time (24 hours) T_6 was closed, the freezing mixture removed from trap (2) and the water vapour expanded into the volume given by T_3, T_4, T_6, which was approximately 100 mls. This was done by manipulating T_{10} so that the pointer of the gauge moved over the range consisting of about 30 divisions either side of the centre of the scale. The gauge was balanced in the usual way. The pressure of the water vapour was never allowed to exceed 8 mm. so that condensation of the vapour was avoided. If this pressure was reached the gauge was re-evacuated and the expansion continued. When the water vapour was expanded into the measuring volume the pressure reading attained decreased slowly due presumably to adsorption of the vapour on the glass walls, thus the initial pressure was recorded. The process was repeated for further periods of time until no further water vapour appeared to be evolved. Throughout all the dehydration experiments the samples were shielded from stray light. The molar quantities of water produced were then calculated from the total pressure of the water vapour evolved and the physical constants of the system in use.

The dissociation pressure of the hydrates were obtained as follows. 10 mgm. quantities of the hydrate were placed in the detachable trap (1) and evacuated as described above. T_4 was then closed, a water bath of the required temperature substituted

for the freezing mixture round trap (1) and the vapour pressure of the hydrate allowed to reach equilibrium. The system was then re-evacuated and the process repeated. This was continued until consistent readings for the dissociation pressure were obtained.

Rates of dehydration are normally followed by weight loss methods. However, a suitable microbalance was not available and the calibrated spring arrangement was regarded as unsatisfactory due to difficulties in obtaining a rapid and accurate temperature control of the dehydrations. Pressure measurements, using small samples of the hydrates, overcame this difficulty but were subject to error on account of the non-perfect behaviour of water vapour. A standard procedure was adopted therefore so that this error was kept to a minimum. 10-15 mgm. quantities were weighed into the detachable trap (1) which was attached to the apparatus and evacuated as before. T_4 was then closed (1) raised quickly to the required temperature with a suitable water bath and (2) surrounded with a cardice/acetone mixture. After a suitable time interval T_6 was closed, the freezing mixture removed from (2) and the water vapour expanded into the measuring volume; as before the initial pressure of the vapour was recorded. The vapour was then pumped off through T_4, T_4 closed, T_6 opened and the carbon dioxide/acetone mixture replaced round (2).

During the period when T_6 was closed (2-3 minutes) a certain amount of water vapour was produced. Allowance was made for this on a time basis by noting the pressure developed on opening T_6 and making an estimation of the time required for this.

However, the pressure developed during this period was limited to the dissociation pressure of the hydrate which, since the volume of (1) was small (4 mls.), represented a small amount of water vapour so that the correction was always small. Soon after the start of the dehydration, the rate fell off such that the correction rapidly became negligible.

SECTION 6: FERRIC OXALATE PREPARATIONS AND DECOMPOSITION PRODUCTS

Attempts to recrystallise the ferric oxalate from water were unsuccessful in that no single crystals were obtained, but the solution finally evaporated to give the same glassy material as was obtained in the preparation of the thin films. Since a weighed quantity of the oxalate powder gave, on solution in water and subsequent evaporation, the same weight of the glassy material, it would appear that they are different forms of ferric oxalate. To investigate this and identify the solid decomposition products, infra red spectra were taken of the two substances, their decomposition products (both photochemical and thermal), ferrous oxalate, sodium oxalate, potassium ferrioxalate and oxalic acid. The results are listed below, the wavenumbers are given in $cm.^{-1}$.

Powdered $Fe_2(C_2O_4)_3.5H_2O$	:	3600, 1740, 1700-1600, 1350, 1270, 820, 755.
Decomposed (photochemically):		3600, 1740, 1700-1600, 1370, 1350, 1270, 810, 750, 710.
Decomposed (thermally)	:	2400, 1700-1600, 1320, 920, 800, 730.
Recrystallised material	:	1725-1575, 1320, 1270, 920, 800, 730.
Decomposed (photochemically):		2400, 1630, 1320, 920, 800, 730.
Decomposed (thermally)	:	2400, 1630, 1320, 920, 790, 730.
Ferrous oxalate	:	1700-1550, 1365, 1320, 920, 820, 770, 720.
Potassium triferrioxalate	:	1715, 1680, 1265, 1250, 890, 800, 775.
Sodium oxalate	:	1890, 1650, 1420, 1340, 1325, 770, 720.
Oxalic acid	:	1700-1600, 1250, 1130, 715.

From a consideration of these results it is reasonable to assume that the powder and the recrystallised material (the latter form of ferric oxalate will be referred to as the recrystallised form throughout this work) are two different physical forms of ferric oxalate, their differences probably being associated with their mode of hydration. Also from the results of the infra red spectra the material produced from both the photochemical and the thermal decomposition are the same, i.e. ferrous oxalate with a certain amount of undecomposed ferric oxalate. The peak at 2400 $cm.^{-1}$, particularly strong with the decomposition product from the re-crystallised sample, suggests the presence of carbon dioxide.

Although X-ray powder photographs of both ferrous and ferric oxalate have been reported (46), the material used in this work showed on X-ray examination little degree of crystallinity, certainly insufficient for identification or comparison. However, the few lines obtained in the photographs did agree with those quoted in (46). Also both forms of the oxalate under a microscope showed anisotropic colours. Therefore it would appear that both forms of ferric oxalate used in this work did have at least some degree of crystallinity.

As described the solid product from both types of decomposition was shown to be ferrous oxalate. In the gaseous phase, two products were obtained which were confirmed as carbon dioxide and water in the following way. After decomposition the gaseous products were trapped in trap (2) (see fig. 4). A solution of sodium carbonate in distilled water was prepared and phenolphthalein added to turn

the solution pink. A drop of this solution was put in the trap (1), which was attached to the apparatus as shown in fig. 4, the solution frozen and the trap evacuated. On warming the solution was still pink, it was then refrozen and the volatile products in trap (2) allowed to distil into it. On warming the pink solution became colourless due to the formation of the bicarbonate by the carbon dioxide.

The second gas was produced in the thermal decomposition and to an almost negligible extent in the photochemical decomposition. By the similarity of its vapour pressure curve with that of water, its easy condensation and rapid absorption by phosphorus pentoxide, it was concluded that it was water. This production of water is explained by the dehydration of the ferric oxalate. No other gases could be detected in the products from the decomposition, and thus at liquid oxygen temperature zero pressure was recorded.

SECTION 7: QUANTITATIVE ANALYSIS OF PRODUCTS

The molar quantities of carbon dioxide produced in the reactions were calculated from the pressure of the gas and the physical constants of the system in use.

To estimate the quantities of ferrous oxalate formed and ferric oxalate remaining the decomposed sample was dissolved in 0.8 N sulphuric acid and made up to a standard volume (50 mls.) with this acid. The absorption of this at 3040 Å was measured on a S.P. 500 spectrometer and from the extinction coefficients (47) quoted below the concentration of ferric iron obtained.

Temp. in °C.	Extinction Coeff. (e)
17°C.	2104
18°C.	2119
19°C.	2135
20°C.	2165
22°C.	2181
23°C.	2197

In the conditions used the iron is not present as the simple ferric ion but almost completely as the $Fe(C_2O_4)^+$ ion (48). However, by measuring the absorption of ferric sulphate solutions in 0.8 N sulphuric acid at 3040 Å and then noting the difference in absorption on the addition of oxalate ions (in the form of potassium oxalate) corresponding to various proportions of ferric and ferrous oxalate, it could be seen that the absorption increased by about 4% and thus due allowance could be made.

The above gave the quantity of ferric iron remaining; the ferrous iron content was obtained by measuring the absorption of ferrous-o-phenanthroline in a solution of pH = 6, at 5100 Å (49,50). The solution for this determination was made up as follows: 2 ml. of the original solution, i.e. in 0.8 N sulphuric acid, were pipetted into a 25 ml. standard flask, 20 ml. of 5 N sodium acetate, 0.8 ml. of 5 N acetic acid and 1 ml. of 0.2% 1:10 o-phenanthroline monohydrate added and the solution made up with distilled water. The calibration results are shown below and the graph in fig. 6.

Concentration of ferrous iron μ moles/25 ml.	$\log \frac{I_o}{I}$
2.66	1.137
2.00	0.854
1.33	0.567
0.66	0.282

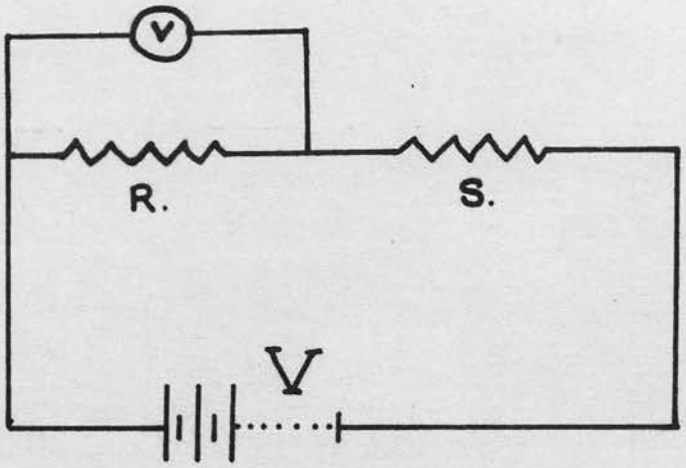

Fig. 7.

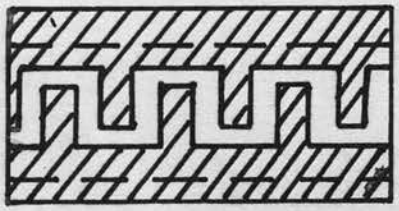

Uncovered silica glass.
Silica glass covered with platinum.
Boundaries of film.

Fig. 8.

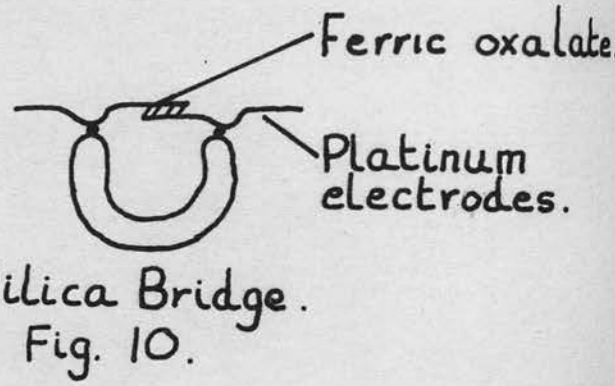

Silica Bridge.
Fig. 10.

Fig. 9.

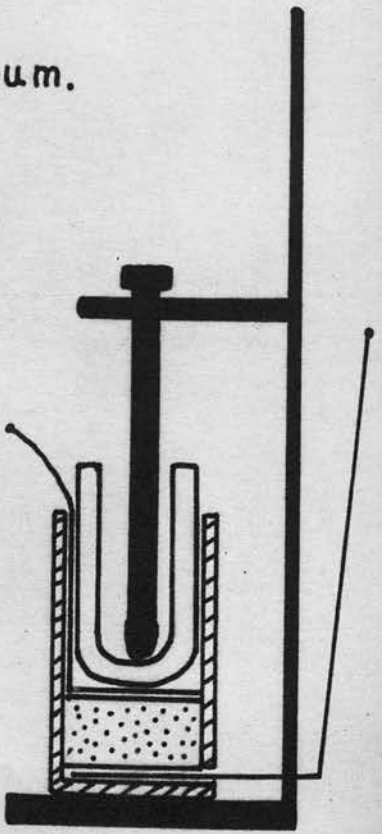

SECTION 8: CONDUCTIVITY MEASUREMENTS

The circuit for the measurement of the electrical conductivity is shown opposite fig. 7. S is the oxalate sample under examination, R a known resistance (10^6, 10^8 or 10^{10} ohms, resistance unit Model 33 B), v the Vibron electrometer (E.I.L. Vibron electrometer) measuring the potential drop across R, and V the potential applied across R and S. This consists of an Ever Ready battery giving voltages from 24–120 volts. If v is the drop across R in millivolts then

$$S = \frac{VR \times 10^3}{v} \text{ ohms.}$$

Three arrangements of the oxalate in the cell were examined. Firstly as a film on silica glass between two platinum contacts (fig. 8), secondly as a compressed pellet screwed down between two platinum electrodes (fig. 9) and finally as a "blob" between two platinum wires on a silica bridge (fig. 10).

To facilitate as far as possible contact between the platinum electrodes by the oxalate, the Johnson Matthey liquid bright platinum G was coated on to a clean piece of silica and the film, deposited from aqueous solution, arranged to cover it as shown (fig. 8). With this system, despite the precautions taken, contact was difficult to obtain. On illumination the film was very liable to split off from the silica glass, thus again breaking the contact.

In the second case, the sample was compressed into a cylindrical pellet of 2.3 mm. length and 6.5 mm. diameter by means of pellet press and vice giving a pressure of 3 tons/in.^{2}. This high compression

avoids any spurious results due to bad contact between individual fragments. The cellholder is shown in fig. 9, by means of the screw the pellet makes good contact with the two platinum electrodes. This arrangement is of great value in obtaining absolute values for the conductivity, but it does not lend itself to photoconductance measurements as only a small fraction of the pellet is illuminated. Also in the case of ferric oxalate uncertainties about the state of hydration of the pellet make the conductivity measurements unreliable.

Thus the third arrangement was developed, with this a paste of the oxalate in distilled water was made up and a little put between the two platinum wires which were in turn held by picene wax to the silica bridge (fig. 10). This was then allowed to dry.

In each of these arrangements the platinum leads attached to the cell were taken out of the vacuum system by means of soda glass seals. Externally the platinum wires were soldered to leads from the high resistance measuring unit. The cell containing the oxalate was shielded against static potential, the shielding being soldered to the screen of the high potential lead from the resistance measuring unit. The high potential lead was of non-microphonic co-axial cable. The output from the vibron electrometer was fed to a recording galvanometer which plotted the potential drop across the standard resistance.

The system was evacuated at 10^{-5} mm. for 48 hours before measurements were made. For illumination a 125 watt, 230 volt Osira lamp was used in conjunction with a focussing device and Chance glass filters.

RESULTS

1. DEHYDRATION EXPERIMENTS

(1) Extent of Dehydration of Ferric and Ferrous Oxalate Hydrates

The extent of dehydration of both forms of ferric oxalate pentahydrate, prepared as described previously, was investigated at room temperature by the two methods described on p. 35. The results of the weight loss experiments are shown below. Column 2 in the table shows the calculated weight of one molecule of water on the basis of the formula $Fe_2(C_2O_4)_3.5H_2O$.

Table 1

Wt. of sample mg.	Wt. of 1 molecule of water mg.	Wt. lost mg.	No. of mols.	Form of the oxalate
99.8	3.8	7.3	1.9	Powder
99.7	3.8	8.0	2.1	
104.3	4.0	12.1	3.0	Recrystallised
105.2	4.1	12.5	3.1	

If the powder form of the oxalate, after dehydration, was allowed to stand in ordinary air the weight returned to its original value. The recrystallised form also returned to its original value, but absorbed a further two-three molecules of water thereafter, i.e. the final state was given by

$$Fe_2(C_2O_4)_3.7\text{-}8\ H_2O$$

The results of measurements by the vapour pressure method are shown below; column 2 in this case shows the calculated quantity in μ moles of one molecule of water on the basis of the formula $Fe_2(C_2O_4)_35H_2O$. One experiment with ferrous oxalate dihydrate (A.R.) was included for comparison ($FeC_2O_4.2H_2O$).

Volume of reaction space = 101.2 ml.
Gauge sensitivity = 0.0608 mm./div.

Table 2

Wt.of sample mg.	μ moles/molecule of H_2O	Press.of H_2O divs.	μ moles of H_2O	No.of molecules	Form of the oxalate
12.4	26.6	169	56	2.1	Powder
31.7	68.0	407	135	2.0	
17.5	37.5	313	104	2.8	Recrystallised
34.4	19.1	31	10.3	0.1	Ferrous

From these results it was concluded that the powder form of the oxalate loses two molecules and the recrystallised form three molecules of water on evacuation at room temperature. No significant quantity of water was obtained from ferrous oxalate under comparable conditions.

The next experiment continued from those above by raising the temperature of the oxalate (dihydrate or trihydrate) until decomposition was complete, to determine any connection between the amounts of water produced and the extent of oxalate decomposition. The results of samples of both forms of ferric oxalate, treated as described are shown below.

Weight of the powder in the form $Fe_2(C_2O_4)_3.5H_2O$ = 31.7 mg.

Therefore 1 molecule of CO_2 or H_2O = 68 μ moles.

Table 3

Extent of heating of trihydrate	Press.of CO_2 divs.	μ moles of CO_2	Press.of H_2O divs.	μ moles of H_2O	H_2O/CO_2
103°C.for 5 hr.	96	32	238	79	2.5
110°C. 5 hr.	129	43	208	69	1.6
110°C. 75 hr.	136	45	59	20	0.4
125°C. 3 hr.	10	3.3	24.5	8.1	2.4
140°C. 3 hr.	27	9.0	66.5	22	2.5
Total gas produced	398	133	596	199	1.5

Weight of the recrystallised sample in the form $Fe_2(C_2O_4)_3.5H_2O$ = 17.5 mg.

Therefore 1 molecule of CO_2 or H_2O = 37.5 μ moles.

Table 4

Extent of heating of dihydrate	Press. of CO_2 divs.	μ moles of CO_2	Press.of H_2O divs.	μ moles of H_2O
103°C. for 21 hr.	101	34	164	54
125°C. 10 hr.	57	19	28	9
135°C. 12 hr.	30	10	15	5
Total gas produced	188	63	207	68

A sample of ferrous oxalate dihydrate was examined under similar conditions.

Weight of ferrous oxalate dihydrate = 34.4 mg.

Therefore 1 molecule of H_2O = 191 μ moles.

Table 5

Extent of heating	Press. of CO_2 divs.	μmoles of CO_2	Press. of H_2O divs.	μmoles of H_2O
115°C. for 22 hr.	11.0	3.7	1102	365
115°C. 6 hr.	5.0	1.7	11	4
Total gas produced	16.0	5.4	1113	369

From the above tables it can be seen that, with both the recrystallised and powder form of ferric oxalate pentahydrate, decomposition was virtually complete in that the final products were anhydrous ferrous oxalate, water and carbon dioxide. Ferrous oxalate dihydrate itself lost no water at room temperature but was completely dehydrated at 115°C.

There appears to be no relation between the rate of dehydration and the rate of decomposition of the oxalate. If the water was produced as the oxalate decomposed, it would be expected that the molar of quantities of water to carbon dioxide obtained would have been in the ratio 3:2 for the powder form and 1:1 for the recrystallised, throughout the course of the decomposition. However, the two reactions appear to be independent although the final states of the decomposition are given by the equations.

$$Fe_2(C_2O_4)_3.5H_2O\ (\text{powder}) \xrightarrow{(-2H_2O)} Fe_2(C_2O_4)_3.3H_2O \longrightarrow 2FeC_2O_4 + 2CO_2 + 3H_2O$$

$$Fe_2(C_2O_4)_3.5H_2O\ (\text{recrystallised}) \xrightarrow{(-3H_2O)} Fe_2(C_2O_4)_3.2H_2O \longrightarrow 2FeC_2O_4 + 2CO_2 + 2H_2O$$

(2) Dissociation Pressure and Rate of Dehydration

The relation between the heat of dissociation and the activation energy for the rate of dehydration of both forms of ferric oxalate pentahydrate was examined. For the powder form this involved the change from the pentahydrate to the trihydrate whereas with the recrystallised the change from the pentahydrate to the dihydrate was involved. In both cases the experiments were conducted below 50°C. for above this temperature further dehydration appeared to be taking place.

The dissociation pressure of both forms of the oxalate hydrate was measured as described on p. 37 and the results are shown below.

Table 6

Powder form. Gauge sensitivity = 0.0263 mm./div.

Temperature °A	$1/T \times 10^3$	Press. divs.	Press (P_m.) mm.	$\log_{10} P_m$. + 1.0
298.0	3.356	6.1	0.160	0.204
305.5	3.274	8.5	0.223	0.348
310.0	3.226	11.2	0.294	0.468
315.8	3.167	13.7	0.360	0.556
321.2	3.113	17.8	0.468	0.670

The plot of $\log_{10} P_m$. against $1/T$ (fig. 11b) is a straight line of slope 1.90×10^3.

Therefore the heat of dissociation = $1.90 \times 10^3 \times 2.303 \times 1.98$ K.cals/mole

= 8.7 K.cals./mole.

Fig. 11. Variation of the dissociation pressure of (a) the recrystallised form, (b) the powder form of $Fe(C_2O_4)_3\,5H_2O$ with temperature.

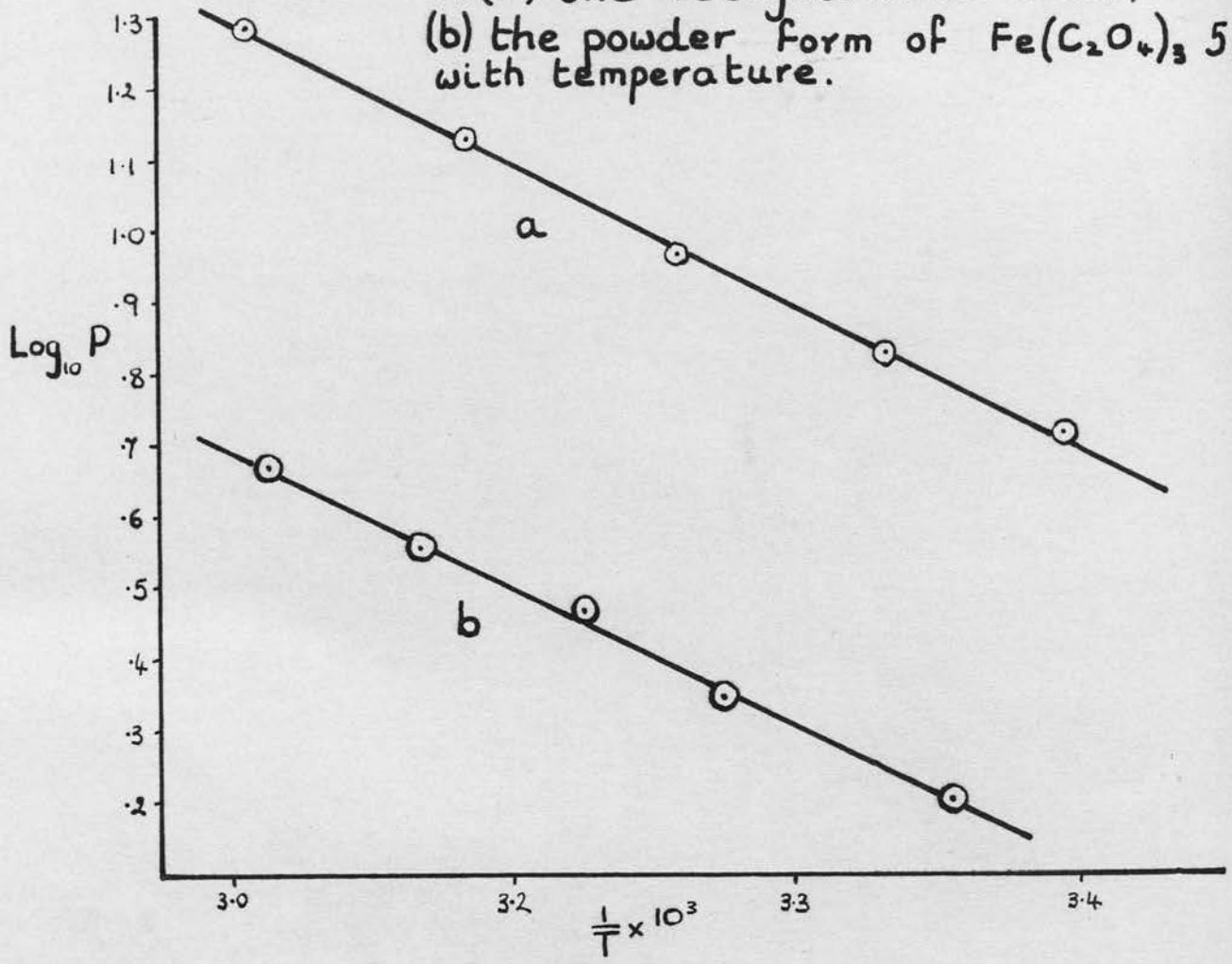

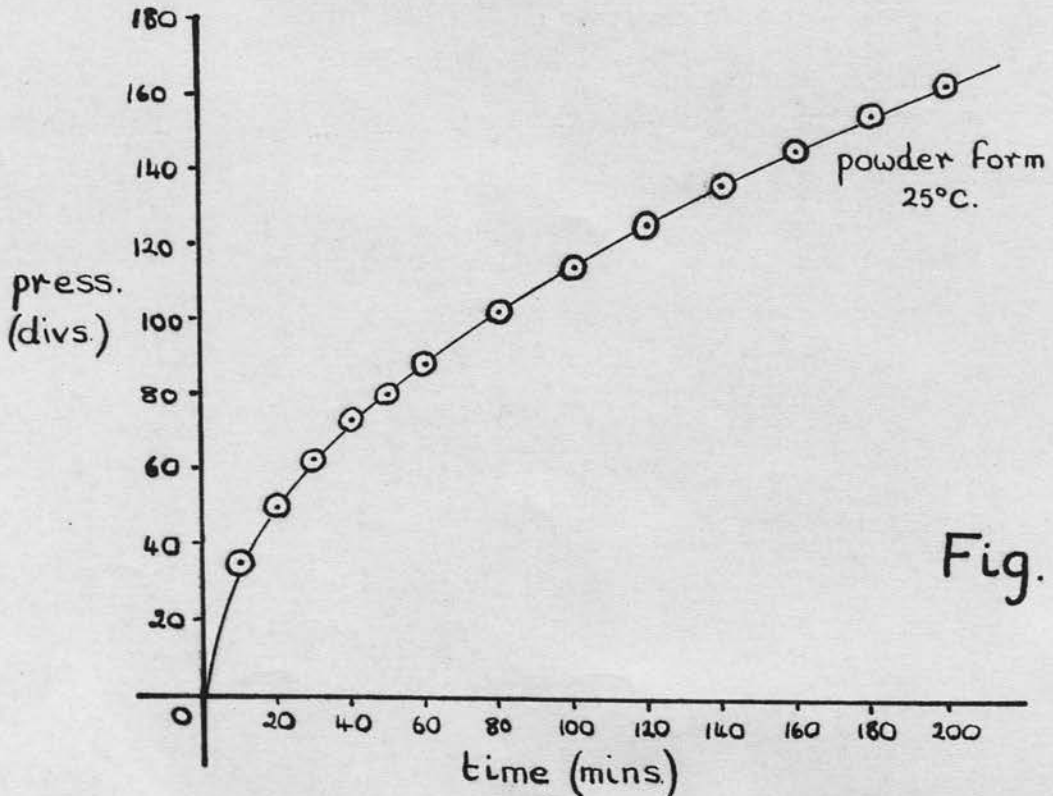

Fig. 12.

Table 7

Recrystallised form. Gauge sensitivity = 0.0608 mm./div.

Temperature °A	$1/T \times 10^3$	Press divs.	(Press (P_m.) mm.	Log_{10} P_m. + 1.0
294.5	3.395	8.5	0.516	0.713
300.0	3.333	11.0	0.669	0.825
306.4	3.264	15.2	0.924	0.966
314.1	3.184	22.1	1.344	1.128
322,0	3.106	31.8	1.934	1.286

From the plot of log_{10} P_m against $1/T$ (fig. 11a) the slope of the line is 2.0×10^3.

Therefore the heat of dissociation = $2.0 \times 10^3 \times 2.303 \times 1.98$ K cals./mole.

= 9.1 K cals./mole.

A maximum percentage error of 3% was calculated from the slopes of the graphs.

Therefore the heat of dissociation of the powder form = 8.7 ± 0.3 K cals./mole.

and the heat of dissociation of the recrystallised form = 9.1 ± 0.3 K cals./mole.

Thus from these results the heats of dissociation for the two forms are approximately the same although the dissociation pressure of the recrystallised form is about four times that of the powder at the same temperature.

Rate of Dehydration

The rate of dehydration was investigated as described on p. 38 utilising 15 mg. samples for the powder form of the oxalate and 10 mg. samples for the recrystallised form. Typical examplesof the pressure-time curves obtained for these samples are illustrated in figs. 12 (powder) and 15 (recrystallised).

Fig. 14.

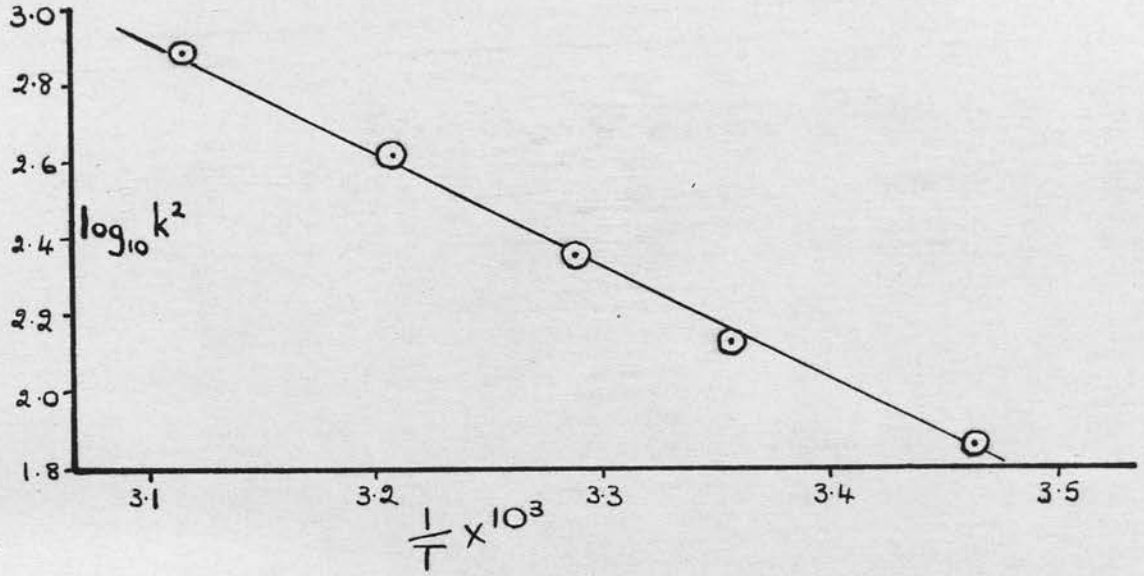
3·0
2·8
2·6
2·4
2·2
2·0
1·8
$\log_{10} k^2$
3·1
3·2
3·3
3·4
3·5
$\frac{1}{T} \times 10^3$

Fig. 13.

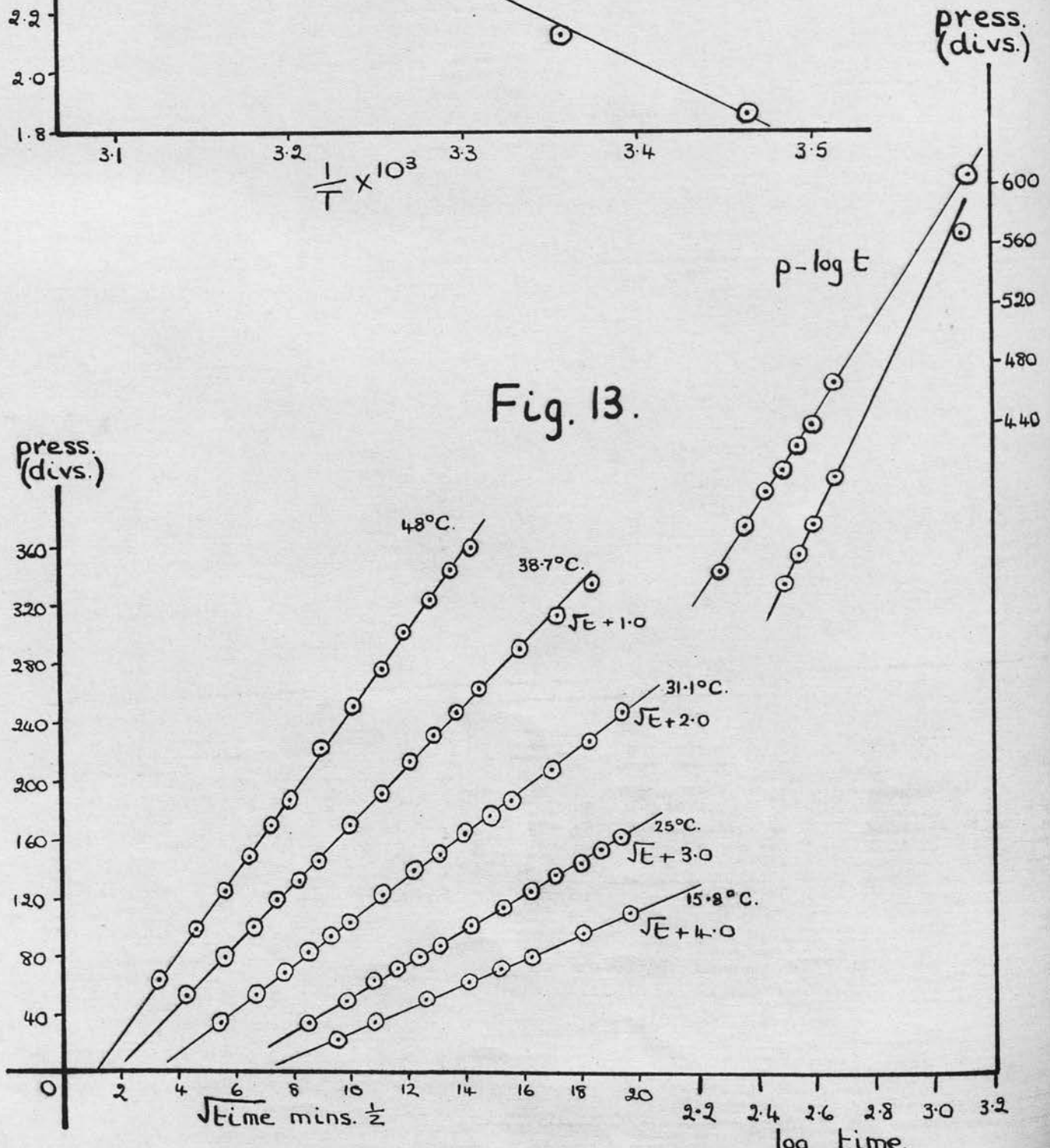
press. (divs.)
600
560
520
480
440
p - log t
press. (divs.)
360
320
280
240
200
160
120
80
40
0
48°C.
38·7°C.
√t + 1·0
31·1°C.
√t + 2·0
25°C.
√t + 3·0
15·8°C.
√t + 4·0
2
4
6
8
10
12
14
16
18
20
√time mins. ½
2·2
2·4
2·6
2·8
3·0
3·2
log time

For the powder form of the oxalate the relationship $p = k\sqrt{t} + c$ (fig. 13) was found to fit the experimental results where p is the total pressure of water evolved in time t and k and c are constants. This relationship described the experimental results up to 50% dehydration (i.e. 50% dehydration from the pentahydrate to the trihydrate), thereafter the results were expressed by the equation $\alpha p = \ln.t + k$ (fig. 13) where p and t have the same meaning as before and α and k are constants. The results are shown below.

Volume of Reaction space = 67.5 ml.
Gauge sensitivity = 0.0263 mm./div.

Table 8.

Temperature °C.			48.0	38.7	33.1	25.0	15.8
Time min.	$\sqrt{\text{Time}}$	Log_{10} time	Press. divs.	Press. divs.	Press. divs.	Press. divs.	Press. divs.
0	0		0	0	0	0	
10	3.16		60	50	32	35	23.5
20	4.47		95	76	51	50	35.0
30	5.48		121	97	66	63	
40	6.33		145	115	80	73	51.0
50	7.07		167	128	91	80	
60	7.75		185	142	101	88	63
80	8.94		220	167	120	102	72
100	10.00		248	189	135	114	80
120	10.95		274	211	148	125	
140	11.83		299	229	162	136	96
160	12.65		321	244	174	145	
180	13.42	2.255	341	260	185	154	110
200	14.1	2.301	358	274		162	
220	14.8	2.342	372	287	206		
260	16.1	2.415	395	310	225		
300	17.3	2.477	414	332	244		
340	18.4	2.532	425	351			
380		2.580	440	373			
420		2.623		389			
460		2.663	468	404			
500		2.699		418			
1250		3.097		568			
1320		3.121	607				

To obtain an activation energy for the process the value of k^2 (where k is the slope of the $p-\sqrt{t}$ line) was used since it is proportional to the linear decay constant or to the specific reaction rate.

$$p^2 = k^2t + c$$

$$\text{then } \frac{dp}{dt} = \frac{k^2}{2p}$$

The values of k were obtained from the $p-\sqrt{t}$ plots (fig. 13).

Table 9

Temperature °A	$1/T \times 10^3$	k	k^2	$\text{Log}_{10} k^2$	α 10^3
288.8	3.462	8.4	70.6	1.849	
298.0	3.356	11.5	132	2.121	
304.1	3.288	15.0	225	2.352	
311.7	3.208	20.2	408	2.611	5.9
321.0	3.115	27.7	767	2.885	8.0

From the plot of $\log_{10} k^2$ against 1/T (fig. 14) the slope of the line is 3.0 $\times 10^3$, with a maximum percentage error of 5%.

Thus the activation energy of dehydration = 3.0 x 2.303 x 1.98
± 5% K cals./mole.
= 13.7 ± 0.7 K cals./mole.

Further information on the second stage of the dehydration, i.e. where the equation $\alpha p = \log t$ applies, was difficult to obtain since at higher temperatures dehydration of the trihydrate took place and at lower temperatures the reaction was too slow for convenient measurement.

As shown in fig. 15 the $p-\sqrt{t}$ relationship did not give a straight line plot with the pressure time data obtained for the dehydration of the recrystallised form of the oxalate. However,

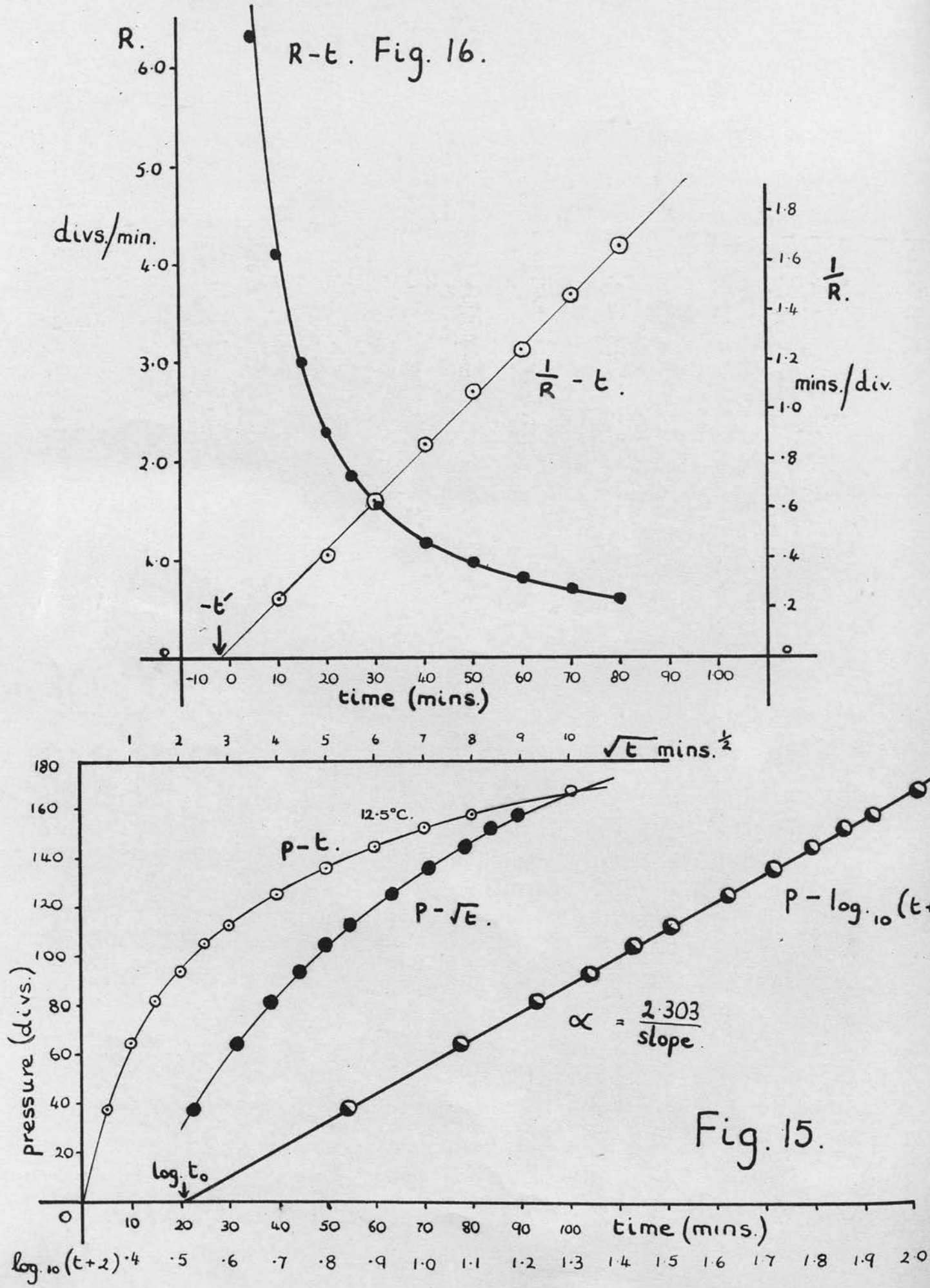
R.
R-t. Fig. 16.
divs./min.
6·0
5·0
4·0
3·0
2·0
1·0
0
1·8
1·6
1·4
1·2
1·0
·8
·6
·4
·2
0
1/R.
mins./div.
1/R - t.
-t'
-10 0 10 20 30 40 50 60 70 80 90 100
time (mins.)
1 2 3 4 5 6 7 8 9 10
√t mins.½
180
160
140
120
100
80
60
40
20
0
12·5°C.
p-t.
P-√t.
P - log.10 (t+2).
pressure (divs.)
log. t0
∝ = 2·303 / slope.
10 20 30 40 50 60 70 80 90 100
time (mins.)
log.10 (t+2) ·4 ·5 ·6 ·7 ·8 ·9 1·0 1·1 1·2 1·3 1·4 1·5 1·6 1·7 1·8 1·9 2·0

Fig. 15.

by consideration of the rates of dehydration a linear relation between $1/R$ and t, where R is the rate of dehydration at time t, was found to fit the experimental results (fig. 16). The values of the rates were found in the following way. Pressure time curves for the dehydration were drawn (fig. 15) and from these measurements of the rate were made. These values were then plotted against time and a smooth curve drawn through the points; from this curve the corrected values of the rate were obtained.

Now $1/R = \alpha(t + t')$ where α and t' are constants

i.e. $$\frac{dp}{dt} = \frac{1}{\alpha(t + t')}$$

Therefore $\alpha p = \ln(t + t') + C$, where C is a constant

by putting $t + t' = t_o$ at $p = 0$, i.e. $C = -\ln t_o$

where t_o is a constant

then $\alpha p = \ln.(t + t') - \ln.t_o$

Thus by using the value of t' obtained from the $1/R - t$ plots, the values of $\log_{10}(t+t')$ were plotted against p to give α and t_o as shown in fig. 15. The dehydrations were conducted between 12.5°C. and 41°C. and the pressure-time data plotted as described above. The results are shown in Table 10 and in graphical form in fig. 17.

Volume of Reaction space = 134.1 ml.
Gauge sensitivity = 0.0263 mm./div.
Temperature = 12.5°C.

Table 10

Press. divs.	Time min.	$\sqrt{\text{time}}$	Rate divs./ min.	Corr. Rate divs./min.	1/R min./ div.	ln.(t+2)
0	0					
38.5	5	2.24	6.3			0.845
65	10	3.16	4.1	4.1	0.24	
82	15	3.87	3.0			1.079
94	20	4.47	2.3	2.35	0.426	1.342
105.5	25	5.00	1.85			1.431
113	30	5.48	1.55	1.58	0.633	1.505
125.5	40	6.33	1.15	1.15	0.870	1.623
136.5	50	7.07	0.98	0.93	1.08	1.716
145	60	7.75	0.80	0.80	1.25	1.792
153	70	8.37	0.68	0.68	1.47	1.857
158.5	80	8.94	0.60	0.60	1.67	1.914
168	100	10.00				

For the other dehydrations, which were conducted at temperatures higher than 12.5°C., it was found that $t' = 0$, and thus α and t_o were obtained by plotting p against $\log_{10}.t$ (fig. 17).

These equations applied to the experimental results up to approximately 55% dehydration. Beyond this stage it was found that the same relationship between pressure and time existed but with different values of α and t' and thus t_o. For dehydrations at 41°C. and 33.1°C. the t' values were found to be -15 minutes and -10 minutes respectively. The results are shown in Table 11.

Fig. 18.

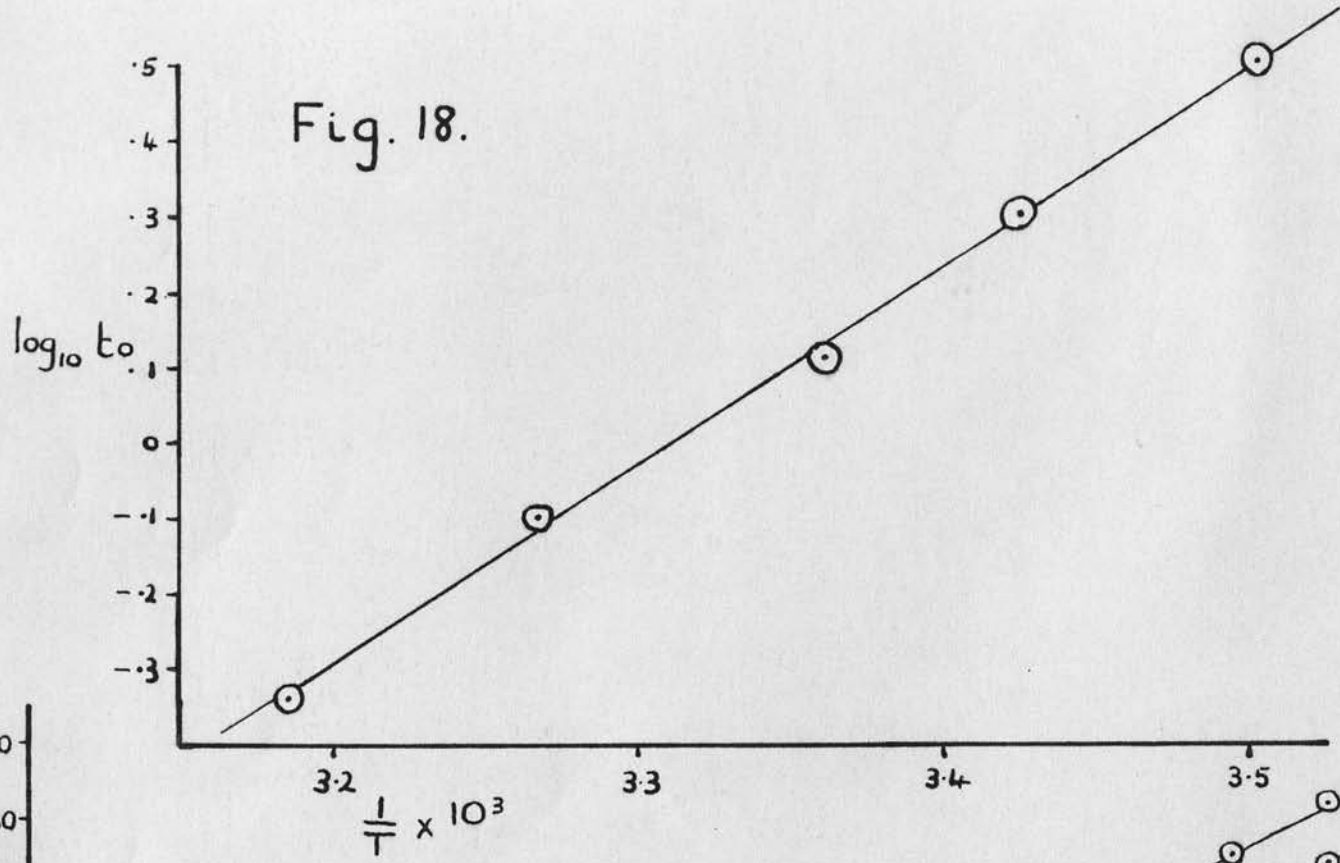
log10 to
·5
·4
·3
·2
·1
0
-·1
-·2
-·3
3·2
3·3
3·4
3·5
1/T x 10³

Fig. 17.

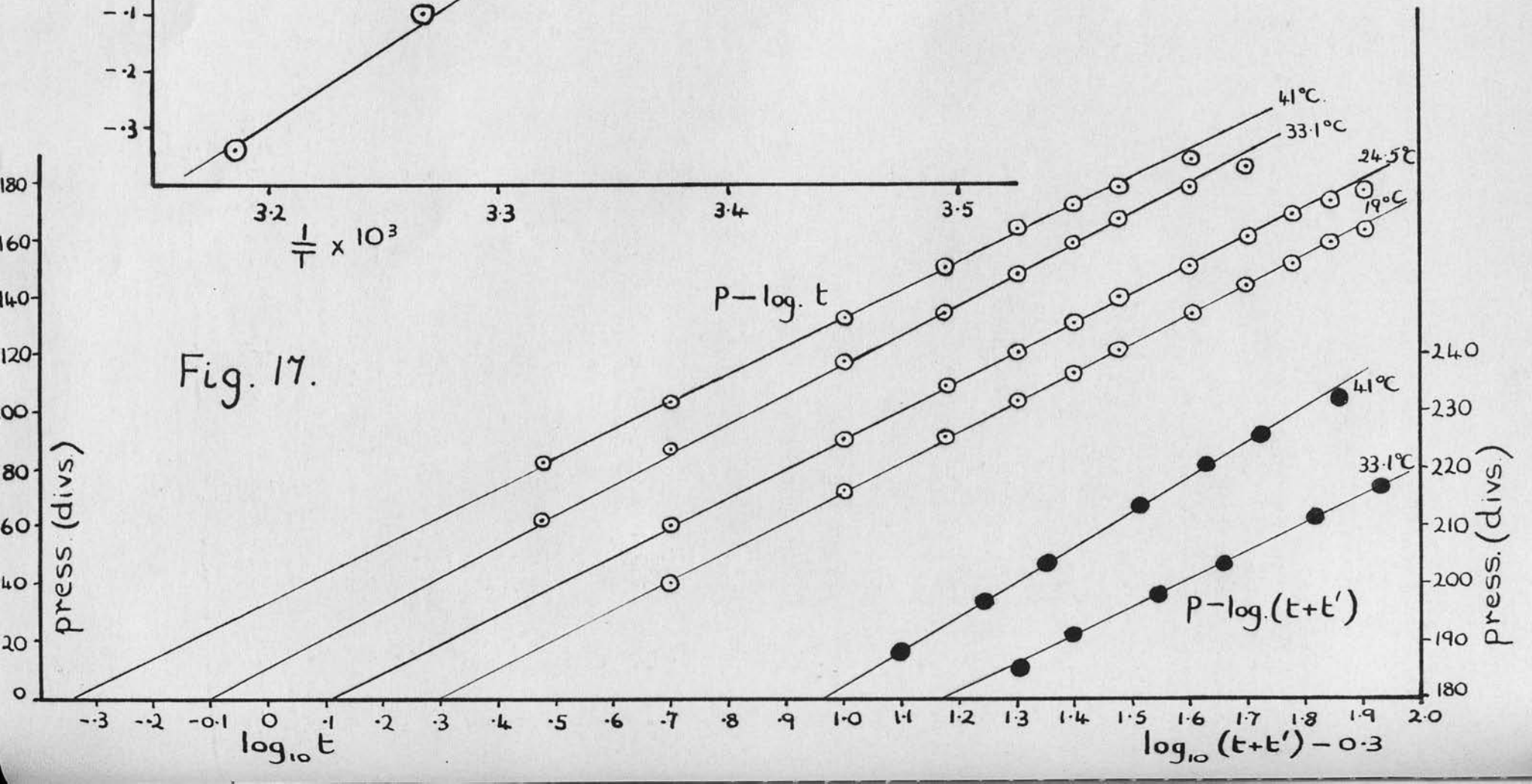
P—log. t
41°C.
33·1°C
24·5°C
19°C
press. (divs.)
0
20
40
60
80
100
120
140
160
180
-·3
-·2
-0·1
0
·1
·2
·3
·4
·5
·6
·7
·8
·9
1·0
1·1
1·2
1·3
1·4
1·5
1·6
1·7
1·8
1·9
2·0
log10 t
P—log.(t+t')
41°C
33·1°C
240
230
220
210
200
190
180
press. (divs.)
log10 (t+t') — 0·3

Table 11

Time min.	Log_{10} t	Temp. 19°C. Press. divs.	24.5°C. Press. divs.	33.1°C. Press. divs.	Log_{10} (t-10)	41°C. Press. divs.	Log_{10} (t-15)
0		0	0	0		0	
3	0.477			62.0		82.0	
5	0.699	40.5	60.5	87.0		103	
10	1.000	73.0	91.0	117.5		132.5	
15	1.176	92.0	109.5	134.5		150.5	
20	1.301	104.0	121.0	148.5		164.0	
25	1.398	114.5	131.5	159.0		172.5	
30	1.477	122.5	140.5	167.5		178.0	
40	1.602	135.0	152.0	179.0	1.477	188.5	1.398
50	1.699	145.0	162.0	185.5	1.602	197.0	1.544
60	1.778	153.0	169.5	191.0	1.699	204.0	1.653
70	1.845	160.0	174.5				
80	1.903	164.5	178.0	198.0	1.845	214	1.813
100	2.000			203.5	1.954	221	1.929
120	2.079					226.5	2.021
140	2.146			211.5	2.114		
160	2.204					233.0	2.161
180	2.255			217.0	2.230		

From the plots of log(t+t') against p it can be seen that the value of α is approximately independent of temperature, whereas t_o increases with decreasing temperature.

$$\alpha p = \ln(t+t') - \ln t_o \text{ or } t+t' = t_o e^{\alpha p}$$

Therefore $$\frac{dp}{dt} = \frac{1}{\alpha t_o} e^{-\alpha p}$$

Since α is temperature independent, then at a definite pressure,

$$\frac{dp}{dt} = \frac{k}{t_o} \quad \text{where k is a constant.}$$

i.e. the reciprocal of t_o is proportional to the specific reaction rate and thus from the plot of $\log_{10} t_o$ against 1/T an activation energy for the dehydration can be obtained in the usual way. The results are shown below and the plot in fig. 18. α_1 and α_2 in the table below refer to the values of α obtained for the first and second stage respectively of the dehydrations at 41°C. and 33.1°C.

t_o is the value obtained from the first stage of the dehydration.

Table 12

Temperature °A	$1/T \times 10^3$	$\alpha_1 \times 10^2$	$\alpha_2 \times 10^2$	$\text{Log}_{10}\ t_o$
314.0	3.185	2.33	3.78	-0.34
306.1	3.267	2.17	4.70	-0.10
297.5	3.361	2.26		+0.11
292.0	3.425	2.22		0.30
285.5	3.503	2.06		0.50

From the plot of $\log_{10} t_o$ against $1/T$ (fig. 18) the slope of the line is 2.6×10^3 with a maximum percentage error of 5%.

Thus the activation energy of dehydration = $2.6 \times 2.303 \times 1.98$ ± 5% K.cals./mole.

= 11.8 ± 0.6 K.cals./mole.

It was hoped to study the further dehydration of the oxalate hydrates and in fact an approximate value of 11 K.cals./mole was obtained for the heat of dissociation of the powder form of the trihydrate. However, the pressures were not very reproduceable. Difficulties with the residue of the initial dehydration, slowness of the pressure to reach equilibrium at lower temperatures and complications with the decomposition of the oxalate at higher temperatures made further study in this respect unsuitable.

Fig. 19.

The relation between the amounts of CO_2 produced and Fe^{++} formed during the photochemical decomposition of thin films.

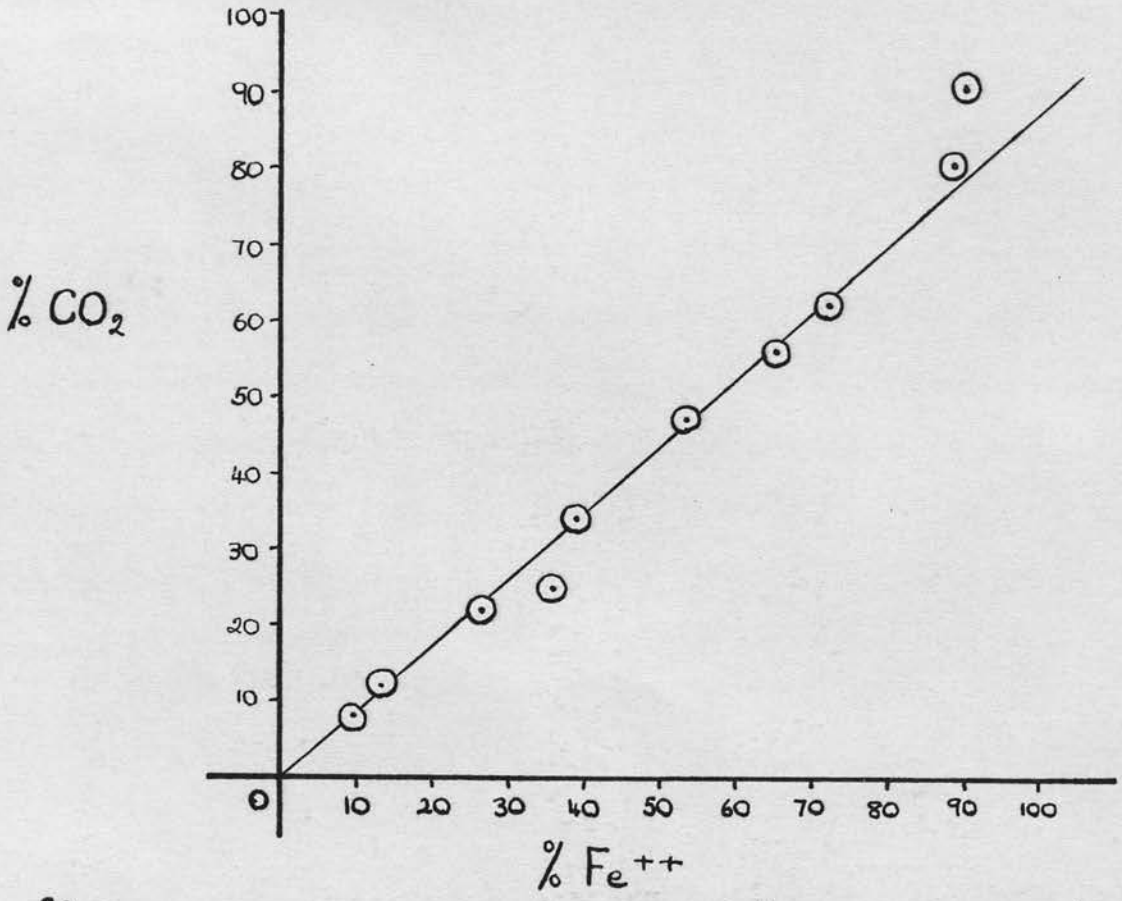

% CO_2 – percentage decomposition as given by CO_2 produced.

% Fe^{++} – percentage decomposition as given by Fe^{++} formed.

2. PHOTOCHEMICAL DECOMPOSITION

A film consisting of 100 mg. of ferrous oxalate was made up as described on p. 30. No reaction, as given by a change in colour or pressure was observed in the dark or on illumination in vacuo or in the presence of carbon dioxide.

Both types of ferric oxalate film were stable in the dark at temperatures up to 50°C., as judged by no observable pressure change over a period of two hours. On illumination of these films with light of wave length less than or equal to 5460Å immediate decomposition, as given by a pressure increase, was observed, the products of which were ferrous oxalate, carbon dioxide and water (p.40).

The table below gives the relative amounts of the products, at various stages of decompositions of the thin films. Columns 1, 2 and 3 give the values of the percentage decomposition as calculated from the pressure of carbon dioxide produced, the quantity of ferrous iron, estimated photometrically, and the quantity of ferrous iron calculated from the initial and final amounts of ferric iron respectively. Column 4 gives the quantity of water produced expressed as a percentage of the carbon dioxide produced.

Table 13

Carbon dioxide(%)	Ferrous iron(1)(%)	Ferrous iron(2)(%)	Water(%)
90	90	89	0.5
80	89	88	1.0
62	71	73	2
56	65	65	0
47	54	52	0.5
34	39	38	0
25	35	35.8	0.3
22	26	26.7	3.0
12.1	12.9	13.6	1.0
8.3	9.3	10.1	0

Fig. 20. Pressure – Time curve for photochemical decomposition of thick film.
(105 mgm. sample.)

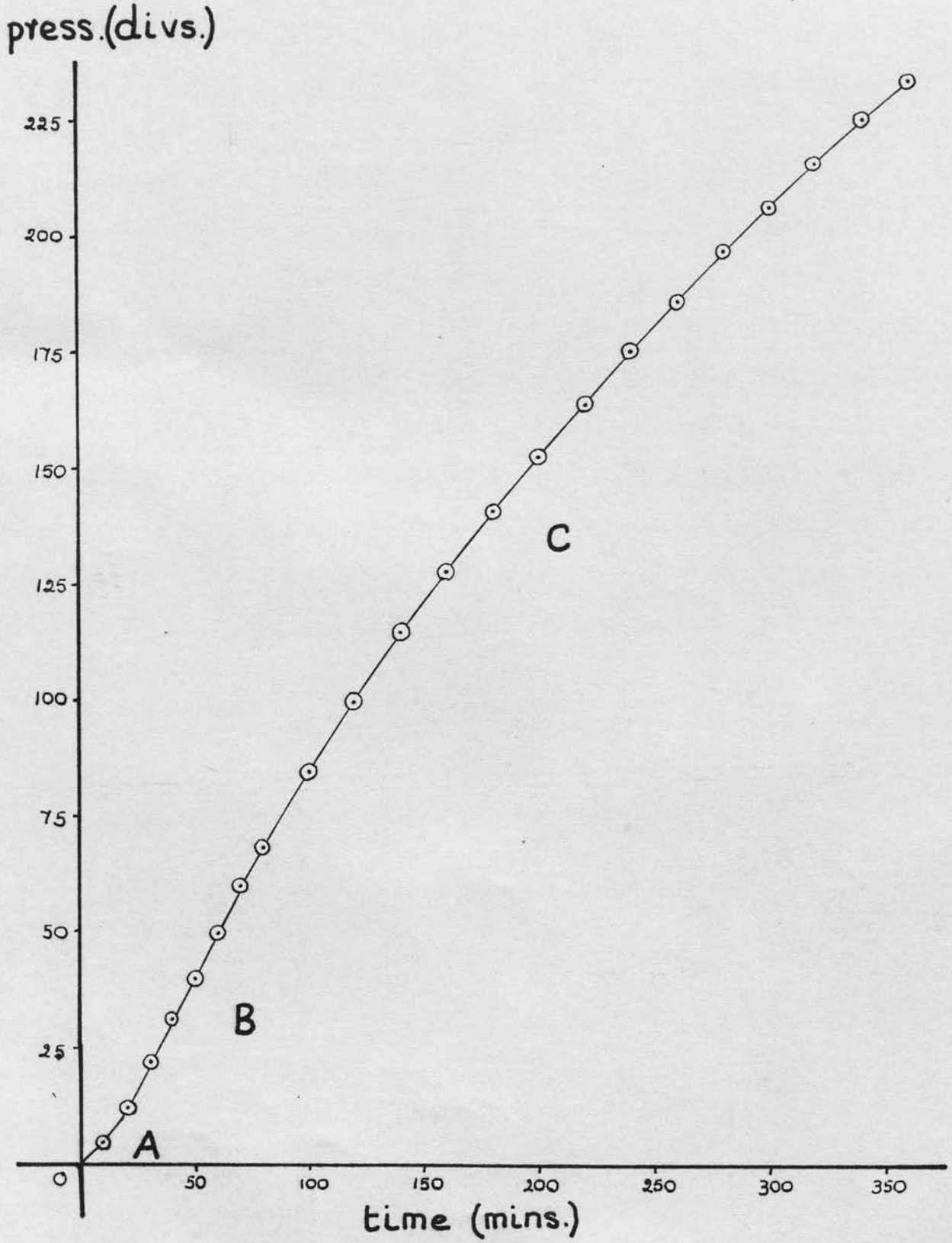

The graph of the relative amounts of carbon dioxide against ferrous iron produced fig. 19, shows that throughout the reaction the ratio CO_2/Fe^{++} is approximately 0.85, i.e. about 15% of the expected carbon dioxide is unaccounted for. This is too large to be an experimental error and was possibly caused by the occlusion of gas in the film. This was to some extent verified by the fact that on dissolving the decomposed film in dilute sulphuric acid, a small effervescence was observed. Similar results were obtained for the thick films. Thus although it is probable that in the initial stages of the reaction $\frac{dCO_2}{dt} = \frac{-dFe^{+++}}{dt}$ this does not necessarily apply as the reaction proceeds.

For both types of film very little water is produced in the gas phase during the reaction and thus it would appear that the photochemical decompositions are given by the equations below.

Recrystallised form: $Fe_2(C_2O_4)_3.2H_2O \longrightarrow 2FeC_2O_4.H_2O + 2CO_2$

Powder form: $Fe_2(C_2O_4)_3.3H_2O \longrightarrow 2FeC_2O_4.\frac{3}{2}.H_2O + 2CO_2$

Photodecomposition of 'thick' films

The general shape of the pressure-time curves obtained for the decomposition of the 'thick' films is shown in fig. 20. These curves consist of three stages: A, a short induction stage up to 0.3% decomposition; B, a constant rate stage from 0.3% up to 2% decomposition, and C, the decay stage thereafter. This stage, however, due to experimental conditions was not studied beyond

15% decomposition.

If at any ~~one~~ stage in the reaction, the illumination was discontinued, a small dark pressure increase was observed, which continued at a decreasing rate for several hours.

Utilising the constant rate stage of the decomposition, the effects of carbon dioxide, oxygen, surface area of the film, temperature and intensity of the incident light on the rate of reaction were examined. For this monochromatic light of wave length 3650 Å was used. However, with this light the duration of this stage of the reaction was short and thus to enable the rate of reaction to be accurately measured, the intensity of the light was reduced to one third by the use of appropriate neutral filters. Using 300 mg. samples of the ferric oxalate and keeping the surface area of the film constant the rate was measurable with an accuracy of ± 2% and was reproduceable to within the same limits.

Effect of Carbon Dioxide and Oxygen

This was studied by introducing 50 mm. of the gases separately into the reaction space during the decomposition. The results are shown below. Unless otherwise specified the experiments, using the constant rate stage of the reaction, were conducted under the following conditions:

Temperature of reaction space = 25.5°C.
Intensity of light = one third full intensity of light of wave length 3650 A.
Surface area of film = 26 cm^2.
Vol. of reaction space = 74.0 ml.

Fig. 22. Dependence of rate of reaction on the intensity of 3650Å Light.

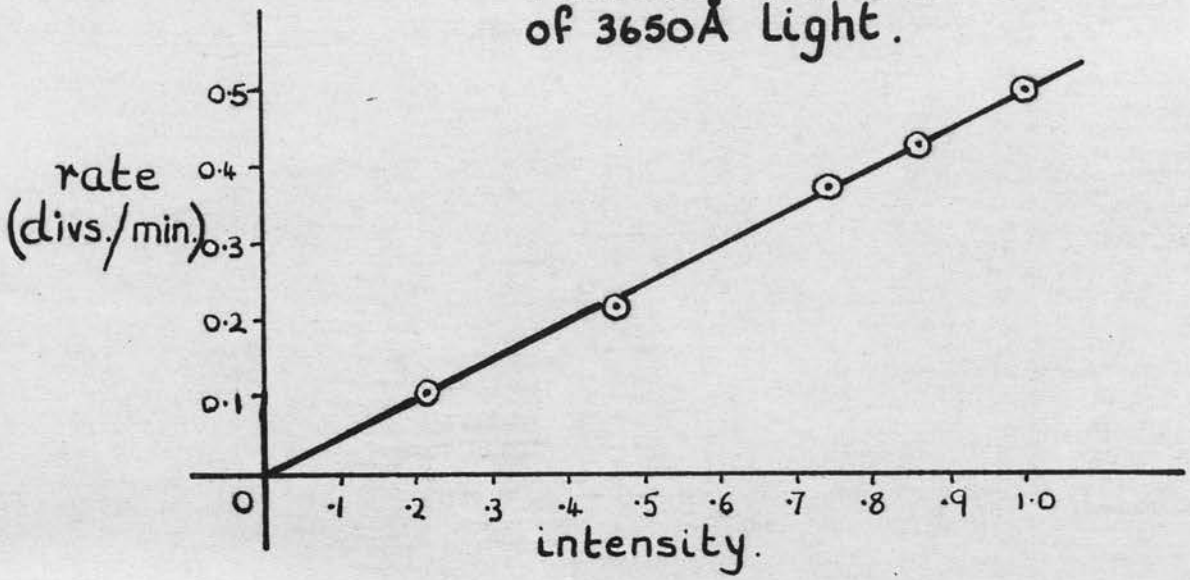

Fig. 21.

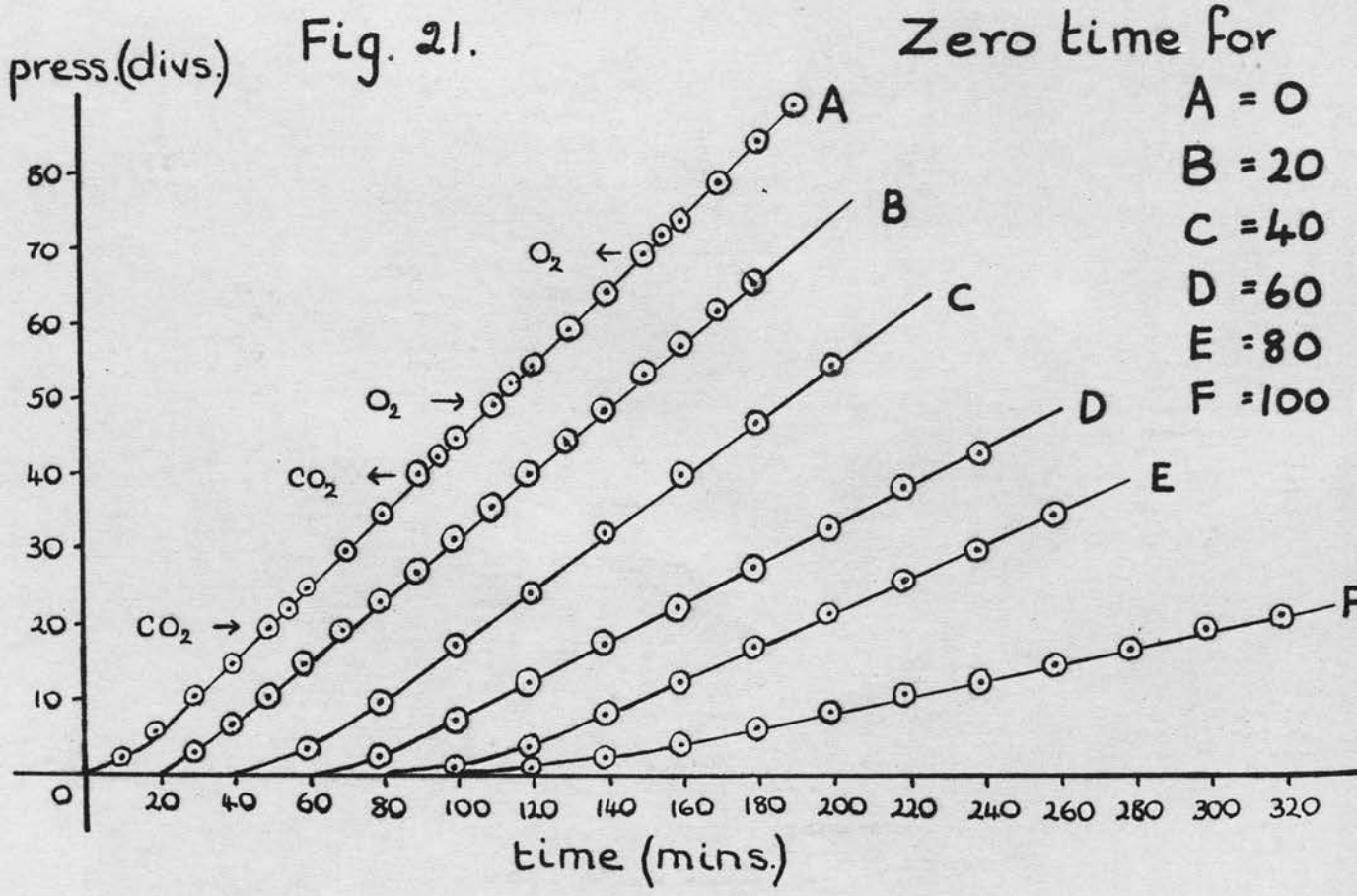

Gauge sensitivity = 0.0103 mm./div.

Table 14

Time min.	Pressure divs.	Time min.	Pressure divs.
0	0	100	44.4
10	1.9	110	49.0
20	5.5	50 mm. O_2 inserted	
30	10.2	115	52.0
40	14.4	120	54.0
50	19.5	130	59.1
50 mm. CO_2 inserted		140	64.2
55	22.1	150	69.0
60	24.8	O_2 removed	
70	29.5	155	71.7
80	34.3	160	73.5
90	40.0	170	78.5
CO_2 removed		180	84.0
95	42.3	190	88.5

From the graph fig. 21A the constant rate of decomposition was apparently unaffected by the introduction of 50 mm. oxygen or carbon dioxide.

Surface Area of Film

To investigate the effect of the surface area of the films on the rate of reaction, the decomposition was repeated using a film of surface area 13 cm^2, i.e. half that used in the previous experiments. The results are shown below.

Table 15

Time min.	Pressure divs.	Time min.	Pressure divs.
0	0	100	22.8
20	3.1	120	28.0
40	7.5	140	33.5
60	13.0	160	38.9
80	18.0	180	43.0

From the previous experiment the rate of decomposition, with a film of surface area of 26 cm^2, was 0.49 divs./min. (fig. 21A). From this experiment the rate of decomposition with a film surface area of 13 cm^2 was 0.25 divs./min. (fig. 21D). Thus for this stage of the reaction the rate is proportional to the surface area of the film.

Variation of the Incident Light Intensity

The decomposition was carried out under the normal conditions, the variations in intensity being achieved by the introduction of further neutral calibrated filters between the light source and the film. The normal value of the light intensity (i.e. one third 3650 Å light) was arbitrarily taken as 1.0 and the other intensities used in this experiment quoted as fractions of this. The results are shown in Table 16.

Table 16

Intensity	1.0	0.86	0.74	0.46	0.21
Time min.	Pressure divs.	Pressure divs.	Pressure divs.	Pressure divs.	Pressure divs.
0	0	0	0	0	0
10	2.5	2.7			
20	7.5	6.5	3.5	1.3	1.0
30	10.9	10.0			
40	16.0	14.6	9.7	3.7	2.1
50	20.8	19.0			
60	25.4	22.3	17.0	8.0	3.9
70	30.3	26.8			
80	35.6	31.1	24.1	12.3	6.0
90	40.4	35.4			
100	45.5	40.0	32.5	17.0	8.0
110	51.0	44.0			
120	55.3	48.2	40.0	21.1	10.5
130	60.5	53.0			
140	65.6	56.9	46.9	25.5	12.0
150	70.9	61.4			
160	75.4	65.3	54.3	30.0	14.5
180				34.2	16.5
200					19.0
220					20.8

The rates of decomposition, with the light intensities mentioned above, were measured from the graphs (fig. 23C and fig. 21B, C, E and F) and are shown below.

Table 17

Intensity	Rate divs./min.
1.0	0.49
0.86	0.42
0.74	0.37
0.46	0.22
0.21	0.105

From the graph (fig. 22) it can be seen that for the constant rate stage of the decomposition the rate of reaction is directly

Fig. 24. Variation of rate of reaction, with light of 3650 Å, with temperature.

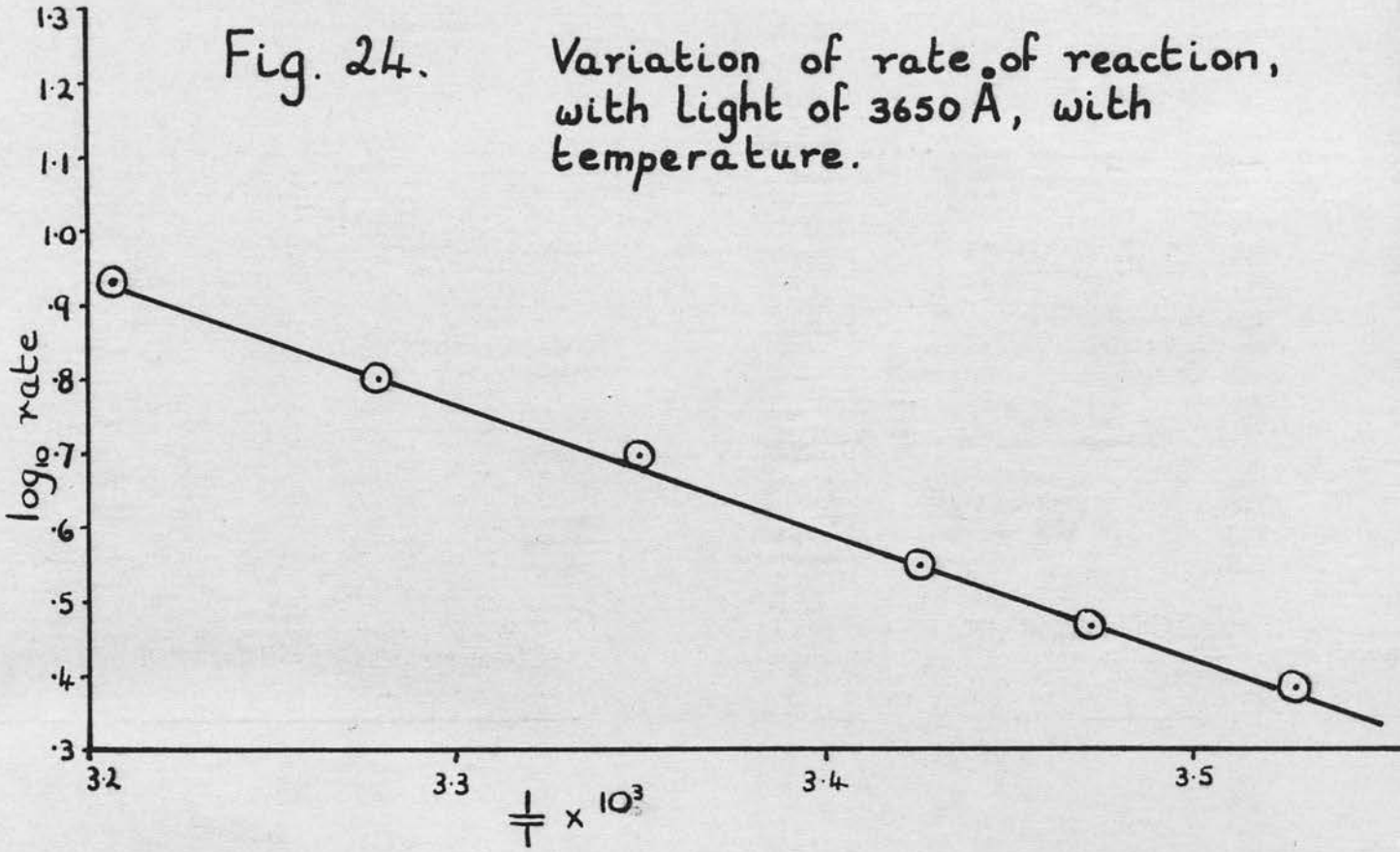

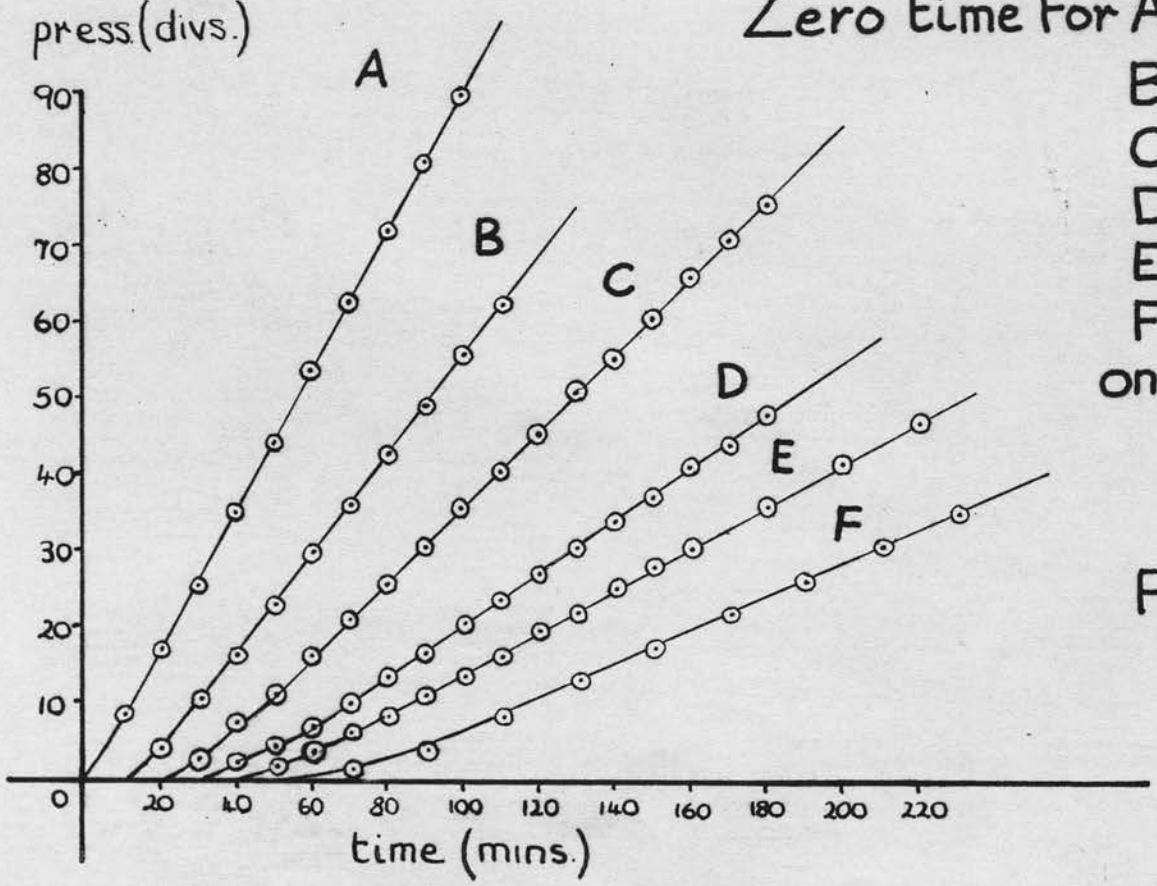

Zero time for A = 0
B = 10
C = 20
D = 30
E = 40
F = 50
on time scale

Fig. 23.

proportional to the incident light intensity.

Variation of Temperature

By adjusting the temperature of the water surrounding the reaction vessel, the decomposition was examined between 10°C. and 40°C. The results are shown below and in fig. 23.

Table 18

Temperature °C.	38.9	32.3	19.0	15.0	10.5
Time min.	Pressure divs.	Pressure divs.	Pressure divs.	Pressure divs.	Pressure divs.
0	0	0	0	0	0
10	8.3	3.9	2.3	1.8	
20	17.0	10.5	4.5	3.9	1.3
30	25.0	16.3	7.2	6.0	
40	35.1	23.0	9.8	8.0	3.7
50	43.8	29.8	13.4	10.7	
60	53.7	36.0	16.2	13.5	8.1
70	62.5	42.6	20.6	16.0	
80	72.2	49.2	23.5	19.5	12.7
90	81.0	55.8	27.0	22.0	
100	90.1	62.0	30.2	25.1	17.1
110			34.0	27.7	
120			37.0	30.3	21.4
130			40.8		
140			43.6	35.5	25.5
150			47.9		
160				41.2	30.0
170					
180				46.4	34.4

To calculate the activation energy for the decomposition, the rates of reaction were adjusted to correspond to a temperature of 25.5°C. for the gas in the reaction space. The correction factor was obtained by comparing the pressure of dry air at the required temperatures with that at 25.5°C. The data for the activation energy plot are shown below and in fig. 24.

Table 19

Temperature °A	$1/T \times 10^3$	Rate divs./min.	Corr. Rate divs./min.	Log_{10} Corr. Rate + 1.0
311.9	3.206	0.92	0.86	0.935
305.3	3.276	0.65	0.63	0.799
298.5	3.350	0.49	0.49	0.690
292.0	3.425	0.34	0.35	0.544
288.0	3.472	0.275	0.290	0.462
283.5	3.528	0.220	0.238	0.377

From the plot of log rate against 1/T (fig. 24) the slope of the line $1.72 \times 10^3 \pm 2\%$

Thus the activation energy = 1.72 x 2.30 x 1.98 K cals./mole

= 7.8 ± 0.2 K.cals./mole.

A further value for the activation energy of the decomposition was obtained using light of wave-length 5460 Å. The procedure was as above and the results are shown in Table 20.

Intensity of light = full 5460 Å light

Volume of reaction space = 65.1 ml.

Gauge sensitivity = 0.0295 mm./div.

Fig. 26 Variation of rate of reaction, with light of 5460 Å, with temperature.

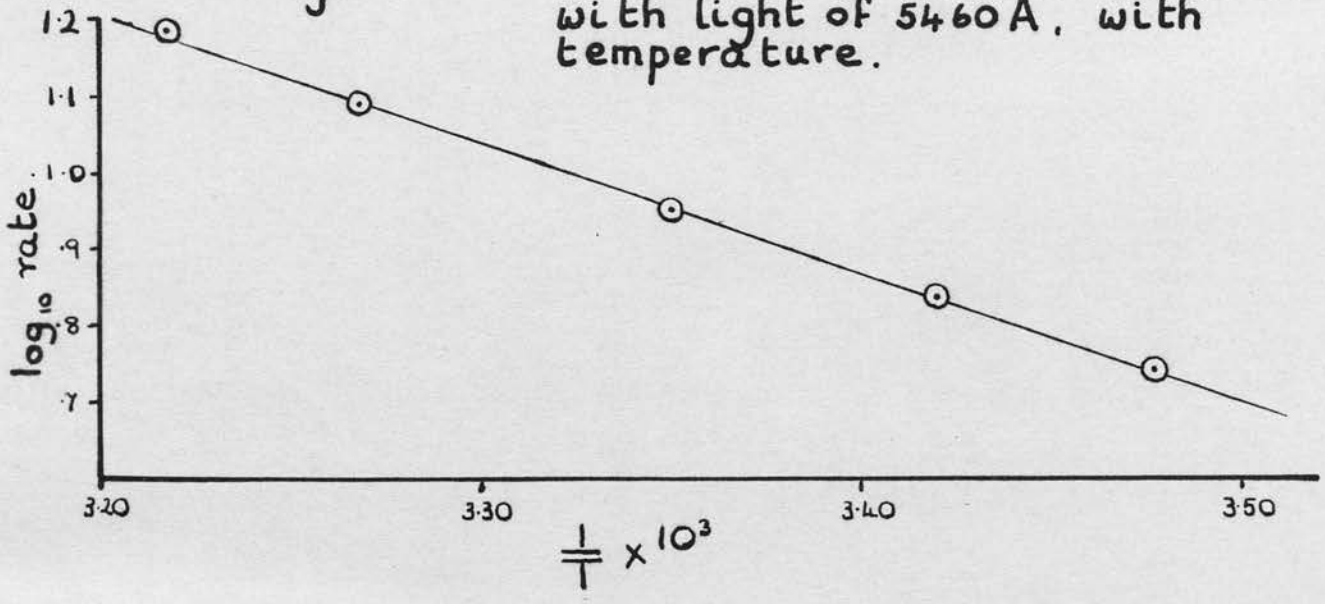

Fig. 25.

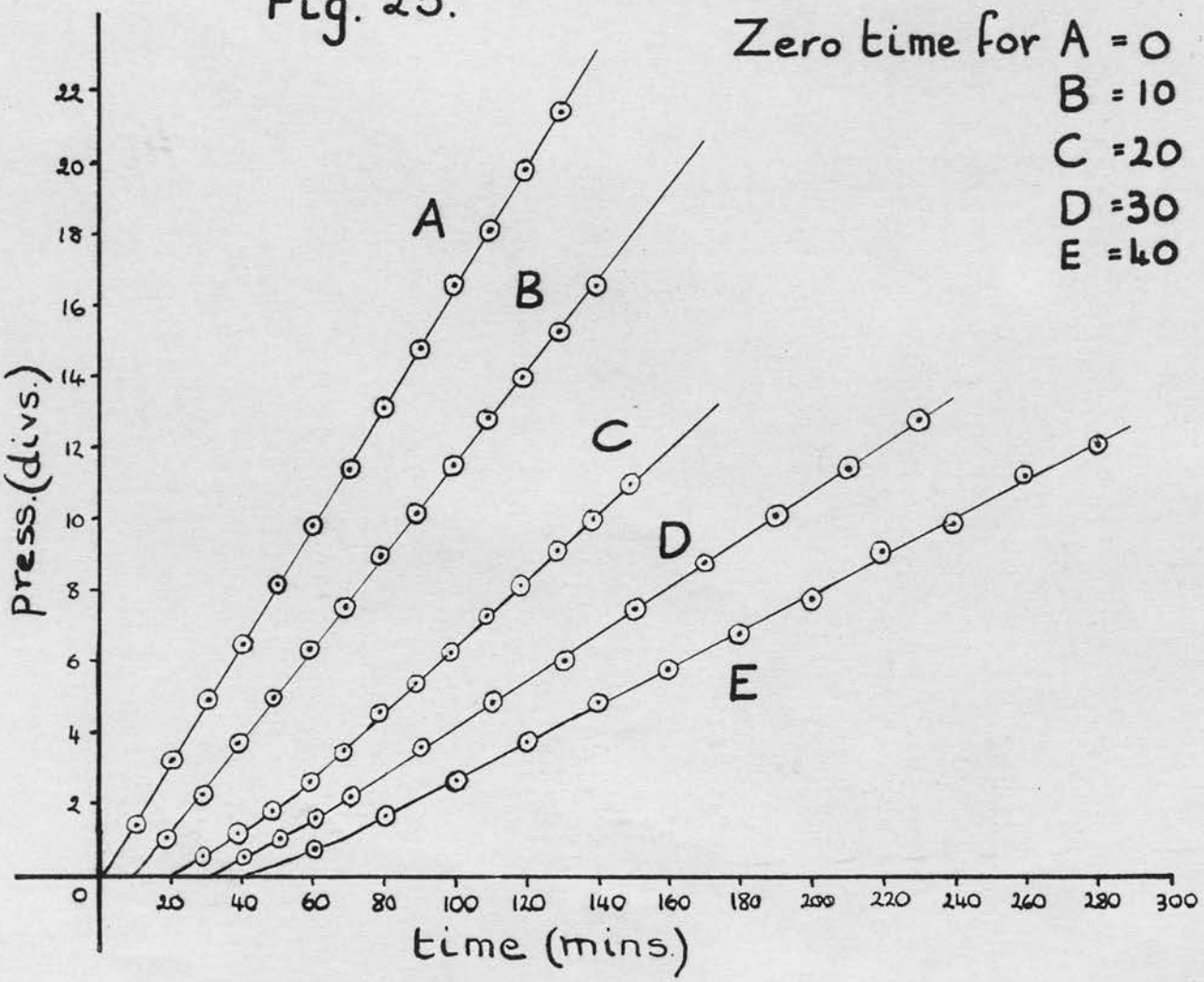

Table 20

Temperature °C.	37.8	33.0	25.5	19.4	14.6
Time min.	Pressure divs.	Pressure divs.	Pressure divs.	Pressure divs.	Pressure divs.
0	0	0	0	0	0
10	1.4	1.1	0.5		
20	3.2	2.2	1.2	1.0	0.8
30	4.9	3.6	2.6		
40	6.5	5.0	3.5	2.1	1.7
50	8.1	6.4	4.6		
60	9.8	7.6	5.4	3.6	2.7
70	11.4	9.0	6.2		
80	13.1	10.2	7.3	4.9	3.7
90	14.7	11.5	8.1		
100	16.6	12.9	9.1	6.0	4.9
110	18.0	14.1	10.0		
120	19.8	15.3	11.0	7.5	5.8
130	21.4	16.6			
140				8.8	6.8
160				10.1	7.8
180				11.4	9.1
200				12.8	9.9
220					11.2
240					12.1

The rates of decomposition measured from the graph (fig. 25) are given below.

Table 21

Temperature °A	$1/T \times 10^3$	Rate divs./min.	Corr. Rate divs./min.	Log_{10} Corr. Rate + 2.0
310.8	3.217	0.166	0.155	1.190
306.0	3.268	0.130	0.124	1.093
298.5	3.350	0.093	0.093	0.969
292.4	3.420	0.066	0.069	0.839
287.6	3.477	0.052	0.055	0.740

From the plot of log rate against 1/T (fig. 26) the slope of the line is $1.70 \times 10^3 \pm 2\%$.

Thus the activation energy = $1.70 \times 2.303 \times 1.98$ K.cals./mole.
= $\underline{7.8 \pm 0.2}$ K.cals./mole.

Fig. 27.

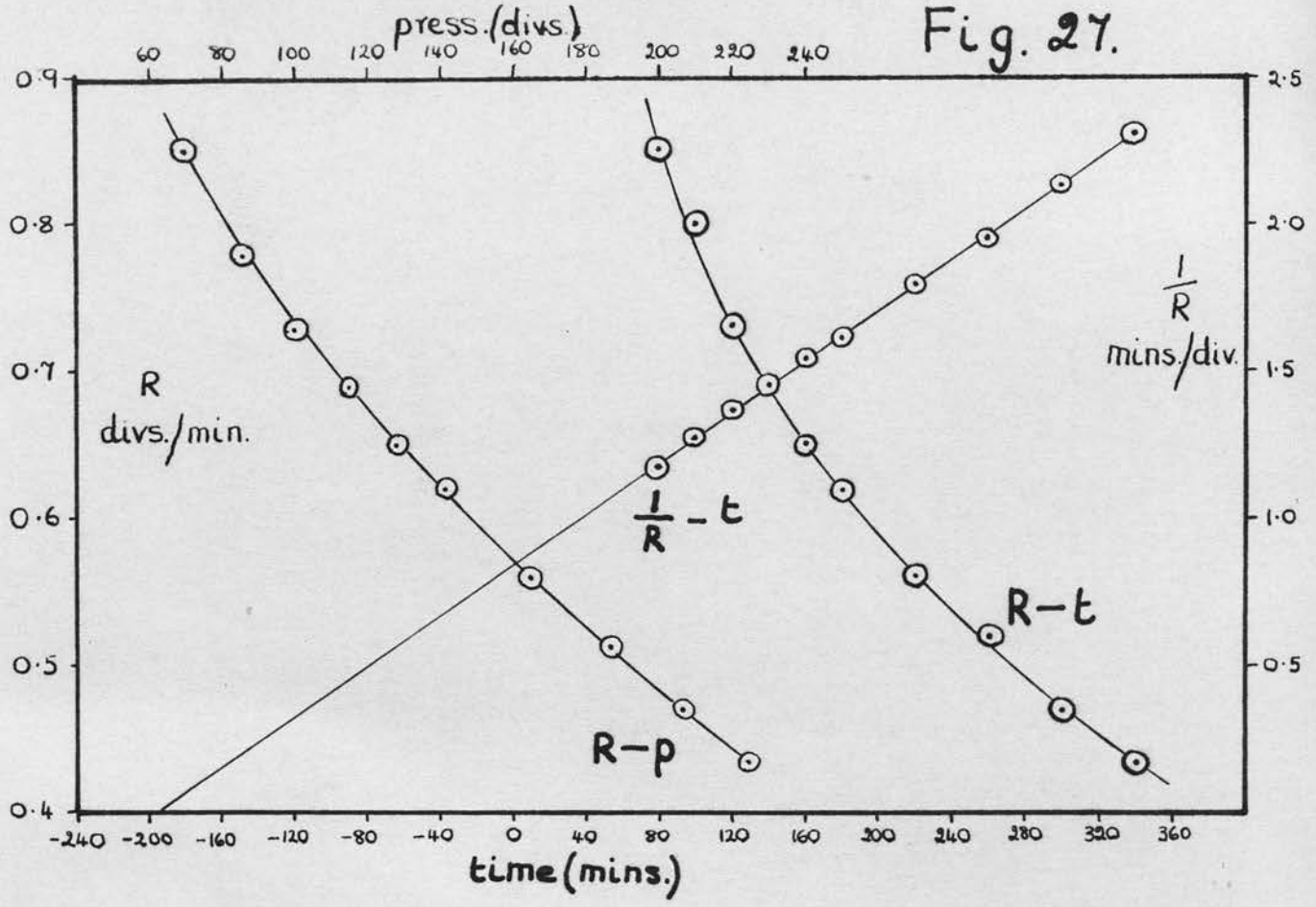
press.(divs.)
60 80 100 120 140 160 180 200 220 240
0·9 0·8 0·7 0·6 0·5 0·4
2·5 2·0 1·5 1·0 0·5
R
divs./min.
1/R
mins./div.
1/R – t
R–t
R–p
-240 -200 -160 -120 -80 -40 0 40 80 120 160 200 240 280 320 360
time (mins.)

Fig. 28.

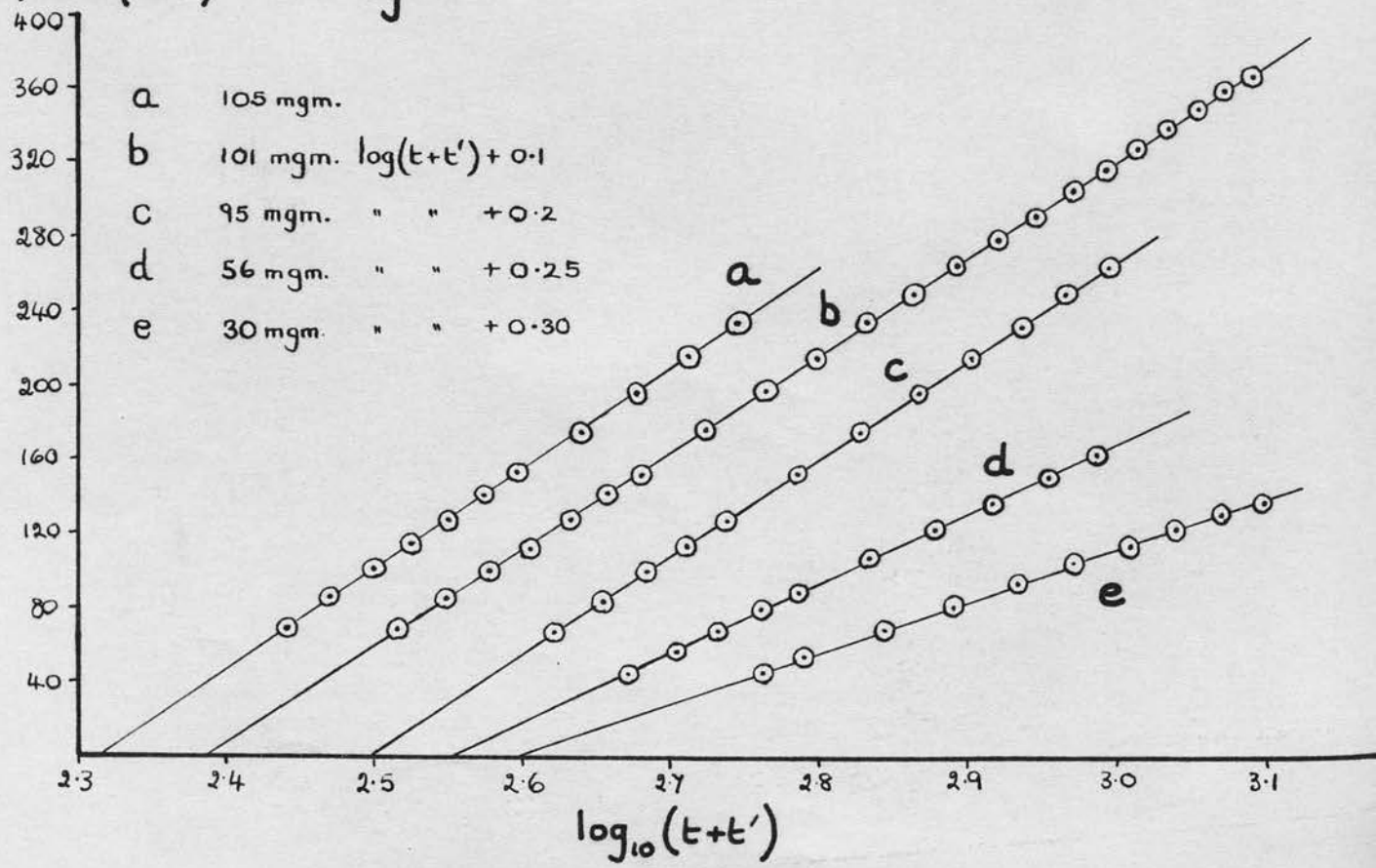
press.(divs.)
400 360 320 280 240 200 160 120 80 40
a 105 mgm.
b 101 mgm. log(t+t') + 0·1
c 95 mgm. " " + 0·2
d 56 mgm. " " + 0·25
e 30 mgm. " " + 0·30
a
b
c
d
e
2·3 2·4 2·5 2·6 2·7 2·8 2·9 3·0 3·1
log10 (t+t')

Constant rate stage - summary

For this stage of the reactions the following results have been obtained.

1. The rate of decomposition was unaffected by the presence of 50 mm. oxygen or 50 mm. carbon dioxide.
2. The rate of decomposition was directly proportional to the surface area of the films.
3. The rate of decomposition was directly proportional to the incident light intensity.
4. The activation energies for the decomposition with light of wave-lengths 3650 Å and 5460 Å were the same, i.e. 7.8 ± 0.2 K.cals./mole.

Decay stage of the reaction

The final stage (C) of the decomposition was examined using the full light of the lamp and 100 mg. samples of the oxalate.

As described previously (p. 55) corrected values for the rate of decomposition were obtained from the pressure-time curves. Using these values, plots of rate against pressure and the reciprocal of rate against time were drawn (fig. 27). From these plots it can be seen that the unimolecular decay equation does not apply, but since $1/R$ is linearly related to t then, as before (p. 55).

$\alpha p = \ln(t+t') - \ln t_o$, where α, t_o and t' are constants and t' is obtained by extrapolation of the $1/R - t$ plot to $1/R = 0$. The results of one such experiment are

shown in Table 22. Unless otherwise specified the following experiments were performed under the conditions shown below.

Temperature of reaction space = 25.5°C.
Light intensity = the full light.
Volume of reaction space = 57.2 ml.
Gauge sensitivity = 0.0465 mm./div.

Table 22 Weight of film = 105 mg.

Pressure divs.	Time min.	Rate divs./min.	Corr. Rate divs./min.	1/Rate min./div.	Log (t + 195)
0	0				
5.0	10				
12.0	20				
21.5	30				
31.5	40				
39.5	50				
49.5	60				
60.0	70				
69.0	80	0.85	0.85	1.18	2.439
85.5	100	0.80	0.78	1.28	2.470
100.0	120	0.73	0.73	1.37	2.498
115.0	140	0.69	0.685	1.46	2.525
128.5	160	0.65	0.65	1.54	2.550
141.0	180	0.62	0.62	1.61	2.574
153.5	200				2.597
164.0	220	0.56	0.56	1.79	
175.0	240				2.639
186.5	260	0.52	0.513	1.95	
196.5	280				2.677
206.0	300	0.47	0.47	2.13	
215.5	320				2.712
224.0	340	0.435	0.435	2.30	
233.0	360				2.744

Similarly films of approximately the same surface area consisting of 30-100 mg. ferric oxalate were decomposed and the results are shown in Tables 23 and 24.

Table 23

Wt. of film (mg.)	101	95	56	30
t' (min.)	180	184	184	190

Fig. 29.

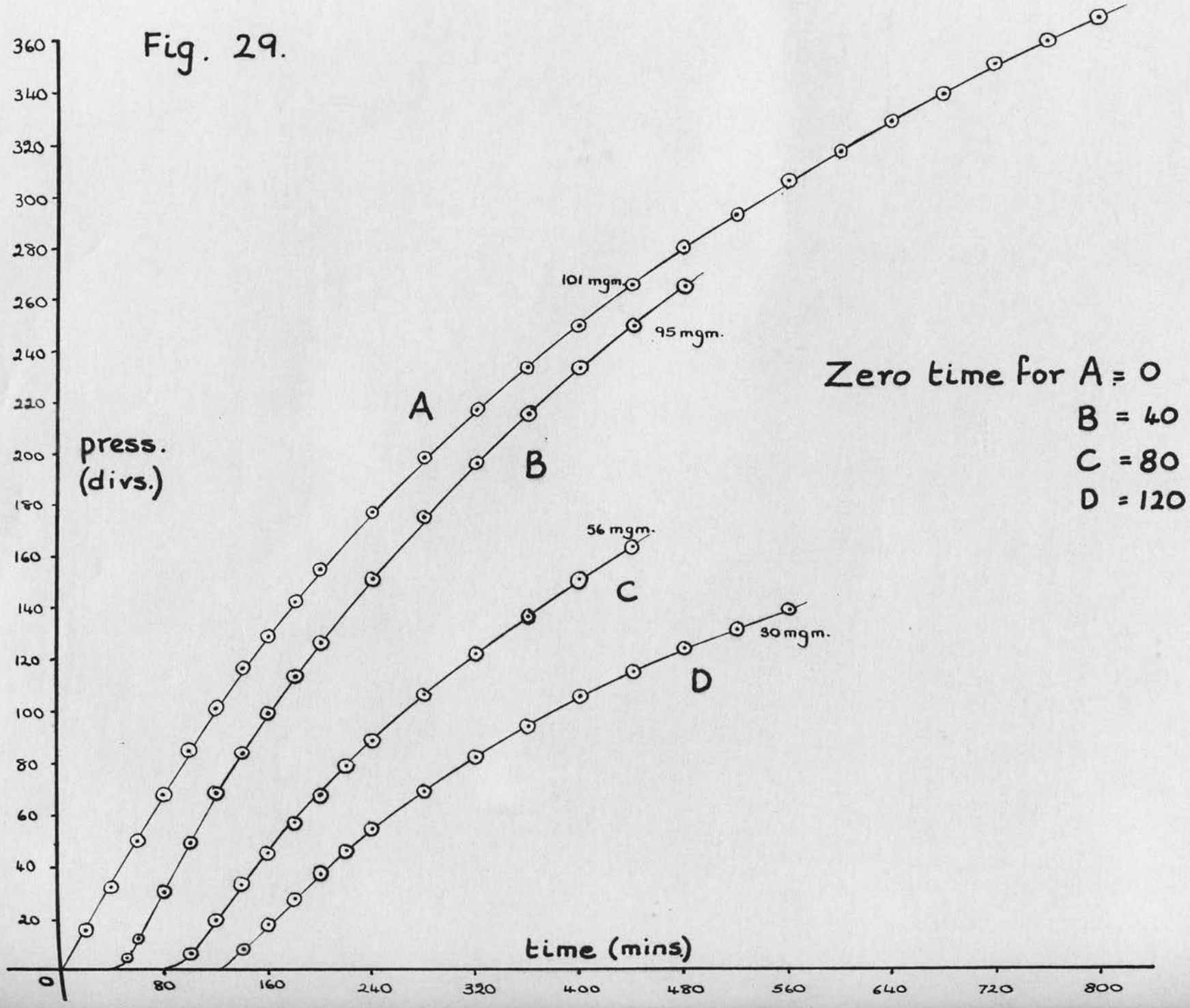
360
340
320
300
280
260
240
220
200
180
160
140
120
100
80
60
40
20
0
press. (divs.)
101 mgm.
95 mgm.
56 mgm.
30 mgm.
A
B
C
D
Zero time for A = 0
B = 40
C = 80
D = 120
time (mins)
80
160
240
320
400
480
560
640
720
800

Table 24

Weight of film mg.	101			95	56		30
Time min.	$Log_{10}(t + 180)$	Press. divs.	$Log_{10}(t + 184)$	Press. divs.	Press. divs.	$Log_{10}(t+190)$	Press. divs.
0							0
20							7.5
40							17.5
60							27.5
80	2.415	68.0	2.422	67.0	45.5		37.0
100	2.447	85.0	2.453	83.0	57.5	2.462	45.5
120	2.477	101.0	2.483	99.5	68.5	2.491	54.0
140	2.505	115.5	2.511	113.5	79.0	2.519	61.5
160	2.532	129.0	2.537	127.0	89.0	2.544	68.5
180	2.556	141.5	2.561	142.5	98.0	2.568	75.5
200	2.580	155.5	2.584	152.0	106.5	2.591	82.5
240	2.623	176.5	2.627	175.5	122.5	2.634	94.5
280	2.663	198.0	2.667	195.5	137.0	2.672	105.0
320	2.699	216.0	2.702	215.0	150.5	2.708	114.5
360	2.732	232.5	2.736	233.0	163.0	2.740	123.0
400	2.763	249.0	2.766	249.5		2.771	131.0
440	2.792	265.5	2.795	264.0		2.799	138.5
480	2.820	279.0					
520	2.845	291.5					
560	2.869	305.0					
600	2.892	316.0					
640	2.914	328.0					
680	2.935	338.5					
720	2.954	349.5					
760	2.973	359.0					
800	2.991	367.0					

Two values of t_o were obtained from the p-log(t+t') plots (fig. 28):

(1) t'_o by extrapolation to p = 0.

(2) t_o'' by extrapolation to $p = p_B$, where p_B was the pressure at the start of the decay stage and was estimated from the pressure-time curves (figs. 20 and 29).

$$\text{Since } \alpha p = \ln(t+t') - \ln t_o$$

$$\text{then } t + t' = t_o\, e^{\alpha p}$$

$$\text{and } \frac{dp}{dt} = \frac{1}{\alpha t_o}\, e^{-\alpha p}$$

Thus the rate of reaction at the beginning of the decay stage (i.e. the initial constant rate) should be equal to $\frac{1}{\alpha t_o}$. Therefore by consideration of the values of $\frac{1}{\alpha t_o}$ and of the initial rates the better value of t_o was selected. In Table 25 t_B is the time equivalent to the pressure p_B.

Table 25

Wt. mg.	$\alpha \times 10^2$	p_B divs.	t_o'	t_o''	Initial Rate divs./ min.	$\frac{1}{\alpha t_o'}$	$\frac{1}{\alpha t_o''}$	t' min.	$t_o''-t'$ min.	t_B min.
105	4.30	70	207	277	0.93	1.12	0.84	195	82	77
101	4.47	70	193	262	0.89	1.16	0.85	180	82	83
95	4.35	70	198	269	0.93	1.16	0.85	184	85	82
56	6.14	50	200	271	0.63	0.81	0.60	184	87	89
30	8.31	40	197	275	0.49	0.61	0.44	190	85	86

From these results three observations may be made:

1. α increased with decreasing weight of film; however, this increase was more probably associated with decreasing surface area of the film, since with the 56 and 30 mg. samples the surface area of the film was unavoidably less than in the other cases.
2. Both t_o' and t_o'' were independent of the mass of the film and, from a comparison of the initial rate with the values of $\frac{1}{\alpha t_o}$ t_o'' was the better value of the two.

Fig. 30.

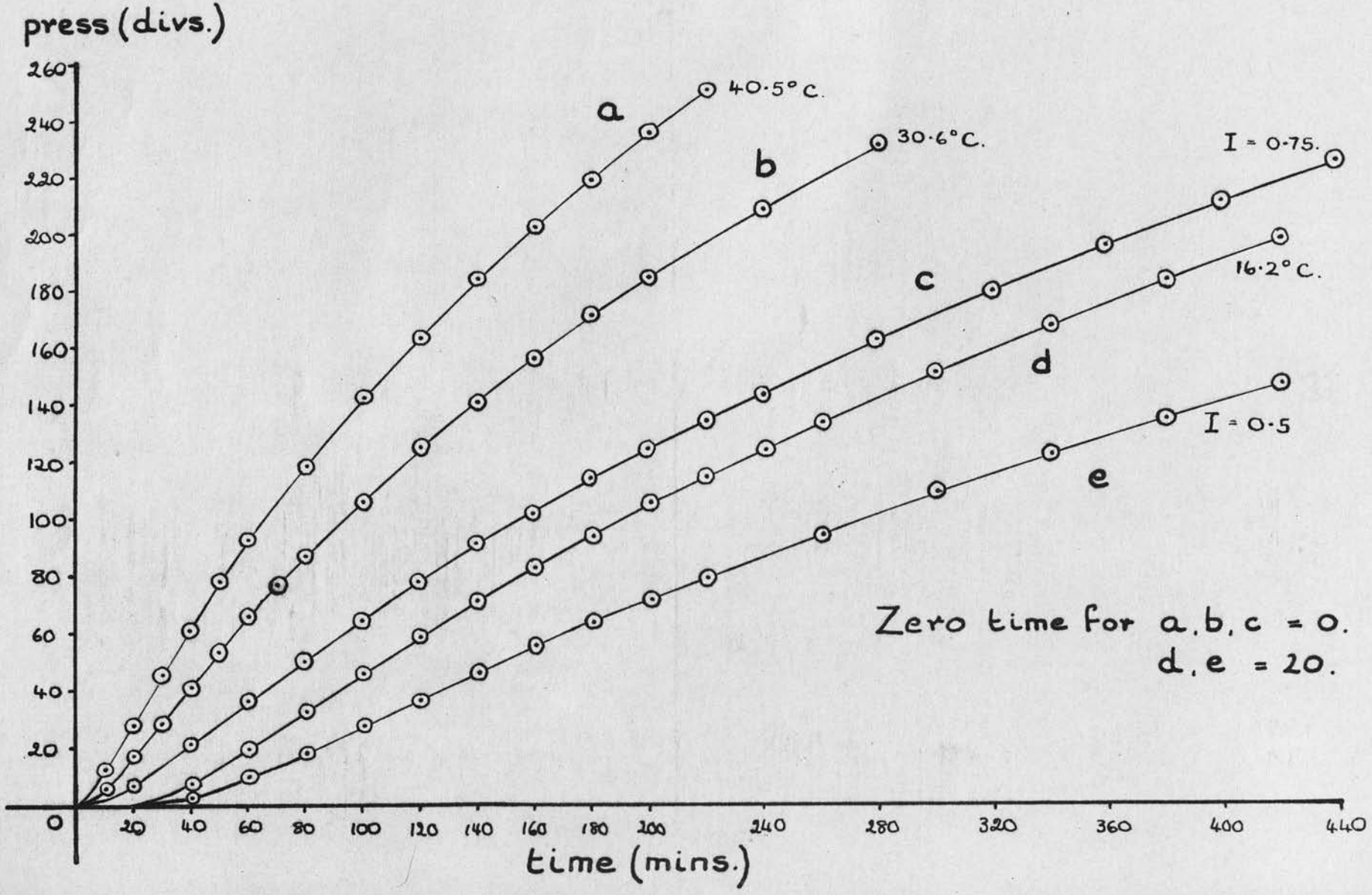
press (divs.)
260
240
220
200
180
160
140
120
100
80
60
40
20
0
20
40
60
80
100
120
140
160
180
200
240
280
320
360
400
440
time (mins.)
a
40·5° C.
b
30·6° C.
c
I = 0·75.
d
16·2° C.
e
I = 0·5
Zero time for a, b, c = 0.
d, e = 20.

3. $t_o'' - t_o'$ was approximately equal to t_B.

Thus from these observations the equation describing the results may be written:

$$\alpha(p-p_B) = \ln(t-t_B + t_o'') - \ln t_o''$$

or $\alpha p^* = \ln(t^* + t_o'') - \ln t_o''$, where p^* and t^* refer to the decay stage of the decomposition.

Variation of intensity

Films of approximately constant surface area consisting of 100 mg. of the oxalate were decomposed at 25.5°C. using various intensities of the full light of the lamp. These variations in intensity were obtained as before. The method of analysis was as in the previous experiment and the results are shown in Table 26.

Table 26

Intensity	0.75		0.5	
Time min.	Pressure divs.	$\log_{10}(t+235)$	Pressure divs.	$\log_{10}(t+390)$
0	0		0	
20	6.5		2.5	
40	21.0		9.5	
60	36.5		18.5	
80	50.0		27.0	
100	64.5		36.0	
120	77.5	2.550	45.5	
140	91.0	2.574	55.0	
160	101.5	2.597	63.5	
180	114.0	2.618	71.0	2.756
200	124.0	2.639	78.5	2.771
220	133.5	2.658		
240	143.0	2.677	93.5	2.799
280	161.5	2.712	108.5	2.826
320	179.5	2.744	121.0	2.851
360	195.0	2.775	134.5	2.875
400	209.5	2.803	146.0	2.898
440	224.0	2.829	156.5	2.919

Fig. 32.

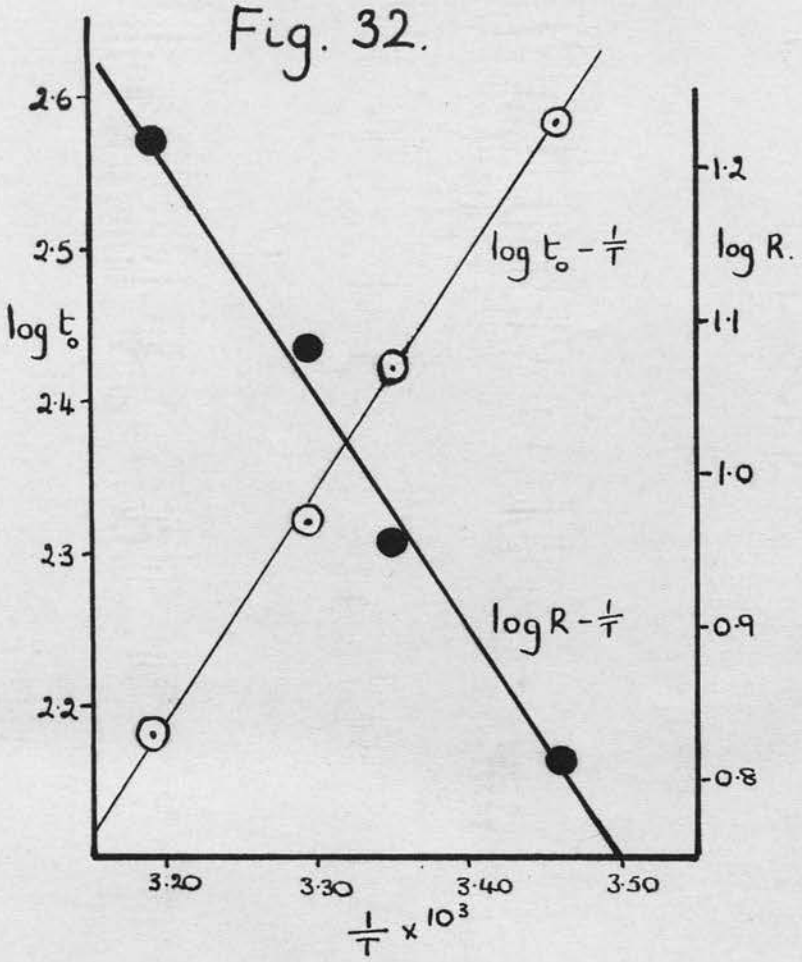

Fig. 33.

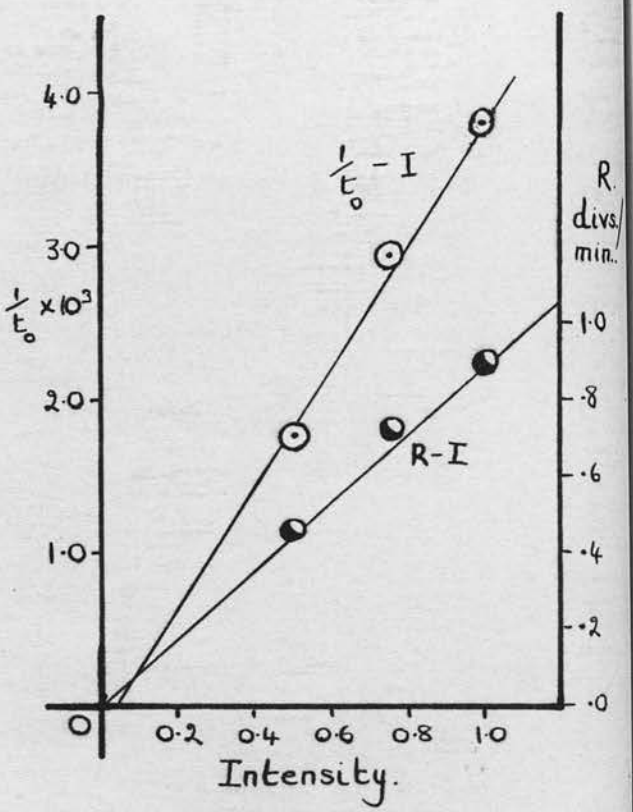

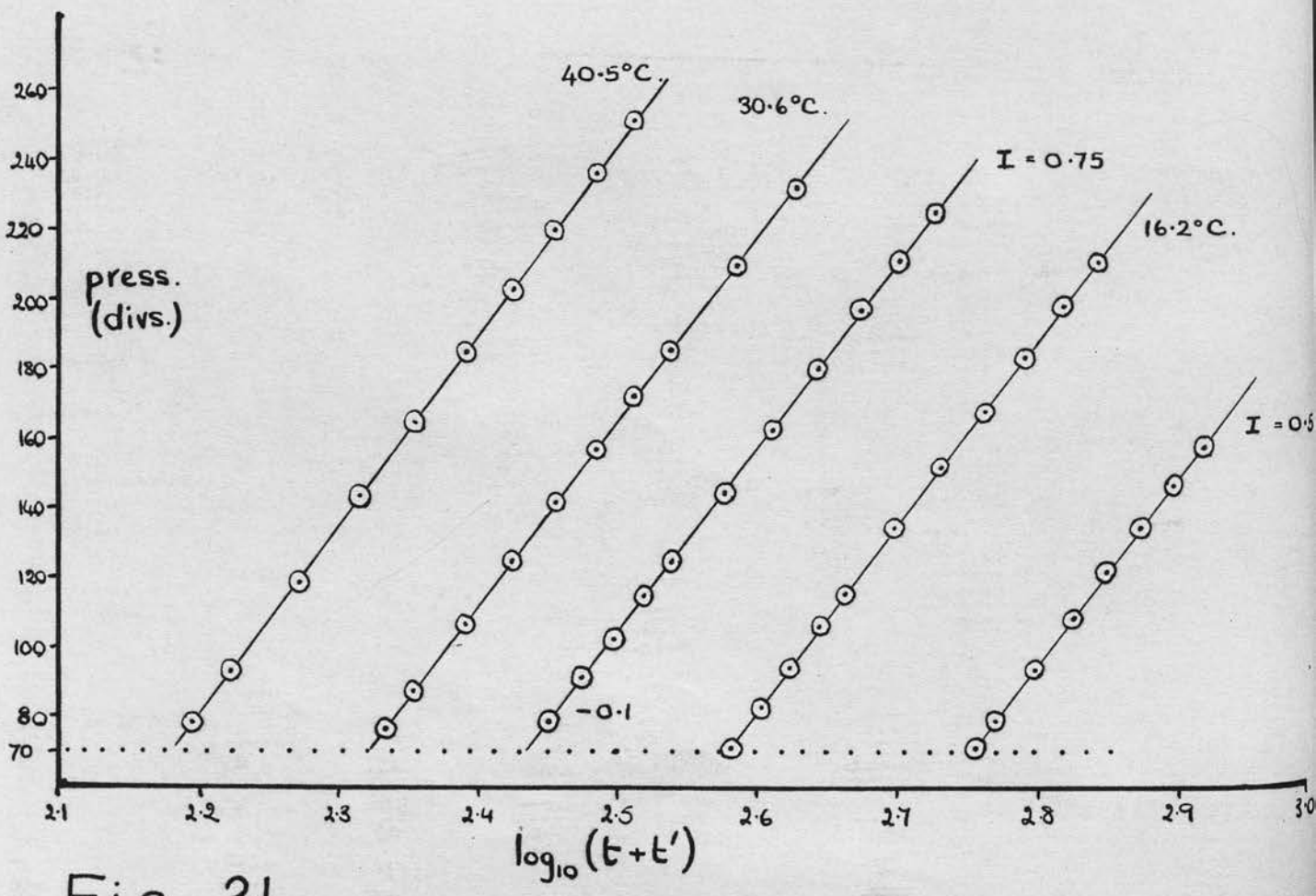

Fig. 31.

In the experiments performed with 100 mg. samples of the oxalate it can be seen from the pressure-time curves (fig. 30) that the extent of the constant rate stage of the decomposition was approximately the same at all the temperatures and light intensities employed, i.e. in the neighbourhood of p = 70 divisions. For purposes of comparison therefore the t_o values shown in Table 27 were obtained from the p-log(t+t') plots at p = 70 divisions.

Figs. 28b and 31 show the p-log(t+t') plots obtained from the decomposition with varying light intensity and from these it can be seen that α was approximately constant whereas t_o increased with decreasing light intensity. The values of t_o are shown in Table 27.

Table 27

Intensity (I)	$\alpha \times 10^2$	t_o	$1/t_o \times 10^3$	It_o	Initial rate(R) divs./min.	$1/\alpha t_o$
1.0	4.47	262	3.82	262	0.89	0.85
0.75	4.42	343	2.92	257	0.72	0.66
0.50	4.35	569	1.76	285	0.46	0.40

Three facts emerge from these results.

1. The initial rate (R) was approximately proportional to the light intensity (I) (fig. 33), in agreement with the results from the last experiment.
2. The initial rate was approximately equal to $1/\alpha t_o$.
3. The reciprocal of t_o was proportional to the light intensity (fig. 33 and column 5 above).

As shown previously $\frac{dp}{dt} = \frac{1}{\alpha t_o} e^{-\alpha p}$

Therefore since α is independent of I, at a definite value of p,

$$\frac{dp}{dt} = \frac{k}{t_o}$$ (where k is a constant)

for the range of light intensities used.

i.e. the rate of decomposition is proportional $\frac{1}{t_o}$, which, from 3. above, is proportional to I, thus the rate of decomposition in the decay stage is proportional to the incident light intensity.

Variation of temperature

Films of approximately constant surface area consisting of 100 mg. of oxalate were decomposed using the full light of the lamp at temperatures between 16°C. and 40°C. In Table 28 the pressures have been corrected to correspond to a temperature of 25.5°C. for the gas in the reaction space.

Table 28

Temperature °C.	40.5		30.6		16.2	
Time min.	$Log_{10}(t+106)$	Pressure divs.	$Log_{10}(t+145)$	Pressure divs.	$Log_{10}(t+260)$	Pressure divs.
0		0		0		0
10		11.5		5.5		
20		28.0		16.5		7.5
30		44.5		28.5		
40		60.0		41.0		19.5
50	2.193	77.5		53.0		
60	2.220	91.5		65.5		33.0
70			2.332	76.5		
80	2.270	118	2.352	87.0		46.0
100	2.314	142	2.389	106.0		58.5
120	2.354	163.5	2.423	125.0	2.580	71.0
140	2.391	184.0	2.455	140.5	2.602	82.5
160	2.425	201.5	2.484	156.0	2.623	93.5
180	2.456	218.5	2.512	171.5	2.644	105.0
200	2.486	235.0	2.538	184.5	2.663	114.5
220	2.513	250.5			2.681	124.0
240			2.586	208.5	2.699	133.5
280			2.628	231.0	2.732	151.0
320					2.763	167.0
360					2.792	182.5
400					2.820	197.0

From the p-log(t+t') plots (fig. 31) it can be seen that α was effectively constant, whereas t_o increased with decreasing temperature. As shown in the dehydration experiments, a value for the activation energy of the process can be obtained from the plots of log t_o against 1/T.

Table 29

Temperature °A	$1/T \times 10^3$	$\alpha \times 10^2$	$Log_{10} t_o$	Initial Rate(R) divs./min.	Log R + 1.0
313.5	3.190	4.27	2.18	1.66	1.22
303.6	3.294	4.39	2.32	1.22	1.09
298.5	3.350	4.47	2.42	0.89	0.95
289.2	3.438	4.41	2.58	0.65	0.81

Fig. 34. Pressure – time curves for photochemical decomposition of thin films.

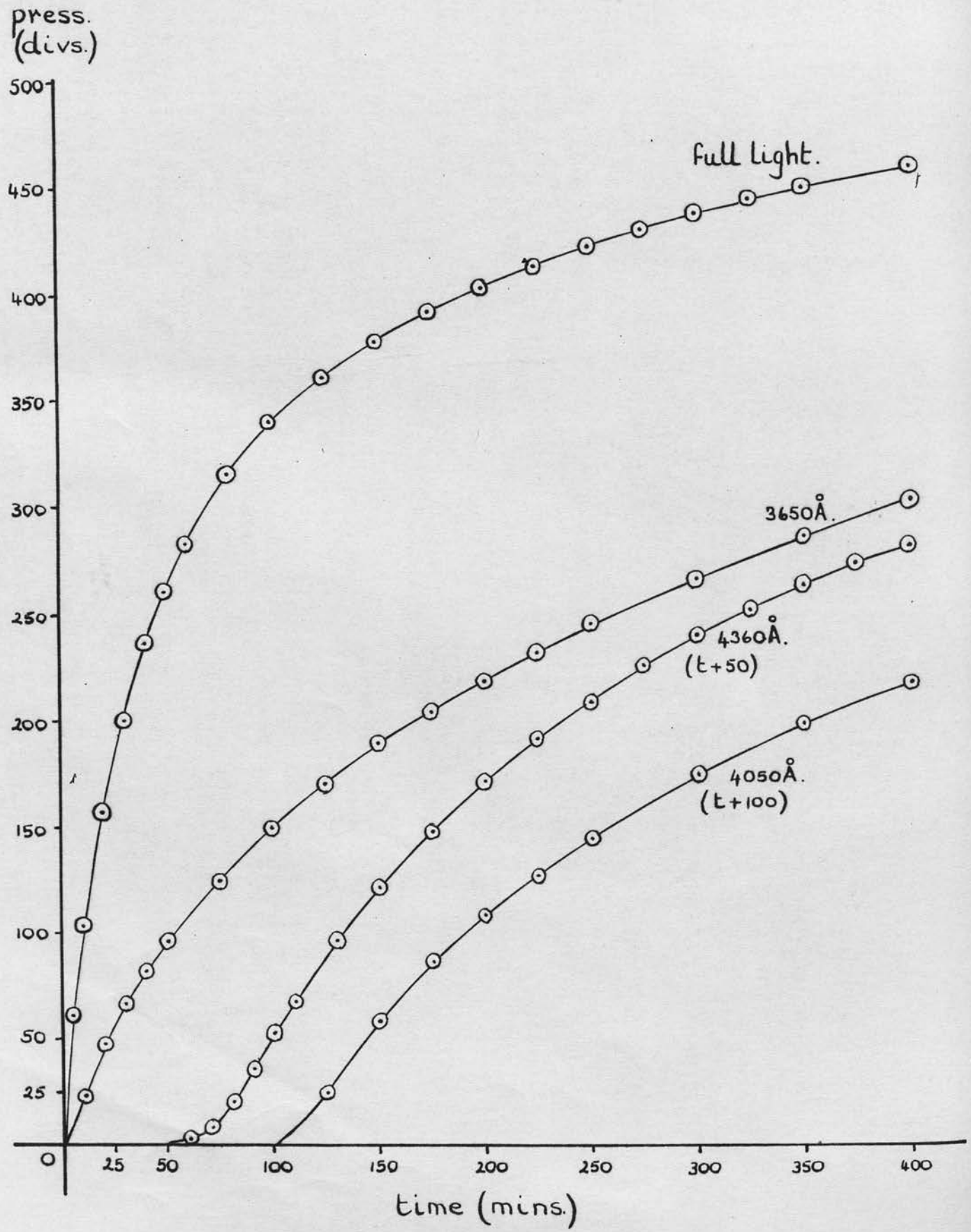

The graph of log t_o - 1/T (fig. 32) gives a reasonable straight line of slope $1.55 \times 10^3 \pm 8\%$,

i.e. the activation energy = 1.55 x 2.303 x 1.98 K.cals./mole.

= 7.2 ± 0.6 K.cals./mole.

Thus the activation energy for the decay stage of the decomposition is in fair agreement with that for the constant rate stage (7.8 ± 0.2 K.cals./mole). ~~and is, within experimental error, equal to the value obtained for the decay stage of the reaction.~~

Photodecomposition of 'thin' films

Due to the physical state of the 'thin' films the reactions were studied over a greater extent of decomposition (up to 90%) than was possible with the 'thick' films. The pressure-time curves for the decomposition of 'thin' films with light of various wavelengths are shown in fig. 34, and it can be seen that they exhibit the same sigmoid shape as the 'thick' films although the extent of the three stages is altered. The acceleration stage A occupied about 3% of the reaction, the constant rate stage B was not so clearly defined as with the 'thick' films and was more a transient stage from the acceleration to decay periods. The decay stage C was followed up to 90% decomposition and it seemed probable that it would continue to completion.

Acceleration stage

The pressure-time data for the acceleration stage were expressed by the equation log p = n log t (fig. 35) where p is the pressure at

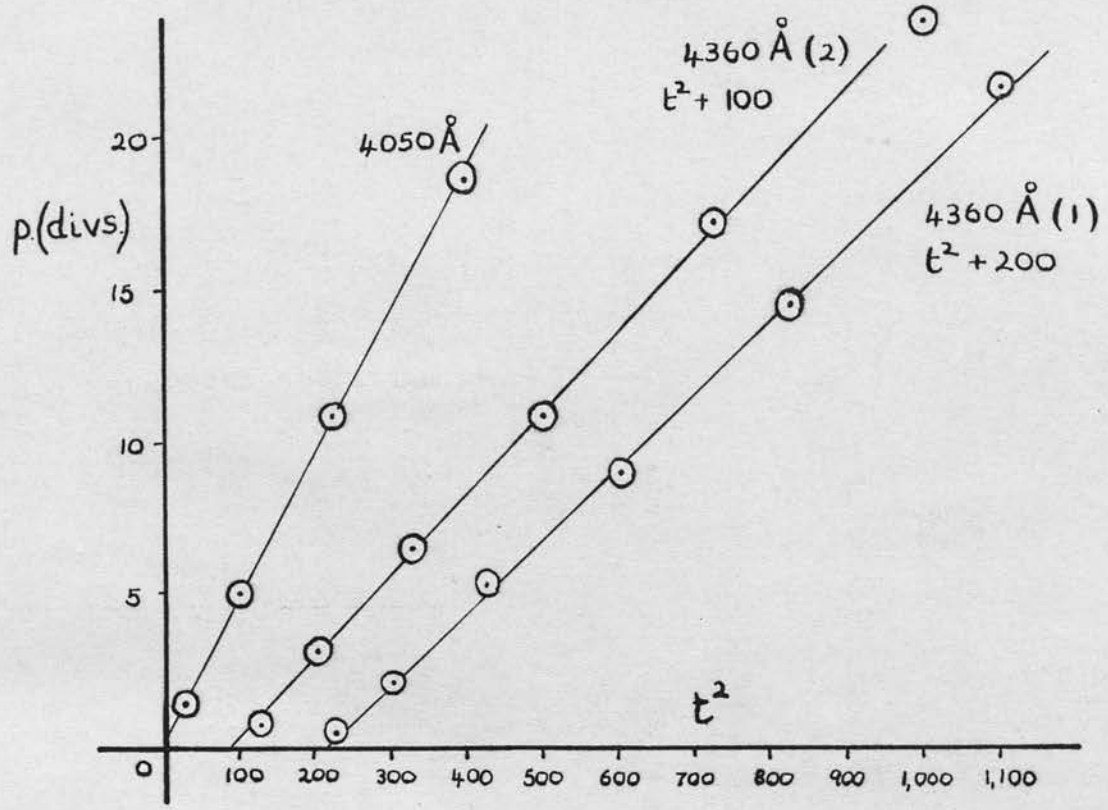
4360 Å (2)
t^2 + 100
4050 Å
4360 Å (1)
t^2 + 200
p (divs.)
20
15
10
5
0
t^2
100
200
300
400
500
600
700
800
900
1,000
1,100

Fig. 36.

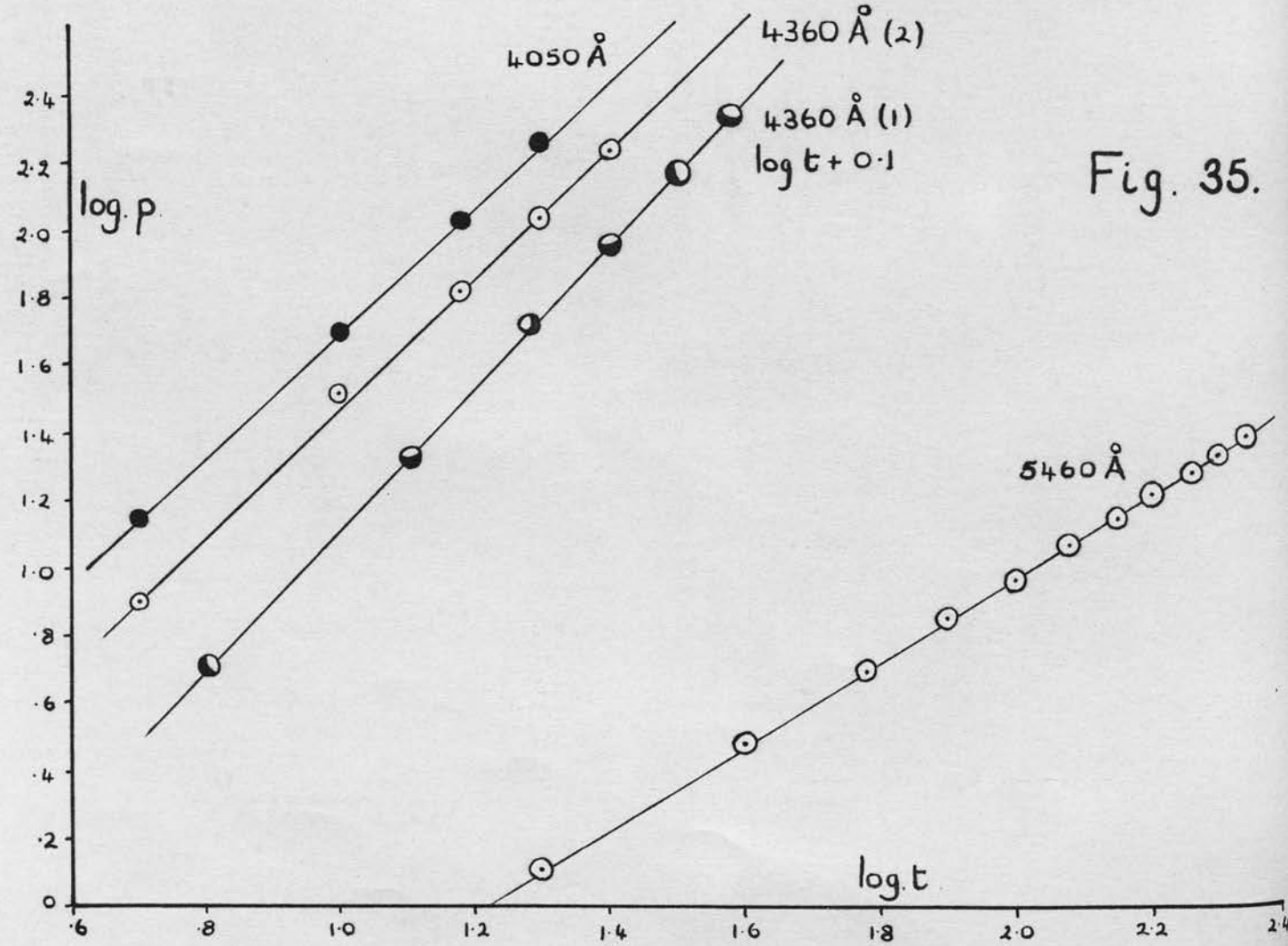
4050 Å
4360 Å (2)
4360 Å (1)
log t + 0·1
log. p
2·4
2·2
2·0
1·8
1·6
1·4
1·2
1·0
·8
·6
·4
·2
0
5460 Å
log. t
·6
·8
1·0
1·2
1·4
1·6
1·8
2·0
2·2
2·4

Fig. 35.

time t and n is a constant giving values of 2 for decomposition with light of wave-length 4050 Å and 4360 Å and 1.2 for 5460 Å,

i.e. $p \propto t^2$ (for 4050 Å, 4360 Å)
and $p \propto t^{1.2}$ (for 5460 Å)

The following experiments were performed under the conditions shown below.

Temperature of reaction space = 25.5°C.
Gauge sensitivity = 0.0225 mm./div.
Volume of reaction space = 43.1 ml.

Table 30

Wave-length of light used Å				4360 (1)		4360 (2)		4050		5460	
Time (t) min.	$Log_{10}t$	t^2	Press. (p) divs.	$Log_{10}p$ + 1.0	p. divs.	$Log_{10}p$ +1.0	p. divs.	$Log_{10}p$. + 1.0	p. divs	$Log_{10}p$.
0										
5	0.70	25	0.5	0.70	0.8	0.90	1.4	1.15		
10	1.00	100	2.1	1.32	3.2	1.51	5.0	1.70		
15	1.18	225	5.3	1.72	6.5	1.81	10.8	2.03		
20	1.30	400	9.0	1.95	10.8	2.03	18.5	2.27	1.3	0.11
25	1.40	625	14.5	2.16	17.1	2.23				
30	1.48	900	21.5	2.33	23.6	2.37				
40	1.60								3.0	0.48
60	1.78								4.9	0.69
80	1.90								7.0	0.85
100	2.00								9.2	0.96
120	2.08								11.5	1.06
140	2.15								13.8	1.14
160	2.20								16.3	1.21
180	2.26								18.8	1.27
200	2.30								21.4	1.33
220	2.34								24.1	1.38

The acceleration constant k from $p = kt^2$ was 0.043 for 4050 Å light and 0.024 and 0.027 for runs (1) and (2) with 4360 Å light (fig. 36), i.e. the constant increased with decreasing wave-length.

Fig. 38.

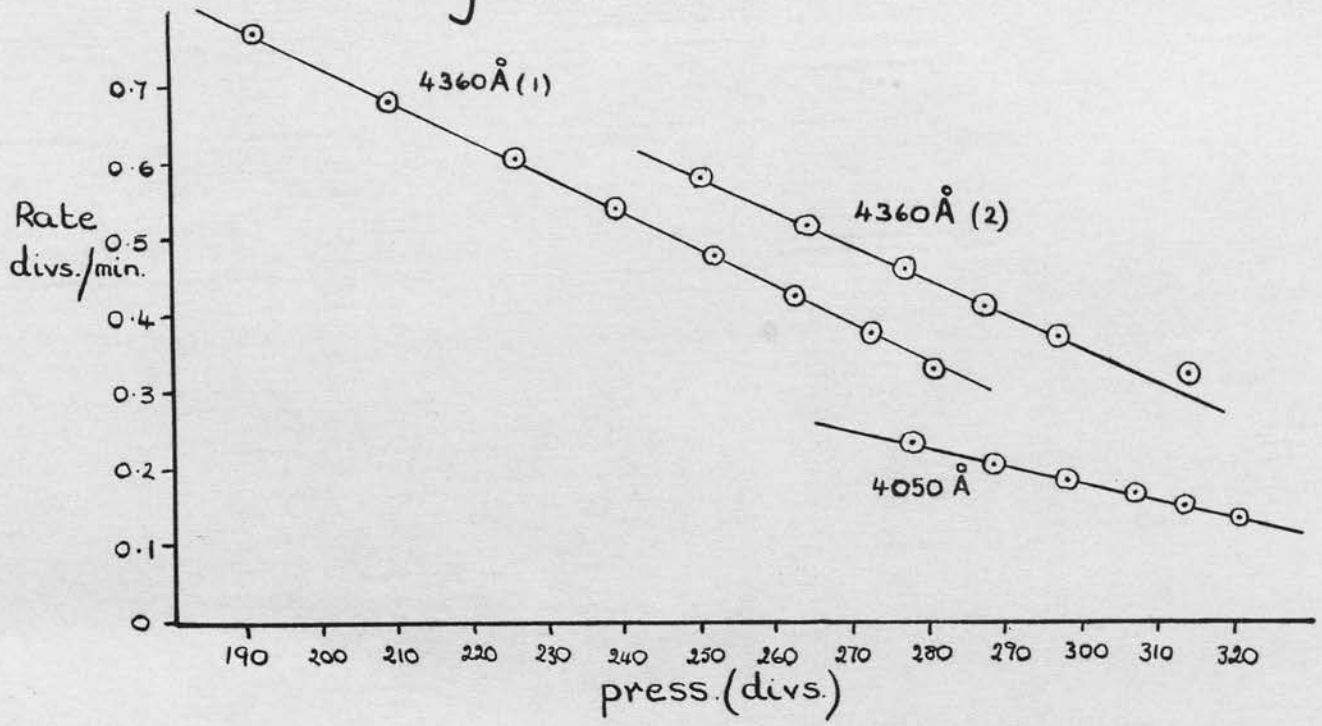
4360Å (1)
4360Å (2)
4050 Å
Rate divs./min.
0·7
0·6
0·5
0·4
0·3
0·2
0·1
0
190 200 210 220 230 240 250 260 270 280 290 300 310 320
press. (divs.)

Fig. 37.

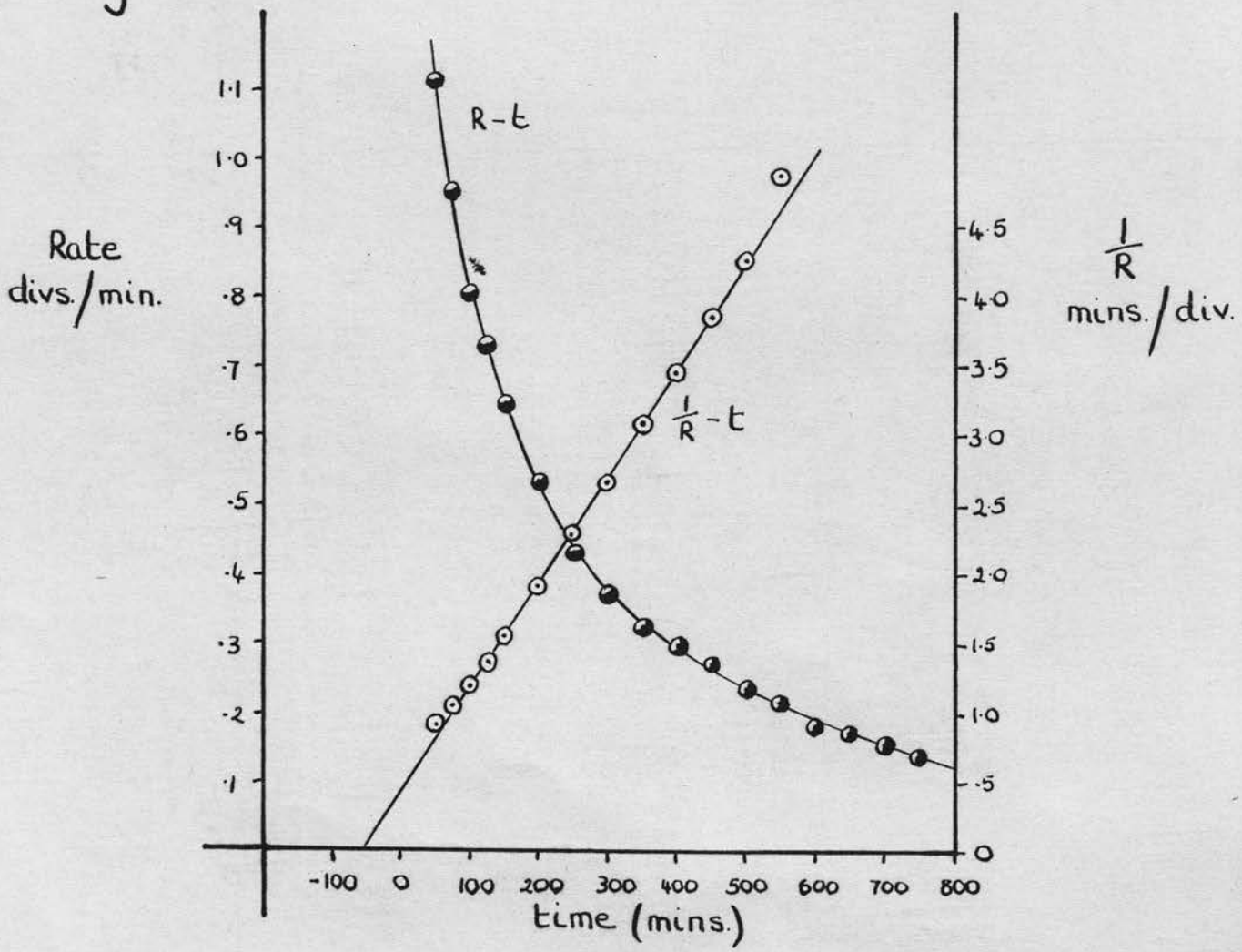
R-t
1/R - t
Rate divs./min.
1/R mins./div.
1·1
1·0
·9
·8
·7
·6
·5
·4
·3
·2
·1
4·5
4·0
3·5
3·0
2·5
2·0
1·5
1·0
·5
0
-100 0 100 200 300 400 500 600 700 800
time (mins.)

Decay stage

The decay stage of the decomposition was similar to that for the 'thick' films in that the results were expressed by the same equation:

$$1/R = \alpha(t+t') \quad \text{(fig. 37)}$$

and thus using the values of t' so obtained the plots of p - log (t+t') were drawn. The complete analysis of one decomposition is shown in Table 31.

Table 31 Wave-length of light = 4050 Å

Time min.	Pressure divs.	Rate divs./min.	Corr. Rate divs./min.	1/R min./div.	$Log_{10}(t+60)$
0	0				
25	25.0				
50	59.0	1.11	1.11	0.90	2.041
75	86.0	0.95	0.95	1.05	2.130
100	108.5	0.80	0.84	1.19	2.204
125	127.5	0.73	0.73	1.37	2.267
150	145.0	0.64	0.645	1.55	2.322
200	174.5	0.535	0.520	1.92	2.415
250	198.0	0.43	0.435	2.30	2.491
300	217.5	0.37	0.375	2.67	2.556
350	235.0	0.325	0.325	3.08	2.613
400	250.5	0.295	0.290	3.45	2.663
450	265.0	0.270	0.260	3.85	2.708
500	278.0	0.235	0.235	4.26	2.748
550	288.5	0.215	0.205	4.88	2.785
600	298.0	0.180	0.185		2.820
650	306.5	0.170	0.170		2.851
700	313.5	0.150	0.150		2.881
750	320.5	0.135	0.135		2.909

The decomposition was repeated at various wave-lengths, three times with 3650 Å light, twice with 4360 Å light and once with the full light. t' values were obtained as above and the p-log(t+t') plots drawn (fig. 39).

Table 32

Light	full		4360 Å (1)			4360 Å (2)		
Time min.	Press. divs.	$Log_{10}t$	Press. divs.	$Log_{10}(t+45)$	$\frac{dp}{dt}$ divs./min.	Press. divs.	$Log_{10}(t+40)$	$\frac{dp}{dt}$ divs./min.
0	0		0			0		
5	61.0	0.699	0.5			0.5		
10	103.0	1.00	2.0			3.0		
20	157.5	1.301	9.0			10.5		
30	200.5	1.477	21.5			23.5		
40	236.0	1.602	36.5			36.5		
50	260.5	1.699	53.0	1.977		54.5	1.954	
60	283.0	1.778	68.0	2.021		71.5	2.000	
80	315.5	1.903	96.5	2.097		102.5	2.079	
100	339.0	2.000	121.0	2.161		127.0	2.146	
		Log(t-25)						
125	360.0	2.000	148.0	2.230		154.5	2.218	
150	377.0	2.097	171.0	2.290		178.5	2.279	
175	390.5	2.176	191.0	2.342	0.77	199.5	2.332	
200	402.0	2.243	209.0	2.389	0.68	218.0	2.380	
225	412.0	2.301	225.5	2.431	0.605	234.5	2.423	
250	421.0	2.352	239.0	2.470	0.54	250.0	2.462	0.58
275	429.0	2.398	251.5	2.505	0.48	265.0	2.498	0.515
300	436.5	2.439	262.5	2.538	0.425	276.5	2.532	0.46
325	443.0	2.477	272.5		0.375	287.5	2.562	0.41
350	448.5	2.512	280.5		0.33	297.0	2.591	0.37
400	459.0	2.574	293.0			314.0		0.32
450	468.0	2.628				329.5		0.30
500	475.5	2.677						
		Log(t-280)						
500	475.5	2.342						
600	487.5	2.505						
700	496.5	2.623						
800	503.0	2.716						
900	508.5	2.792						
1000	513.0	2.857						
1400	527.0	3.049						
1600	531.0	3.121						

Fig. 39.

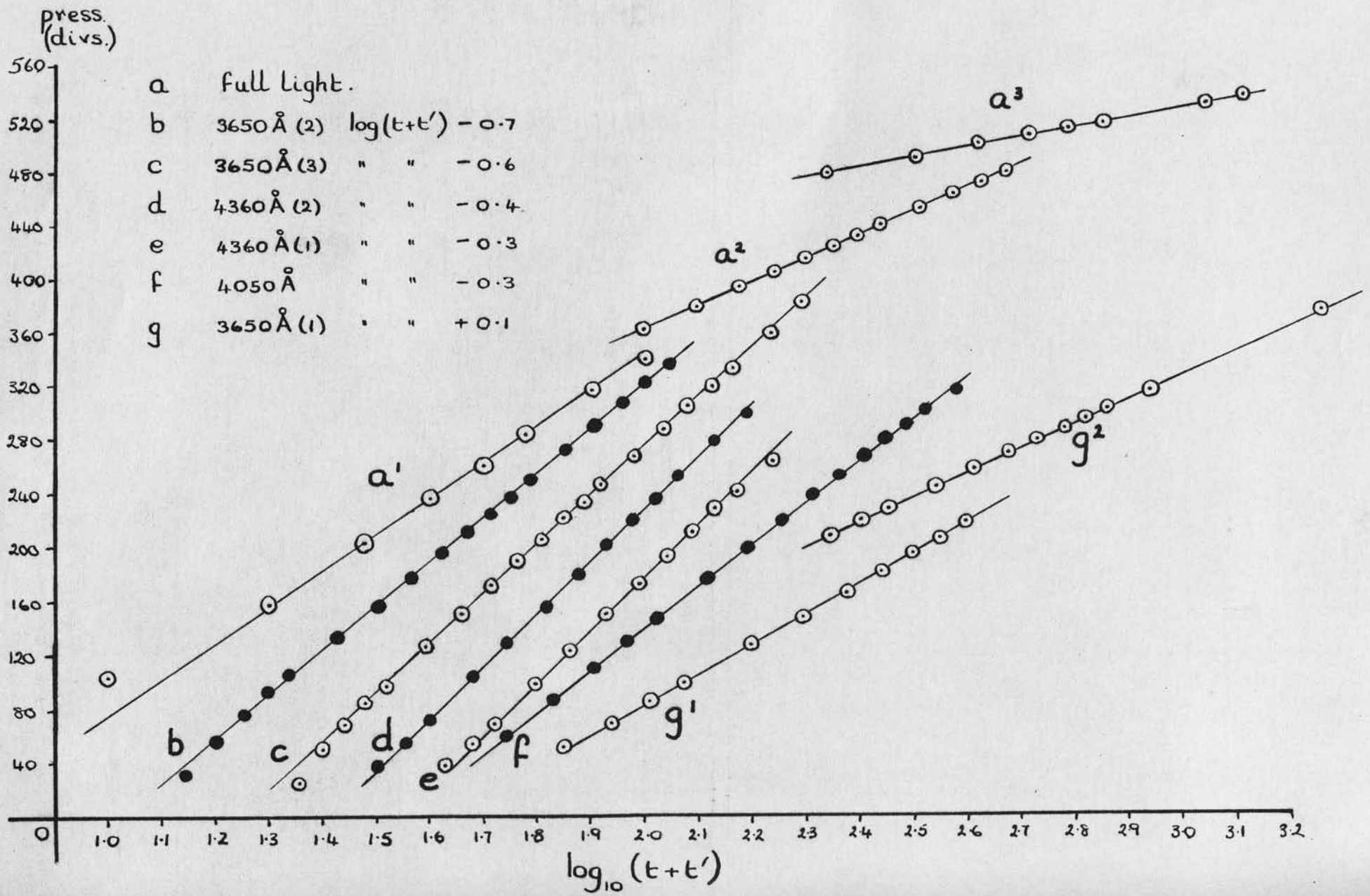
press. (divs.)
560
520
480
440
400
360
320
280
240
200
160
120
80
40
0
a Full Light.
b 3650 Å (2) log(t+t′) − 0·7
c 3650 Å (3) " " − 0·6
d 4360 Å (2) " " − 0·4
e 4360 Å (1) " " − 0·3
f 4050 Å " " − 0·3
g 3650 Å (1) " " + 0·1
a¹
a²
a³
b
c
d
e
f
g¹
g²
1·0 1·1 1·2 1·3 1·4 1·5 1·6 1·7 1·8 1·9 2·0 2·1 2·2 2·3 2·4 2·5 2·6 2·7 2·8 2·9 3·0 3·1 3·2
log10 (t+t′)

Table 33 Wave-length of light = 3650 Å

Time min.	Press. divs.	(1) Log(t+ 25)	Log(t- 25)	Press. divs.	(2) Log(t+ 60)	Press. divs.	(3) Log(t+ 80)
0	0			0			
10	29.0	1.544		32.0	1.845	24.0	1.954
20	52.5	1.653		57.0	1.903	48.0	2.000
30	70.0	1.740		78.0	1.954	67.0	2.041
40	86.5	1.813		92.5	2.000	82.5	2.079
50	99.0	1.875		105.5	2.041	96.0	2.114
75	126.5	2.000		134.0	2.130	124.5	2.190
100	147.5	2.097		156.5	2.204	150.0	2.255
125	165.5	2.176		177.5	2.267	170.0	2.312
150	181.0	2.243		195.5	2.322	189.0	2.362
175	194.5	2.301	2.176	211.0	2.371	204.0	2.407
200	206.0	2.352	2.243	224.5	2.415	218.5	2.447
225	216.5	2.398	2.301	237.0	2.455	231.0	2.484
250	225.5		2.352	250.0	2.491	244.5	2.519
300	241.5		2.438	271.5	2.556	265.5	2.580
350	255.0		2.512	290.0	2.613	285.0	2.634
400	266.5		2.574	306.5	2.663	302.0	2.681
450	266.5		2.628	321.5	2.708	317.0	2.725
500	284.0		2.677	335.0	2.748	331.0	2.763
550	292.0		2.720			344.0	2.799
600	299.0		2.760			357.0	2.833
650	306.0		2.796			368.5	2.863
700	312.5		2.829			379.0	2.892
750	318.5		2.860			388.5	2.919
1475	375		3.161				
1700	386		3.224				

As for the 'thick' films t_o was obtained from the p-log(t+t') plots at $p = p_B$, where p_B is the pressure at the start of the decay stage of the decomposition. In the above experiments p_B was taken to be 60 divisions, this value being chosen on examination of both the pressure-time curves (fig. 34) and the p-log(t+t') plots (fig. 39).

Values of the intensity of light of wave-length 3650 Å, 4050 Å and 4360 Å emitted by a 125 watt Osira mercury lamp were

obtained from (51), these values being corrected for the transmission of the appropriate filters; column 2 in Table 34 gives the approximate relative light intensities, as a fraction of the value for 3650 Å, incident on the film at these wave-lengths. In the next experiment the intensity (I) is shown to be proportional to $1/t_o$. Thus using this fact and the intensities shown in Table 34, the values of t_o were corrected to correpond to an intensity of 1.0 (see column 8, Table 34).

In the table, t_B is the time corresponding to the pressure p_B and the final column gives the percentage decomposition described by the 1/R - t relationship.

Table 34

Wave length Å		Intensity	$\alpha \times 10^3$	t' min.	t_o	$1/\alpha t_o$	Rate for stage B divs./min.	Corr. t_o	$t_o - t'$	t_B min.	%
3650	1	1.0	10.3	25	50	1.94	2.7	50	25	23	
	2	1.0	7.0	60	81	1.76	2.6	81	21	20	60
	3	1.0	6.3	80	103	1.54	2.5	103	23	21	
4050	1	0.42	7.5	60	110	1.21	1.4	46	50	50	43
4360	1	0.47	5.9	45	100	1.70	1.67	47	55	55	29
	2	0.47	5.9	40	93	1.82	1.7	44	53	53	38
Full light			8.5	0	9.3	12.7	12.2		9.3	5	50

For the extent of decomposition shown in the last column in Table 34 the $1/R = \alpha(t+t')$ equation expressed the results with one value of α; thereafter the decomposition characteristics varied according to the wave-length of light used. One exception to this

was experiment (1) with 3650 Å light, the $1/R - t$ plot in that case consisted of two straight lines the break occurring at 31% decomposition. However, as this was in marked contrast to the other runs at this wave-length, it was considered that the break was caused by a change in the condition of the film - some of it becoming detached from the reaction vessel - giving new α and t_o values.

From Table 34, three facts emerge for this stage of the reaction.

1. α appears to be approximately constant whereas to, with respect to a constant light intensity, varies with the wave-length of light used.
2. $1/\alpha t_o$ is approximately equal to the maximum rate of reaction, i.e. the rate at the beginning of the decay stage.
3. $t_o - t'$ is approximately equal to t_B.

Thus the equation describing this part of the decay stage is:

$$\alpha p^* = \ln(t^* + t_o) - \ln t_o$$, where p^* and t^* refer to the decay stage of the decomposition.

As can be seen from the tables the $\alpha p - \log(t+t')$ relationship agreed with the experimental results for 3650 Å light for the extent of the reactions investigated (approximately 60% decomposition). However, this was not the case for the other wave-lengths of light used, in these cases the relationship expressed the results up to between 30% and 50% decomposition. For the experiments with 4360 Å and 4050 Å light, it was found that for

a further 6-12% decomposition $\frac{dp}{dt} \propto p$ (fig. 38), i.e. the reaction obeyed a unimolecular decay mechanism. On the other hand the results for the decomposition with the full light were expressed by the equation $\alpha p = \ln(t+t') - \ln t_o$ with two further values of α and t_o (fig. 39 a^2, a^3). A table of the constants for the appropriate equations and the extent of their agreement is shown below (Table 35).

Table 35

Wave-length Å		k x 10^3	α x 10^2	Extent of agreement %
Full light			1.3	50-55
			3.2	55-90
4050		2.3		43-49
4360	1	4.7		29-41
	2	4.5		38-46

where k is given by $\frac{dp}{dt} = kp + C$ (where C is a constant)
and α by $\alpha p = \log(t+t') - \log t_o$.

The Effect of Temperature and Light Intensity on the Decay Stage of the Reaction with 'thin' films.

The films for these experiments were made by pipetting 1 ml. portions of a solution of known concentration (9.8 mg./ml.) of ferric oxalate into the reaction vessel. This was preferred to the previous method since the quantities used could be more accurately controlled. 4360 Å light was used for the decomposition, and the experimental procedure was as before.

The decompositions were performed at (1) varying temperatures

and constant light intensity and (2) varying intensity and constant temperature; the methods of analysis were as before and the results are shown in Tables 36 and 37.

Gauge sensitivity = 0.0870 mm./div.
Volume of reaction space = 27.2 ml.

Table 36 (1) Decomposition at varying temperatures

Temperature °C.		32	25.5		16.5		6.5	
Time min.	Log(t-1)	Press. divs.	Log(t+1)	Press. divs.	Log(t+2)	Press divs.	Log(t+10)	Press divs.
0								
20	1.279	47.5	1.322	41.0	1.342	32.5	1.477	32.0
40	1.591	74.5	1.613	60.5	1.623	55.0	1.699	50.0
60	1.771	90.0	1.785	73.0	1.792	68.5	1.845	62.0
80	1.898	101.5	1.909	82.0	1.914	78.0	1.954	71.0
100	1.996	110.0	2.004	88.5	2.009	86.0	2.041	78.5
120	2.076	116.5	2.083	93.5	2.086	92.0	2.114	84.5
140	2.143	121.5	2.149	98.5				
160	2.201	126.0	2.207	102.5	2.207	101.5	2.230	93.5
180	2.253	129.5						
200	2.300	133.0	2.303	109.0	2.305	109.0	2.322	101.0
240			2.382	114.0	2.382	115.0		

Table 37 (2) Decomposition with varying intensity

Intensity		0.86	0.62		0.38	
Time min.	log(t+3)	Press divs.	log(t+12)	Press. divs.	log(t+11)	Press. divs.
0		0		0		0
20	1.362	38.5	1.505	27.5	1.491	15.0
40	1.633	61.5	1.716	47.0	1.708	32.5
60	1.799	75.5	1.857	60.5	1.851	45.0
80	1.919	86.5	1.964	70.5	1.959	54.0
100	2.013	94.5	2.049	78.0	2.045	61.0
120	2.090	101.0	2.121	85.0	2.117	67.5
140	2.155	106.5	2.182	90.5	2.179	72.5
160	2.212	111.0	2.236	96.0	2.233	77.0
180						
200	2.308	118.5	2.326	104.5	2.324	85.0
240	2.386	124.0	2.418		2.400	92.0
280					2.464	97.5
320					2.520	102.0

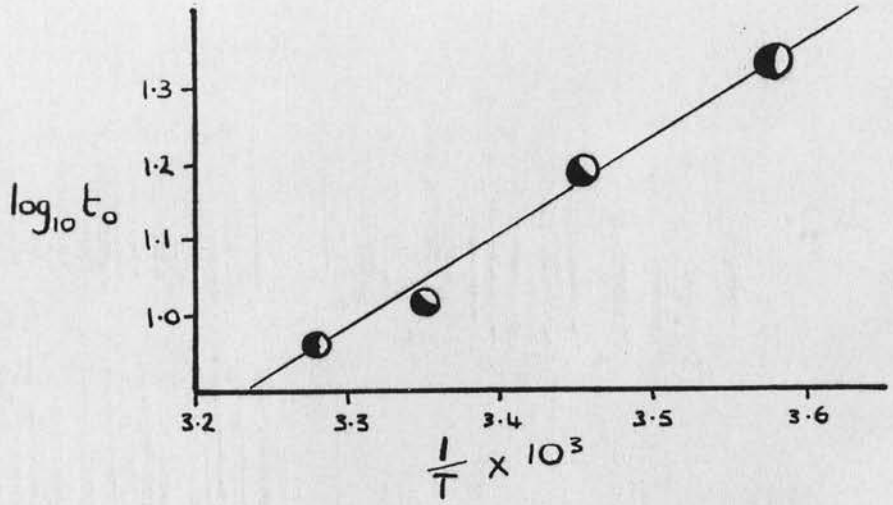
$\log_{10} t_0$
1·3
1·2
1·1
1·0
3·2
3·3
3·4
3·5
3·6
$\frac{1}{T} \times 10^3$

Fig. 41.

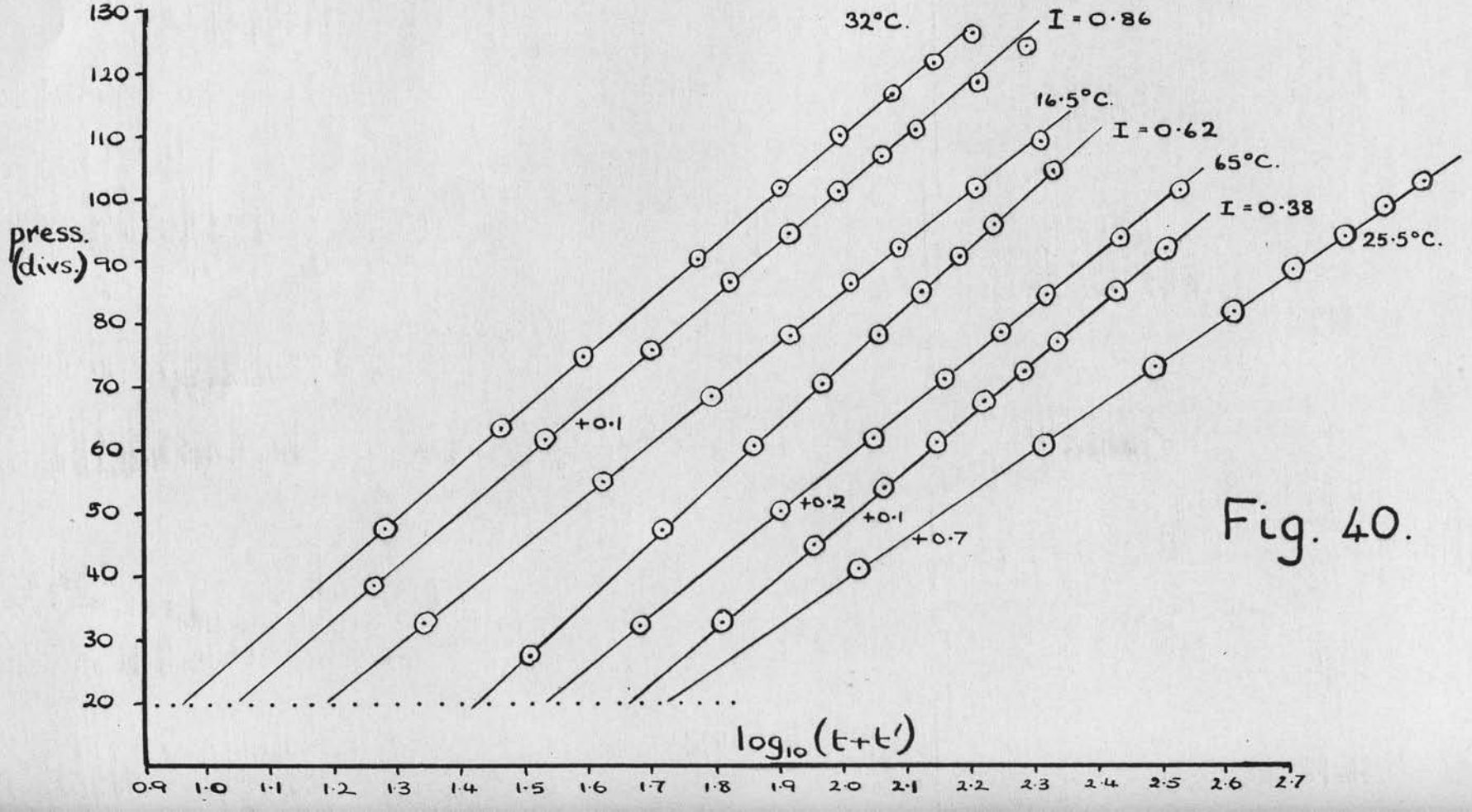
press. (divs.)
130
120
110
100
90
80
70
60
50
40
30
20
32°C.
I = 0·86
16·5°C.
I = 0·62
65°C.
I = 0·38
25·5°C.
+0·1
+0·2
+0·1
+0·7
$\log_{10}(t+t')$
0·9
1·0
1·1
1·2
1·3
1·4
1·5
1·6
1·7
1·8
1·9
2·0
2·1
2·2
2·3
2·4
2·5
2·6
2·7

Fig. 40.

From the p - log(t + t') plots (fig.40) it can be seen that α is approximately constant whereas t_o (obtained from the plots at p = 20 divs.) increased with both decreasing light intensity and decreasing temperature.

Table 38

Temp. A	1/T x 10^3	α x 10^2	Log t_o
305	3.279	2.69	0.96
298.5	3.350	3.31	1.02
289.5	3.454	2.87	1.19
279.5	3.577	2.81	1.33

Table 39

Intensity (I)	α x 10^2	t_o	It_o
1.0	3.31	10.5	10.5
0.86	2.69	14	12.0
0.62	2.48	26	16.0
0.38	2.68	36	14.0

From fig. 41 it can be seen that the plot of log t_o - 1/T is a reasonable straight line of slope 1.3 x 10^3, giving an activation energy of the order of 6 K cals./mole. Also in the table the It_o values are approximately constant, i.e. the reciprocal of t_o is approximately proportional to the incident light intensity. Thus although the reproducibility of these experiments was poor, the results on the whole conform to the general pattern as was observed with the 'thick' films.

Effect of water vapour on the decomposition

Two decompositions of 'thin' films were performed using the full light of the lamp. The first under normal conditions, the second in the presence of 8.2 mm. of water vapour. The results were analysed in the usual way and are shown in Table 40.

Gauge sensitivity = 0.0470 mm./div.

Volume of reaction space = 37.4 ml.

Fig. 43.

Effect of water vapour on photochemical decomposition.

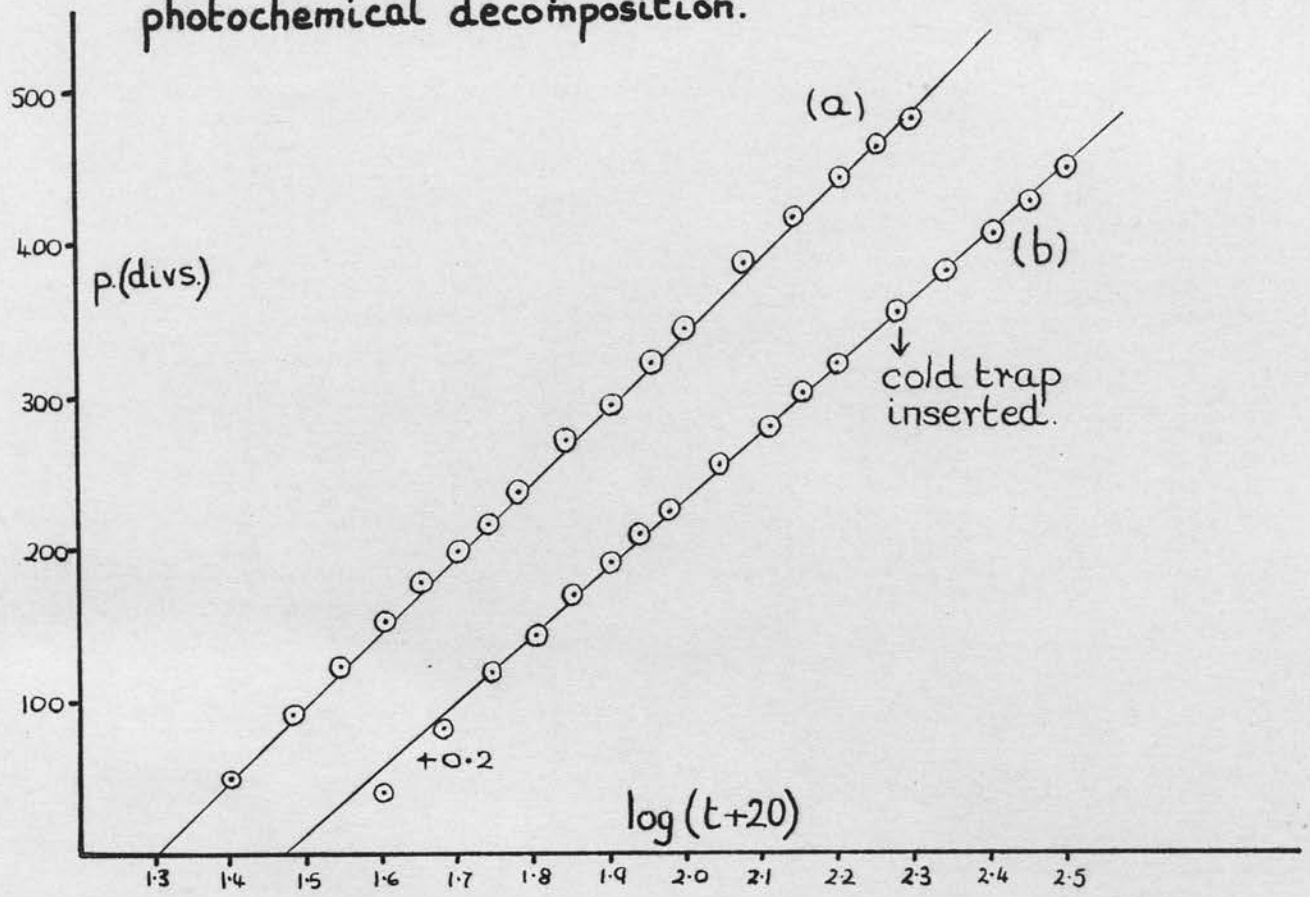

Fig. 42.

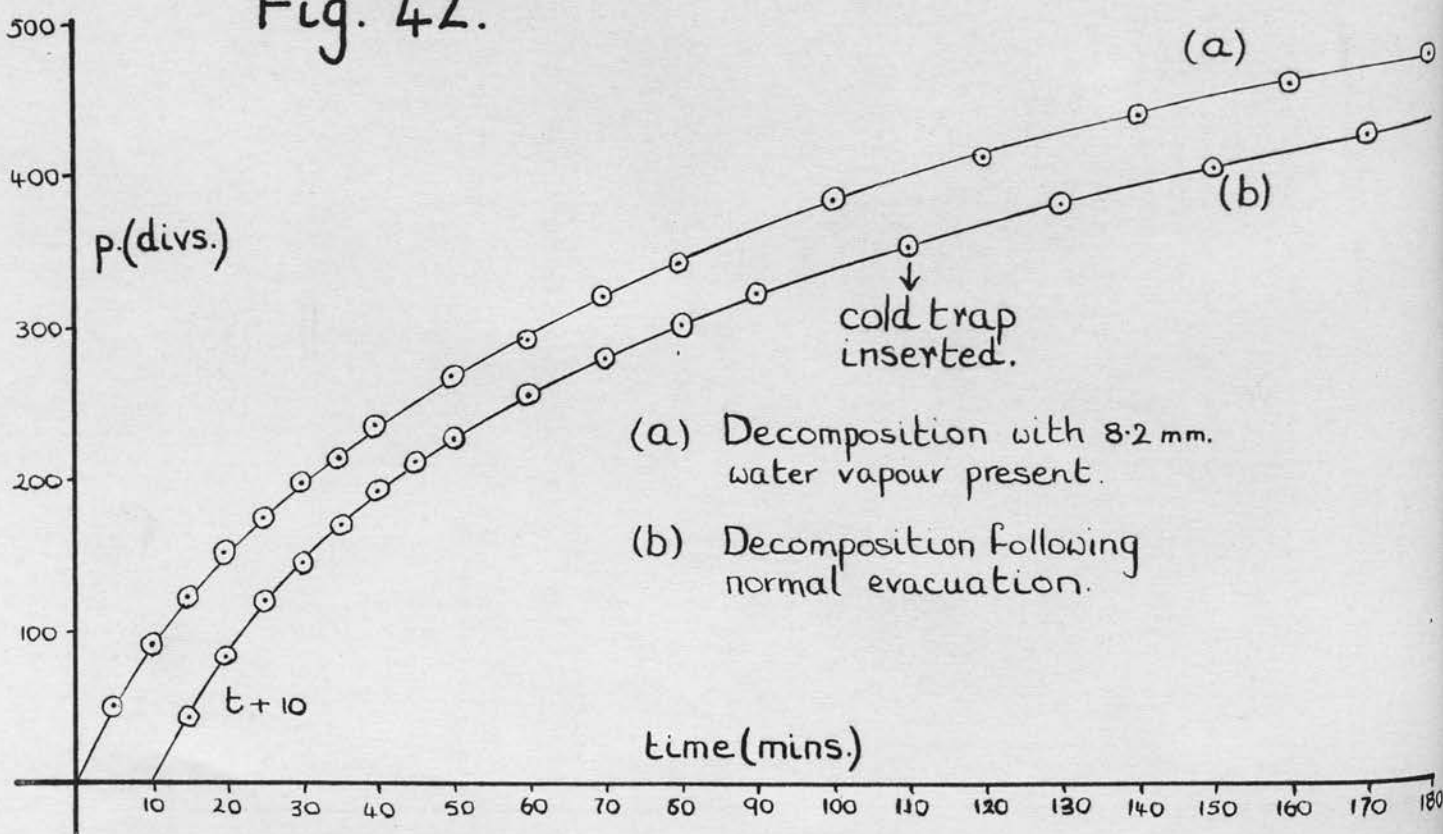

Table 40

Conditions	Normal		+ H_2O vapour
Time min.	Pressure divs.	Log(t + 20)	Pressure divs.
0	0		0
5	42.5	1.398	49.5
10	83.0	1.477	90.0
15	119.5	1.544	121.5
20	144.5	1.602	151.0
25	170.0	1.653	175.5
30	192.0	1.699	198.0
35	210.5	1.740	215.5
40	226.0	1.778	236.0
50	255.0	1.845	267.5
60	279.5	1.903	293.0
70	301.0	1.954	320.0
80	320.0	2.000	342.0
100	351.5	2.079	384.0
120	381.0	2.146	414.0
140	404.5	2.204	438.5
160	426.0	2.255	459.5
180	447.0	2.301	478.0

For purposes of comparison the t_o values were obtained from the p - log(t +t') plots at p = 0 (fig. 43).

Table 41

Conditions	t' min.	α x 10^3	t_o
8.2 mm. H_2O vapour	20	4.70	20
normal	20	4.85	18.5

The value of α and t_o above show an excellent agreement. Also, as a confirmation of these results, at time = 100 min. in the experiment performed under normal conditions, a trap near the reaction vessel was surrounded by a cardice acetone mixture; this

removed any small amounts of water vapour formed during the reaction. As can be seen from the p - log(t + t') plots this treatment did not significantly alter the subsequent kinetics of the decomposition. Thus from these results the presence of small amounts of water vapour had no appreciable effect on the decomposition.

Quantum efficiency

Blue light of wave-length 4360 Å was used. A circular aperture in the reaction vessel thermostat jacket limited the area of the incident beam so that all of the beam fell on the rear face of the reaction vessel. A barrier type photo cell in series with a standard mirror galvanometer and scale was used to measure the relative transmitted light intensities. 'Thin' films were made up in the usual way with quantities of the oxalate from 1.5 mg. up to 25 mg.

Using the reaction vessel as an uranyl oxalate actinometer (52) the number of quanta of wave-length 4360 Å entering the solution was measured. A correction for the interface reflection gave the quanta incident on the rear face of the reaction vessel when empty. Two measurements were made and the results are shown below.

1. Normality of potassium permanganate solution = 0.0986 N.

   Normality of uranyl oxalate solution = 0.0998 N.

   Initial volume of oxalate solution = 11.93 ml. ≡ 12.08 ml. of permanganate solution

   After illumination, vol.of permanganate solution required = 10.96 ml.

Therefore oxalate decomposed ≡ 1.12 ml. of 0.0986 N $KMnO_4$ soln.

Time of illumination = 2.3×10^4 sec.

Cell filled with	H_2O	Oxalate soln.	Empty
Galvanometer deflection (divs.)	30.0	23.1	24.6

$$\text{Quantum efficiency} = 0.6 = \frac{0.5 \times 1.12 \times 0.0986 \times 6.02 \times 10^{23} \times \frac{24.6}{30.0}}{I \times 1000 \times \left(1 - \frac{23.1}{30.0}\right) \times 2.3 \times 10^4}$$

Therefore the intensity incident on the rear face of the reaction vessel (I) = 8.8×10^{15} quanta/sec.

2. Vol. of oxalate decomposed ≡ 11.74 - 10.32 ml. = 1.42 ml. of 0.0986 N-$KMnO_4$

Cell filled with	H_2O	Oxalate soln.	Empty
Galvanometer deflection (divs.)	28.9	22.5	24.0

Time of illumination = 2.844×10^4 sec.

$$\text{Therefore } I = \frac{0.5 \times 1.42 \times 0.0986 \times 6.02 \times 10^{23} \times \frac{24.0}{28.9}}{2.844 \times 0.6 \times 1000 \times \left(1 - \frac{22.5}{28.9}\right) \times 10^4}$$

$$= 9.1 \times 10^{15} \text{ quanta/sec.}$$

Therefore Average I = 9.0×10^{15} quanta/sec.

To allow for the reflection of the film itself, the relative values of the intensity of light transmitted, of wave-length 5790 Å

were taken with and without the film on the reaction vessel. At this wave-length ferric oxalate does not absorb light appreciably so that the fraction of light reflected could be calculated. Although the reflection of the film was not necessarily the same at both wave-lengths, the value obtained should serve an an approximation. The results are shown below.

Weight of film = 25.8 mg.

Reaction vessel with		water	film	empty
Galvanometer deflection (divs.)	4360 Å	48.6	14.3	40.7
	5790 Å		27.8	33.8

Fraction of light absorbed and reflected $= 1 - \frac{14.3}{40.7} = 0.649$

Fraction of light reflected $= 1 - \frac{27.8}{33.8} = 0.177$

Therefore fraction of light absorbed = 0.472

Maximum rate of evolution of CO_2 = 1.50 divs./min. in a reaction vessel of 32.9 ml. and with a gauge sensitivity of 0.0305 mm./div.

Therefore rate of decomposition $= \frac{1.50 \times 273 \times 0.0305 \times 32.9 \times 6.02 \times 10^{23}}{60 \times 299 \times 760 \times 22400}$ molecules/sec.

$= 8.1 \times 10^{14}$ molecules/sec.

Quantum efficiency $= \frac{8.1 \times 10^{14}}{9.0 \times 10^{15} \times 0.472}$

$= 0.19$

Results for different weights of film were obtained in an exactly similar way and are shown in Table 42.

Fig. 45. Temperature effect on the dark reaction.

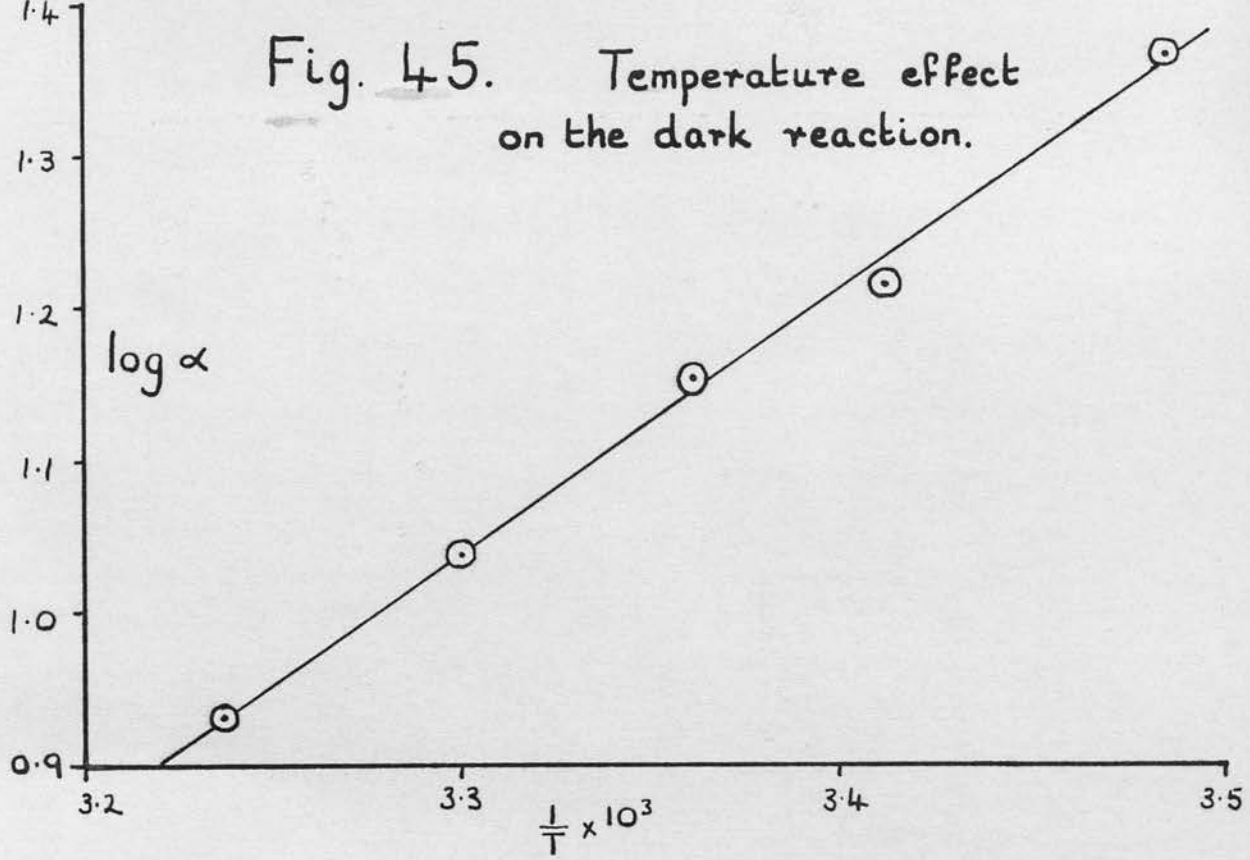

Fig. 44.

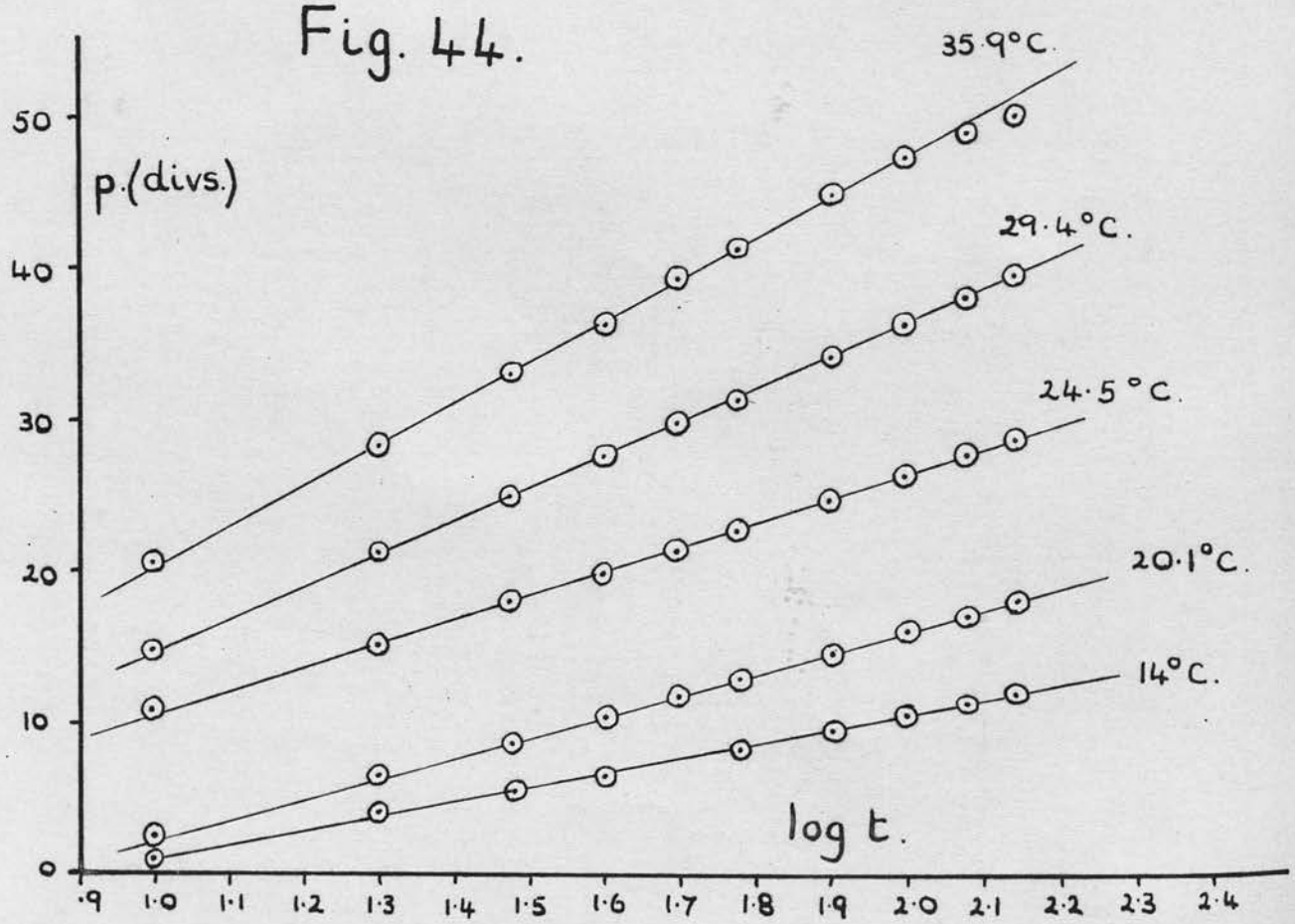

Table 42

Weight mg.	Rate of decomposition	Light absorbed and reflected	Light reflected	Light absorbed	Quantum efficiency
25.8	8.1×10^{14}	0.649	0.177	0.472	0.19
10.0	7.1×10^{14}	0.506	0.134	0.372	0.21
5.0	4.4×10^{14}	0.297	0.100	0.197	0.25
1.5	3.7×10^{14}	0.179	0.040	0.139	0.30

Thus the quantum efficiency increases with decreasing thickness of the film giving a limiting value of approximately 0.35.

Reaction after cessation of illumination

After the illumination ceased a pressure increase was observed which continued at a steadily decreasing rate.

It was found that the results were expressed by the equation $\alpha p = \log t + k$ (fig. 44) where p is the pressure developed in time t for the dark reaction and α and k are constants. Thus the kinetics of the reaction are similar to those for the photo decomposition of the film. However, in contrast to the latter experiments, on re-examining the dark reaction at a higher temperature, it was found that the value of α had altered. Thus to investigate the change in α with temperature the following procedure was adopted. The film, 10 mg. in weight, was decomposed for 18 min. at 24.5°C. by the full light, which was then removed and the temperature rapidly adjusted to that required. This method ensured that the photodecomposition prior to the dark reaction was approximately the same for each determination. If

this was not so the determination was repeated. The results are shown in Table 43.

Table 43

Temperature °C.		35.9	29.4	24.5	20.1	14.0
Time min.	$Log_{10}t$	Pressure divs.	Pressure divs.	Pressure divs.	Pressure divs.	Pressure divs.
		Photodecomposition at 24.5°C.				
0		0	0	0	0	0
5		13.1	12.6	14.3	14.3	15.2
10		33.2	30.7	34.1	33.8	37.2
15		50.8	49.5	49.7	49.2	48.9
18		60.3	59.5	57.1	57.2	56.8
		Dark reaction				
0						
10	1.000	20.4	14.8	10.8	2.5	1.0
20	1.301	28.2	21.2	15.1	6.6	4.1
30	1.477	33.0	25.0	18.0	8.7	5.5
40	1.602	36.2	27.6	19.9	10.5	6.6
50	1.699	39.3	29.8	21.4	11.9	
60	1.778	41.2	31.3	22.8	13.0	8.4
80	1.903	44.7	34.2	24.8	14.7	9.7
100	2.000	47.2	36.3	26.3	16.3	10.7
120	2.079	48.8	38.0	27.7	17.2	11.5
140	2.146	50.0	39.5	28.7	18.2	12.1

The values of α obtained from the p - log t plots were corrected to correspond to a temperature 24.5°C. for the gases in the reaction space as before and are shown in Table 44.

Table 44

Temperature °A	1/T x 10^3	α x 10^2	Corr. α x 10^2	Log Corr. α + 2
308.9	3.237	8.41	8.55	0.932
303.0	3.300	10.76	10.9	1.037
297.5	3.361	14.2	14.2	1.152
293.2	3.411	16.4	16.3	1.215
287.0	3.484	23.5	23.0	1.362

From the plot of log α - 1/T (fig. 45) the slope of the line is 1.75 x 10^3 ± 5%, α is associated with an activation energy = 1.75 x 2.303 x 1.98 = 8.0 ± 0.4 K.cals./mole.

Unfortunately the methods employed do not give absolute values of the pressure and thus the effect of temperature on the constant k was not obtained.

The dark reaction was considered to be due to one of two processes or the combination of both:

(1) A slow diffusion of gas out of the film following photo-decomposition.

(2) The slow decomposition of some metastable excited state, formed during the photodecomposition.

To investigate the possibility of the formation of an excited state, two experiments were performed. Firstly the effect of oxygen on the dark reaction was examined. Oxygen might be expected to deactivate excited states if they were present, particularly on the surface of the film, causing a considerable decrease in rate. This was not observed, the

reaction rate being unaffected by the introduction of 50 mm. of oxygen. Secondly a film of ferric oxalate was made between sodium chloride plates. This was then exposed to a high intensity projection lamp for five minutes and immediately its infra red absorption spectra examined. This was repeated with longer times of exposure until the film was green indicating considerable decomposition had taken place. The results are shown in Table 45. In the first column 1 is pure ferric oxalate, 2, 3 and 4 are the progressively decomposed samples. The frequencies are given in wave numbers, cm^{-1}.

Table 45

Sample						
1		1725-1575	1320 1270	920	800	730
2	2400	1700-1600	1320-1270	920	800	730 *
3	2400	1700-1600	1320-1270	920	800	730 *
4	2400	1630	1320		800	

* indicates a small peak

As can be seen from Table 45, no peaks which did not appear on the ferric or ferrous oxalate spectra were observed except that due to carbon dioxide. This suggests that the dark reaction is more probably associated with diffusion than with the decomposition of excited states produced in appreciable amounts as a result of illumination.

It would then be expected that a second illumination after the dark period would not immediately show the same rate of pressure increase as when the light was cut off, since the assumed diffusion

process must again be built up. This was found to be so; a second illumination following a period of examination of the dark reaction, showed initially an induction period, whether or not one had been evident in the first illumination. After this induction period the reaction continued at a rate in agreement with that expected from the first illumination and corresponded to the percentage decomposition given by the combined pressures of the primary photochemical and dark reaction. This applied to both 'thick' and 'thin' films.

---

3. THERMAL DECOMPOSITION

As measured by the pressure increase a sample of 10 mg. of ferrous oxalate was decomposed to less than 0.3% on heating at temperatures up to 150°C. for fourteen hours both in vacuo and in the presence of carbon dioxide.

The thermal decomposition of both forms of ferric oxalate was investigated between 70°C. and 140°C. and, as in the photochemical reaction, the products were carbon dioxide, ferrous oxalate and water. Columns 1, 2 and 3 in Tables 46 and 47 give the percentage decomposition as calculated from the pressure of carbon dioxide produced, the quantity of ferrous iron estimated photometrically and the quantity of ferrous iron calculated from the initial and final amounts of ferric iron respectively.

Table 46 Products for powder form of oxalate

Carbon dioxide %	Ferrous iron (1) %	Ferrous iron (2) %
90.9	90.0	90.4
88.0	91.2	90.0
86.5	84.9	84.5
86.2	83.8	86.0
65.4	64.2	66.5
54.9	58.0	56.5
30.0	31.4	31.0
20.1	21.0	22.1
1.3	2.3	1.6

Table 47 Products for recrystallised form

Carbon dioxide %	Ferrous iron(1) %	Ferrous iron(2) %	Carbon dioxide % from powder
* 66.5	74.5	75.0	90
60.3	78.9	77.7	80
56.8	76.5	77.0	78
40.2	51.5	53.0	52
21.1	29.0	30.2	27

From these tables it can be seen that, for the powder form of the oxalate, the ferrous oxalate and carbon dioxide were produced in approximately stoichiometric proportions. On the other hand the quantity of carbon dioxide produced from the recrystallised material was a constant fraction (≈ 0.75) of the ferrous iron formed except with (*) where the decomposition was continued for 24 hours. The others were decomposed for periods not exceeding 400 minutes. The fourth column in the table above is an estimate of the percentage decomposition given by the pressure of carbon dioxide which would be produced from the powder form under the same conditions and in the same time as the values quoted for

Fig. 46. Pressure-time curves for recrystallised samples.

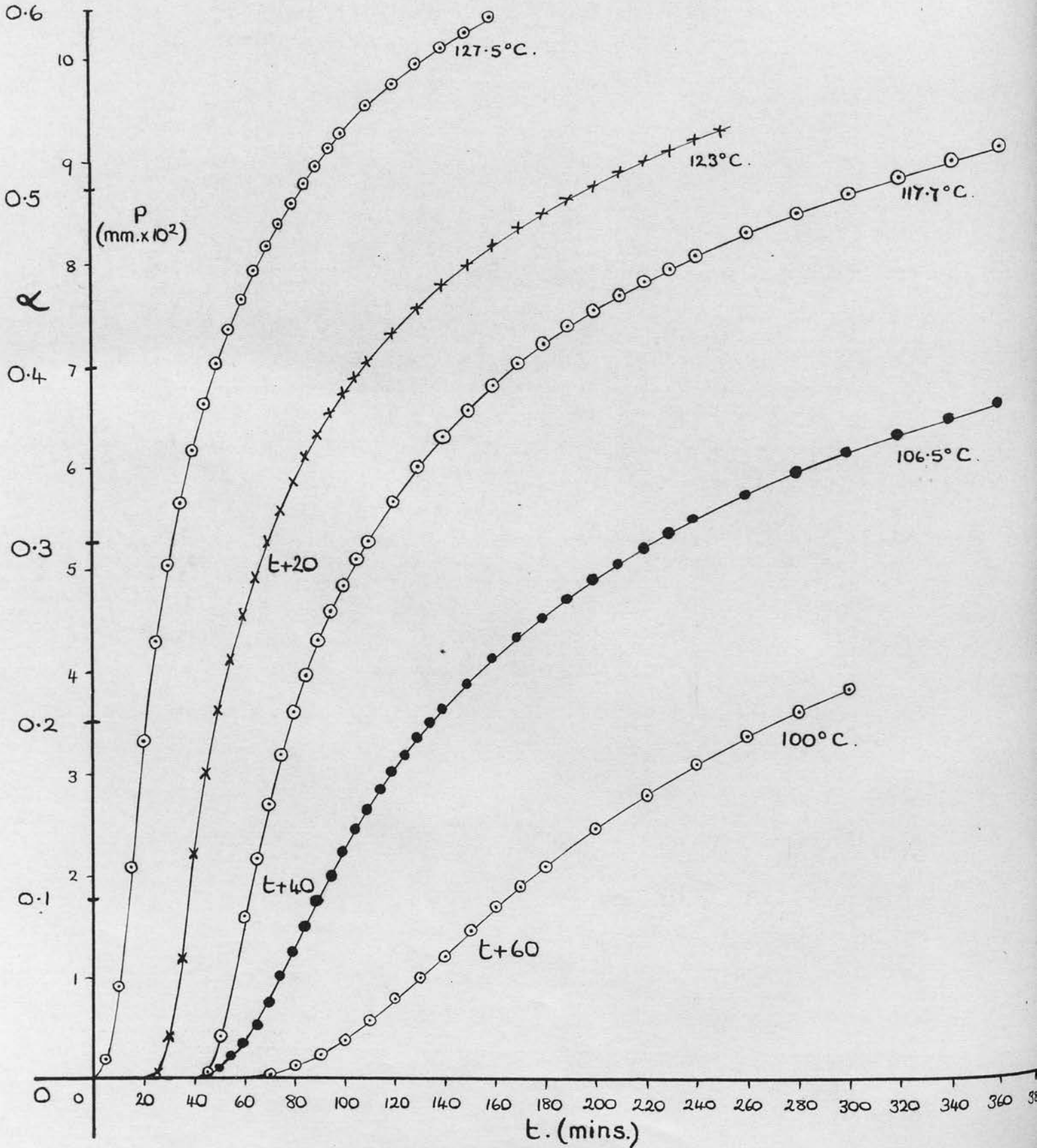

the recrystallised samples. They show an excellent agreement with the percentage decomposition calculated from the ferrous content and it seems probable that with the recrystallised samples the missing gas was retained in the material.

However, it was considered possible that the decomposition resulted in an intermediate compound which on exposure to oxygen in the atmosphere might decompose further to give the missing carbon dioxide and ferrous oxalate. If this occurred, then by the methods of analysis used the extent of decomposition as given by the ferrous content would be greater than that given by the carbon dioxide produced. To test this possibility, the recrystallised sample was decomposed in vacuo, allowed to cool and then exposed to 50 mm. oxygen. No significant uptake of oxygen or formation of carbon dioxide was observed. The experiment was repeated with 100 mm. oxygen with the same result. The formation of such an intermediate compound therefore was not supported by the experimental evidence.

Thus for both types of the oxalate it was probable that in the early stages, the rate of decomposition of the oxalate was given by the rate of production of carbon dioxide, however, particularly with the recrystallised form, this was not necessarily the case in the later stages of the reaction.

Visual examination of ferric oxalate

By means of sieves of known sizes, the greatest linear dimension of the particles used in the decompositions was found

Fig. 47. Pressure-time curves for powder samples.

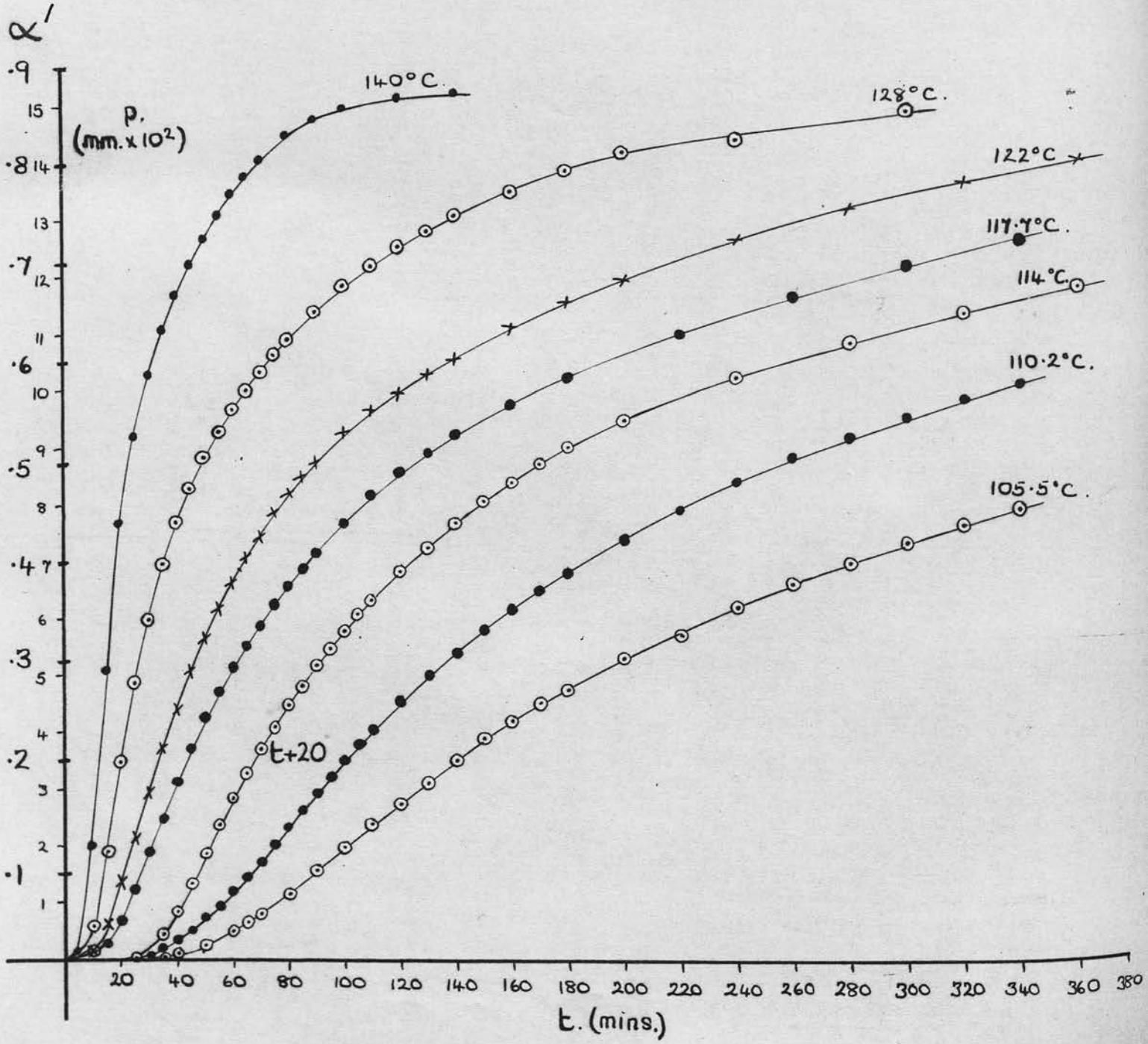

to be between 1/100" and 1/200", i.e. the average linear dimension was 1/150" or 1.7 x 10^{-2} cm. From an examination under the microscope it was seen that the particles in the powder form of the oxalate were approximately spherical, whereas the recrystallised form was comprised of thin flakes.

The density of ferric oxalate was estimated by suspending ferric oxalate particles in several fluids and observing in which one the particles remained suspended after standing for several hours. The specific gravity of this fluid was then the same as the density of ferric oxalate. Thus the density was found to be 2.28 g./cc.

Both the recrystallised and powder forms of the oxalate were examined on a hot stage microscope from room temperature up to 150°C. No physical change in the materials could be observed on decomposition except that the colour changed from yellow to green.

Kinetics of thermal decomposition

The pressure-time curves obtained from the decomposition of both forms of the oxalate were sigmoid in shape and are shown in figs. 46 and 47. α' in these diagrams is the theoretical degree of decomposition.

The recrystallised material gave decomposition results reproducible to within 5%. The powder results, however, with samples from a fresh preparation were about 10% faster than those when the preparation was a few days old. Thereafter the results

Fig. 48. Pressure-time curves for thermal decomposition of powder and recrystallised forms.

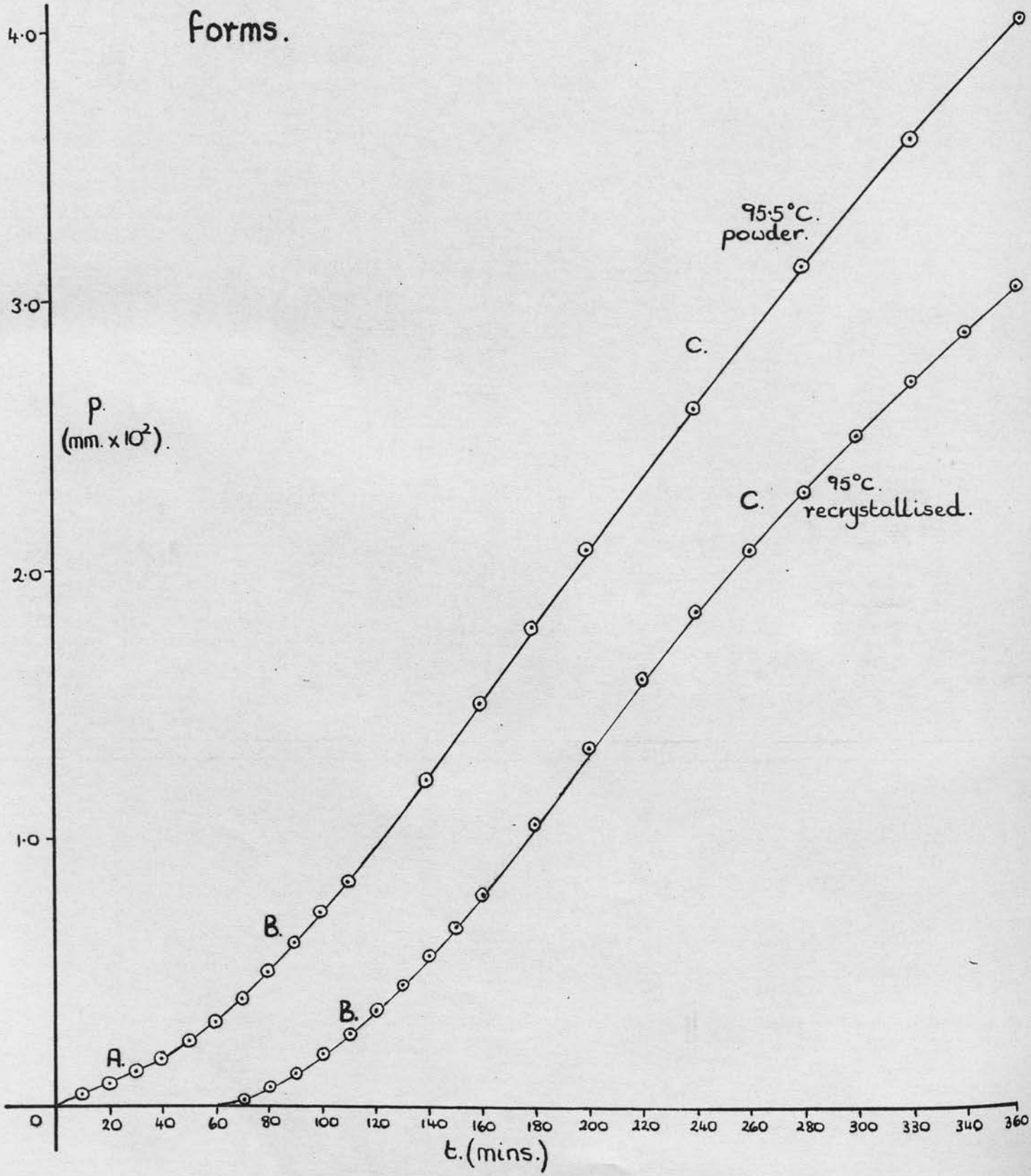

were of the same order of reproducibility as the recrystallised material.

For the powder form of the oxalate the decomposition was divisible into three stages (fig. 48):

(A) - a constant rate process up to 1% decomposition.

(B) - an acceleration stage up to 6% decomposition.

(C) - the decay stage for the rest of the decomposition.

For the recrystallised form no constant rate stage was detected at a temperature of 85°C. and the decomposition was thus comprised of two stages (fig. 48):

(B) - the acceleration stage up to 5% decomposition.

(C) - the decay stage for the rest of the decomposition.

In all the following experiments, the pressures quoted refer to 10 mg. of the oxalate and a temperature of 22°C. for the gases in the reaction space.

Constant rate stage (A) for decomposition of powder

To investigate this stage of the decomposition, the reaction was studied between 67°C. and 95°C. The results are shown in Table 48.

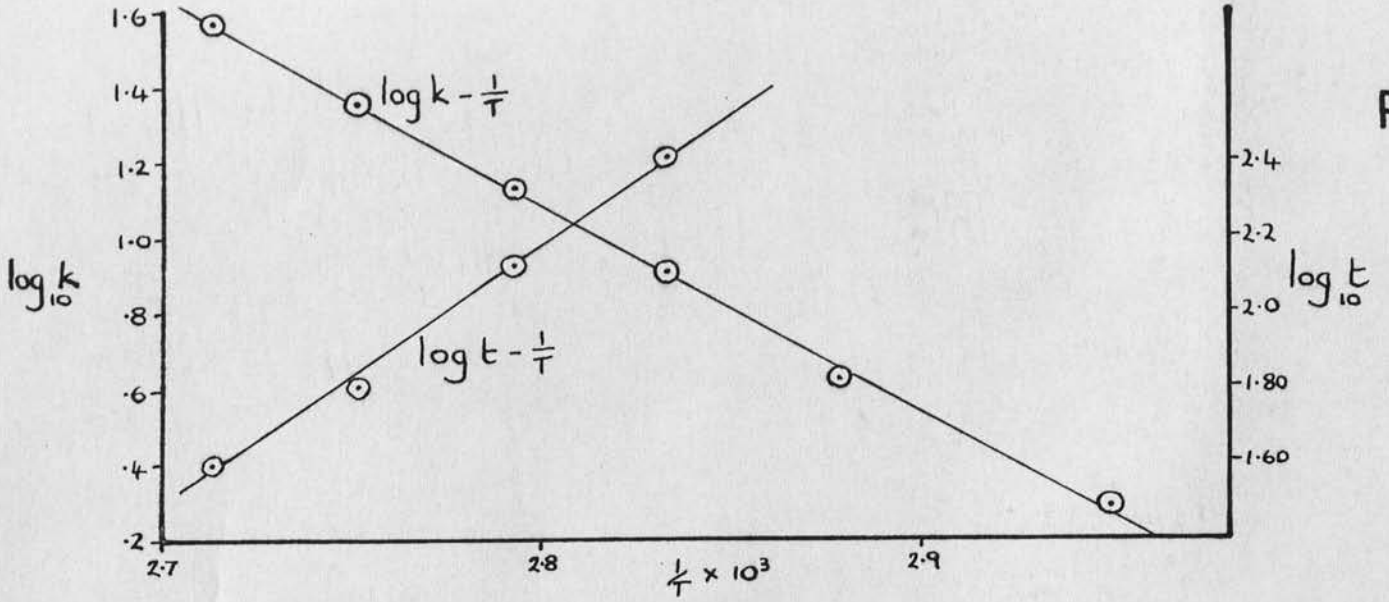
log k - 1/T
log t - 1/T
log k 10
log t 10
1/T x 10³
1·6
1·4
1·2
1·0
·8
·6
·4
·2
2·4
2·2
2·0
1·80
1·60
2·7
2·8
2·9

Fig. 50.

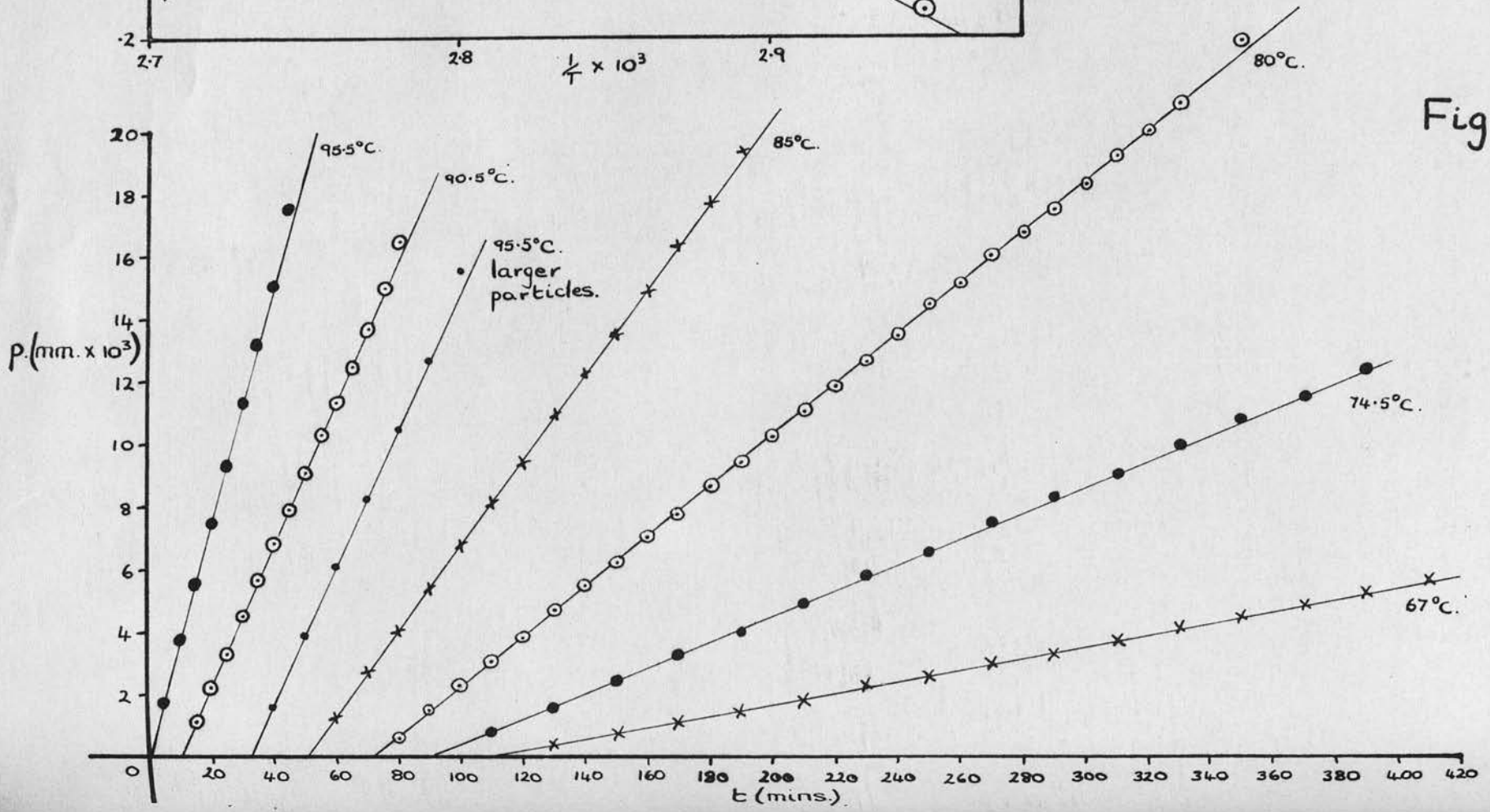
95·5°C.
90·5°C.
95·5°C.
larger
particles.
85°C.
80°C.
74·5°C.
67°C.
p.(mm. x 10³)
t (mins.)
0
2
4
6
8
10
12
14
16
18
20
40
60
80
100
120
140
160
180
200
220
240
260
280
300
320
340
360
380
400
420

Fig. 49.

Table 48 Volume of reaction space = 542 ml.

Temperature °C.	95.5	90.5	85.0	80.0	74.5	67.0
Time min.	Pressure mm.x10³	Pressure mm.x 10³	Pressure mm.x 10³	Pressure mm.x 10³	Pressure mm.x 10³	Pressure mm.x 10³
0	0	0	0	0	0	0
5	1.80	1.11				
10	3.83	2.23	1.29	0.65		
15	5.57	3.27				
20	7.45	4.51	2.75	1.55	0.80	0.35
25	9.34	5.64				
30	11.3	6.82	4.05	2.30		
35	13.2	7.93				
40	15.1	9.08	5.42	3.08	1.58	0.71
45		10.3				
50		11.3	6.85	3.91		
55		12.5				
60		13.7	8.15	4.68	2.41	1.12
65		15.0				
70		16.5	9.50	5.49		
80			10.95	6.25	3.25	1.45
90			12.3	7.09		
100			13.5	7.85	4.06	1.83
110			14.9	8.73		
120			16.4	9.52	4.92	2.31
130			17.8	10.3		
140			19.4	11.1	5.79	2.62
150				11.9		
160				12.7	6.54	3.00
170				13.5		
180				14.5	7.48	3.31
190				15.2		
200				16.1	8.28	3.80
210				16.8		
220				17.6	9.02	4.15
230				18.4		
240				19.3	9.97	4.54
250				20.1		
260				21.0	10.77	4.93
280					11.5	5.30
300					12.4	5.65

Fig. 51. Pressure-time curve for acceleration stage for recrystallised form.

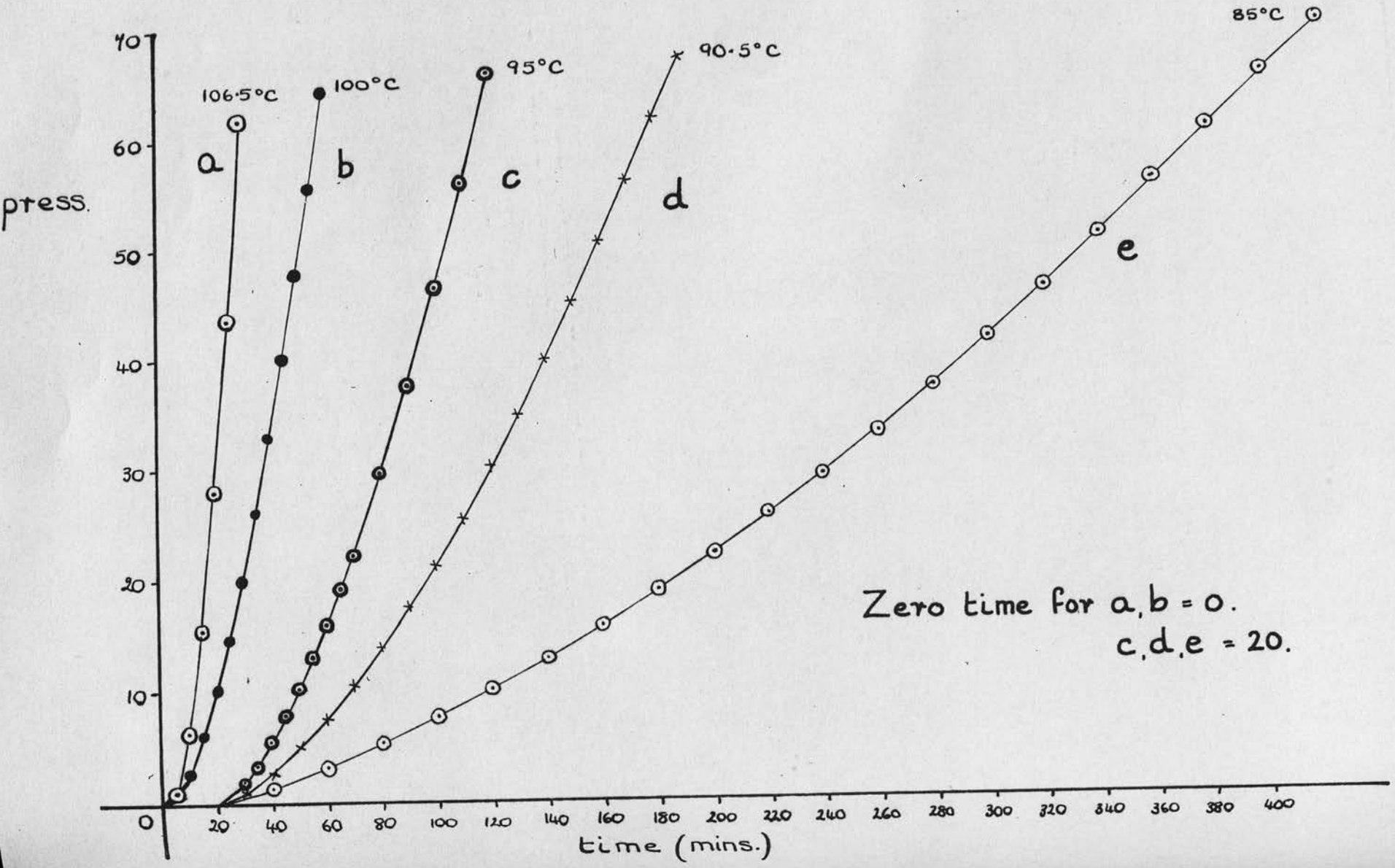

From the pressure time plots (fig. 49) it can be seen that at p = 0, t = 1-2 minutes, i.e. the sample was taking one to two minutes to reach the temperature of the reaction.vessel. This is in agreement with the time estimated previously (p. 34).

The rate constants (k) and the ~~times~~ durations λ(t) of the constant rate stage with the corresponding temperatures are shown in Table 49.

Table 49

Temperature °A	1/T x 10^3	k mm./min. x 10^5	Log k + 5.0	t min.	Log t
368.5	2.713	37.5	1.574	40	1.60
363.5	2.751	22.8	1.358	65	1.81
358.0	2.793	13.6	1.134	135	2.13
353.0	2.833	8.1	0.909	260	2.42
347.5	2.878	4.2	0.623		
340.0	2.941	1.9	0.279		

From the straight line plots of log k - 1/T and log t - 1/T (fig. 50), the slopes of the lines are 5.70 x 10^3 ± 5% and 7.2 x 10^3 ± 10%. Thus the activation energy for the process is 5.7 x 1.98 x 2.303 K.cals./mole = 26.2 ± 1.3 K.cals./mole. and the activation energy associated with the duration of the process = 7.2 x 2.303 x 1.98 K.cals./mole = 32.8 ± 3.3 K.cals./mole.

Acceleration stage (B)

This stage of the reaction was investigated at temperatures between 80°C. and 106°C. The pressure-time curves for both forms of the oxalate were similar and fig. 51 shows the shape of those

Fig. 52.

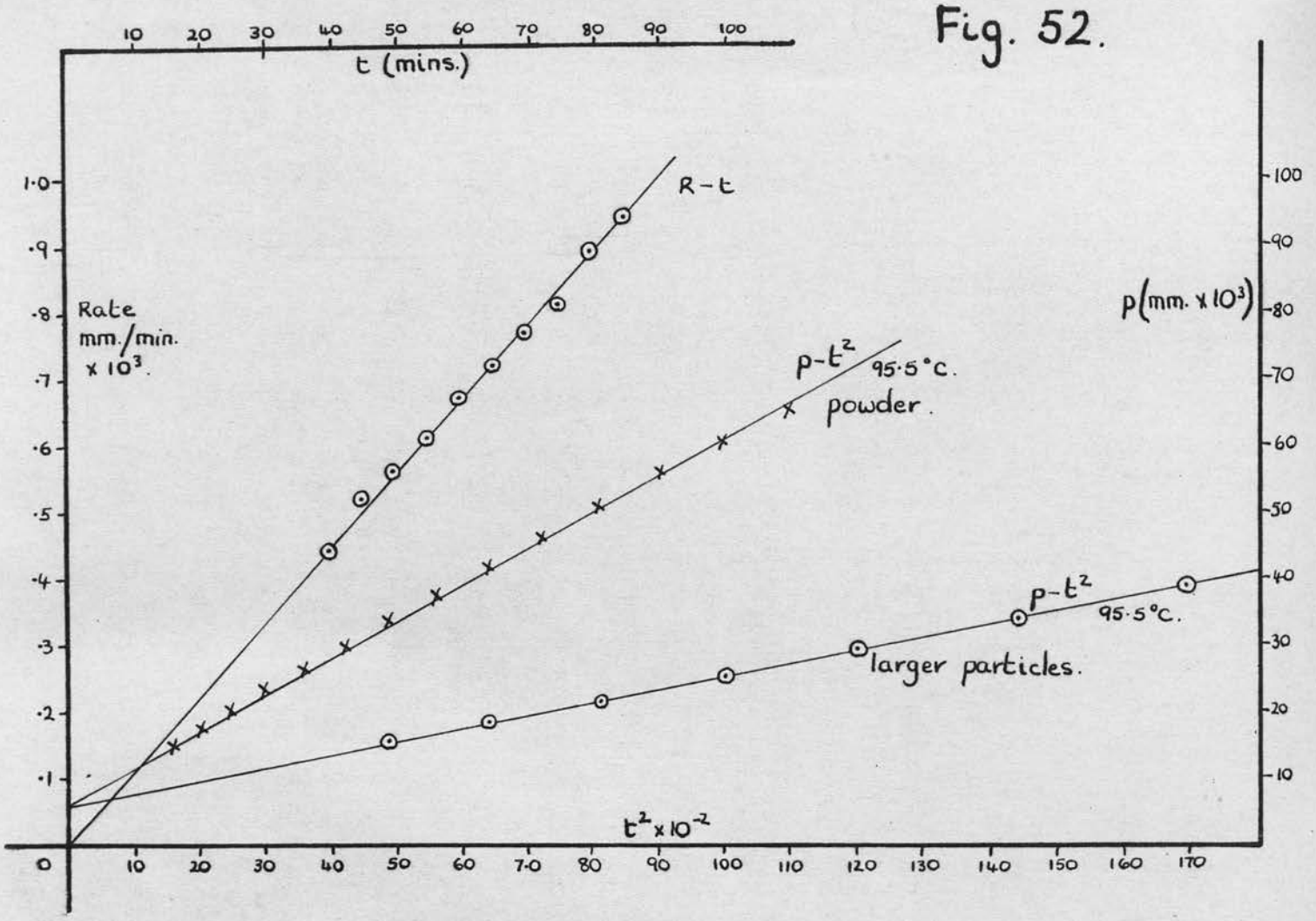
t (mins.)
R-t
Rate mm./min. x 10³.
p-t² 95·5°C. powder.
p-t² 95·5°C. larger particles.
p (mm. x 10³)
t² x 10⁻²

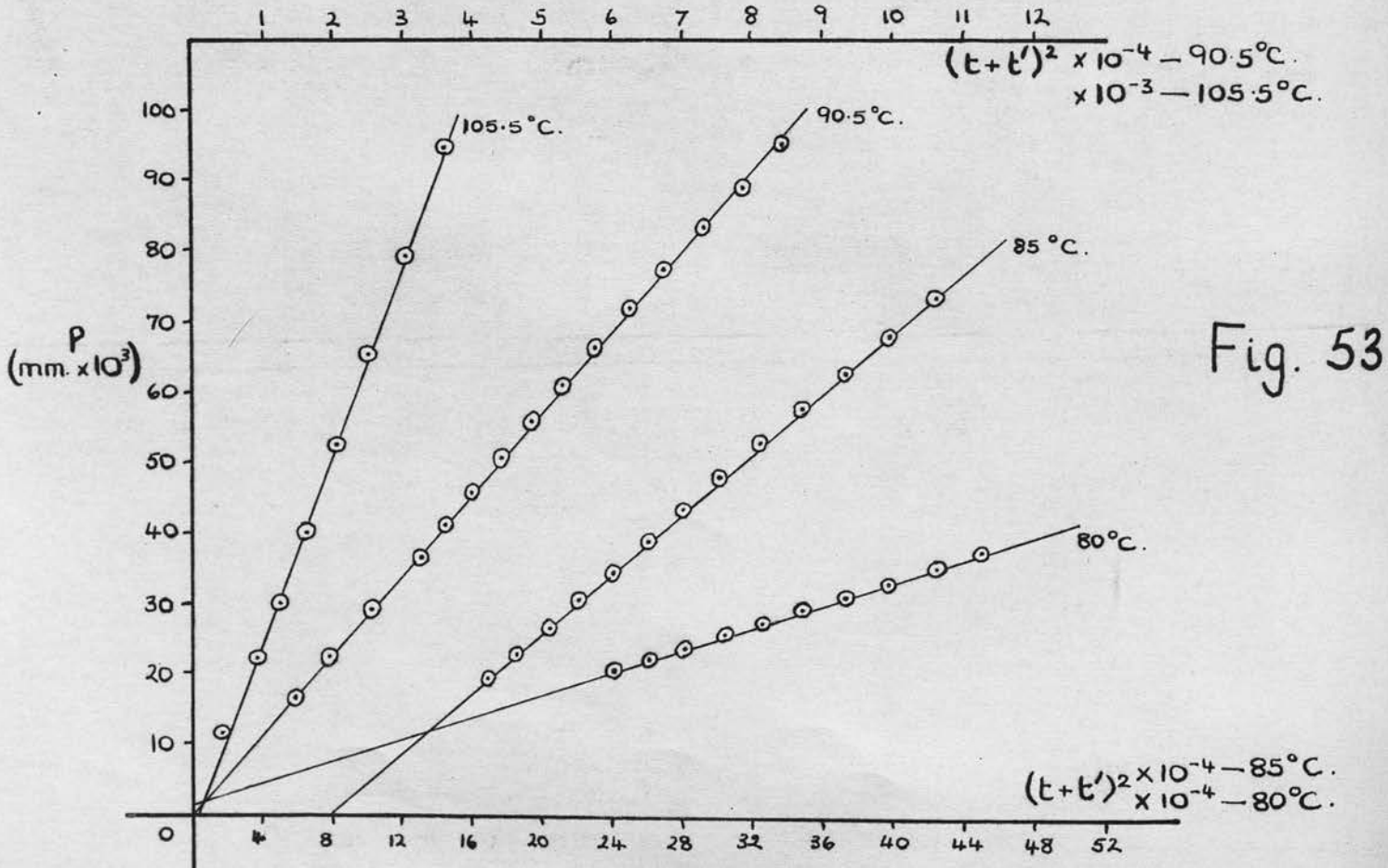
(t+t')² x 10⁻⁴ — 90·5°C.
x 10⁻³ — 105·5°C.
105·5°C.
90·5°C.
85°C.
80°C.
P (mm. x 10³)
(t+t')² x 10⁻⁴ — 85°C.
x 10⁻⁴ — 80°C.

Fig. 53.

obtained with the recrystallised material.

Again for both forms of the oxalate, rates of decomposition measured from the pressure-time curves, were found to be linear with time(fig. 52). Thus an equation of the form:

$p + p' = k(t + t')^2$ where p', t' and k are constants

(figs. 52, 53 and 54) describes the results for this stage of the reaction. The values of t' were obtained by extrapolation of the dp/dt - t plots to dp/dt = 0. A typical analysis of one such experiment is shown in Table 50.

Table 50 Acceleration stage for powder at 95.5°C. Volume of reaction space = 542 ml.

Time(t) min.	Pressure mm. x 10^3	Rate mm./min. x 10^4	t^2 min.^{2} x 10^{-2}
40	15.1	4.4	16.0
45	17.6	5.2	20.3
50	20.3	5.6	25.0
55	23.3	6.1	30.3
60	26.5	6.7	36.0
65	29.9	7.2	42.3
70	33.8	7.7	49.0
75	37.6	8.1	56.3
80	41.8	8.9	64.0
85	46.5	9.4	72.3
90	51.2	9.8	81.0
95	56.3	9.5	90.3
100	60.7	9.2	100
105	65.5	9.8	110.3
110	70.5		

Similarly values of t' were obtained for the other decompositions and the results for both forms of the oxalate are shown in Tables 51 and 52.

Table 51 Powder form of oxalate (figs. 52, 53)

Temperature °C.	105.5		90.5		85.0		80.0	
Time min.	$t^2 \times 10^{-2}$	Press. mm. x 10^3	$(t+50)^2 \times 10^{-4}$	Press. mm. x 10^3	$(t+270)^2 \times 10^4$	Press. mm. x 10^3	$(t+230)^2 \times 10^{-4}$	Press. mm.x 10^3
0		0						
20	4.0	11.5						
30	9.0	22.2						
35	12.3	30.0						
40	16.0	40.0						
45	20.3	52.7						
50	25.0	65.6						
55	30.3	79.6						
60	36.0	94.7						
70			1.44	16.5				
80			1.69	19.3				
90			1.96	22.3				
100			2.25	25.6				
110			2.56	29.0				
120			2.89	32.8				
130			3.24	36.7				
140			3.61	41.0	16.8	19.4		
150			4.00	45.7				
160			4.41	50.7	18.5	22.9		
170			4.84	55.8				
180			5.29	61.1	20.3	26.7		
190			5.76	66.5				
200				71.9	22.1	30.7		
210				77.6				
220				83.5	24.0	34.7		
230				89.3				
240				95.2	26.0	39.0		
260					28.1	43.5	24.0	21.0
280					30.3	48.2	26.0	22.5
300					32.5	53.0	28.1	24.2
320					34.8	57.8	30.3	26.0
340					37.2	62.8	32.5	27.8
360					39.7	68.1	34.8	29.7
380					42.3	73.5	37.2	31.6
400							39.7	33.5
420							42.3	35.6
440							44.9	37.8

Table 52 Recrystallised form of oxalate (fig. 54).

Temperature °C.	106.5		100.0		95.0	
Time min.	t^2	Press. mm.x 10^3	$(t+12)^2$ x 10^{-2}	Press. mm.x 10^3	$(t+40)^2$ x 10^{-3}	Press. mm.x 10^3
0	0	0		0		
5	25	0.82	2.89	0.41		
10	100	6.34	4.84	2.63	2.5	1.32
15	225	15.4	7.29	6.04		
20	400	28.0	10.2	10.00	3.6	5.50
25	625	43.5	13.7	14.8		
30	900	61.8	17.6	20.0	4.9	10.2
35			22.1	26.1		
40			27.0	32.8	6.4	16.0
45			32.5	40.0		
50			38.4	47.7		
60					10.0	29.7
70					12.1	37.5
80					14.4	46.4
90					16.9	55.9
100					19.6	65.9

Fig. 55.

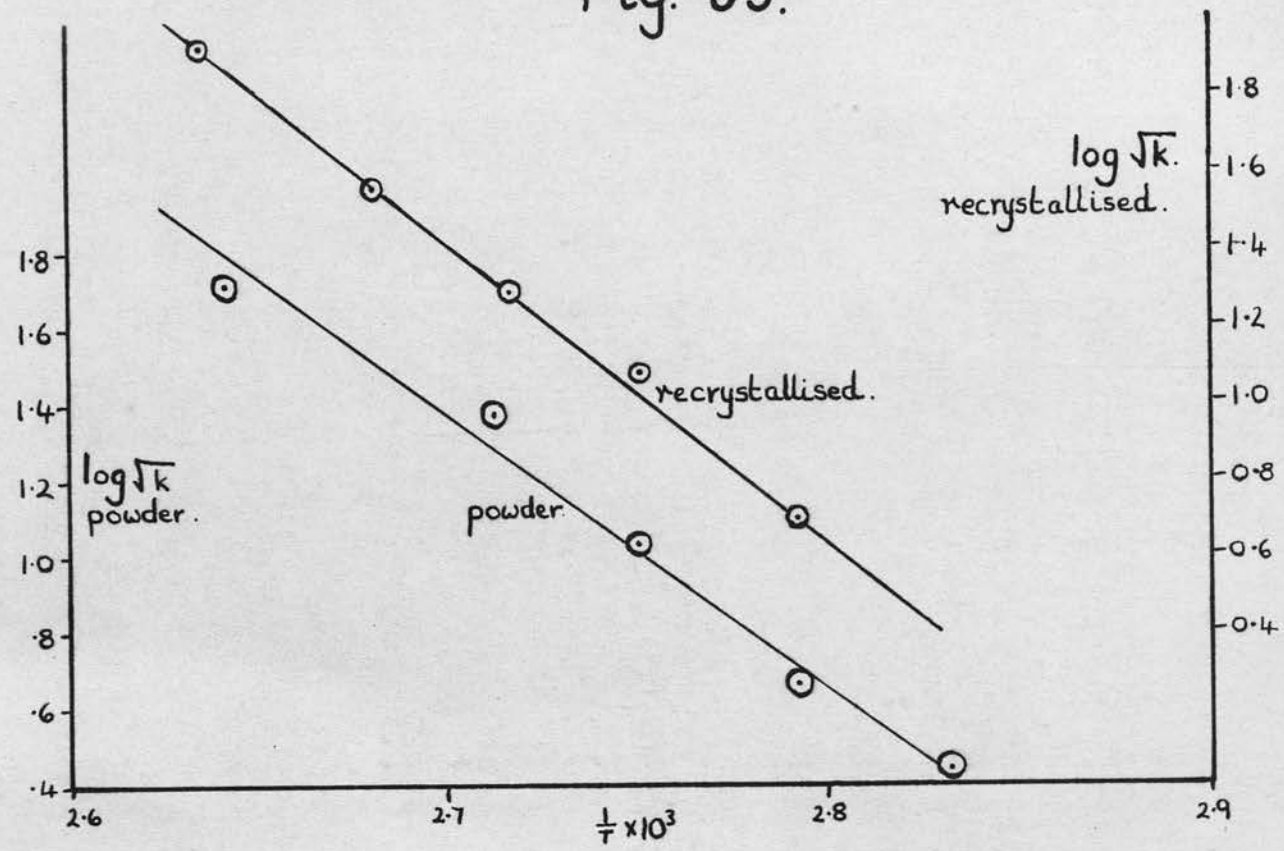
log √k.
recrystallised.
recrystallised.
log √k
powder.
powder.
1·8
1·6
1·4
1·2
1·0
·8
·6
·4
2·6
2·7
2·8
2·9
1/T x10³

Fig. 54.

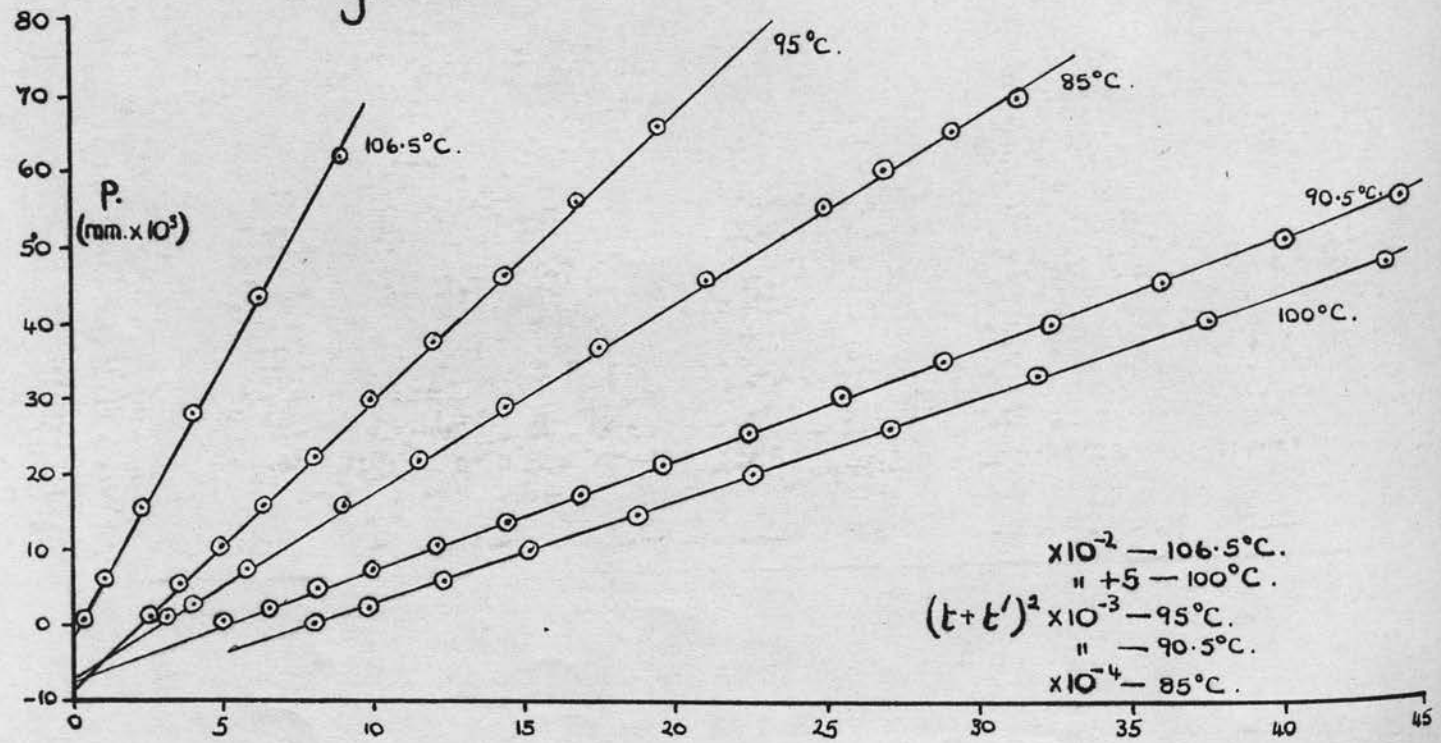
P.
(mm. x 10³)
106·5°C.
95°C.
85°C.
90·5°C.
100°C.
x10⁻² — 106·5°C.
" +5 — 100°C.
(t+t')² x10⁻³ — 95°C.
" — 90·5°C.
x10⁻⁴ — 85°C.
80
70
60
50
40
30
20
10
0
-10
0
5
10
15
20
25
30
35
40
45

Table 52 continued

Temperature °C.	90.5		85.0		85.0		
Time min.	$(t+60)^2 \times 10^{-3}$	Press. mm.x 10^3	$(t+160)^2 \times 10^{-4}$	Press. mm.x 10^3	Time min.	$(t+160)^2 \times 10^{-4}$	Press. mm. x 10^3
0		0					
10	4.9	0.80			160	10.2	18.8
20	6.4	2.63	3.24	1.21	180	11.6	22.0
30	8.1	5.00			200	13.0	25.5
40	10.0	7.51	4.00	3.13	220	14.4	29.0
50	12.1	10.50			240	16.0	32.8
60	14.4	13.9	4.84	5.28	260	17.6	36.9
70	16.9	17.4			280	19.4	41.3
80	19.6	21.2	5.76	7.60	300	21.2	45.8
90	22.5	25.5			320	23.0	50.4
100	25.6	30.1	6.76	10.0	340	25.0	55.3
110	28.9	34.8			360	27.0	60.1
120	32.4	39.9	7.84	12.7	380	29.2	65.1
130	36.1	45.1			400	31.4	69.6
140	40.0	50.5	9.00	15.7			
150	44.1	56.0					

To obtain the activation energies for the acceleration process of the two forms the log of the linear growth constant, i.e. $\sqrt{k}$ was plotted against 1/T.

Table 53 Powder form.

Temperature °A	$1/T \times 10^3$	$k \times 10^8$ mm./sec.^{2}	$\sqrt{k} \times 10^4$	$\text{Log}_{10} \sqrt{k} + 4.0$
378.5	2.642	2710	52.1	1.717
368.5	2.713	550	23.5	1.371
363.5	2.751	114	10.7	1.029
358.0	2.793	21.3	4.62	0.664
353.0	2.833	8.0	2.83	0.452

From the plot of log $\sqrt{k}$ - 1/T (fig. 55) the slope of the line is $7.2 \times 10^3 \pm 10\%$.

Thus the activation energy = 7.2 x 2.303 x 1.98 K.cals./mole.
= 33 ± 3 K. cals./mole.

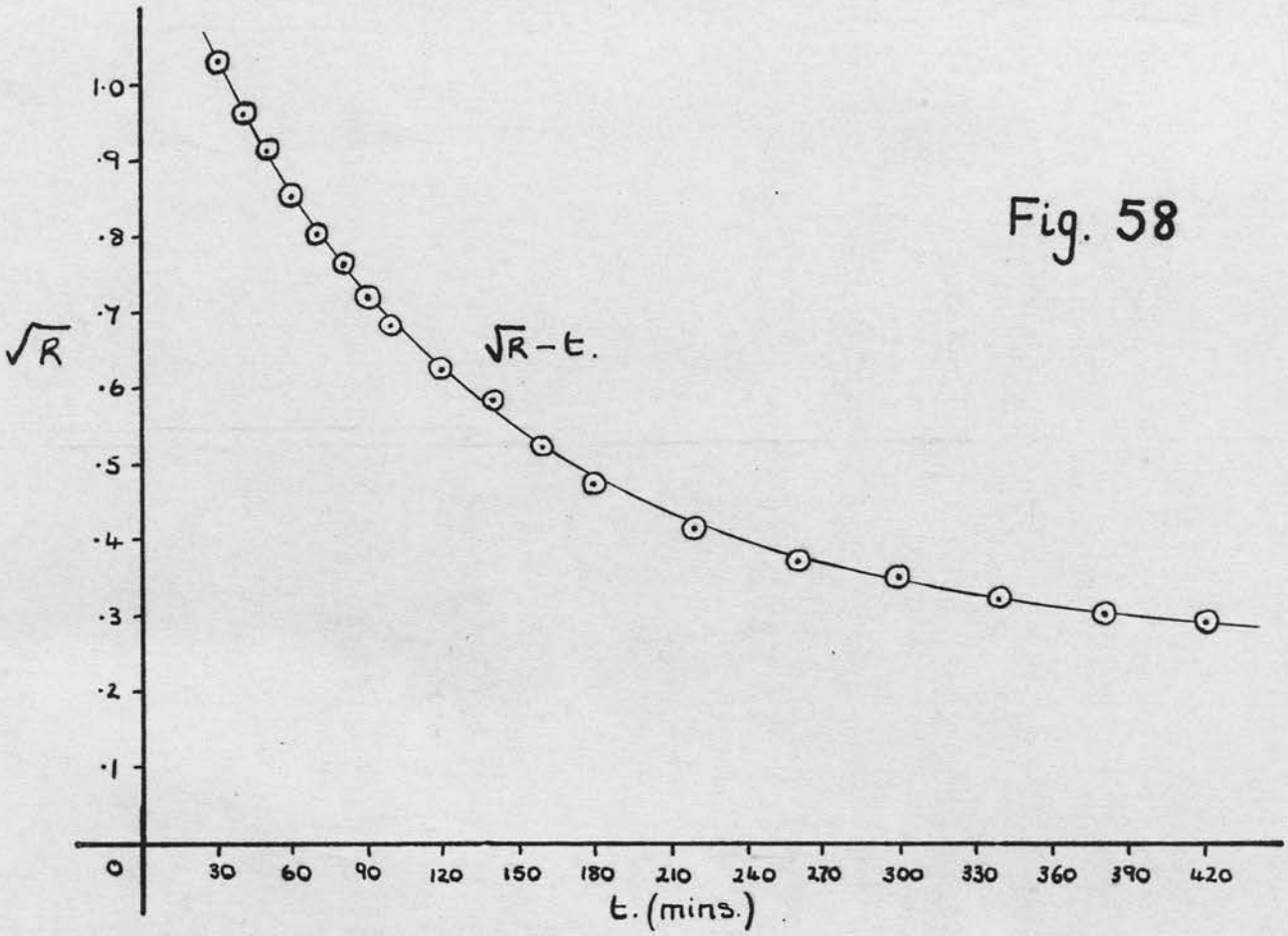
√R
√R – t.
1·0
·9
·8
·7
·6
·5
·4
·3
·2
·1
0
30 60 90 120 150 180 210 240 270 300 330 360 390 420
t. (mins.)

Fig. 58

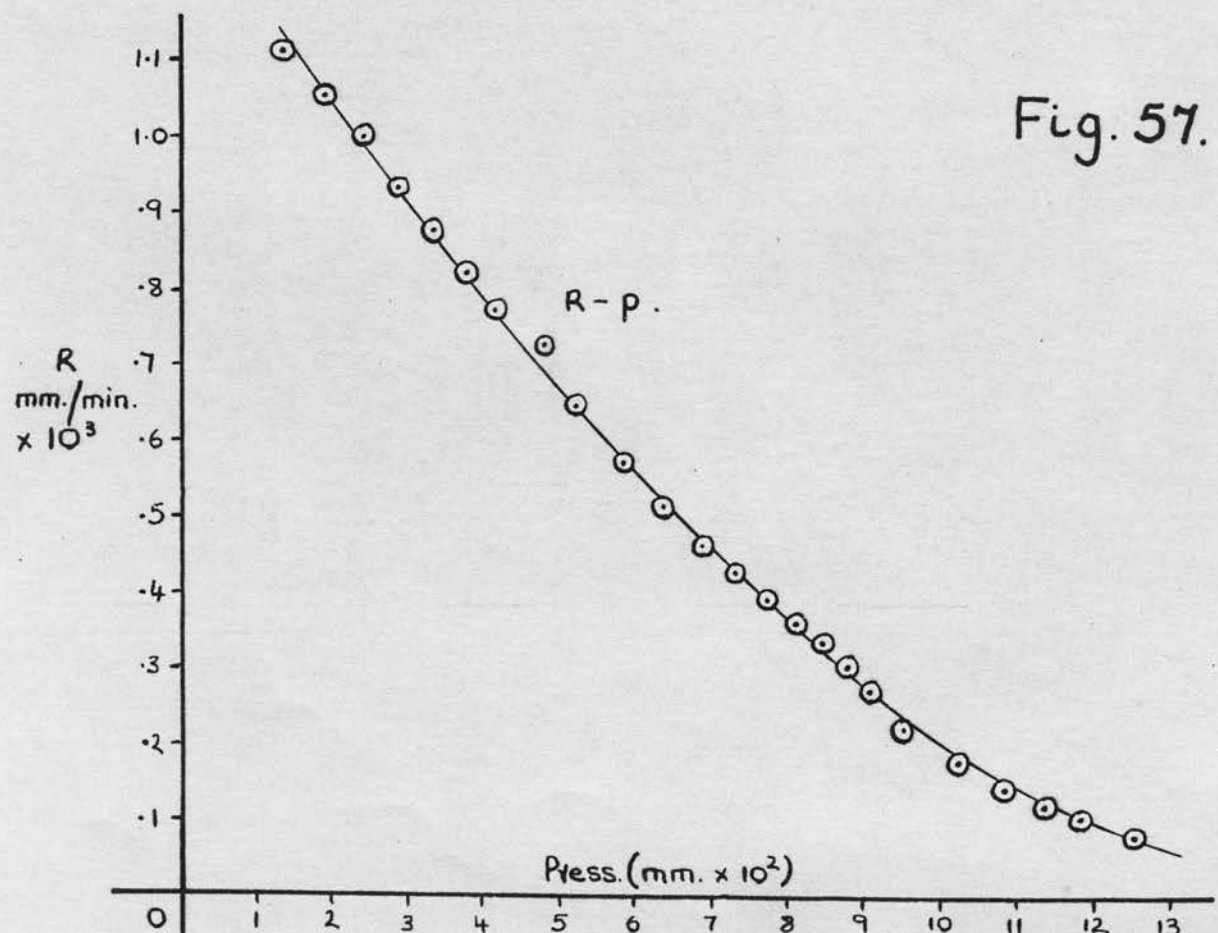
R
mm./min.
× 10³
R – p.
1·1
1·0
·9
·8
·7
·6
·5
·4
·3
·2
·1
0
Press. (mm. × 10²)
1 2 3 4 5 6 7 8 9 10 11 12 13

Fig. 57.

Table 54 Recrystallised form

Temperature °A	1/T x 10^3	k x 10^8 mm./sec.²	$\sqrt{k}$ x 10^4	$Log_{10}\sqrt{k}$ + 4.0
379.5	2.635	7000	83.7	1.923
373.0	2.681	1350	36.7	1.565
368.0	2.717	377	19.4	1.288
363.5	2.751	143	12.0	1.079
358.0	2.793	24.7	4.97	0.696

From the plot of log $\sqrt{k}$ - 1/T (fig. 55) the slope of the line is $7.80 \times 10^3 \pm 5\%$.

Thus the activation energy = 7.8 x 2.303 x 1.98 = 35.5 ± 1.8 K.cals./mole.

Decay stage (C)

The rates of decomposition for both forms of the oxalate were measured from the pressure-time curves. As shown by the plots of $\frac{dp}{dt}$ - p and $\left(\frac{dp}{dt}\right)^{\frac{1}{2}}$ - t (figs. 57 and 58) neither the unimolecular decay nor contracting sphere equations applied to the results. Thus the relationship 1/R - t was investigated and was found to fit the results for both forms of the oxalate (fig. 56).

For the powder form it was found that this relationship described the results up to 90% decomposition. However, as can be seen from fig. 56a and b, the 1/R - t plot consists of three straight lines, the breaks occurring at approximately 25% and 50% decomposition. Using the values of t' obtained by extrapolation of the 1/R - t lines the plots of p - log(t + t') were

Fig. 56 (b).

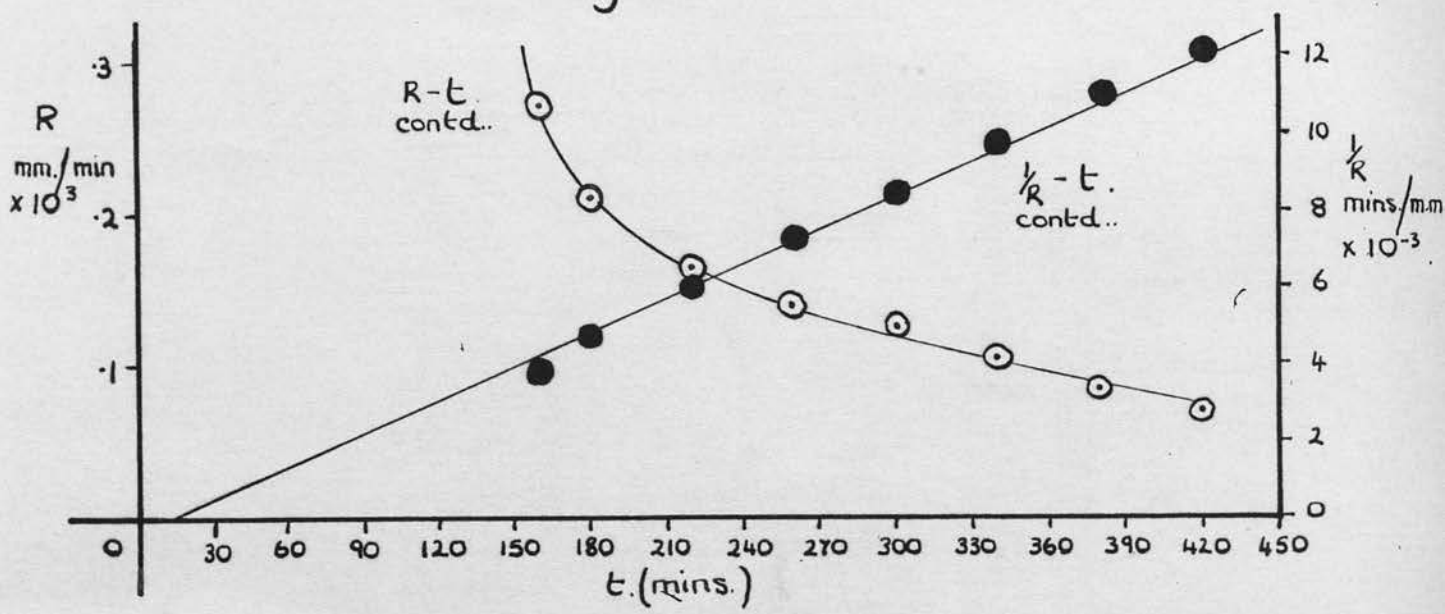

Fig. 56 (a).

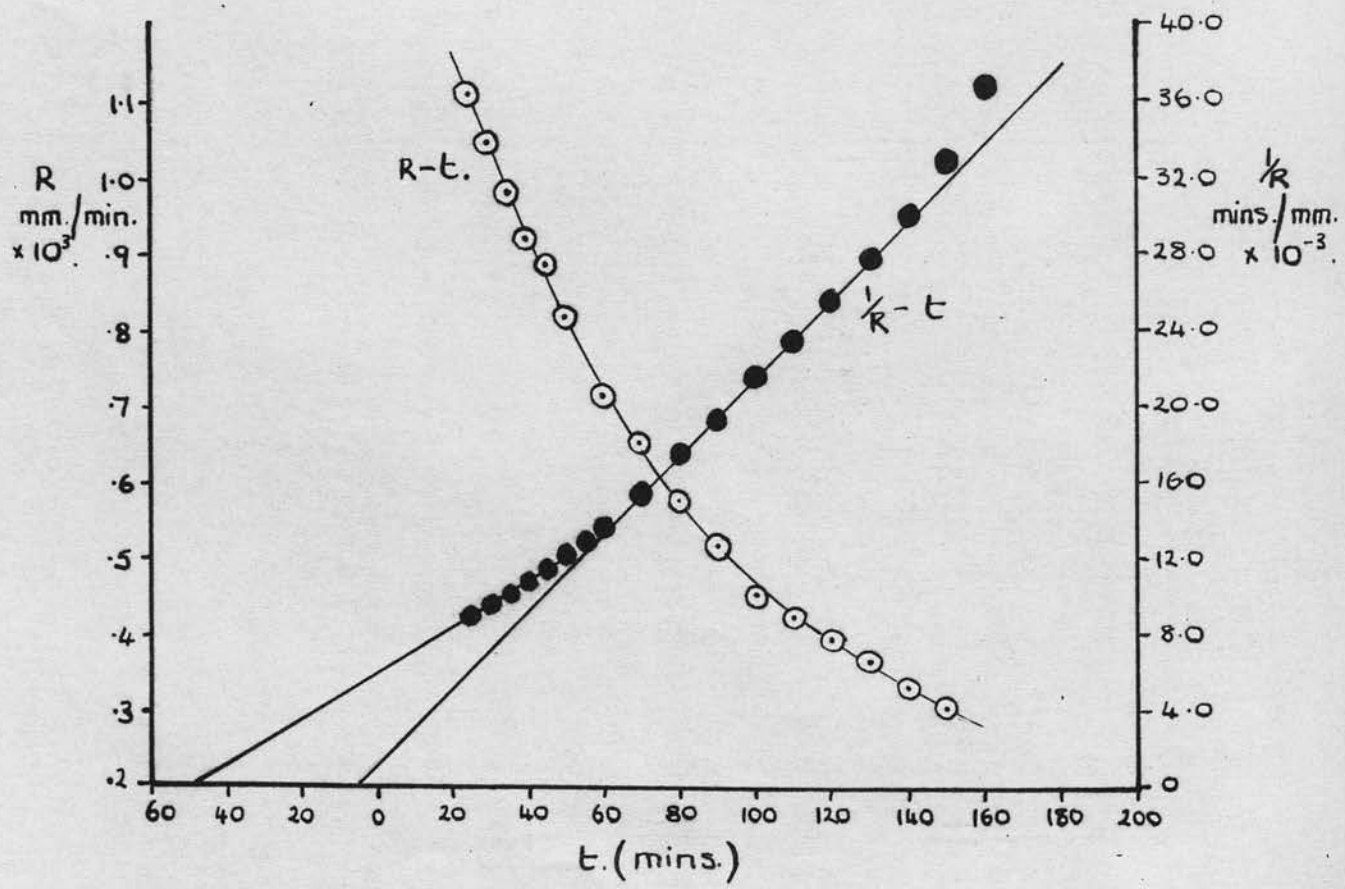

made. The full analysis of a typical decomposition is shown in Table 55.

Table 55 Temperature = 114°C.
Volume of reaction space = 4520 ml.

Pressure mm. x 10^2	Time min.	Rate mm./min. x 10^3	Corr.rate (R). mm./min. x 10^3	1/R min./mm. x 10^{-3}	$R^{1/2}$.	log (t+50)
1.35	25	1.11	1.11	0.90		1.875
1.89	30	1.05	1.05	0.95	1.03	1.903
2.40	35	0.985	0.99	1.01		1.929
2.86	40	0.925	0.93	1.08	0.96	1.954
3.31	45	0.89	0.875	1.14		1.978
3.75	50	0.82	0.82	1.22	0.91	2.000
4.13	55	0.75	0.77	1.30		2.021
						log(t+6)
4.80	60	0.720	0.725	1.38	0.85	1.820
5.19	70	0.655	0.645	1.55	0.80	1.881
5.81	80	0.580	0.57	1.75	0.76	1.935
6.36	90	0.520	0.515	1.94	0.72	1.935
6.85	100	0.456	0.460	2.17	0.68	2.025
7.27	110	0.424	0.425	2.35		2.065
7.69	120	0.397	0.390	2.56	0.62	2.100
8.07	130	0.368	0.360	2.78		2.134
8.42	140	0.333	0.335	2.99	0.58	2.164
8.74	150	0.302	0.302	3.31		2.193
						log(t-14)
9.02	160	0.270	0.270	3.70	0.52	2.164
9.48	180	0.210	0.210	4.76	0.47	2.220
10.20	220	0.163	0.167	6.00	0.41	2.314
10.78	260	0.139	0.139	7.19	0.37	2.391
11.31	300	0.124	0.119	8.40	0.35	2.456
11.77	340	0.104	0.103	9.71	0.32	2.513
12.14	380	0.091	0.091	11.0	0.30	2.563
12.50	420	0.083	0.083	12.1	0.29	2.609
12.81	460					2.649

The three values of t_o were obtained from the appropriate $p - \log(t + t')$ plots at p = 1.0, 4.0 and 9.0 mm. x 10^{-2} respectively. These values of the pressure, which were estimated from the $p - \log(t + t')$ plots indicate the stage of the reaction where the breaks in these plots occur. The fifth and seventh columns in Table 56 give the time and rate of reaction corresponding to these pressures.

Table 56

α	t_o	t' min.	$t_o - t'$	t break min.	$1/\alpha t_o \times 10^3$	Rate mm./min. $\times 10^3$	p break mm. $\times 10^2$
11.7	72	50	22	22	1.19	1.10	1.0
20.0	60	6	54	53	0.83	0.79	4.0
29.5	145	-14	159	160	0.23	0.27	9.0

From these results it can be seen that there is an excellent agreement between the values of $t_o - t'$ and the time corresponding to the break in the $p - \log(t + t')$ plots and between $1/\alpha t_o$ and the rate of reaction at this stage. Thus, similarly to the photochemical decompositions, the equation describing the results may be written:

$\alpha p^* = \ln(t^* + t_o) - \ln t_o$, where p^* and t^* refer to the stage of the reaction where the corresponding values of α and t_o apply.

The results of decompositions at other temperatures were analysed in a similar way and the results are shown in Table 57 At higher temperatures, where the duration of the initial stage was short, t' was taken empirically to give the best agreement with experiment.

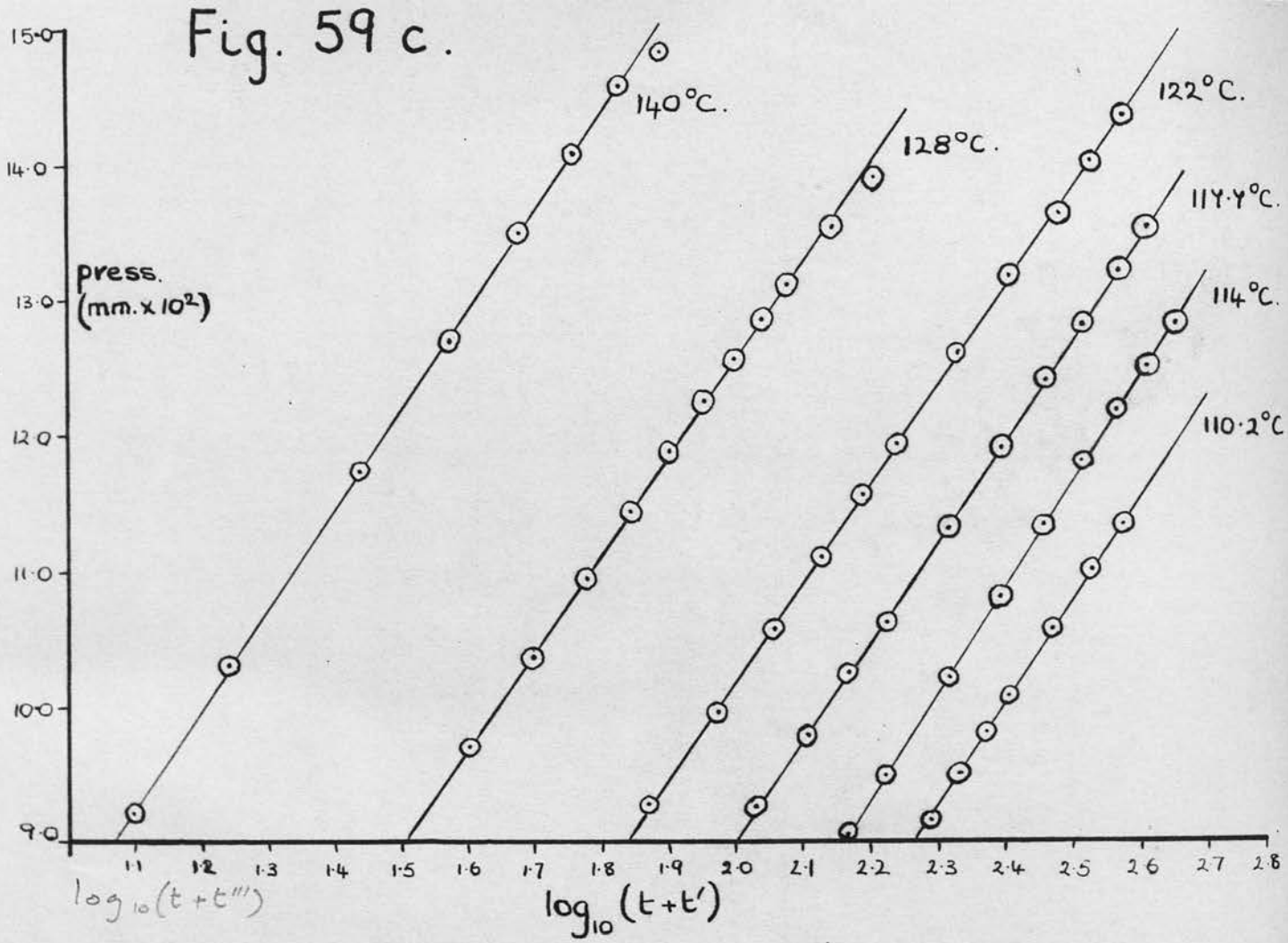
Fig. 59 c.
140°C.
128°C.
122°C.
117·7°C.
114°C.
110·2°C
press.
(mm.×10²)
15·0
14·0
13·0
12·0
11·0
10·0
9·0
1·1 1·2 1·3 1·4 1·5 1·6 1·7 1·8 1·9 2·0 2·1 2·2 2·3 2·4 2·5 2·6 2·7 2·8
log₁₀(t+t''')
log₁₀(t+t')

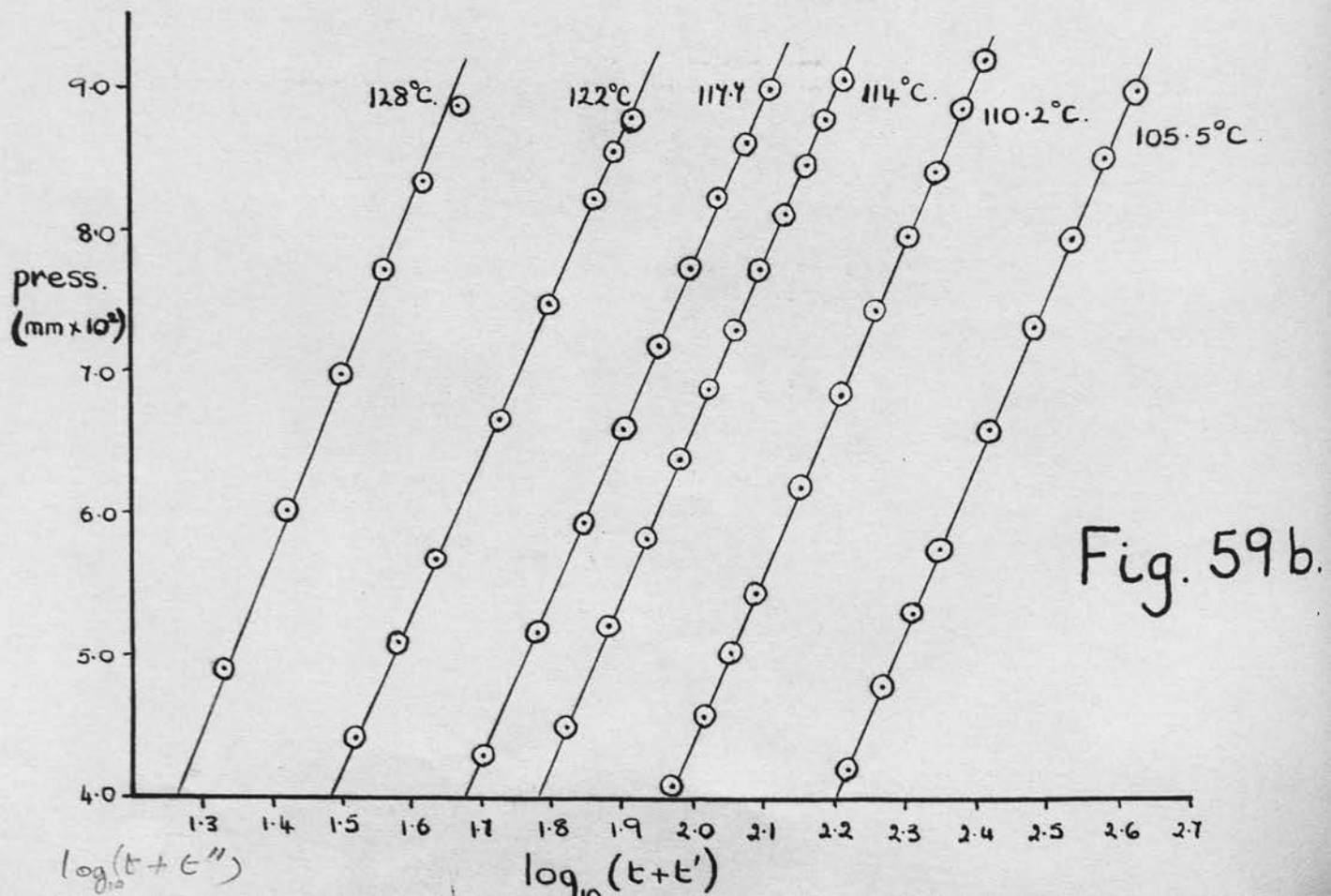
128°C.
122°C
117·7
114°C.
110·2°C.
105·5°C
press.
(mm×10²)
9·0
8·0
7·0
6·0
5·0
4·0
1·3 1·4 1·5 1·6 1·7 1·8 1·9 2·0 2·1 2·2 2·3 2·4 2·5 2·6 2·7
log₁₀(t+∈'')
log₁₀(t+t')

Fig. 59b.

Table 57

Temperature °C.		140.0		128.0		122		117.7
Time min.	Log(t-12.5)	Press. mm. x 10^2	Log(t-3.5)	Press. mm. x 10^2	Log(t-7)	Press. mm. x 10^2	Log(t+32)	Press. mm. x 10^2
0		0		0		0		0
15	0.398	5.10		1.92		0.58		0.34
20	0.875	7.70	1.218	3.50		1.28		0.71
25	1.097	9.22	1.332	4.89		2.10	1.756	1.25
30	1.243	10.32	1.423	6.00		2.94	1.792	1.90
35	1.352		1.698	6.97		3.73	1.826	2.53
40	1.439	11.73	1.562	7.70	1.519	4.41	1.857	3.16
45	1.512		1.618	8.32	1.580	5.08	1.887	3.75
50	1.574	12.68	1.668	8.85	1.634	5.67	log t	
50			log(t-20)					
60	1.677	13.47	1.602	9.69	1.724	6.65	1.778	5.15
70	1.760	14.05	1.699	10.35	1.799	7.46	1.845	5.92
80	1.829	14.50	1.778	10.93	1.863	8.20	1.903	6.58
90	1.889	14.78	1.845	11.42	1.919	8.76	1.954	7.17
					log(t-26)			
100		14.95	1.903	11.86	1.869	9.27	2.00	7.71
110			1.954	12.22	1.924		2.041	8.20
120		15.14	2.000	12.53	1.973	9.95	2.079	8.59
130			2.041	12.82	2.017		2.114	8.95
							log(t-33)	
140		15.23	2.079	13.07	2.057	10.55	2.029	9.25
160			2.146	13.50	2.127	11.07	2.104	9.77
180			2.204	13.85	2.188	11.53	2.167	10.23
200					2.241	11.91	2.223	10.61
240					2.330	12.57	2.316	11.30
280					2.405	13.13	2.393	11.10
320					2.468	13.58	2.458	12.38
360					2.524	13.97	2.515	12.80
400					2.573	14.30	2.565	13.18
440							2.610	13.52

Table continued on p.109.

Table 57 contd.

Temperature °C.		114.0		110.2	105.5		95.5	
Time min.	Log(t+ 50)	Press. mm. x 10^2	Log(t+ 75)	Press. mm. x 10^2	Log(t+ 120)	Press. mm. x 10^2	Log.(t+ 440)	Press. mm. x 10^2
0								
25	1.875	1.35						
30	1.903	1.89						
35	1.929	2.40						
40	1.954	2.81						
45	1.978	3.31	2.079	1.35				
50	2.000	3.75	2.097	1.71				
55	log(t+ 6)		2.114	2.03				
60	1.820	4.48	2.130	2.35	2.255	1.13		
70	1.881	5.19	2.161	2.96	2.279	1.55		
80	1.935	5.81	2.190 log(t+ 3)	3.53	2.301	1.97		
90	1.982	6.36	1.969	4.07	2.322	2.37		
100	2.025	6.85	2.013	4.55	2.342	2.76		
110	2.065	7.27	2.053	5.00	2.362	3.14		
120	2.100	7.69	2.090	5.42	2.380	3.52		
130	2.134	8.07			2.398 log(t+ 25)	3.89		
140	2.164	8.42	2.155	6.17	2.218	4.18	2.763	1.22
150	2.193 log t+ 14)	8.74						
160	2.164	9.02	2.212	6.82	2.267	4.76	2.778	1.51
180	2.220	9.48	2.263	7.40	2.312	5.28	2.792	1.79
200			2.308	7.92	2.352	5.73	2.806	2.07
220	2.314	10.20	2.348	8.37				
240			2.386 log(t -66)	8.80	2.423	6.57	2.833	2.59
260	2.391	10.78	2.288	9.15				
280		11.05	2.330	9.49	2.484	7.28	2.857	3.11
300	2.456	11.31	2.369	9.79				
320		11.54	2.403	10.06	2.538	7.90	2.881	3.58
360		11.97	2.468	10.55	2.586	8.46	2.903	4.03
400		12.30	2.524	10.98	2.628	8.93		
440		12.58	2.573	11.32				

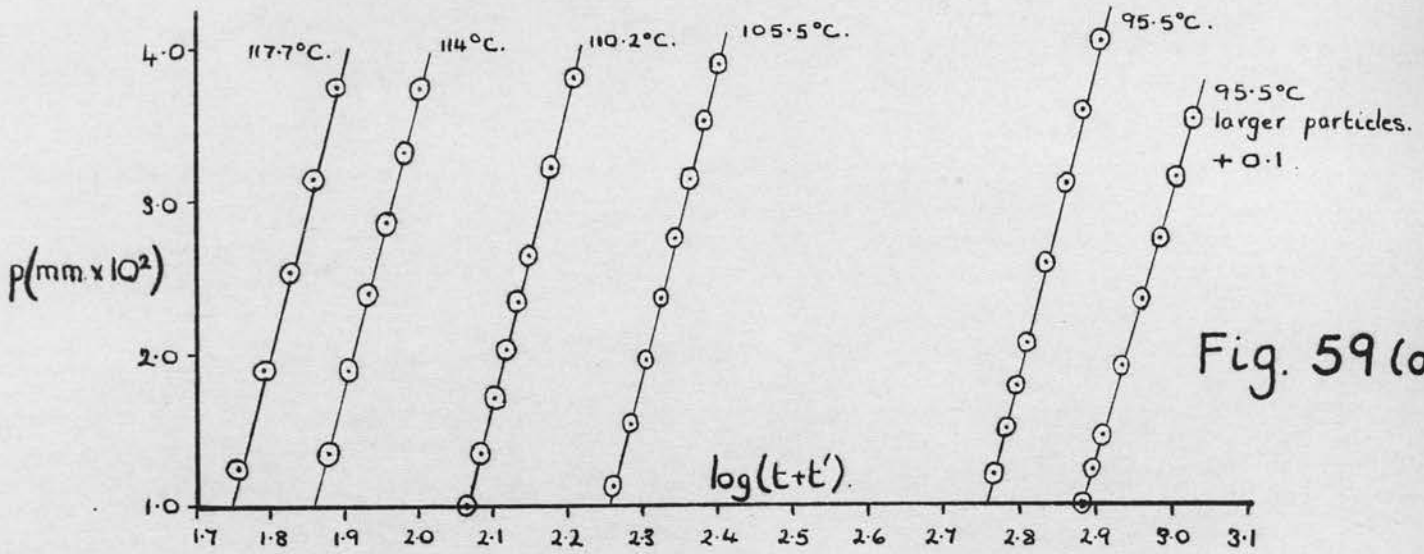

Fig. 59 (a)

Fig. 60.

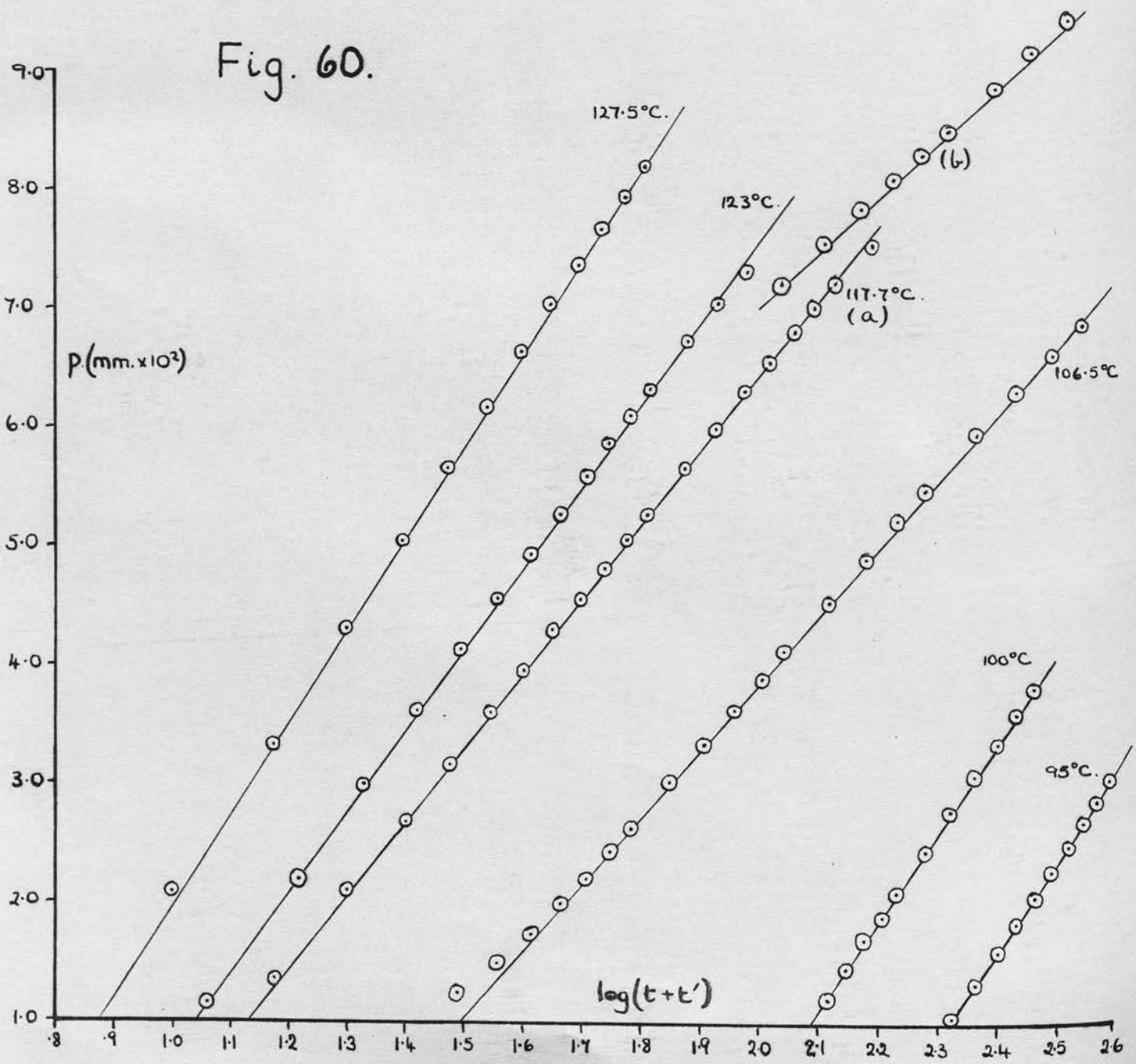

From the p - log(t + t') plots (fig. 59a, b and c) it can be seen that the corresponding values of α are temperature independent, whereas the t_o values increase with decreasing temperature.

The breaks in the plots varied a little with temperature, however for activation energy calculations the breaks were taken to occur at p = 1.0, 4.0 and 9.0 mm. x 10^{-2}. Thus log t_o values were obtained from the plots at these pressures and are shown in Table 58, as are the values for the maximum rate of decomposition at each temperature.

Table 58

Temp. °A	1/T x 10^3	α_1	log t_o'	α_2	log t_o''	α_3	log t_o'''	Max. rate (R) mm./min. x 10^4	log R + 4.0
413.0	2.421					31.8	1.065	70	1.85
401.0	2.494			18.8	1.26	28.5	1.505	29	1.46
395.0	2.532			19.5	1.485	30.8	1.83	16.8	1.23
390.7	2.560	11.7	1.745	20.2	1.675	30.7	2.005	12.5	1.10
387.0	2.584	11.7	1.860	20.0	1.78	29.5	2.16	10.2	1.01
383.2	2.610	11.5	2.060	20.1	1.965	30.1	2.265	5.7	0.76
378.5	2.642	11.5	2.255	19.8	2.20			4.1	0.61
368.5	2.713	11.5	2.750					1.5	0.18

As can be seen in fig. 61 the plots of log t_o - 1/T give reasonable straight lines of slope 6.8 x 10^3, 6.3 x 10^3 and 6.3 x 10^3 for t_o', t_o'' and t_o''' respectively with a maximum error of 6%. Thus the activation energies associated with them are

Fig. 62.

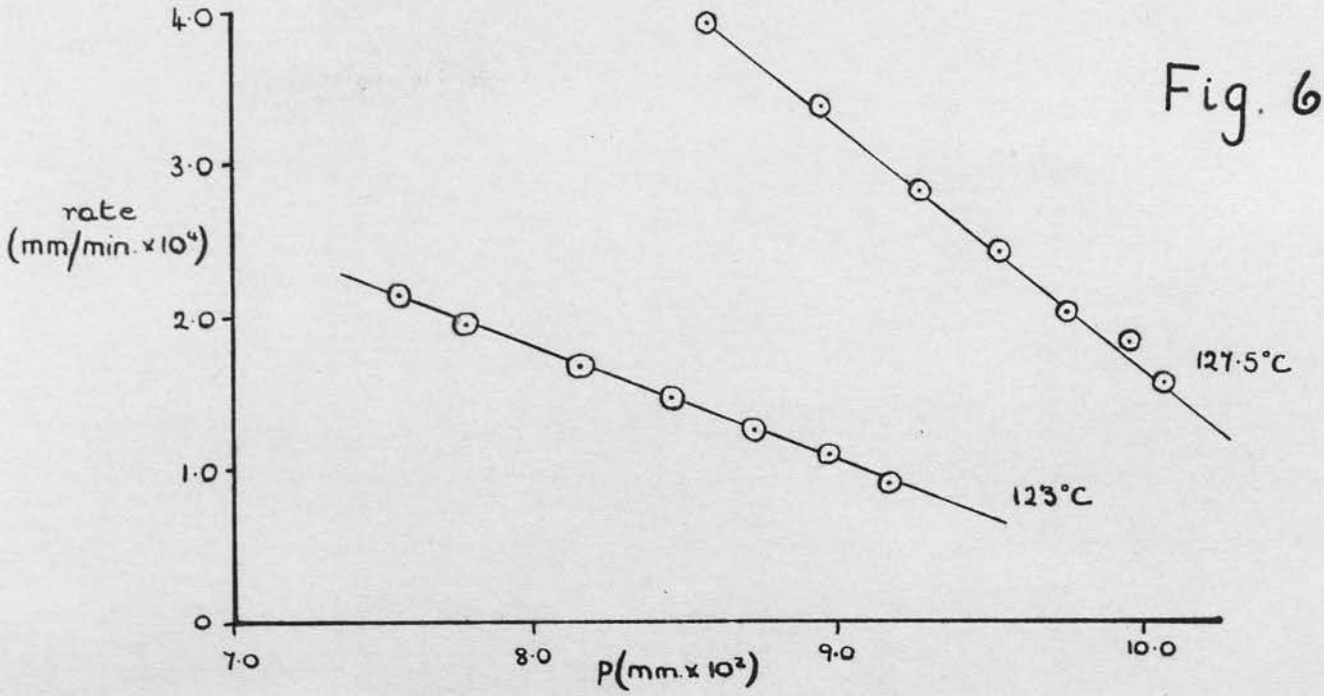
4·0
3·0
2·0
1·0
0
rate
(mm/min. x 10⁴)
127·5°C
123°C
7·0
8·0
9·0
10·0
P(mm. x 10²)

Fig. 61.

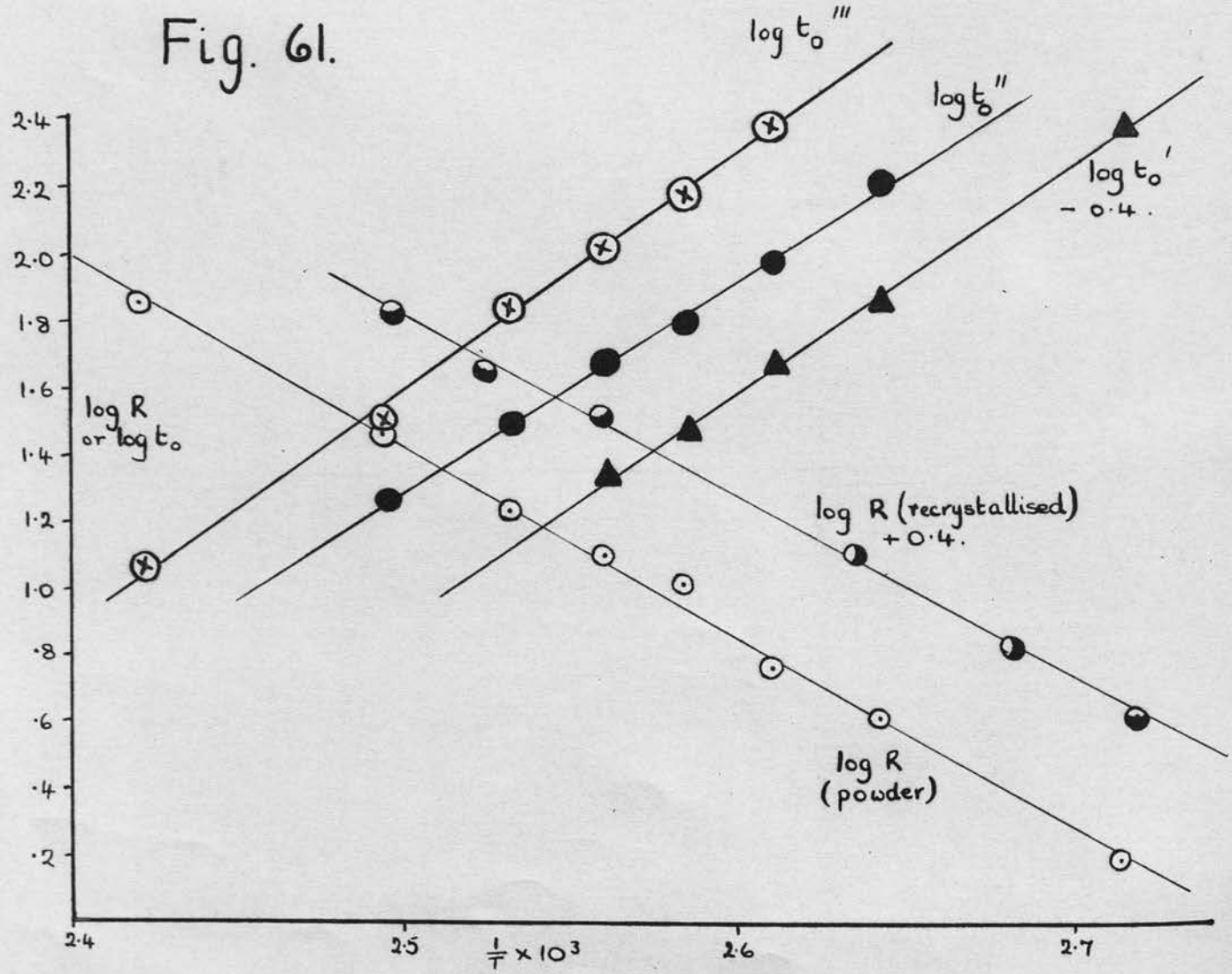
log t₀'''
log t₀''
log t₀'
- 0·4.
2·4
2·2
2·0
1·8
1·6
1·4
1·2
1·0
·8
·6
·4
·2
log R
or log t₀
log R (recrystallised)
+ 0·4.
log R
(powder)
2·4
2·5
2·6
2·7
1/T x 10³

for t_o' $6.8 \times 1.98 \times 2.303 = 31 \pm 2$ K.cals./mole

t_o'' $6.3 \times 1.98 \times 2.303 = 29 \pm 2$ K.cals./mole

t_o''' $6.3 \times 1.98 \times 2.303 = 29 \pm 2$ K.cals./mole

Also from fig. 61 the plot of log maximum rate - 1/T is a reasonably straight line of slope $5.7 \times 10.3 \pm 10\%$ giving for the activation energy of the reaction a value of $5.7 \times 1.98 \times 2.303 = 26 \pm 3$ K.cals./mole, which agrees within the experimental error with the values obtained above.

For the recrystallised material only one value of α was required; however, the 1/R - t relationship only applied up to approximately 40% decomposition.

Values of t' were obtained as before and the results of decomposition carried out at various temperatures are shown in Table 59.

Table 59 Recrystallised material

Temperature °C.		127.5		123		117.7
Time min.	Log(t-5)	Press. mm. x 10^2	Log(t-3.5)	Press. mm. x 10^2	Log(t-5)	Press. mm. x 10^2
0						
15	1.000	2.07	1.061	1.16		1.00
20	1.176	3.33	1.218	2.21	1.176	1.35
25	1.301	4.31	1.322	3.00	1.301	2.10
30	1.398	5.04	1.423	3.62	1.398	2.68
35	1.477	5.66	1.498	4.14	1.477	3.16
40	1.544	6.17	1.562	4.56	1.544	3.60
45	1.602	6.63	1.618	4.93	1.602	3.97
50	1.653	7.02	1.668	5.27	1.653	4.30
55	1.699	7.35	1.712	5.58	1.699	4.57
60	1.740	7.65	1.752	5.87	1.740	4.83
65	1.778	7.92	1.789	6.10	1.778	5.06
70	1.813	8.17	1.823	6.32	1.813	5.27
	Rate mm./min. x 10^4					
80	3.9	8.58	1.884	6.72	1.875	5.66
90	3.35	8.95	1.937	7.03	1.929	5.99
100	2.8	9.27	1.985	7.30	1.977	6.29
			Rate mm./min. x 10^4			
110	2.4	9.53	2.15	7.55	2.021	6.55
120	2.0	9.75	1.95	7.77	2.061	6.79
130	1.8	9.95			2.097	7.00
140	1.55	10.07	1.65	8.15	2.130	7.18
160			1.45	8.45	2.190	7.52
					log(t-30)	
180			1.25	8.72	2.176	7.80
200			1.08	8.97	2.230	8.04
220			0.90	9.17	2.279	8.25
240					2.322	8.45
280					2.398	8.80
320					2.462	9.12
360						

Table 59 contd.

Temperature °C.		106.5		100		95
Time min.	Log(t-9)	Press. mm. x 10^2	Log(t+50)	Press. mm. x 10^2	Log(t+90)	Press. mm. x 10^2
40	1.491	1.25				
45	1.556	1.50				
50	1.613	1.75				
55	1.663	2.00				
60	1.708	2.23				
65	1.748	2.45				
70	1.785	2.64				
80	1.851	3.02	2.114	1.21		
90	1.909	3.34	2.146	1.47		
100	1.959	3.63	2.176	1.70		
110	2.004	3.90	2.204	1.90		
120	2.045	4.13	2.230	2.09	2.322	1.05
140	2.117	4.53	2.279	2.45	2.362	1.33
160	2.179	4.89	2.322	2.78	2.398	1.59
180	2.233	5.22	2.362	3.08	2.431	1.84
200	2.281	5.48	2.398	3.35	2.462	2.06
220			2.431	3.59	2.491	2.27
240	2.364	5.93	2.462	3.81	2.519	2.48
260					2.544	2.68
280	2.433	6.30			2.568	2.86
300					2.591	3.03
320	2.493	6.60				
360	2.545	6.86				

As can be seen from the p - log(t + t') plots (fig. 60) α in these experiments was not constant over the range of temperatures employed, thus the values of t_o could not be used to evaluate an activation energy for the process; for this purpose therefore the maximum rate of reaction, measured at approximately 10% decomposition, was used.

Table 60

Temperature °A	1/T x 10^3	α	$Log_{10}t_o$	Max. rate(R) mm./min. x 10^3	$Log_{10}R$ + 4.0
400.5	2.497	29.8	0.87	2.55	1.41
396.0	2.525	34.0	1.04	1.73	1.24
390.7	2.560	36.9	1.13	1.25	1.10
379.5	2.635	41.0	1.49	0.50	0.70
373.0	2.681	31.1	2.08	0.26	0.42
368.0	2.717	31.4	2.32	0.16	0.20

From fig. 61 the slope of the line log R - 1/T is 5.4 x 10^3 ± 10%, thus the activation energy for the decomposition is 5.4 x 2.303 x 1.98 = 25 ± 2.5 K.cals./mole.

For the decomposition beyond 40% different kinetics applied at different temperatures. At 127.5°C. and 123°C. the results were expressed by the equation $dp/dt \propto p$ (fig. 62); thus the decomposition proceeded by a unimolecular decay mechanism. The decay constant decreased from 127.5°C. to 123°C. (1.6 and 0.7 respectively). At 117.7°C, however, the results were described by the equation $\alpha p = \ln(t - 30) - \ln t_o$ (fig. 60) where α had a larger value than applied to the first stage of the decay (58 and 39 respectively).

Decompositions using a larger particle size

For comparison with the results obtained with the crushed powder (p. 23), the decomposition of an uncrushed piece of ferric oxalate was examined. The sample was not a single crystal but rather an aggregate of smaller particles, similar to those used in the

previous decompositions. The kinetics for the reaction were the same as for the crushed powder and the results are shown in Table 61.

Table 61 Temperature = 95.5°C. Volume of reaction space = 542 ml.

Time(t) min.	Press. mm. x 10^3	t^2 x 10^{-3}	Time min.	Press. mm. x 10^3	t^2x 10^{-3}	Log(t + 400)
0	0		140	44.6	19.6	
10	1.60		150	50.7	22.5	
20	3.92		160	57.2	25.6	
30	6.08		170	64.0	28.9	
40	8.33		180	71.2	32.4	
50	10.5					
60	12.7		200	Volume of reaction space = 4520 ml. 1.02 mm.x 10^2		2.778
70	15.6	4.9	220	1.22		2.792
80	18.5	6.4	240	1.47		2.806
90	21.6	8.1	280	1.91		2.833
100	25.2	10.0	320	2.35		2.857
110	29.2	12.1	360	2.75		2.881
120	33.7	14.4	400	3.15		2.903
130	38.8	16.9	440	3.52		2.924

A table of the constants derived from this experiment and from that with the crushed powder is shown (Table 62). k_1 and p_1 are the rate and extent of the constant rate process (fig. 49), k_2 the acceleration constant (fig. 52) and α and t_o are as before (fig. 59a).

Table 62

Material	k_1 mm./min. x 10^4	p_1 mm. x 10^3	k_2 x 10^6	t' min.	α	t_o
Crushed	3.8	12.5	5.5	440	11.5	560
Uncrushed	2.2	15.0	2.1	400	12.8	600

Thus both the rate constant for the initial and acceleration processes have been doubled by crushing the powder, although the extent of the initial reactibn was not much affected. For the decay stage neither α nor t_o altered considerably on crushing.

The uncrushed sample, at about 30% decomposition was removed from the reaction vessel crushed and replaced. On continuing the decomposition, the rate of reaction was found to be approximately half its former value. When the crushed powder was removed and further crushed it was found that the ensuing rate of decomposition was unchanged.

Finally the following experiments were performed.

(1) The oxalate sample was removed from the furnace during both the acceleration and decay stages of the reaction. The evolution of carbon dioxide ceased immediately and on readmitting the oxalate some hours later the reaction continued unchanged without any induction period, this being in contrast to the photochemical reaction.

(2) The decomposition of a mixture of ferric oxalate and the decomposition product from a previous experiment was examined. No significant change in the kinetics or rate of decomposition was observed.

4. Thermal decomposition following various degrees of photochemical decomposition

The following effects were investigated:

(1) Effect of photodecomposition on initial stages of the subsequent thermal decomposition of the powder form.

(2) Effect of photodecomposition on the initial stages of the subsequent thermal decomposition of the recrystallised form.

(3) Effect of photodecomposition on the decay stage of the subsequent thermal decomposition of the recrystallised form.

(1) The preparation and evacuation of the reaction vessel were as before, except that a small glass bucket replaced the platinum one used previously. The sample was then exposed to the full light of a 250 watt mercury lamp for the appropriate time (5-15 minutes);to prevent heating the sample an infra red filter was placed between it and the lamp. In order to make the decomposition as uniform as possible the sample was slowly rotated during the illumination. When the lamp was removed the sample was shielded from stray light and allowed to stand for a period of four hours. At the end of this time the dark rate was negligible and thus recording the total extent of decomposition the thermal decomposition was started. This method was not ideal in that the decomposition was limited to the surface of the powder, but it did allow an exact knowledge of the extent of this decomposition.

Following varying degrees of photodecomposition (0-1%), the powder was decomposed at temperatures between 85°C. and 95°C. No

Fig. 63. Thermal decomposition of powder following photo-decomposition.

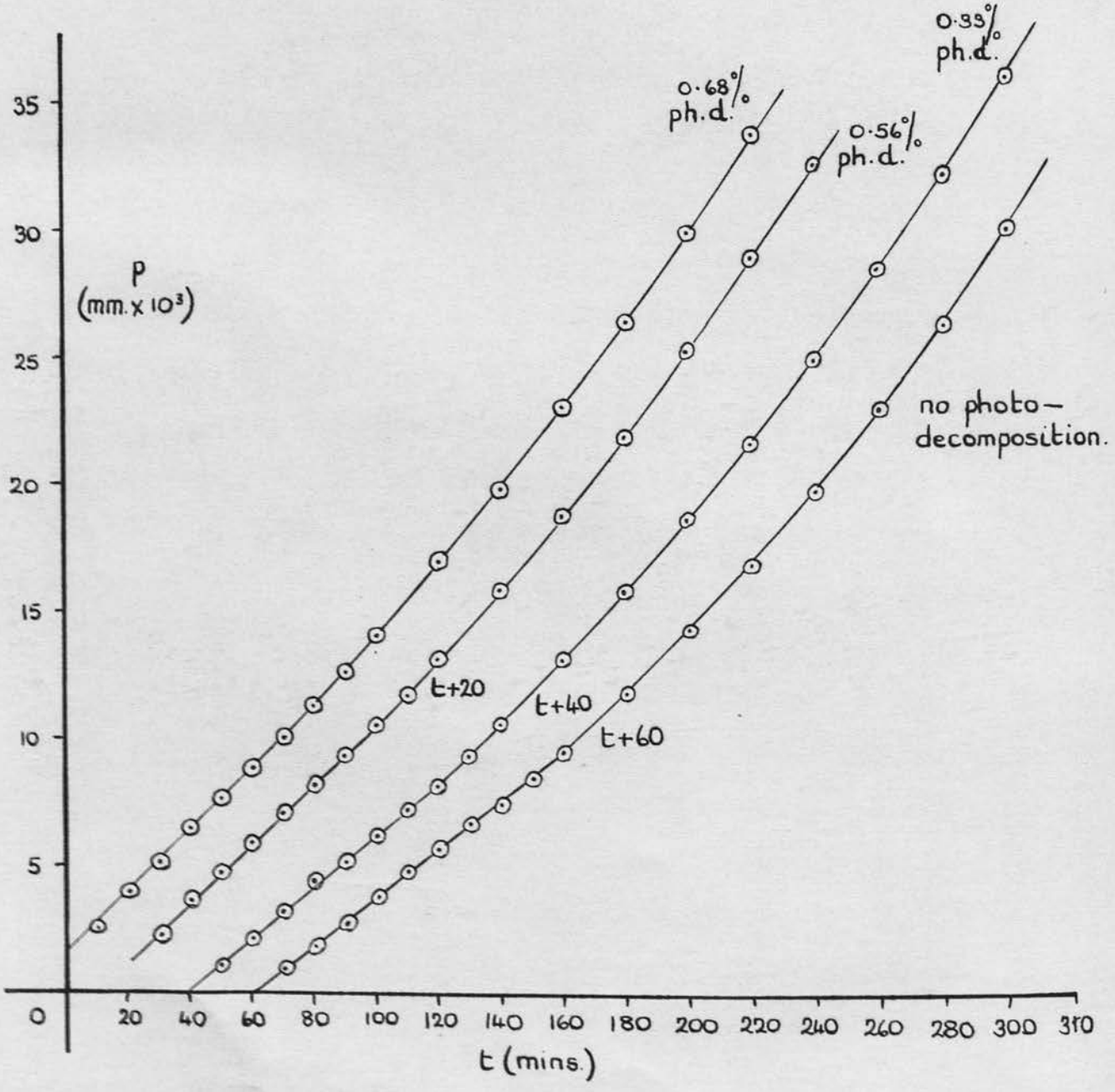

new features were introduced by the photodecomposition, as can be seen from the p - t and p - $(t + t')^2$ plots for the decomposition at 85°C. shown in figs. 63 and 64; thus the results were analysed as before and are shown in Table 63. Similar p - t and p -$(t + t')^2$ plots were constructed for the decompositions at 89°C. and 94°C. from which the constants shown in Table 66 were derived.

Table 63 Temperature = 85°C. Volume of reaction space = 642 ml.

Photo-decomposition %	0		0.33		0.56		0.68	
Time min.	$(t+70)^2$ x 10^{-4}	Press. mm. x 10^3	$(t+150)^2$ x 10^{-4}	Press. mm. x 10^3	$(t+160)^2$ x 10^4	Press. mm. x 10^3	$(t+170)^2$ 10^4	Press. mm.x 10^3
0		0		0		0		0
10		0.93		1.05		2.06		2.51
20		1.85		2.02		3.45		3.88
30		2.71		3.15		4.59		5.13
40		3.75		4.08		5.76		6.39
50		4.75		5.07		6.87		7.55
60		5.60		6.12		8.00		8.79
70		6.58		7.10		9.22		10.02
80		7.41	5.29	8.05	5.76	10.40		11.3
90		8.41	5.76	9.20	6.25	11.6	6.76	12.6
100	2.89	9.33	6.25	10.5	6.76	13.0	7.29	14.0
120	3.61	11.8	7.29	13.0	7.84	15.7	8.41	16.9
140	4.41	14.2	8.41	15.6	9.00	18.6	9.61	19.7
160	5.29	16.7	9.61	18.4	10.24	21.7	10.9	22.9
180	6.25	19.6	10.9	21.5	11.6	25.0	12.3	26.2
200	7.29	22.8	12.3	24.7	13.0	28.6	13.7	29.7
220	8.41	26.1	13.7	28.2	14.4	32.3	15.2	33.5
240	9.61	29.8	15.2	31.9				
260			16.8	35.7				

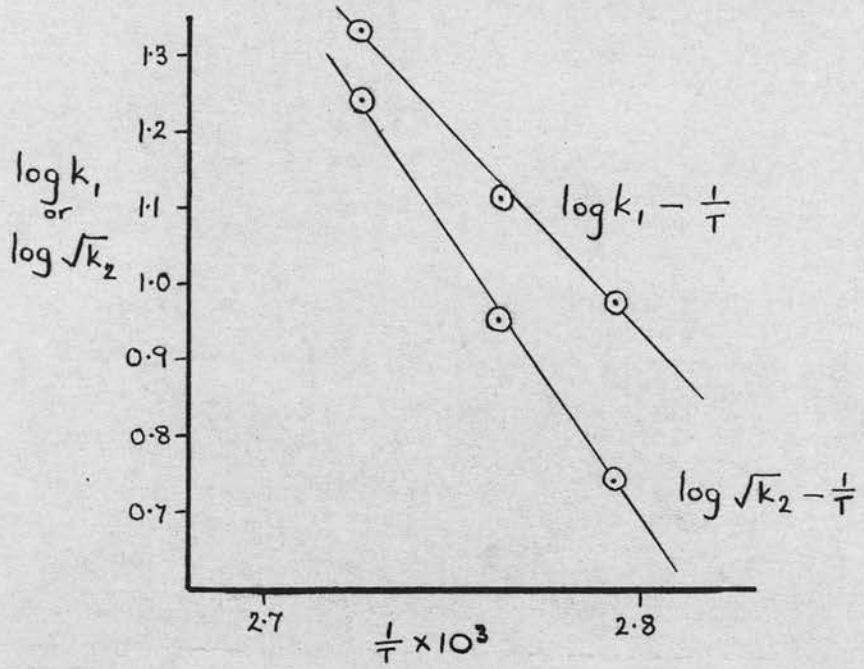
1·3
1·2
1·1
1·0
0·9
0·8
0·7
log k1 or log √k2
log k1 – 1/T
log √k2 – 1/T
2·7
1/T × 10³
2·8

Fig. 65.

Fig. 64.

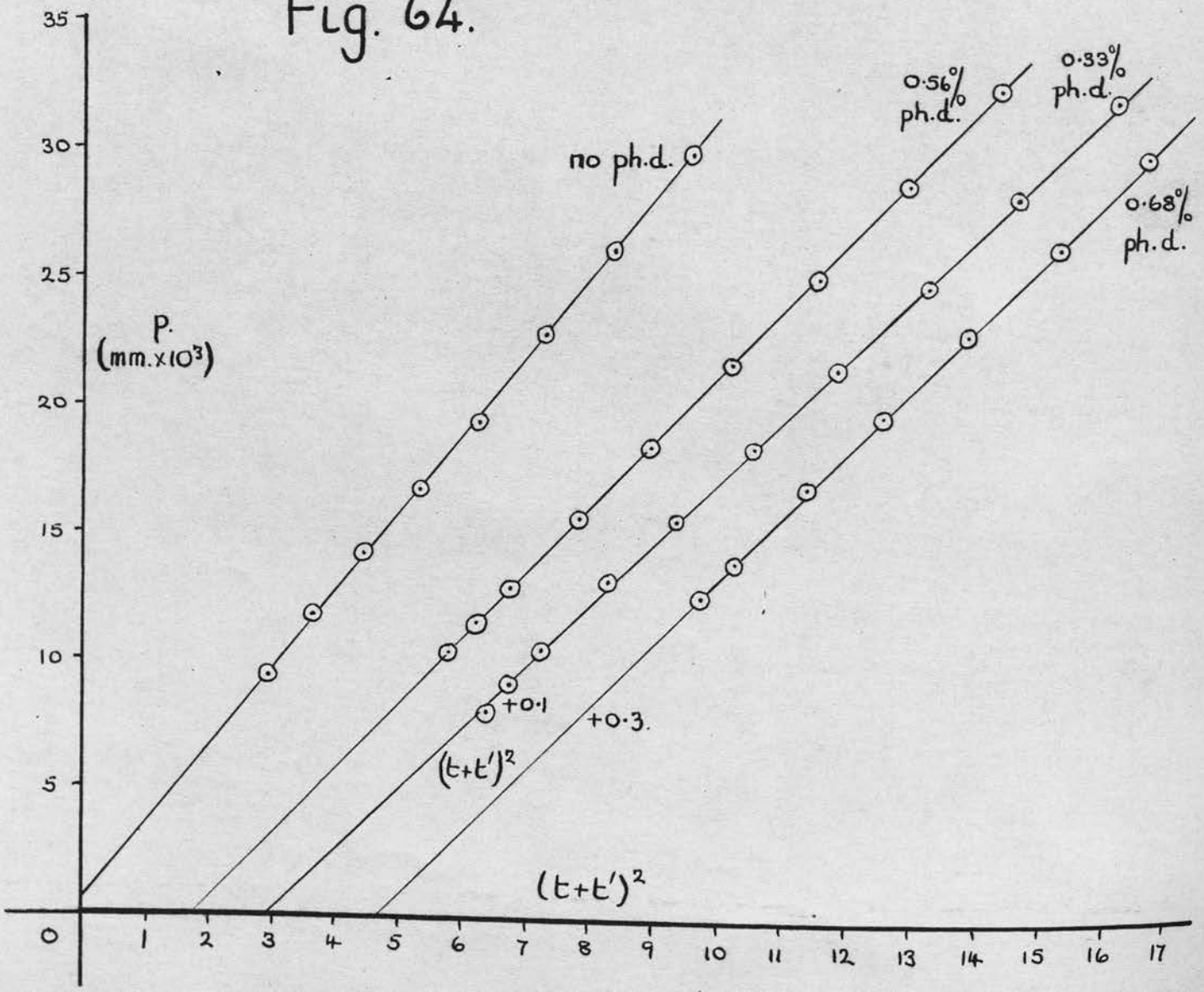
35
30
25
20
15
10
5
0
P. (mm. × 10³)
no ph.d.
0·56% ph.d.
0·33% ph.d.
0·68% ph.d.
+0·1
+0·3.
(t+t')²
(t+t')²
1
2
3
4
5
6
7
8
9
10
11
12
13
14
15
16
17

Table 64 Temperature = 89°C. Volume of reaction space = 642 ml.

Photodecomposition %		0		0.33		0.48
Time (t) min.	$(t + 12)^2 \times 10^{-3}$	Press. mm. x 10^3	$(t + 12)^2 \times 10^{-3}$	Press. mm. x 10^3	$(t + 40)^2 \times 10^{-3}$	Press. mm. x 10^3
0		0		0		0
5		1.05		1.60		2.01
10		2.05		2.73		3.85
15		3.21		3.98		5.26
20		4.33		5.06		6.82
25		5.36		6.37		8.13
30		6.38		7.50		9.72
35	2.21	7.60	2.21	9.11	5.63	11.30
40	2.70	8.77	2.70	10.7	6.4	13.3
50	3.84	12.2	3.84	14.2	8.1	17.8
60	5.18	16.5	5.18	18.1	10.0	23.3
70	6.72	21.0	6.72	22.8	12.1	28.9
80	8.46	26.0	8.46	28.3	14.4	35.4
90	10.4	31.7	10.4	34.3	16.9	42.4
100	12.5	38.0	12.5	41.0	19.6	49.9
110	14.9	45.2	14.9	48.3	22.5	57.7
120	17.4	53.0			25.6	66.0

Table 66 shows the constants derived from these results.

Table 65 Temperature = 94°C. Volume of reaction space = 642 ml.

Photo-decomposition %	0		0.23		0.68	
Time min.	$(t + 36)^2 \times 10^{-3}$	Press. mm. x 10^3	$(t + 70)^2 \times 10^{-4}$	Press. mm. x 10^3	$(t + 180)^2 \times 10^{-4}$	Press. mm. x 10^3
0		0				
10		1.27		2.47		4.15
20		2.45		4.12		6.21
30		3.78		5.85		8.04
40		5.03		7.50		10.20
50		6.33		9.09		12.2
60	9.22	7.70	1.69	10.85	5.86	14.3
70	11.2	9.41	1.96	12.5	6.25	16.8
80	13.5	11.3	2.25	14.4	6.76	19.4
100	18.5	15.5	2.89	18.5	7.84	24.9
120	24.3	20.1	3.61	23.4	9.00	31.0
140	31.0	25.1	4.41	28.7	10.2	37.4
160	38.4	31.2	5.29	34.5	11.6	44.3
180	46.7	37.8	6.25	40.6	13.0	51.7
200	55.7	45.3	7.29	47.5	14.4	59.3
220	65.5	53.0	8.41	54.7		

Table 66

Temp. °A	1/T x 10^3	Photo-decompn. mm. x 10^3	Photo-decompn. %	$k_1 x$ 10^4	Log k_1 + 5.0	t' mm.	$k_2 x$ 10^7	Log $\sqrt{k_2}$ + 4.0
		0	0	0.93	0.97	70	3.04	0.74
358	2.793	4.0	0.33	1.01		150	2.40	
		6.7	0.56	1.16		160	2.54	
		8.1	0.68	1.23		170	2.45	
		0	0	1.29	1.11	36	8.12	0.95
362	2.762	2.8	0.23	1.70		70	6.53	
		8.1	0.68	2.05		180	5.15	
		0	0	2.15	1.33	12	30.2	1.24
367	2.725	4.0	0.33	2.35		12	30.9	
		5.7	0.48	2.95		40	27.6	

From this table and the graph (fig. 63) it can be seen that increasing photodecomposition increased both the extent and rate constant (k_1) though not the duration for the initial stage of the reaction. The change, however, was small. For the acceleration stage, the acceleration constant decreased slightly whereas the value of t' increased considerably with increasing photodecomposition. Also, although the rate constants for the decomposition with no photodecomposition are different from those obtained previously, they give comparable activation energies (fig. 65): 24 K.cals./mole and 34 K.cals./mole for the rate constant for the initial and acceleration stages respectively.

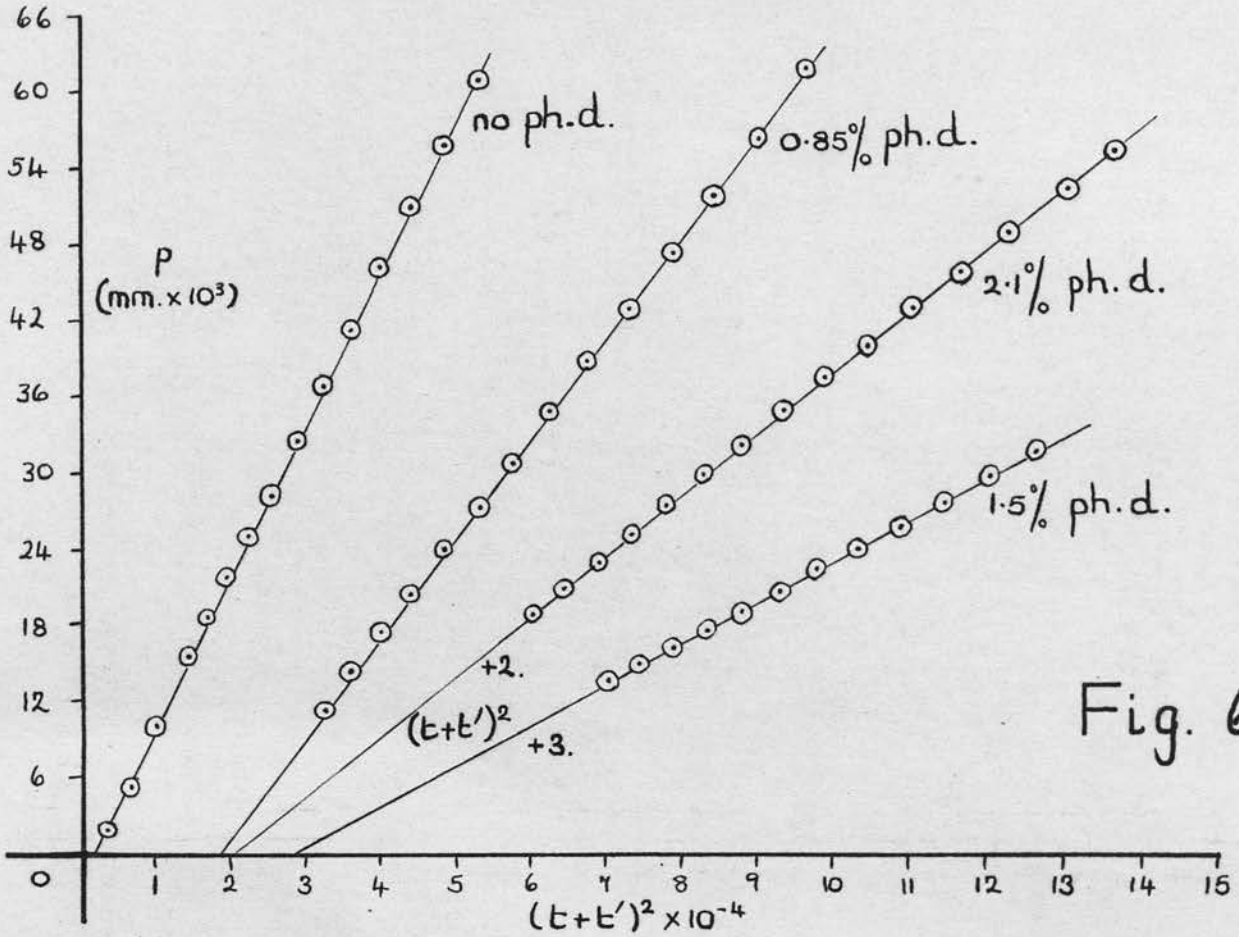
66
60
54
48
42
36
30
24
18
12
6
0
P
(mm. × 10³)
no ph.d.
0·85% ph.d.
2·1% ph.d.
1·5% ph.d.
+2.
(t+t')²
+3.
1
2
3
4
5
6
7
8
9
10
11
12
13
14
15
(t+t')² × 10⁻⁴

Fig. 67.

Fig. 66.

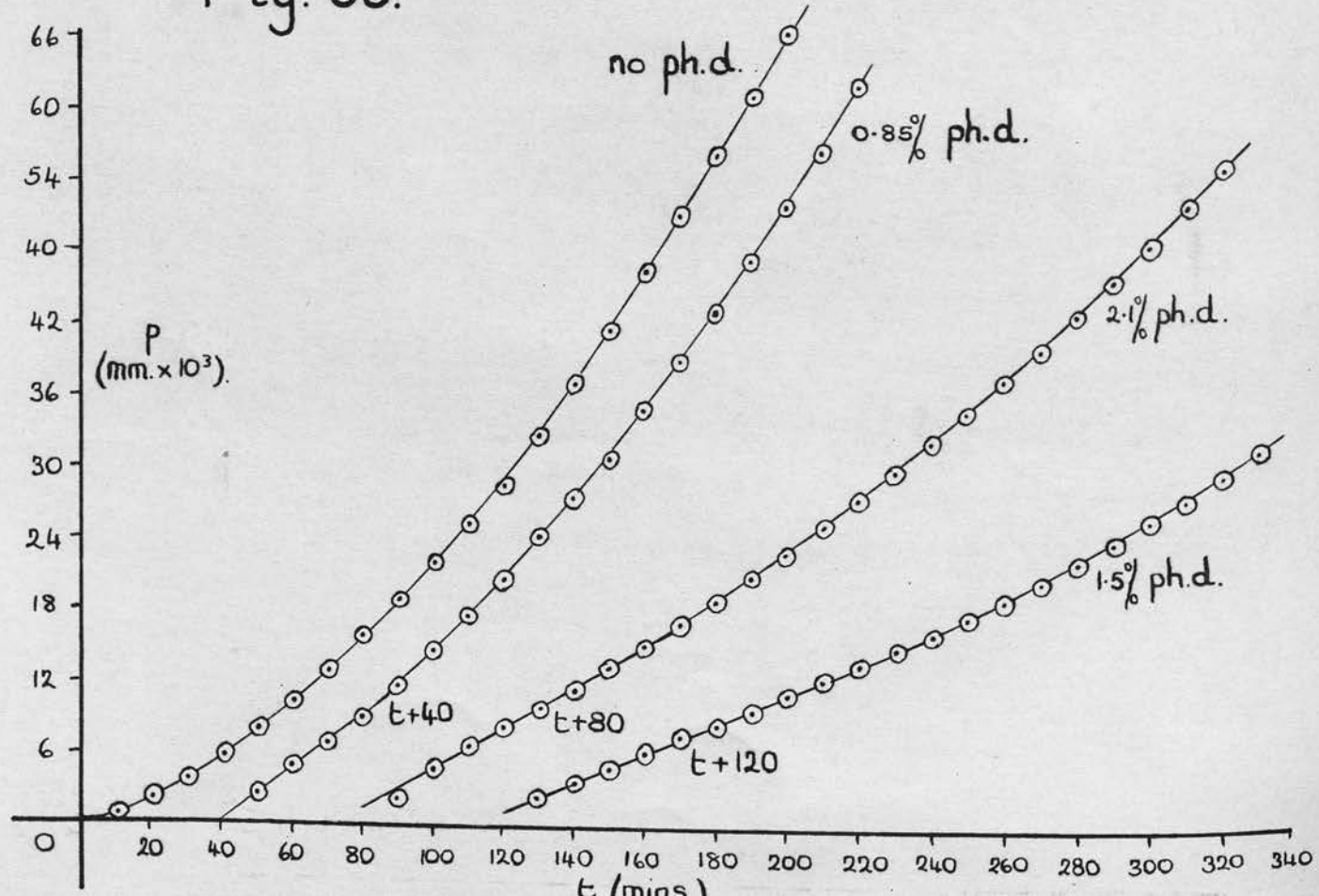
66
60
54
40
42
36
30
24
18
12
6
0
P
(mm. × 10³).
no ph.d.
0·85% ph.d.
2·1% ph.d.
1·5% ph.d.
t+40
t+80
t+120
20
40
60
80
100
120
140
160
180
200
220
240
260
280
300
320
340
t (mins.)

(2) Thermal decomposition following photodecomposition with recrystallised samples.

The procedure was exactly as before, except that the sample was left for 20 hours after photodecomposition before commencing thermal decomposition. The decomposition was carried out at 90°C. following 0-2% degrees of photodecomposition.

In these experiments photodecomposition did introduce a new feature into the thermal decomposition, namely an initial constant rate stage which occupied approximately 1% of the decomposition (fig. 66). Thereafter the reaction accelerated in the usual way (fig. 67). The results are shown in Table 67.

Table 67 Temperature = 90°C. Volume of reaction space = 642 ml.

Photodecomposition %	0		0.85		1.5		2.1	
Time min.	$(t + 40)^2 \times 10^{-3}$	Press. mm. x 10^3	$(t + 130)^2 \times 10^{-4}$	Press. mm. x 10^3	Press. mm. x 10^3	$(t + 100)^2 \times 10^{-4}$		Press. mm. x 10^3
0		0		0	0			
10	2.5	0.68		2.53	2.44			2.65
20	3.6	2.05		4.67	3.62			4.61
30	4.9	3.71		6.77	4.83			6.49
40	6.4	5.55		8.81	6.06			8.11
50	8.1	7.72	3.24	11.7	7.51			9.84
60	10.0	10.20	3.61	14.4	8.55			11.50
70	12.1	12.8	4.00	17.4	9.83			13.3
80	14.4	15.5	4.41	20.5	11.04			15.0
90	16.9	18.5	4.84	24.0	12.3			16.8
100	19.6	21.7	5.29	27.3	13.6		4.00	18.8
110	22.5	25.0	5.76	30.6	14.9		4.41	20.7
120	25.6	28.2	6.25	34.7	16.0		4.84	22.8
130	28.9	32.5	6.76	38.7	17.4		5.29	25.0
140	32.4	36.8	7.29	42.8	18.9		5.76	27.3
150	36.1	41.2	7.84	47.1	20.4		6.25	29.7
160	40.0	46.1	8.41	51.6	22.1		6.76	32.0
170	44.1	50.8	9.00	56.0	23.8		7.29	34.5
180	48.4	55.7	9.61	61.5	25.6		7.84	37.2
190	52.9	60.8			27.4		8.41	39.7
200	57.6	65.8			29.3		9.00	42.5
210					31.3		9.61	45.4
220							10.24	48.5
230							10.9	51.6
240							11.6	54.8

In Table 68 p_1 and k_1 are the extent and rate of the initial process and t' and k_2 are given by the equation $p + p' = k_2(t+t')^2$.

Table 68

Photo-decompn. mm. x 10^3	Photo-decompn. %	p_1 mm.x 10^3	p_1 %	k_1 x 10^4	t' mins.	k_2 x 10^7
0	0				40	12.0
10.5	0.85	8.6	0.72	2.10	130	7.74
18.8	1.5	16.0	1.34	1.25	100	3.18
26.3	2.1	16.0	1.34	1.74	100	4.77

As can be seen from this table photochemical decomposition decreased the value of k_2 and increased the value of t'. However, the effect on these constants of further photodecomposition was inconclusive.

Fig. 69.

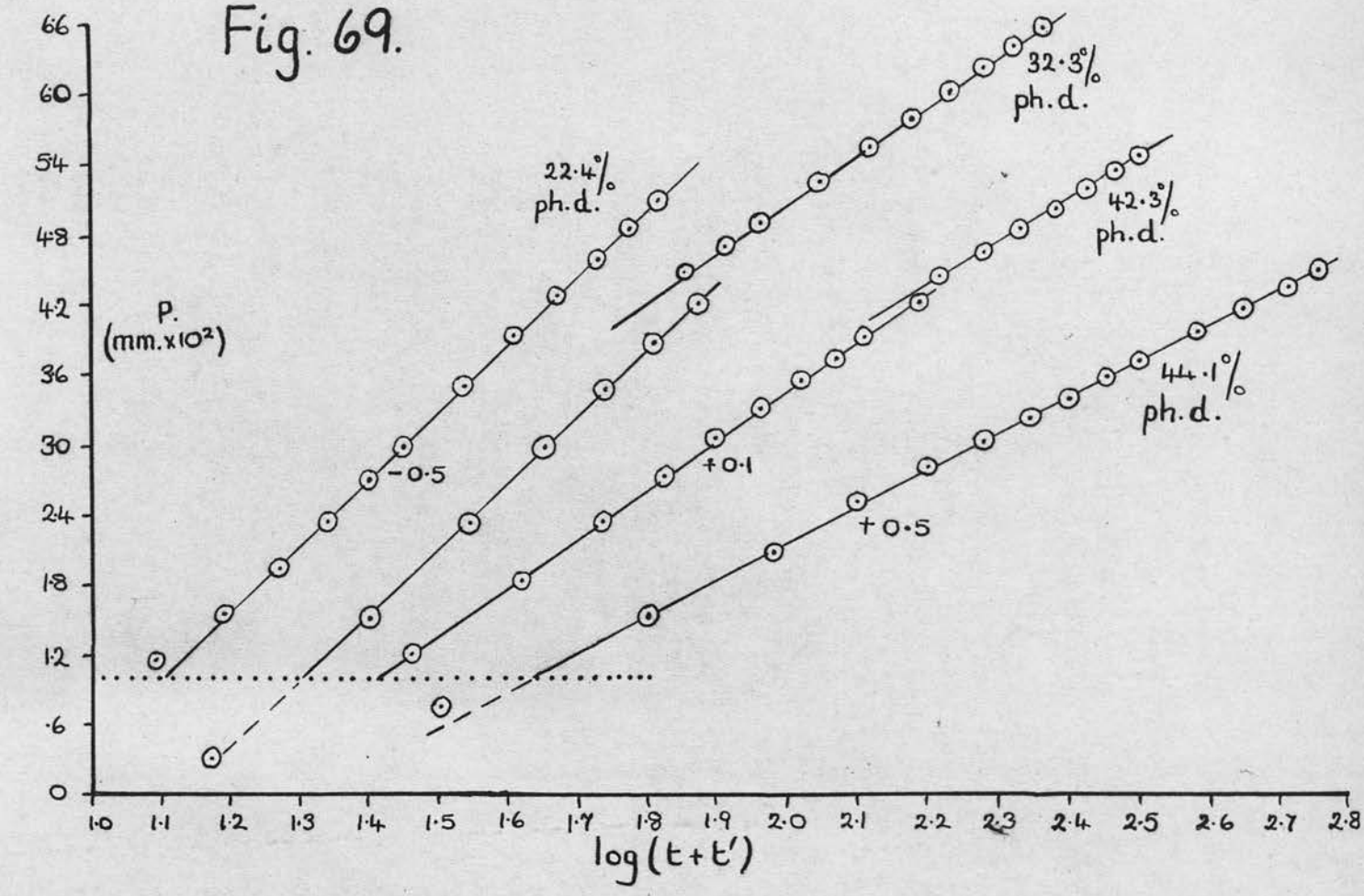
P.
(mm.x10²)
66
60
54
48
42
36
30
24
18
12
·6
0
1·0 1·1 1·2 1·3 1·4 1·5 1·6 1·7 1·8 1·9 2·0 2·1 2·2 2·3 2·4 2·5 2·6 2·7 2·8
log (t+t')
32·3% ph.d.
22·4% ph.d.
42·3% ph.d.
44·1% ph.d.
−0·5
+0·1
+0·5

Fig. 68.

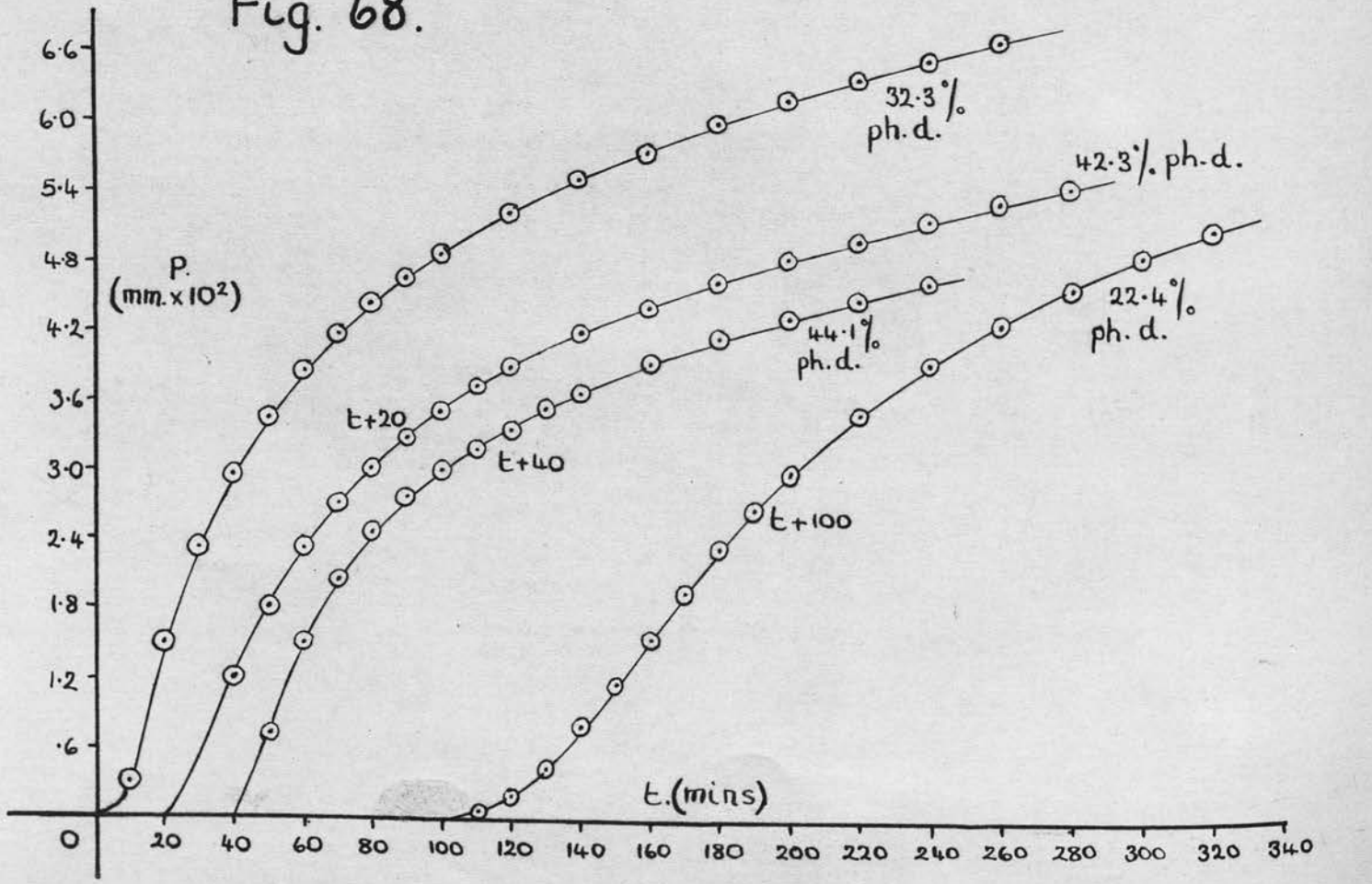
P.
(mm.x10²)
6·6
6·0
5·4
4·8
4·2
3·6
3·0
2·4
1·8
1·2
·6
0
20 40 60 80 100 120 140 160 180 200 220 240 260 280 300 320 340
t.(mins)
32·3% ph.d.
42·3% ph.d.
44·1% ph.d.
22·4% ph.d.
t+20
t+40
t+100

(3) Effect of photochemical decomposition on the decay stage of the subsequent thermal decomposition.

In this experiment 'thin' films, using approximately 15 mg. of the oxalate, were made up and photochemically decomposed in the manner described on p. 30 . After cessation of illumination the sample was left under vacuum for a further twenty-four hours; the full extent of decomposition was then recorded. Quantities of this photochemically decomposed material, corresponding to 10 mg. of undecomposed material were then thermally decomposed at 117.7°C. in the usual way.

The pressure-time curves obtained with these samples were very similar to that with no photodecomposition (fig. 68) and the same relationship was found to apply (fig. 69), i.e.

$$\propto p = \ln.(t + t') - \ln t_o$$

One sample (22.4% photodecomposed) was kept for one week before thermal decomposition. In this case a pronounced acceleration period, for a further 5% decomposition, was observed (fig. 68) and this was expressed by the equation:

$$p + p' = k^2(t + t')^2$$

Thereafter the results were expressed as above. The results of these experiments are shown in Table 69.

Table 69 Temperature = 117.7°C. Volume of reaction space = 4520 ml.

Photodecompn. %		22.4		32.3		42.3		44.1	
Time (t) min.	$t_2 \times 10^{-2}$	Press. mm. x 10^{-2}	Log(t+5)	Press. mm. x 10^2	Log(t+3)	Press. mm. x 10^2	Log t	Press. mm. x 10^2	
0		0		0		0			
5	0.25	0.025							
10	1.00	0.068	1.176	0.31	1.114		1.00	0.74	
15	2.25	0.127							
20	4.00	0.205	1.398	1.52	1.362	1.20	1.301	1.52	
25	6.25	0.310							
30	9.00	0.455	1.544	2.33	1.519	1.83	1.477	2.07	
35	12.3	0.625							
40	16.0	0.805	1.653	2.96	1.634	2.33	1.602	2.47	
	log(t-11)								
50	1.591	1.17	1.740	3.44	1.724	2.71	1.699	2.76	
60	1.690	1.55	1.813	3.84	1.799	3.02	1.778	2.98	
70	1.771	1.95	1.875	4.17	1.863	3.28	1.845	3.18	
			log(t-8)						
80	1.839	2.33	1.857	4.43	1.919	3.51	1.903	3.35	
90	1.898	2.67	1.914	4.65	1.969	3.70	1.954	3.52	
100	1.949	2.97	1.964	4.85	2.013	3.87	2.00	3.65	
120	2.037	3.48	2.049	5.19	2.090	4.17	2.079	3.90	
					log(t-9)				
140	2.111	3.90	2.121	5.48	2.117	4.40	2.146	4.12	
160	2.173	4.23	2.182	5.72	2.179	4.60	2.204	4.28	
180	2.228	4.54	2.236	5.95	2.233	4.79	2.255	4.45	
200	2.277	4.81	2.283	6.15	2.281	4.96	2.301	4.60	
220	2.320	5.04	2.326	6.32	2.324	5.13			
240			2.366	6.48	2.364	5.28			
260			2.401	6.63	2.400	5.40			

The acceleration constant (k) quoted for the non-photo-decomposed sample in Table 70 was obtained by extrapolation of the activation energy plot (fig.55), since the period of acceleration

was too short for the constant to be experimentally determined. Also in the table α_1, t_1' and t_o', and α_2, t_2' and t_o'' refer to the α p - log(t + t') plots for the two stages of the decay. The t_o values were obtained from these plots at p = pressure at which the corresponding equation first applies. Thus for all the experiments t_o' was obtained at p = 1.0. However, t_o'' was obtained at p = 4.0 for the photodecomposed samples and p = 7.0 for the non-decomposed sample. The last column in Table 70 shows the extent of decomposition corresponding to the first stage of the decay.

Table 70

Photo-decompn. %	α_1	t_1' min.	t_o'	α_2	t_2' min.	t_o''	k x 10^3	%
0	36.9	-5	13.5	51.2	-30	100	34	41
22.4	38.5	-11	41				2.2	26
32.3	41.0	5	20	56.1	- 8	58		24
42.3	56.5	3	21	64.9	- 9	101		24
44.1	75.0	0	14					26

Three facts emerge from this experiment.

(1) α_1 was increased by increasing photodecomposition, whereas α_2 and the two values of t_o were not significantly altered.

(2) The extent of decomposition described by the α_1 p = ln(t + t_1') - lnt_o' equation was reduced by 20% photodecomposition, but was not further decreased by increased decomposition.

(3) Photodecomposition did not reduce the extent of the acceleration stage, but reduced the acceleration constant (k) to approximately one-twentieth of its calculated value.

On the assumption that the dark reaction following the photochemical reaction was a slow diffusion of gas from the material, then it is probable that after a week the process was complete and thus the subsequent thermal decomposition of the sample left for this period was not complicated by any residual gas from the photochemical reaction. However, it is possible that in the samples left for twenty-four hours there was a small residue of gas, which on thermal decomposition was expelled from the sample. Thus the acceleration stage would in these cases be obscured by this pressure increase.

---

5. Electrical conductivity in the dark and on illumination.

The resistance (r) of pellets of both ferrous and ferric oxalate were measured as described on p. 45. The specific conductivities of the materials were obtained from these resistances and the dimensions of the pellets, which were measured with a micrometer screw gauge.

Specific conductivity = $\frac{l}{R.a}$ where l is the thickness in cm., a the cross-sectional area in $cm.^2$ and R the resistance of the pellet in ohms.

Tables 71 and 72 give the specific conductivities of both ferrous and ferric oxalate at temperatures between 0°C.-50°C. Column (3) in the table gives the potential drop (v) across the standard resistance R_1, which in all the following experiments, unless otherwise specified, was 10^{10} ohms.

Fig. 70.

Variation of the conductivity of the iron oxalate samples with temperature.

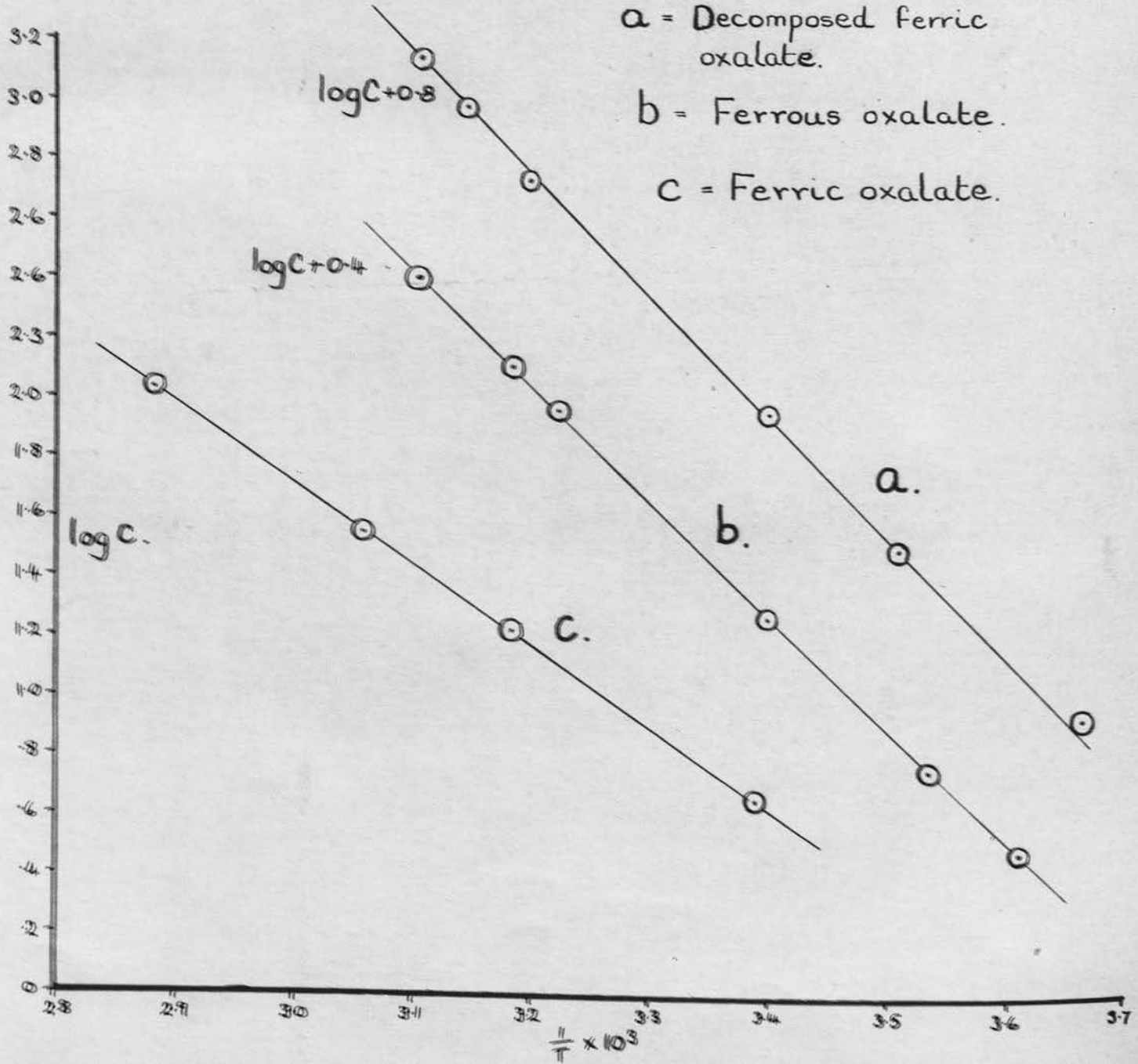

Table 71 Ferric oxalate 1/a = 0.807.

Temp. °A	1/T 10^3	v m.volts	r ohms x 10^{-12}	Sp.conduct. (C) x 10^{15}	Log C + 15
322	3.106	318	3.77	214	2.33
318	3.145	220	5.45	148	2.17
312.5	3.200	123	9.75	82.1	1.92
294	3.401	21	57.2	14.1	1.15
285	3.509	7.5	160	5.04	0.70
273	3.663	2.0	600	1.35	0.130

From the plot of log C - 1/T (fig. 70) the slope of the line is 4.0 x 10^3 ± 2%, thus the activation energy of the conductivity is 4.0 x 2.303 x 1.98 K.cals./mole = 18.2 ± 0.4 K.cals./mole.

Also from fig. 70 log C = -12.26 when $1/T = 3.0 \times 10^{-3}$. If A is the pre-exponential constant, then $\log_{10}A = -12.26 + 4.0 \times 10^3 \times 3.0 \times 10^{-3}$

$= -0.26 = \bar{1}.74$

Therefore A = 0.55 ± 2%

= 0.55 ± 0.01

Thus the conductivity is given by $C = 0.55\, e^{\frac{-18,200}{RT}}$

Table 72

Temperature °A	1/T x 10^3	v m.v.	Sp.conduct. C x 10^{15}	Log C + 15
322	3.106	138	97.5	1.99
314	3.185	71	50.2	1.70
310	3.225	51	36.1	1.56
294	3.401	10.5	7.42	0.87
283	3.535	3.2	2.27	0.36
277	3.610	1.7	1.20	0.08

From the plot of log C - 1/T (fig. 70), the slope of the line is 3.8 x 10^3 ± 2%, thus the activation energy of conductivity is

$3.8 \times 2.303 \times 1.98 = \underline{17.3 \pm 0.3 \text{ K.cals./mole.}}$

Also from fig. 70 $\log A = -12.61$ at $1/T = 3.0 \times 10^{-3}$

Therefore $\log A = -12.61 + 11.4 = -1.21 = 2.79$

Therefore $A = 0.061 \pm 0.01$.

Therefore the conductivity is given by $C = \underline{0.061\, e^{\frac{-17,300}{RT}}}$

However, the ferric oxalate used in the first determination was not very pure, being about 5% decomposed by exposure to day light, etc. So a pellet of pure ferric oxalate was used, and with this no significant reading was obtained, thus the resistance of the pellet was of the order of 10^{15} ohms (a factor of 10 greater than the last experiment). However, to verify the results obtained for ferrous oxalate, also to check that contact was being made between the pellet and the electrodes, the pellet was thermally decomposed in situ. The conductivity immediately rose by a factor of 200, but on cooling after an estimated 10-20% decomposition no significant reading was obtained. The increase in conductivity on heating was probably due to some extent to a release of water vapour from the oxalate. The pellet was then heated at 150°C. for two hours, by which time the pellet was almost completely decomposed to give anhydrous ferrous oxalate (the ferrous oxalate used before was in the form of the dihydrate). After cooling to room temperature the resistance of the pellet was found to be 10^{11} ohms - a factor of 10^4 less than before decomposition. This therefore confirms that the pellet was making contact between the electrodes, and thus the resistance of the original pellet was

of the order of 10^{15} ohms.

As a check on the previous result for ferrous oxalate, the change in conductivity with temperature of the decomposed pellet was examined and the results are shown in Table 73.

Table 73 $1/a = 0.55$, the standard resistance (R) = 10^8 ohms.

Temperature °A	1/T x 10^3	v m.v.	Spec. conduct.(C) 10^{12}	Log C + 12
347	2.882	2900	106	2.03
327	3.058	960	35.2	1.55
314	3.185	450	16.5	1.22
295	3.390	125	4.6	0.66

From the plot of log C - 1/T (fig. 70), the slope of the line is $2.73 \times 10^3 \pm 2\%$, and thus the activation energy of conductivity is $2.73 \times 1.98 \times 2.303 =$ 12.4 ± 0.2 K.cals./mole.

Also from fig.70 log C = 10.28 when $1/T = 3.0 \times 10^{-3}$

Therefore log A = -10.28 + 8.19 = -2.08 = 3.91.

Therefore $A = 8.1 \times 10^{-3}$.

The conductivity is given by $C = 8.1 \times 10^{-3} \, e^{\frac{12.400}{RT}}$

The differences in these results may well be related to the presence of water present in some form in the bulk of the pellet, particularly in the case of the ferric oxalate pellets.

Photoconductivity of ferric oxalate

With the sample of ferric oxalate in the form of a film on silica glass between two platinum connections (fig. 8), photoconductivity was observed. However, for the reasons mentioned previously (p. 45), this system was not used for systematic

measurements. Thus the final technique (p. 46) with the oxalate as a bridge between two platinum wires was employed as shown in fig. 10.

With ferrous oxalate as the bridge, a dark conductivity was observed, the sample having a resistance of the order of 10^{13} ohms; however, on illumination with the full light of the lamp for three hours no increase in conductivity was observed. On the other hand, when ferric oxalate completed the bridge, photo-conductivity, using 5460 Å light was observed almost immediately. The conductivity then rose at a gradually decreasing rate for a period of several hours until it reached an approximately constant value. This final value corresponded to a resistance of the order of 10^{13} ohms. If at any stage during the increase of conductivity, the illumination was stopped the conductivity fell gradually to a value between the initial and final readings obtained during illumination. Even when the constant conductivity stage had been reached a small decrease in conductivity was observed after the illumination was stopped. These facts could be explained on the assumption that the ferrous oxalate formed during the illumination contributed to the conductivity and that when the illumination was stopped the increase in dark conductivity was due to this ferrous oxalate. Thus on this assumption the photoconductivity of the ferric oxalate at any stage during the illumination was the difference between the total and dark conductivity at that stage and was thus inconvenient and difficult to measure.

Information on the effect of temperature and light intensity was therefore obtained from a consideration of the rate of conductivity increase. By keeping the intensity of illumination low, the rate of increase of conductivity was approximately constant for a period of 2-3 hours.

The rate of increase of the total conductivity equalled the rate of increase of the ferrous oxalate conductivity (if the photoconductivity of ferric oxalate was constant at a fixed temperature and light intensity, which should be so at least in the initial stages of illumination). Since the rate of increase of ferrous oxalate conductivity is proportional to the rate of formation of ferrous oxalate and on the assumption that this rate of formation was directly proportional to the photoconductivity of the ferric oxalate, then the rate of increase of the total conductivity is proportional to the photoconductivity of the ferric oxalate.

Thus by measuring the relative rates of conductivity increase at various temperatures and light intensities the effect of these variables on the photoconductivity of ferric oxalate was obtained.

The following procedure was therefore adopted. The ferric oxalate bridge was made up as described on p. 46 and evacuated at 10^{-5} mm. for 48 hours. The illumination with 5460 Å light was then started; after allowing a few minutes for the rate of conductivity increase to become constant, the rate was measured. The temperature was then raised and the process repeated.

Fig. 72.

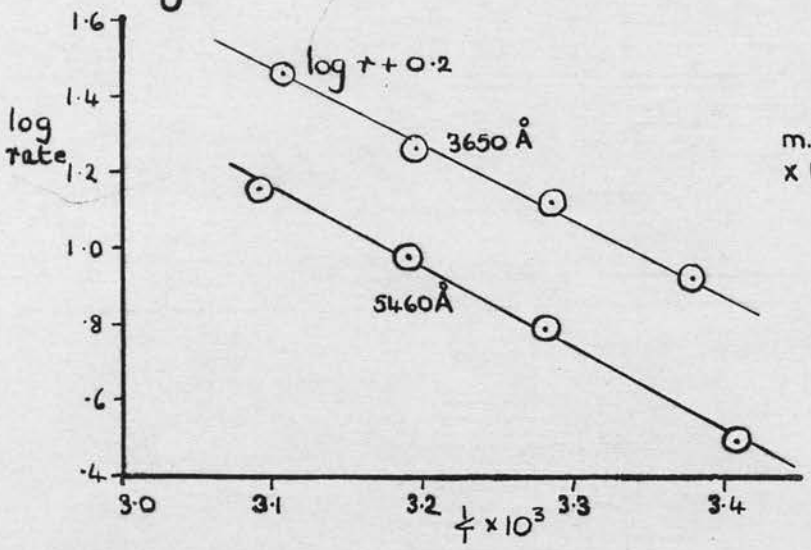

Fig. 73.

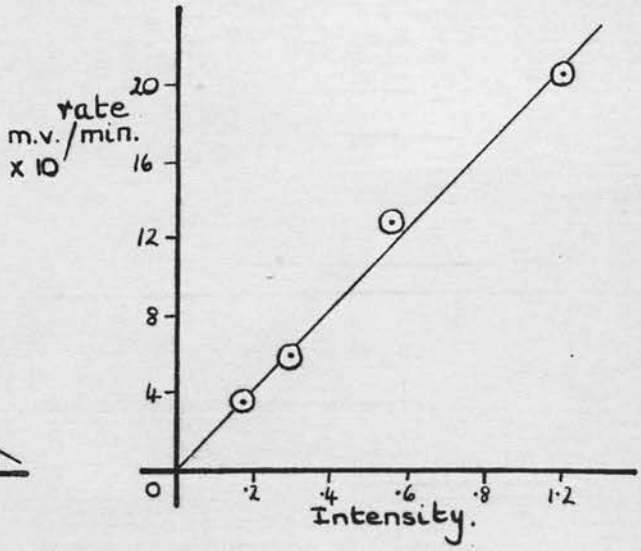

Fig. 71. The effect of temperature and light intensity on the photo-conductivity of ferric oxalate.

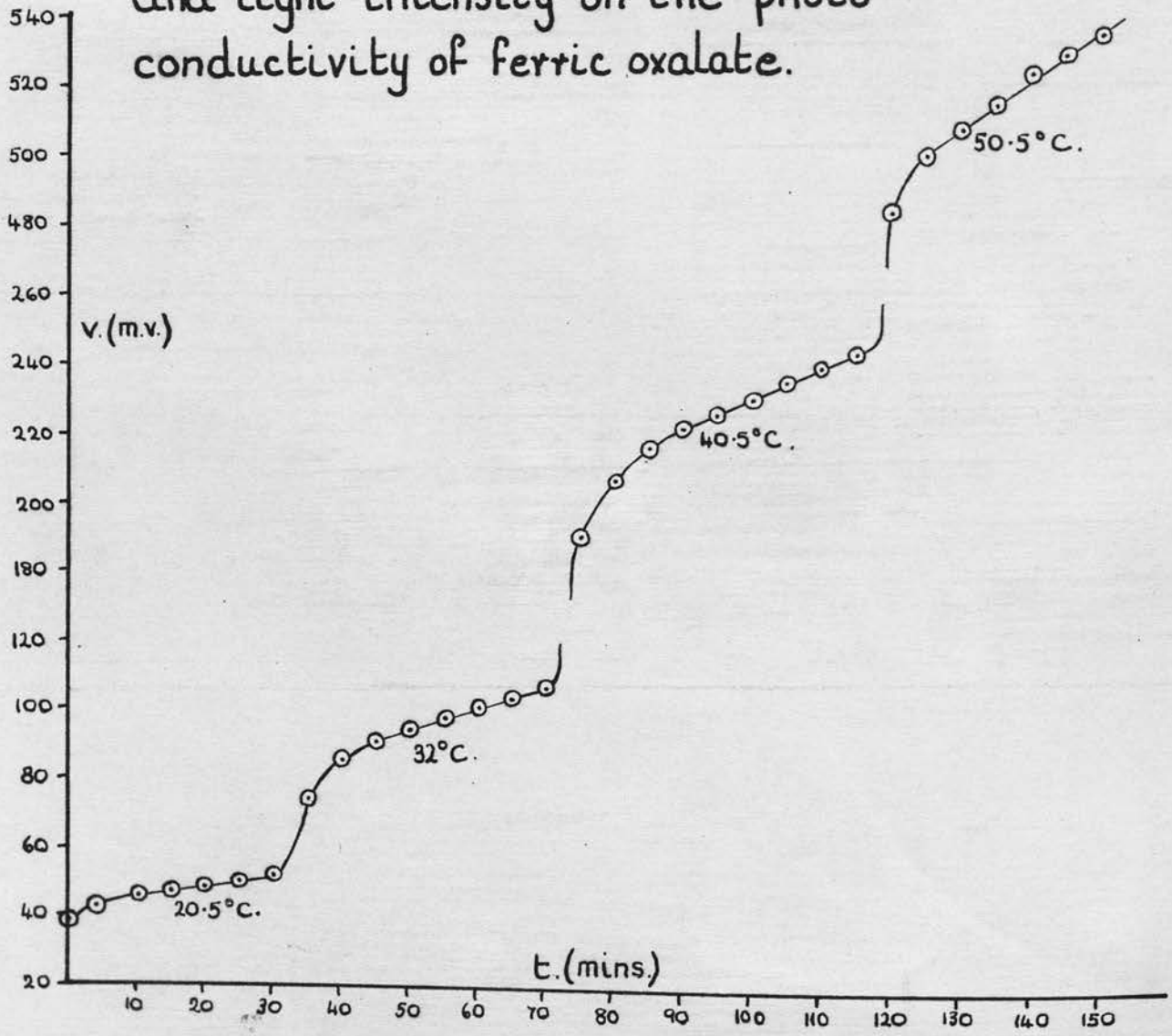

Measurements of the rate were made at four temperatures, the entire operation lasting approximately two and a half hours. The results of one complete experiment are shown in Tables 74 and 75.

Table 74

Temp. °C.	20.5		32.0		40.5		50.5	
Time min.	v m.v.	Time min.	v m.v.	Time min.	v. m.v.	Time min.	v. m.v.
0	39.0	35	74.5	75	191	120	485
2	42.0	40.	85.5	80	207.5	125	501
4	43.1	45	91.0	85	217.0	130	509
6	44.0	50	94.5	90	223.0	135	516
8	44.7	55	98.5	95	227.0	140	525
10	45.5	60	101.0	100	231.0	145	530
15	47.0	65	103.5	105	236.0	150	536
20	48.5	70	107.0	110	240.0		
25	50.0			115	244.5		
30	51.5						

The rates of conductivity increase, measured from the graph (fig. 71) are shown in Table 75.

Table 75

Temp. °A	$1/T \times 10^3$	Rate m.v./ mm. x 10	Log rate + 1.0
323.5	3.091	14.0	1.15
313.5	3.190	9.3	0.97
305.0	3.279	6.0	0.78
293.5	3.407	3.1	0.49

From the plot of log rate - 1/T (fig. 72) the slope of the line is $2.2 \times 10^3 \pm 5\%$ e, thus the activation energy of photo-conductivity is $2.2 \times 2.303 \times 1.98 =$ 10.0 ± 0.5 K.cals./mole.

This was then repeated using 3650 Å light. However, the intensity in this case was reduced to one-third with neutral filters.

Table 76

Temp. °A	1/T x 10^3	Rate m.v./ min. x 10	Log rate + 1.0
322.0	3.106	18.0	1.26
313.0	3.195	11.5	1.06
304.5	3.284	8.2	0.91
296.0	3.378	5.1	0.71

From the plot of log rate - 1/T (fig. 72), the slope of the line is 2.0 x 10^3 + 5% and thus the activation energy of photoconductivity is 2.0 x 1.98 x 2.303 = 9.2 ± 0.5 K.cals./mole. Thus the activation energies of photoconductivity are approximately the same with both 5460 Å light and 3650 Å light.

Finally the effect of the light intensity on photoconductivity was examined as above by the removal of calibrated neutral filters from between the light source and the sample.

Table 77 Photoconductivity with 3650 Å light

Intensity	Rate m.v./min. x 10
0.17	3.6
0.30	6.0
0.55	12.8
1.00	20.8

An intensity of 1.0 in this case referred to two-thirds of the 3650 Å light.

From the plot of intensity against rate (fig. 73) it can be seen that the photoconductivity of ferric oxalate was directly proportional to the incident light intensity.

DISCUSSION

The experiments have confirmed that ferric oxalate is decomposed both photochemically and thermally to give ferrous oxalate and carbon dioxide, and that there are no significant side reactions at temperatures below 150°C.

Before discussing the results in detail it is of interest to study the results as a whole and for this purpose the equations used to describe the reactions are shown in Table 78.

Table 78

Form of oxalate	Photochemical decomposition % decompn.	Equation	Thermal decomposition % decompn.	Equation	Dehydration % decompn.	Equation
Powder	0-0.3	induction	0-1	constant rate	0-50	$p^2=kt$
	0.3-2	constant rate	1-6	$p=k(t+t')^2$	50-90	$\alpha p=\ln\frac{t+t'}{t_o}$
	2-15	$\alpha p=\ln\frac{t+t'}{t_o}$	6-90	$\alpha p=\ln\frac{t+t'}{t_o}$		
Recrystallised	0-3	$p = kt^2$	0-5	$p=k(t+t')^2$		
	3-9	approx. const. rate	5-40	$\alpha p=\ln\frac{t+t'}{t_o}$	0-70	$\alpha p=\ln\frac{t+t'}{t_o}$
	9-90	$\alpha p=\ln\frac{t+t'}{t_o}$				

As can be seen from this table the initial stages of both the photochemical and thermal decompositions are described by conventional equations, but the bulk of these decompositions and of the dehydrations is described by the equation $\alpha p = \ln(t + t') - \ln t_o$. This form of equation has been of considerable value in

chemisorption studies (53), but has not previously been encountered in the field of solid state decompositions.

It was mentioned in the Introduction that this work was undertaken with a view to providing further information on solid state oxalate salt decompositions. However, although the pressure-time curves obtained from the decomposition of ferric oxalate are of the same sigmoid shape as those for other oxalate salt decompositions, the equations describing the former curves have no obvious counterpart in other systems, and thus comparison between them and those for the other oxalate salts is difficult.

The results can be divided into three sections: photochemical decomposition, thermal decomposition and dehydration. The photochemical reaction itself can be divided into two sections - the initial stage and the decay stage. For the powder form of the oxalate the initial stage was comprised of a short induction period followed by a 2% decomposition at a constant rate. For the recrystallised form this stage was comprised of a 3% induction (or acceleration) period followed by an approximately constant rate stage of a further 6%. For comparison with the reactions discussed in the Introduction the powder film is obviously more suitable, since in this case the decomposition, by the physical nature of the film, will take place at the surface of the film, whereas with the 'thin' film the reaction will take place at various depths within the film giving rise to complicated intensity effects. From the results on p.50, the 'thin' films will be in the form $Fe_2(C_2O_4)_3.2H_2O$

at the start of the reaction, whereas the 'thick' films will be in the form $Fe_2(C_2O_4)_3.3\text{-}4H_2O$, the dehydration to the trihydrate being probably incomplete. This is due to the slower rate of dehydration of the powder and the considerably larger quantities used; however, as was shown (p. 85), the presence of small amounts of water vapour does not significantly affect the rate of decomposition, so that the incomplete dehydration should not be important. A table of the results obtained for the constant rate stage with the 'thick' films as well as the photoconductivity results is shown in Table 79.

Table 79

	Intensity (I)	Activation energy K.cals./mole	Surface area (S.A.)
Rate of reaction (R)	$\propto I$	8	$R \propto$ S.A.
Photoconductivity	$\propto I$	10	

For comparison a summary of the azide results is shown in Table 80.

Table 80

	Covalent azide	Barium azide	Thallous azide
Intensity (I)	$R \propto I$ No photo-conductivity	$R \propto I^2$ No photo-conductivity	$R \propto I$ Photoconductivity $E = 8$ K.cals./mole
Activation energy K.cals./mole	8	5	8
Surface area	$R \propto$ S.A.	$R \propto$ S.A.	$R \propto$ S.A.

From these tables it can be seen that there is a similarity between the results for ferric oxalate and for thallous azide. In the latter case the activation energies of photoconductivity and decomposition are the same. This is considered to be due to the fact that in each case this energy is associated with the thermal dissociation of the optically formed exciton, the resultant electron and positive hole giving rise to the observed conductivity and the reaction involving two positive holes to give the product gas.

A similar state of affairs may exist with ferric oxalate. However, before discussing possible courses of decomposition, it is of interest to consider the ionic structure of ferric oxalate. Unfortunately, no details are available from X-ray examinations, but the following three ions have been shown to exist in ferric oxalate solutions of varying acidity and oxalate ion concentration (48):

$pH \leq 1$	$\left[Fe(C_2O_4)\right]^+$	(a)
$pH = 2.5$	$\left[Fe(C_2O_4)_2\right]'$	(b)
neutral soln. with excess of oxalate ions	$\left[Fe(C_2O_4)_3\right]'''$	(c)

From a consideration of these ions there are two probable forms for the overall neutral structure associated with the solid ferric oxalate:

$\left[Fe(C_2O_4)\right]^+ \quad \left[Fe(C_2O_4)_2\right]'$	(1)
$Fe^{+++} \left[Fe(C_2O_4)_3\right]'''$	(2)

If ferric oxalate exists in form (2) then it would be expected that its infra-red absorption spectra would be similar to that of potassium ferrioxalate since the latter is of the form $3K^{+}\left[Fe(C_2O_4)_3\right]'''$. As can be seen (p. 40) this is not so, and form (1) seems more probable. Thus with form (1) representing ferric oxalate, a possible course of decomposition is shown schematically below:

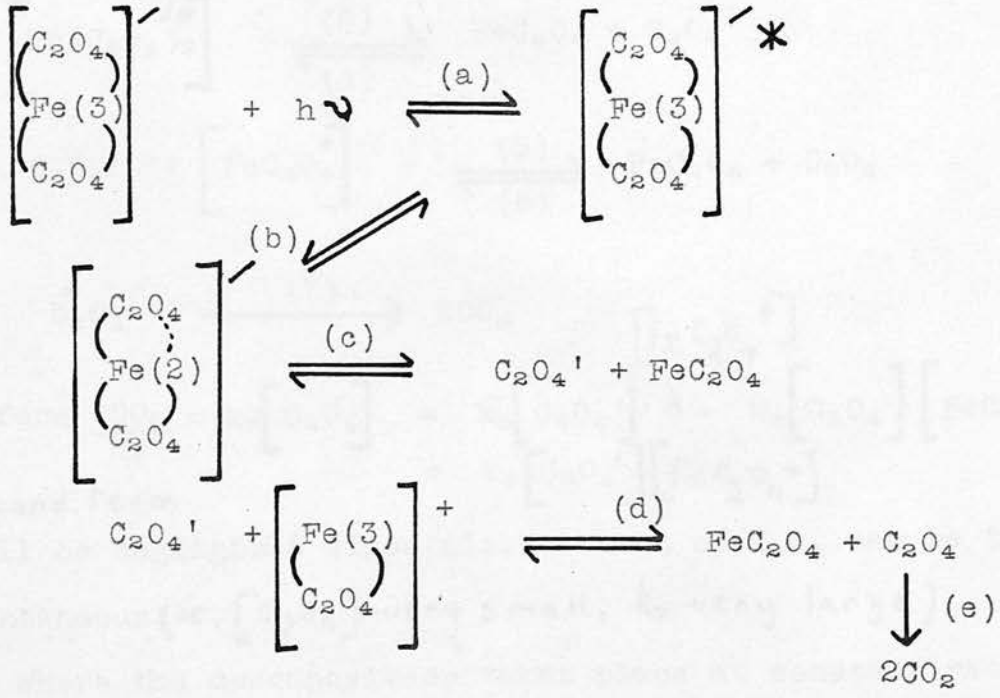

where Fe(3) and Fe(2) represent the trivalent and divalent states respectively.

It is probable that the electron transferred from the oxalate to the iron in step (b) is associated with the complex throughout and thus will not be available for conductivity. However, the oxalate radical C_2O_4' is a positive hole and thus would contribute to the observed photoconductivity. Although this C_2O_4' radical was not observed in infra-red absorption

measurements, it has been postulated as a possible intermediate in silver oxalate decomposition (54) and in decompositions of ferric oxalate in solution (12).

The above scheme may be kinetically represented as follows:

$$\left[Fe(C_2O_4)_2'\right] + h\nu \underset{(2)}{\overset{(1)}{\rightleftharpoons}} \left[Fe(C_2O_4)_2'^*\right]$$

$$\left[Fe(C_2O_4)_2'^*\right] \underset{(4)}{\overset{(3)}{\rightleftharpoons}} FeC_2O_4 + C_2O_4'$$

$$C_2O_4' + \left[FeC_2O_4^+\right] \underset{(6)}{\overset{(5)}{\rightleftharpoons}} FeC_2O_4 + C_2O_4$$

$$C_2O_4 \xrightarrow{(7)} 2CO_2$$

Therefore $\frac{dCO_2}{dt} = k_7\left[C_2O_4\right] = k_5\left[C_2O_4'\right]\lambda - k_6\left[C_2O_4\right]\left[FeC_2O_4^+\right]$

$= k_5\left[C_2O_4'\right]\left[FeC_2O_4^+\right]$

The second term λ will be negligible since dissociation of C_2O_4 can be taken as instantaneous (ie. $[C_2O_4]$ very small, k_7 very large).

Where the decomposition takes place at constant rate, then the concentrations of the intermediate entities will be effectively constant and thus by application of the steady state treatment values for $\left[C_2O_4'\right]$ etc. may be found.

$$\frac{d[C_2O_4']}{dt} = k_3[Fe(C_2O_4)_2'^*] - k_4[FeC_2O_4][C_2O_4'] - k_5[FeC_2O_4^+][C_2O_4'] = 0$$

$$\text{Therefore } [C_2O_4'] = \frac{k_3[Fe(C_2O_4)_2'^*]}{k_4[FeC_2O_4] + k_5[FeC_2O_4^+]}$$

On the assumption that $k_5 \gg k_4$

$$[C_2O_4'] = \frac{k_3[Fe(C_2O_4)_2'^*]}{k_5[FeC_2O_4^+]}$$

$$\frac{d[Fe(C_2O_4)_2'^*]}{dt} = k_1[Fe(C_2O_4)_2']I - k_2[Fe(C_2O_4)_2'^*] - k_3[Fe(C_2O_4)_2'^*] = 0$$

$$\text{Therefore } [Fe(C_2O_4)_2'^*] = \frac{k_1[Fe(C_2O_4)_2']\ I}{k_2 + k_3}$$

$$\text{Therefore } \frac{dCO_2}{dt} = \frac{k_1 . k_3}{k_2 + k_3}[Fe(C_2O_4)_2']I$$

which gives the correct dependence of the rate of reaction on the light intensity and surface area (since for a film, the amount is proportional to the surface area). Variations on steps 5 and 6 are possible but do not alter the essential course of the decomposition.

The above expression is very similar to that obtained for the decomposition of thallous azide. In that case since the quantum efficiency for the reaction was low (0.01) k_1 and k_2

were much greater than k_3 (where the k values refer to a scheme similar to the above, shown on p. 5) and thus the expression reduced to:

$$\frac{dN_2}{dt} = \frac{k_1 k_3}{k_2} (N_3') I$$

and $E = E_1 + E_3 - E_2 \approx E_3$ (since $E_1 \approx E_2$)

Thus the activation energy for the decomposition is approximately equal to the activation energy associated with the dissociation of the exciton and thus, in agreement with experiment, is the same as that for the photoconductivity. However, although approximately the same activation energies were obtained for the decomposition and photoconductivity of ferric oxalate, the quantum efficiency was found to be 0.3 (p. 87) and thus the same simplification cannot be made in the expression above.

After this initial constant rate stage, the rate fell off and as described previously the pressure-time data for the decomposition was described by the equation

$$\alpha p = \ln(t + t') - \ln t_o$$ where α, t' and t_o are constants.

This on differentiation becomes

$$\frac{dp}{dt} = \frac{1}{\alpha t_o} e^{-\alpha p} \qquad (2)$$

These equations apply to both types of film.

For reactions involving the extents of decomposition encountered in this work (up to 15% for the 'thick' films and up to

90% for the 'thin' films), the intensity of light falling on the undecomposed parts of the film will decrease as the reaction proceeds, since the ferrous oxalate formed will absorb and reflect a considerable amount of the light falling on it, especially when the film is in the powder form. Thus the equation (2) above could be obtained empirically on the assumption that the reaction continues as before at a rate dependent on the incident light intensity which decreases according to the equation:

$I = I_o \ e^{-\alpha p}$ where I_o is the initial incident light intensity and p, the pressure, gives a measure of the thickness of the decomposed layer. Thus when $p = 0$, $I = I_o$ and when p is large $I \longrightarrow 0$,

now since the rate of reaction $\propto I$

Therefore $\frac{dp}{dt} = kI_o \ e^{-\alpha p} = K \ e^{-\alpha p}$, where k and K are constants, which is the same as equation (2). However, this equation also describes the thermal decompositions, the dehydration and the dark reaction results, where the explanation given above cannot apply. So although the effective light intensity must decrease during the course of the reaction this may not alone explain the equation.

It was mentioned (p. 60) that although carbon dioxide and ferrous oxalate were produced in stoichiometric proportions in the early stages of the reaction, this was not so as the decomposition proceeded. Thus the observed rate of pressure increase was in

all probability less than the actual rate of decomposition (i.e. $-d\,\frac{Fe_2(C_2O_4)_3}{dt}$ and this applied to both photochemical and thermal decompositions. If this discrepancy in the rates was due to the slow diffusion of the product gas from the interior of the oxalate film or particles, it would explain why the equations describing the decay for both the photochemical and thermal decompositions are the same and why there was a continued pressure increase after the illumination was discontinued. Several facts support this theory that diffusion has an important role in the decomposition kinetics. (1) Fresh ferric oxalate is very soluble in water. Ferric oxalate slightly (5%) decomposed by sunlight is very insoluble even when ground to a fine powder. This lack of solubility must be due to the close adhesion of the insoluble ferrous oxalate to the ferric oxalate. This firm binding of the ferrous to the ferric oxalate probably takes place either by hydrogen bonding of the water molecules present or by the easy incorporation of the new phase in the lattice of the old due to their similar structures or more probably a combination of both. Hydrogen bonding in both ferrous oxalate dihydrate and ferric oxalate pentahydrate is clearly demonstrated, particularly when compared with anhydrous sodium oxalate, by the breadth of the peaks in the respective infra-red absorption spectra. Thus the cracked and fissured structure usually obtained after a small percentage decomposition of an ionic salt due to the strain associated with the formation of the new phase in the old is probably not obtained with ferric oxalate for the reasons mentioned

above and thus slow diffusion of the product gas from the crystals is quite feasible. Also in this connection both ferric and ferrous oxalate readily form a paste with a little water which on drying forms a hard residue. This material does not readily break or crumble back into the original powder and appears to be unaffected by evacuation. It is probable that the powder used for the thermal decompositions is a similar aggregate of still smaller particles. Thus the ferric oxalate particles and films (which are bound with water) in physical appearance seem very likely to give rise to the diffusion effects proposed.

(2) The equation describing the pressure change during the dark reaction was the same as that for the photochemical reaction. If during the illumination the diffusion of gas out of the film is the rate determining process, then on discontinuing the illumination the diffusion should continue at a decreasing rate and the equations describing these processes should be similar. This, as mentioned previously, was observed.

(3) On re-illumination after the dark period an induction period was always observed. This can be accounted for by the diffusion theory, since it will be the time taken for the diffusion pressure to build up inside the film.

(4) Although only a 0.3% induction period was observed with the 'thick' films 3% was observed with the 'thin' films. This too can be

explained on the basis of diffusion. With the 'thick' films the light will almost entirely be reflected or absorbed in the surface layers and thus the reaction will take place on the surface of the film. On the other hand, the thin almost transparent film, from the quantum efficiency measurements (p. 87) reflects from 10-30% of the incident light, the remaining 70-90% of the light being absorbed at varying depths in the film depending on the wave-length of light used. Thus for light of 5460 Å or 4360 Å, at which wave-lengths ferric oxalate does not absorb strongly, the majority of light absorbed will be in the bulk of the film and consequently the greater part of the reaction will take place in the bulk also. Thus if there is a slow diffusion of the gas out of the film, the rate of pressure ~~of~~ increase will be initially slow due to the small amount of surface decomposition but will increase as the gas produced by the reaction in the film diffuses out, the overall effect being the induction or acceleration period observed. This increase in rate will continue until the diffusion rate is a maximum and then decrease as the actual rate of decomposition decreases. Ferric oxalate absorbs 3650 Å light more strongly and thus more of the reaction will take place in the surface layers of the film than before and as a result there is virtually no induction period at this wave-length.

(5) After both photochemical and thermal decomposition when the sample was dissolved in 0.8 N-sulphuric acid for estimation purposes an effervescence was observed. Since this effervescence was not observed with undecomposed samples, it is probable that it is due to the release of carbon dioxide occluded in the decomposition samples. This is to some extent verified by the fact that in the absorption spectra for the decomposed, but not the undecomposed, samples a peak at 2400 $cm.^{-1}$, presumably due to carbon dioxide, was observed (p. 40).

(6) Finally the rate of diffusion of the gas will be proportional to the internal pressure of the gas which in turn will be determined by the actual rate of decomposition. Thus if the decay stage is related to the rate of diffusion of the gas, then the same relationship between the rate of reaction and light intensity should exist for this stage as existed for the constant rate stage. This was observed for both types of film.

Thus from a consideration of these facts a theory based on the diffusion of the gas out of the film appears to explain generally the phenomena observed. This is not an isolated example and gas occlusion following ionising radiation has been observed by Hennig, Lees and Matheson with nitrate salts (55).

Consider the equation $$\frac{dp}{dt} = \frac{1}{\alpha t_o} e^{-\alpha p}$$

For the 'thick' films, decomposition takes place principally on the surface, thus as the decomposition proceeds, the thickness of the

decomposed layer will increase, i.e. the gas will have to diffuse through an increasing distance. Thus where p (the pressure increase) is a measure of the thickness of the decomposed layer, then the observed rate of reaction, i.e. the rate of diffusion of the gas, might be given by:

$$\frac{dp}{dt} = A\, e^{-\alpha p} \qquad \text{where A and } \alpha \text{ are constants.}$$

This equation fulfils the conditions that at $p = 0$ $\frac{dp}{dt} = A$ (the initial constant rate of decomposition) and as $p \longrightarrow \infty$ $\frac{dp}{dt} \longrightarrow 0$ and is the same as that obtained:

$$\frac{dp}{dt} = \frac{1}{\alpha t_o}\, e^{-\alpha p}$$

where $\frac{1}{\alpha t_o}$ = initial rate of decomposition.

Similarly with the thin films, although the reaction does not exclusively take place at the surface of the film, the average distance through which the gas has to diffuse will increase as the reaction proceeds and thus the same equation can be developed.

The effects of varying temperature, light intensity and amount on the constants α and t_o are shown in Table 81.

Table 81

	'Thick' films			'Thin' films	
	Mass (M)	Light intensity (I)	Temperature (E in K.cals./mole).	Intensity	Temperature
α	dependent on M	constant	constant	constant	constant
t_o	constant	$1/t_o \propto I$	$\log t_o \propto 1/T$, $E = 8$	$1/t_o \propto I$	$\log t_o \propto 1/T$, $E = 5$

For both types of film $1/\alpha t_o$ = constant rate of reaction. As mentioned previously (p. 71) α is more probably dependent on the effective surface area of the film than on the mass.

Like the photochemical reaction, the thermal decomposition may be divided into two sections: the initial stage up to 5-6% decomposition and thereafter the decay stage for both forms of the oxalate. For the powder this initial stage consists of a constant rate stage up to 1% decomposition followed by an acceleration ($p = k(t + t')^2$) for a further 5%, whereas with the recrystallised form there is no significant constant rate stage and the acceleration ($p = k(t + t')^2$) applies up to 5%.

There are two possible explanations for the acceleration stage in the light of the equation $p = k(t + t')^2$:

(1) A two dimensional growth of rapidly formed nuclei over the surface of the particles, similar to the decomposition of mercury oxalate (43).

(2) An induction period due to a build up of an internal diffusion pressure similar to that observed in the photochemical decompositions of the thin films.

For (1) a high degree of nucleation is required at the start of the decomposition, the acceleration being given by the growth of these nuclei. This high degree of nucleation is probable in the case of ferric oxalate for the following reasons:

(a) As a precipitated microcrystalline solid, nucleus forming sites will be plentiful.

(b) Dehydration on evacuation of the hydrated solid will leave spaces in the lattice and positions suitable for nucleus formation.

(c) As has been discussed earlier (p.144) ferrous and ferric oxalate appear to have similar crystal structures and thus the strain energy associated with nucleus formation will be small, so that nuclei could be formed at any minor imperfections in the structure.

(d) Grinding of the precipitated fragments into powder and unavoidable exposure to light will create nuclei at these sites.

From these considerations it would appear that ferric oxalate could be highly nucleated soon after the start of the decomposition and thus the extent of acceleration would be small - as was observed. However, on this basis there is no obvious explanation for the constant rate stage. It is unlikely that this stage is related to the expulsion of water vapour from the partially dehydrated samples since the activation energy associated with the duration of the constant rate process was 33 K.cals./mole. Had the constant

rate stage been associated with this water removal a lower activation energy would have been expected.

On the other hand if it is to be accepted that the later stages of the reaction are governed by the rate of diffusion of the product gas out of the sample, then the picture created in (1) of a highly nucleated structure suggesting lattice imperfections, sub grain boundaries, etc. is misleading. It is more probable therefore that the ferric oxalate used was comprised of a mass of independent microcrystalline fragments firmly bound together, with the decomposition taking place simultaneously throughout all these fragments. The acceleration could then be envisaged as the time taken for the internal diffusion pressure to build up to its maximum value and thereafter the observed rate of reaction would decrease as the amount of undecomposed material decreased. If diffusion of the gas was rapid then the observed rate of reaction would be a maximum at the start of the decomposition and would probably decrease in accordance with the unimolecular decay law.

Also on the basis of the diffusion process the initial constant rate stage of the powder can be explained as the decomposition of the surface layers (which will gradually decrease) plus the increasing effect from the bulk of diffusion, giving the overall constant rate observed, this in turn developing into the acceleration as the rate of diffusion increases.

For the recrystallised samples no constant rate period was observed, possibly because with the thinner flakes there was no

time lag in the centre of the flakes reaching the reaction vessel temperature and because of an increased rate of diffusion. In support of the latter view is the fact that the acceleration constant for the recrystallised samples was greater than that for the powder at the same temperature.

The effects of photochemical decomposition on the subsequent thermal decomposition throw more light on the problem. The results obtained with the two types of material are as follows. For the powder form, the rate of the constant rate stage of the reaction was slightly increased, whereas the duration of this stage was unchanged. The rates thereafter were increased although the maximum rate was not much affected and thus t' increased with photodecomposition. Now if the acceleration stage is considered to be due to the two dimensional growth of nuclei, then the probable effects of pre-photodecomposition would be to advance this process by the amount of photodecomposition and at the same time to increase the number of nuclei. Thus the initial rates of reaction (for the acceleration stage) and t' should be increased, whereas the extent of acceleration decreased. Also it would be expected that the extent of the initial stage would be decreased.

With respect to a diffusion theory if the photodecomposition took place principally in the surface layers (which is very probable), then the initial rate might be increased by gas retained from the photodecomposition (although the amount of undecomposed oxalate has been reduced), but the duration of this stage should be unaffected;

as before the constant rate would be made up of the surface decomposition + diffusion. The initial acceleration rates will be faster, but the maximum rate and the duration of the acceleration should be unchanged and thus t' will be increased.

Of the two possibilities the latter seems more plausible, although from acceleration evidence there is little to differentiate them. However, the constant rate stage is more satisfactorily explained by the latter, firstly for its existence and secondly that its duration is unchanged by photodecomposition. If the constant rate stage was in some way connected with a movement of anion vacancies or some other pre-nucleation step, it would be reasonable to assume that photodecomposition would have a more marked effect than was observed.

For the recrystallised form, photodecomposition introduced a constant rate stage and reduced the resultant acceleration rates, the latter in contrast to the powder form. Since the full light of the lamp was used it is probable that decomposition in depth was obtained, and some gas was almost certainly retained in the bulk of the samples. Thus when the thermal decomposition was started, this retained gas would be expelled at a decreasing rate and this in conjunction with the normal acceleration would give rise to the observed constant rate. The acceleration rates thereafter were slower than before, due to the overall decomposition prior to this acceleration. ~~Like the powder~~ The appearance of this constant rate stage is not easily explained on the basis of a nucleation theory, nor would a nucleation theory account for the decreased acceleration rates; rather it

would be expected that the acceleration would be advanced by an amount in proportion to the surface photodecomposition. Further confirmation for the diffusion theory comes from the results for decompositions at 117.7°C. (p. 124). In this case the acceleration period was only observed with the sample which was kept for a week after photodecomposition (this giving time for the retained gas to diffuse out of the sample). The other samples which were only kept for twenty-four hours probably still contained gas from the photodecomposition, which on thermal decomposition would be expelled from the sample obscuring the acceleration period. The lower acceleration constant for the 22% decomposed sample than that for the undecomposed sample is presumably due to the decreased amount of undecomposed ferric oxalate.

From the evidence it appears that the acceleration is best explained on the basis of an increasing rate of diffusion. Thus although the actual rate of reaction is probably a maximum at the start of the decomposition and decreases thereafter, due to the slow diffusion of the product gas out of the sample the observed maximum rate did not occur until 5-6% decomposition.

Now from Fick's Law (56) the rate of diffusion of the gas (R), $\propto$ the concentration gradient and for both forms of the oxalate, the average distance through which the gas has to diffuse is constant, so that $R \propto P$, where P is the diffusion pressure.

Now in the initial stages, i.e. the first 5% decomposition, if the actual rate of decomposition is given by the unimolecular decay law

then $P \propto t$ (approximately)

and thus R, when p is small is linearly related to t, which is the relationship that was experimentally determined.

The activation energies associated with the acceleration stage were 35 K.cals./mole and 33 K.cals./mole for the recrystallised and powder forms of the oxalate respectively, i.e. some 7-9 K.cals./mole greater than that for the actual rate of decomposition, as given by the constant rate stage of the decomposition (26 K.cals./mole). This difference is possibly due to the activation energy associated with the diffusion coefficient of the samples, which for solid gas systems is usually between 5-10 K.cals./mole.

It was noted in the Introduction that rates of dehydration of crystalline hydrates were generally of two types:
(1) Dehydration takes place from a transition layer existing between the hydrated and dehydrated material with a consequent constant rate of dehydration. In an example of this kind, eg. chrome alum, the activation energy (E) associated with the rate of dehydration was considerably greater than the heat of dissociation (H). Also the vibration frequency (γ) obtained from the Polanyi-Wigner equation was much greater than the theoretical value (10^{12}).

(2) The dehydration initially takes place at a constant rate, but due to the impedance of the dehydrated layer, the rate decreases as the dehydration proceeds. E in this case may be approximately equal to H and the vibration frequency ~~is~~ normal (eg. copper sulphate).

The dehydration of both forms of ferric oxalate appears to be similar to the second class of dehydration, although the impedance from the dehydrated layer is greater than that encountered in the dehydration of copper sulphate pentahydrate (15) a typical example of (2) above, and E is somewhat greater than H; the difference (3-5 K.cals./mole) may be associated with this increased impedance. To find the vibration frequency the value of N, the number of molecules/cm^2 of interface, and r, the rate of reaction in molecules/cm^2. sec. are required. Since the powder form of the oxalate is made up of approximately spherical particles of about 1.7×10^{-2} cm. diameter, it was considered that the area of interface, at least initially was the total surface area of the particles and thus by calculation of this area the rate of reaction could be determined and by calculation from the density of ferric oxalate the value of N could be obtained as shown below:

Radius of the particles = 8.5×10^{-3} cm.

Therefore Volume of particle = $\frac{4}{3}\pi (8.5 \times 10^{-3})^3$ c.c.

Since the density of ferric oxalate = 2.28 g./c.c.

then wt. of a particle = $\frac{4}{3}\pi (8.5 \times 10^{-3})^3 \times 2.28$ g.

the total weight of the sample = 1.5×10^{-2} g.

Therefore the number of particles = $\frac{1.5 \times 10^{-2} \times 3}{4\pi (8.5 \times 10^{-3})^3 \times 2.28}$

the surface area of a particle = $4\pi (8.5 \times 10^{-3})^2$ cm^2.

Therefore the total surface area = $\frac{4\pi (8.5 \times 10^{-3})^2 \times 3 \times 10^{-2} \times 1.5 \text{ cm}^2}{4\pi (8.5 \times 10^{-3})^3 \times 2.28}$

$= \underline{2.3 \text{ cm}^2.}$

The density of ferric oxalate = 2.28 g./c.c.

$$= \frac{2.28 \times 6.02}{466} \times 10^{23} \text{ molecules/c.c.}$$

Therefore 1 molecule occupies $\frac{466}{2.28 \times 6.02} \times 10^{-23}$ c.c.

if the radius of the molecule = r cm.

then $\frac{4}{3}\pi r^3 = \frac{466}{2.28 \times 6.02} \times 10^{-23}$

Therefore $r = \sqrt[3]{\frac{4660 \times 3}{4\pi \times 2.28 \times 6.02}} \times 10^{-8}$ cm.

$$= \underline{4.3 \times 10^{-8} \text{ cm.}}$$

the surface area of the molecule = $4\pi (4.3 \times 10^{-8})^2$ cm².

Half the surface area of the molecule will contribute to the area of the interface and 2 molecules of water are obtained per molecule of ferric oxalate.

Therefore number of molecules/cm² (N) $= \frac{2 \times 2 \times 10^{16}}{4\pi \times (4.3)^2}$

$$= \underline{1.7 \times 10^{14}}$$

At 298°A the initial rate of reaction (r) = 3 divs./min.

$$= \frac{273 \times 3.0 \times 0.0263 \times 67.5 \times 6.02 \times 10^{23}}{298 \times 60 \times 760 \times 22400 \times 2.3} \text{ molecules/sec.cm}^2.$$

$$= \underline{1.3 \times 10^{15} \text{ molecules/sec.cm}^2.}$$

From the Polanyi-Wigner equation

$$1.3 \times 10^{15} = 1.7 \times 10^{14} \times \gamma \times e^{\frac{13,700}{1.98 \times 298}}$$

Therefore $\log_{10} \gamma = 0.88 + 10.1$

Therefore $\gamma = \underline{10^{11} \text{ sec.}^{-1}}$

On the assumption that the surface area/g. of the recrystallised samples is of the same order as that for the powder, then the surface area of interface = $\frac{10}{15}$ x 2.3 cm^2 = $\underline{1.5\ cm^2.}$

In this case 3 molecules of water are produced per molecule of ferric oxalate

Therefore $N = \frac{1.7 \times 3}{2} \times 10^{14} = \underline{2.5 \times 10^{14}\ \text{molecules}/cm^2.}$

At 298° the initial rate of dehydration (r) = 9 divs./min.

$$= \frac{9 \times 273 \times 134.1 \times 0.0263 \times 6.02 \times 10^{23}}{60 \times 298 \times 760 \times 22400 \times 1.5} \text{ molecules/sec. } cm^2$$

Therefore $r = \underline{1.2 \times 10^{16}}$ molecules/sec. cm^2.

Therefore $1.2 \times 10^{16} = 2.5 \times 10^{14} \times \gamma \times e^{\frac{11,800}{1.98 \times 298}}$

Therefore $\log_{10} \gamma = 1.7 + 0.87$

Therefore $\gamma = \underline{10^{10}\ sec.^{-1}}$

Thus for both the powder and the recrystallised forms of ferric oxalate pentahydrate, the vibration frequency is of approximately the expected order.

The experiments on the rates of dehydration provide the only example in the examination of ferric oxalate where the kinetics of the reactions for the two forms of the oxalate radically differ and thus supports the view that the main difference between these forms is the type of hydration of each form.

The equation $\alpha\ p = \ln(t + t') - \ln t_o$ is of the same form as the Roginsky and Zeldovich equation (57) ($q = \ln(t + t_o) - \ln t_o$,

where q is the amount of gas adsorbed in time t) which has been of considerable value in chemisorption problems. It is of interest therefore to examine the theoretical aspects of this equation with a view to comparing them with the results obtained in this work.

It has frequently been found that in chemisorption processes the adsorption consisted of two stages, an initial fast uptake followed by a slow uptake. The rate of adsorption in both stages is often given by the equation

$$\frac{dq}{dt} = a\, e^{-bq}$$ where a and b are constants

Where this equation only describes the slow process, there are indications that the constants a and b are relatively insensitive to variations in the pressure of the gas and so the process is probably determined by changes in the solid due to the chemisorbed gas.

Roginsky and Zeldovich pointed out that a rate of chemisorption which decreased exponentially with coverage would be consistent with an activated adsorption occurring with an increasing activation energy.

This condition is fulfilled if chemisorption is considered to be taking place as an activated adsorption on a non-uniform surface, where the sites are of various adsorption potential (χ) and the activation energy required for the adsorption to take place at these sites is linearly related to χ. Stone (58) using this model of the adsorption deduced an expression for the

surface coverage due to one value of χ, which by making certain assumptions can be summed for all values of χ present in the solid giving:

θ_t = constant x ln(t + constant), where θ is the degree of surface coverage

and since $q \propto \theta$, then q = constant x ln(t + constant).

The treatment which leads to this equation is valid for any model in which sites become occupied as a result of adatoms having overcome a potential barrier whose height steadily increases with coverage. Thus the model described by Porter and Tompkins (59) which involves activated migration of the adatoms can also lead to this equation. Their results point to a rapid adsorption at sites of low potential (B-sites) followed by activated migration to sites of high potential (A-sites), which cannot be reached directly from the gas phase.

The results obtained from the decomposition of ferric oxalate can be envisaged as the reverse of the second model described above, i.e. a kind of activated desorption. Two main differences distinguish these processes:

(1) The barrier which is to be overcome in the chemisorption case is of a chemical nature, whereas in the decomposition case it is probably entirely associated with the physical obstruction of the solid to the diffusing gas, rather than with any form of sorption of the gas on the solid.

(2) In the chemisorption case the adsorption potential increases with increasing degree of coverage. In contrast the energy barrier offered by the ferric and ferrous oxalate to the diffusing gas should be of the same order throughout the decomposition, for the reasons mentioned previously. However, this constancy of the barrier is offset by the fact that the diffusion pressure (P) will decrease during the course of the reaction and this in effect is the same as the barrier increasing.

Despite these differences, the overall pictures of these processes are comparable. Thus for the chemisorption, the process is considered as the movement of the adatoms from the sites of low potential over the energy barrier to those of high potential. While for the decomposition the process is reversed, the gas passing over the energy barrier from the sites of high 'potential', i.e. in the bulk of the material to those of low 'potential', i.e. at the surface where the gas passes readily into the reaction space.

In support of this theory are the activation energies determined in this work.

(a) For the dehydration experiments the activation energy associated with the rate of dehydration is some 3-5 K.cals./mole greater than the heat of dissociation.

(b) The activation energies for the acceleration and decay stages of the thermal decomposition (both considered to be determined by a diffusion mechanism) are some 5-10 K.cals./mole greater than that for the constant rate stage.

These differences may well be associated with the energy barrier proposed.

The fact that the activation energy for the constant rate and for the decay stage of the photochemical reactions are approximately the same may indicate that the decreasing intensity is the rate determining factor in that case.

This concept of diffusion as the rate determining factor has been discussed by Gafner (60) and he showed that if the gas escapes out of the solid by a lattice diffusion method rather than by means of sub grain boundaries, etc. (which seems probable for ferric oxalate), then the rate of diffusion of the gas is likely to be rate determining.

The only method of confirming these theories is by devising some method of following the actual and observed rates of reaction simultaneously. However, like the thermal decompositions of potassium manganese trioxalate trihydrate and potassium cobalt trioxalate trihydrate (44), it does seem probable that diffusion plays a predominant part in the kinetics of the reactions examined.

REFERENCES

1. Plotnikow. Lehrbuch der Photochemie (Walter de Gruyter & Co., Berlin, 1920) 316.
2. Frenkel. Phys. Rev., 37 (1931) 17.
3. Deb and Yoffe. Proc. Roy. Soc. A.256 (1960) 528.
4. Thomas and Tompkins. Proc. Roy. Soc. A.209 (1951) 550.
5. Deb and Yoffe. Proc. Roy. Soc. A.256 (1960) 514.
6. Gray and Waddington. Proc. Roy. Soc. A.241 (1957) 110.
7. Finch, Jacobs and Tompkins. J. Chem. Soc. (1954) 2053.
8. Allmand and Webb. J. Chem. Soc. (1929) 1518.
9. Allmand and Young. J. Chem. Soc. (1931) 3079.
10. Livingston. J. Phys. Chem. 44 (1940) 601.
11. Parker. Trans. Faraday Soc. 50 (1954) 1213.
12. Parker and Hatchard. J. Phys. Chem. 63 (1959) 22.
13. Polanyi and Wigner. Z. phys. Chem. A.139 (1928) 439.
14. Garner and Tanner. J. Chem. Soc. (1930) 47.
15. Smith and Topley. Proc. Roy. Soc. A.134 (1931) 224.
16. Hartshorne. Discuss. Faraday Soc. 5 (1949) 194.
17. Cooper and Garner. Proc. Roy. Soc. A.174 (1948) 487.
18. Topley and Hume. Proc. Roy. Soc. A.120 (1928) 210.
19. Cottrell. Progress in Metal Physics., vol. 1, Chap. 2. (Butterworths, London, 1949).
20. Hedges and Mitchell. Phil. Mag. 44(7)(1953) 223.
21. Wischin. Proc. Roy. Soc. A.172 (1939) 314.

22. Bright and Garner. J. Chem. Soc. (1934) 1872.

23. Prout and Tompkins. Trans. Faraday Soc. 43 (1947) 148.

24. Garner and Gomm. J. Chem. Soc. (1931) 2123.

25. Garner and Reeves. Trans. Faraday Soc. 51 (1955) 694.

26. Bartlett, Tompkins and Young. J. Chem. Soc. (1956) 3323.

27. Tompkins and Young. Trans. Faraday Soc. 52 (1956) 1245.

28. Tompkins and Young. J. Chem. Soc. (1956) 3331.

29. Tompkins. Trans. Faraday Soc. 44 (1948) 206.

30. Thomas and Tompkins. Proc. Roy. Soc. A.210 (1951) 111.

31. Garner and Hailes. Proc. Roy. Soc. A.139 (1933) 576.

32. Prout and Tompkins. Trans. Faraday Soc. 40 (1944) 488.

33. David. Bull. Soc. Chim. France. (1960) 719.

34. Scaife and Allen. J. Phys. Chem. 58 (1954) 667.

35. Wendlandt. Anal. Chem. 31 (1959) 408.

36. Akalan. Rev. fac. sci. univ. Istanbul. 21C (1956) 184.

37. Freeman and Carroll. J. Phys. Chem. 62 (1958) 394.

38. Benton and Cunningham. J. Amer. Chem. Soc. 57 (1935) 2227.

39. Tompkins. Trans. Faraday Soc. 44 (1948) 206.

40. MacDonald. J. Chem. Soc. (1936) 832.

41. Haynes and Young. Discuss. Faraday Soc. 31 (1961) in press.

42. Bircumshaw and Harris. J. Chem. Soc.(1948) 1898.

43. Prout and Tompkins. Trans. Faraday Soc. 43 (1947) 148.

44. Hennig. Thesis, Buffalo. 1941, see reference 60.

45. Weinland and Rein. Z. anorg. Chem. 178 (1929) 219.

46. X-Ray Powder Data File, ed. Smith (A.S.T.M., Baltimore 1959) 3-0117, 1-0292.

47. Miller. Thesis, Edinburgh, 1958.

48. Babko and Dubovenko. Zhur. Obschei. Khim. 26 (1956) 660, 996. See Chem. Rev. 61 (1961) 228.

49. Fortune and Mellon. Ind. Eng. Chem. 10 (1938) 60.

50. Cumming and Kay. Quantitative Chemical Analysis, 11th ed. (Oliver and Boyd, Edinburgh 1956) 294.

51. Bowen and Wokes. Fluorescence of Solutions (Longmans, Green & Co., London 1953) 59.

52. Leighton and Forbes. J. Amer. Chem. Soc. 52 (1930) 3139.

53. Low. Chem. Rev. 60 (1960) 267.

54. MacDonald. Discuss. Faraday Soc. 2 (1947) 210.

55. Hennig, Lees and Matheson. J. Chem. Phys. 21 (1953) 665.

56. Barrer. Diffusion in and through Solids (Camb. Univ. Press, Camb. 1951) Chap. 1.

57. Roginsky and Zeldovich. Acta Phys. 1 (1934) 449, 554, 595, 651.

58. Stone. Chemistry of the Solid State. ed. Garner. (Butterworths, London 1955) Chap. 15.

59. Porter and Tompkins. Proc. Roy. Soc. A.217 (1953) 529.

60. Gafner. Trans. Faraday Soc. 55 (1959) 981.

ACKNOWLEDGEMENTS

I would like to thank Dr Mowbray Ritchie for his guidance and encouragement throughout the course of this work. I would also like to thank Professors J.P.Kendall, E.L.Hirst and T.C. Cottrell for the provision of laboratory facilities, and the Department of Scientific and Industrial Research for the award of a Research Studentship (1958-1961).

Finally I am indebted to my wife for drawing the diagrams and for giving me much encouragement during the last three years.